GEOMETRY AND CONSTRAINT EFFECTS IN MIXED MODE FRACTURE

BY

Majid Reza Ayatollahi

November 1998

A dissertation submitted to the University of Bristol
in accordance with the requirements of
the degree of Doctor of Philosophy
in the Department of Mechanical Engineering
in the Faculty of Engineering

Number of words: 52250

ABSTRACT

It is known that the mode I fracture toughness depends on the geometry and the level of constraint in cracked bodies. The crack tip parameters T and Q can be used to quantify the crack tip constraint in mode I. In this thesis the geometry and constraint effects are investigated in mixed mode I/II loading for both linear elastic and elastic-plastic materials.

The higher order terms of elastic stress are obtained for an internal crack specimen using a binomial series expansion. The effect of these terms on the crack tip stresses and the plastic zone size are studied.

A new method is successfully used to determine the T-stress in mode I and mixed mode loading using finite element analysis. It is shown that the T-stress can be significant in mode II.

The maximum tangential stress criterion is modified to include the T-stress. The effect of T on the direction of fracture initiation and the onset of fracture is quantified for linear elastic materials.

A new shear specimen is used to study experimentally the effect of T-stress in mode II brittle fracture. The PMMA test specimen provides significant positive and negative values of T-stress when subjected to positive and negative shear loads. It is shown that T-stress influences significantly the direction of fracture initiation and the mode II fracture toughness.

A method is described to determine Q for mixed mode loading in elastic-plastic materials. A mode II boundary layer formulation is used to show the effect of T on the plastic zone and the near crack tip stresses and to obtain a relation between Q and T. The variation of Q with load is obtained for several shear specimens and is compared with that predicted by the Q-T diagram.

ACKNOWLEDGEMENTS

I am grateful to my supervisors Professor David Smith and Dr Martyn Pavier for their advice, technical input and encouragement throughout the course of this research.

I wish also to extend my special thanks to Troy Swankie, whose experimental project complemented this research, for not only being helpful with my work, but also being a good friend. Troy has always been willing to share his experimental expertise with me through lots of useful discussions. His assistance for the experimental part of this study is also gratefully acknowledged.

Thanks also to my nice friends in the Fracture Research Group for providing a friendly and enjoyable working atmosphere. I would also like to thank the technical staff in the Group, Ian Milnes and Ashley Davis for manufacturing the test specimens.

I wish to acknowledge gratefully the financial sponsorship for this research which was provided by the Iran University of Science and Technology through a PhD scholarship. I would also like to thank British Energy plc for providing additional financial assistance particularly for the course of the experimental work in this study.

Finally, my greatest debt of gratitude must go to my family, especially my wife for her support, devotion and patience throughout this research.

AUTHOR'S DECLARATION

I declare that the work in this dissertation was carried out in accordance with the Regulations of the University of Bristol. The work is original except where indicated by special reference in the text and no part of the dissertation has been submitted for any other degree.

Any views expressed in the dissertation are those of the author and in no way represent those of the University of Bristol.

The dissertation has not been presented to any other University for examination either in the United Kingdom or overseas.

Majid R. Ayatollahi

Date: 29/1/1999

PUBLICATIONS

The following publications have resulted from this research:

a. Journal publications

1) Ayatollahi M.R., Pavier M.J. and Smith D.J. (1998) Determination of *T*-stress from finite element analysis for mode I and mixed mode I/II loading, *International Journal of Fracture* , accepted for publication.

2) Smith D.J., Ayatollahi, M.R., Davenport, J.C.W. and Swankie, T.D. (1998) Mixed mode brittle and ductile fracture of a high strength rotor steel at room temperature. *International Journal of Fracture*, Submitted for publication.

3) Ayatollahi M.R., Smith D.J. and Pavier M.J. (1998) A method for calculating *T*-stress for mixed mode problems, *Key Engineering Materials*, Volumes 145, pp 83-88.

4) Ayatollahi M.R., Pavier M.J. and Smith D.J. (1996) On mixed mode loading of a single edge notched specimen, *International Journal of Fracture*, Volume 82, pp R61-R66.

b. Conference Proceedings

5) Smith, D.J. , Swankie, T.D., Ayatollahi, M.R. and Pavier, M.J. (1998) Brittle and ductile failure under mixed mode loading. *Proceedings of the 12th European Conference on Fracture (ECF12)*, Sheffield, UK, Vol. 2, 661-666.

6) Ayatollahi M.R., Smith D.J. and Pavier M.J. (1997) Displacement based approach to obtain *T*-stress using finite element analysis, *Proceedings of ASME-PVP Conference*, Atlanta, GA, Volume 346, pp 149-154.

CONTENTS

- **Abstract** ii
- **Acknowledgements** iii
- **Declaration** iv
- **Publications** v
- **List of Tables** xi
- **List of Figures** xii
- **Nomenclature** xvi

Chapter 1. Introduction 1

1-1. The role of geometry and constraint in fracture mechanics 1
1-2. Introduction to the thesis 4

Chapter 2. Literature Review 6

2-1. Introduction 6
2-2. Stresses near the crack tip 6
2-2-1. Elastic stresses and displacements 6
2-2-2. Plastic zone around the crack tip 9
2-2-3. Stresses and strains inside the plastic zone 11
2-3. Mechanisms of crack growth 15
2-4. Linear elastic fracture mechanics (LEFM) 17
2-4-1. LEFM - Mode I 17
Stress approach 17
Energy approach 18
2-4-2. LEFM - Mixed mode 18
Maximum tangential stress (MTS) criterion 19
Maximum energy release rate (MERR) criterion 21
Minimum strain energy density (SED) criterion 22
Remarks on mixed mode fracture criteria 24
2-4-3. Brittle fracture in PMMA 25
Mechanisms of yielding in polymers 25
Mixed mode experiments on PMMA 27

2-4-4. Statistical modelling of brittle fracture 28
2-5. Elastic-plastic fracture mechanics (EPFM) 30
2-5-1. EPFM - Mode I 30
2-5-2. EPFM - Mixed mode 31
Brittle fracture 31
Ductile fracture 32
2-6. Methods of calculating the crack tip parameters 33
2-6-1. Stress intensity factors, K_I and K_{II} 33
2-6-2. T-stress 35
2-7. Constraint effects in fracture mechanics 36
2-7-1. J-dominance 37
2-7-2. Methods of quantifying the crack tip constraint 39
J-T approach 39
J-Q approach 40
J-A_2 approach 41
A critical review of three approaches 42
2-7-3. Constraint effects in mixed mode fracture 43
2-7-4. Constraint effects in mode I ductile fracture 44

Chapter 3. Higher Order Terms of Stresses in An Internal Crack Problem 46

3-1. Introduction 46
3-2. Binomial expansion of the exact stresses 46
3-3. Plastic zone size 48
3-3.1. Plastic zone size-Tresca yield criterion 49
3-3.2. Plastic zone size-von Mises yield criterion 50
3-4. Discussion 51
3-4-1. Higher order terms of stresses 51
3-4-2. Effect of higher order terms on the plastic zone size 53
3-5. Concluding remarks 54

Chapter 4. Methods for Calculating T-stress in Mode I and Mixed Mode Problems 56

4-1. Introduction 56

4-2. Mixed mode crack tip stresses 57
4-3. Determining T using finite element analysis 58
4-3-1. Mode I 58
4-3-2. Mixed mode I/II 60
4-4. Finite element results 61
4-4-1. Mode I 61
4-4-2. Mixed mode I/II 62
4-5. Application to a mixed mode test fixture 63
4-5-1. Finite element modelling 63
4-5-2. Effect of loading configuration 65
4-5-3. Influence of crack length for mixed mode 66
4-6. Discussion 67
4-6-1. Stress method versus displacement method 67
4-6-2. T in the present mixed mode specimen 67
4-7. Concluding remarks 68

Chapter 5. A Generalised MTS Criterion 70

5-1. Introduction 70
5-2. Mixed mode crack tip parameters 71
5-3. Angled internal crack specimen 72
5-4. K-T formulation for the MTS criterion 74
5-5. Discussion 76
5-5-1. Angled crack specimen 76
5-5-2. Generalised MTS criterion 77
5-6. Concluding remarks 79

Chapter 6. Experimental Study of T-stress Effects in Mode II 80

6-1. Introduction 80
6-2. Theory 81
6-3. Experiments 82
6-3-1. Material 82
6-3-2. Specimens 82
6-3-3. Finite element analysis 83
6-3-4. Test method 84

6-3-5. Experimental results 85
6-3-6. Statistical distribution of K_{IIf} data 87
6-4. Discussion 88
6-4-1. Effect of T in mode II fracture - Theory 88
6-4-2. Effect of T in mode II fracture - Experiments 89
6-4-3. Mechanism of crack growth 91
6-4-4. Fractography of the fracture surfaces 92
+T shear specimens 92
-T shear specimens 94
6-4-5. Statistical modelling 95
6-5. Concluding remarks 97

Chapter 7. Effects of Geometry and Constraint in Mixed Mode Loading 99

7-1. Introduction 99
7-2. Quantifying Q for mixed mode problems 100
7-2-1. Boundary layer formulation 100
7-2-2. Determination of the constraint parameter Q 101
7-3. Constraint effects in mode II brittle fracture 102
7-3-1. Finite element modelling for boundary layer formulation 102
7-3-2. T-stress effect on mode II crack tip stresses 103
7-3-3. Relation between T and Q in mode II loading 104
Mode I - Validation 105
Mode II 105
7-3-4. Variation of Q in mode II crack geometries 107
Mode I - Validation 107
Mode II - Shear loading in the mixed mode specimen 108
7-4. Constraint effects in initiation of mode II ductile fracture 109
7-4-1. Mechanism of void growth and coalescence 109
7-4-2. Mechanism of shear decohesion 110
7-5. Discussion 111
7-5-1. Boundary layer formulation 111
7-5-2. Plastic zone in mode II 112
7-5-3. Effect of constraint for brittle fracture 112
J-dominance in mode II 113

Mode II constraint parameter Q_{II} 114
Finite geometry shear specimens 115
7-5-4. Effect of constraint for ductile fracture 116
7-6. Concluding remarks 117

Chapter 8. General Discussion 119

8-1. Introduction 119
8-2. Higher order terms of stress 120
8-3. *T*-stress in mixed mode loading 121
8-4. *K-T* formulation for linear elastic mixed mode fracture 122
8-5. Brittle fracture in mode II 124
8-6. Constraint effects in mode II 125
8-6-1. Brittle fracture 125
8-6-2. Ductile fracture 128

Chapter 9. Conclusions and Recommendations for Future Work 131

9-1. General conclusions 131
9-2. Potential future work 133

References 135

Appendix A5. Generalised MTS Criterion - Solution Method 147
A5-1. Direction of fracture initiation 147
A5-2. Onset of fracture, *K-B* formulation 148
A5-3. Onset of fracture, *K-T* formulation 149

- **Tables** 150
- **Figures** 156

LIST OF TABLES

Tables in Chapter 4

Table 4-1. Mode I results for the biaxiality ratio B, for the single edge notched specimen.
Table 4-2. The biaxiality ratio B, for the three connection models with different crack length ratios.

Tables in Chapter 6

Table 6-1. Results for the $+T$ shear test specimens.
Table 6-2. Results for the $-T$ shear test specimens.
Table 6-3. Results for the mode I test specimens.
Table 6-4. Results for fitting parameters in the Wallin's model used for probability analysis of the mode I and mode II fracture toughness results.

Tables in Chapter 7

Table 7-1. The variation of the direction of maximum tangential stress θ_o in mode II versus T/σ_o for n=3, 8 and 13.
Table 7-2. The mode II constraint parameter Q_{II}, calculated along the direction of maximum tangential stress, versus T/σ_o for n=3, 8 and 13.

LIST OF FIGURES

Figures in Chapter 2

Figure 2-1. Crack tip coordinates and stresses in the Cartesian and polar coordinate systems.
Figure 2-2. Three modes of loading in cracked specimens.
Figure 2-3. Mixed mode fracture in the angled internal crack specimen predicted based on the MTS criterion
Figure 2-4. Boundary layer model to simulate small scale yielding in a finite element model.
Figure 2-5. Effect of positive and negative T on the tangential stress ahead of the crack tip in a modified boundary layer model (mode I).
Figure 2-6. The constraint parameter Q versus T/σ_o for different values of hardening coefficient n. (O'Dowd and Shih, 1995).

Figures in Chapter 3

Figure 3-1a. An elliptic hole in a large plate.
Figure 3-1b. A sharp crack in a large plate.
Figure 3-2. First 6 terms in series expansion for σ_{yy}. (Internal crack in a large plate).
Figure 3-3. Effects of the higher order terms on improving the results for normalised σ_{yy}. (Internal crack in a large plate).
Figure 3-4. Effects of the higher order terms on improving the results for normalised σ_{xx}. (Internal crack in a large plate).
Figure 3-5. Plastic zone size along the crack line versus external load. Plane strain, Tresca yield criterion. a. Uniaxial loading, b. Biaxial loading.
Figure 3-6. Plastic zone size along the crack line versus external load. Plane strain, von Mises yield criterion. a. Uniaxial loading, b. Biaxial loading.
Figure 3-7. Plastic zone size along the crack line versus external load. Plane stress, Tresca yield criterion. a. Uniaxial loading, b. Biaxial loading.
Figure 3-8. Plastic zone size along the crack line versus external load. Plane stress, von Mises yield criterion. a. Uniaxial loading, b. Biaxial loading.

Figures in Chapter 4

Figure 4-1. Single edge notched (SEN) and double edge notched (DEN) specimens.
Figure 4-2. Mesh pattern for one half of the SEN specimen and one quarter of the DEN specimen.
Figure 4-3. Normalised T in a single edge notched specimen of a/W=0.4.
Figure 4-4. Normalised T in a double edge notched specimen of a/W=0.2.
Figure 4-5. T-stress determined using the displacement method, compared with results calculated by Kfouri (1986) for SEN and DEN specimens of different crack length.

Figure 4-6. An inclined edge crack in a large square plate subjected to a uniform tensile load.
Figure 4-7. Normalised T in an angled edge crack in a large square plate (loading angle β=70°)
Figure 4-8. Normalised T for different loading angles, FE results compared with those presented by Seed and Nowell (1994).
Figure 4-9. Test apparatus designed for mixed mode fracture tests. (Davenport and Smith, 1993).
Figure 4-10. Three models used to simulate the link between the specimen and the fixture.
Figure 4-11. Finite element mesh for the SEN specimen.
Figure 4-12. Finite element mesh for one half of the fixture.
Figure 4-13. Biaxiality ratio in the mixed mode test rig for crack depth to specimen width ratio (a/W) of 0.5.
Figure 4-14. Biaxiality ratio in the mixed mode test rig in the case of pin loading alone (pinned model) for crack depth to specimen width ratios (a/W) of: 0.1, 0.5 and 0.7.
Figure 4-15. Biaxiality ratio in the mixed mode test rig in the case of pin loading plus contact elements (contact model) for different crack depth to specimen width ratios (a/W).
Figure 4-16. Variation of biaxiality ratio with respect to crack length to specimen width (a/W) for modes I and II in the contact model.
Figure 4-17. A sample of loading condition to produce antisymmetric loading.

Figures in Chapter 5

Figure 5-1. Elastic tangential stress along the direction of fracture initiation θ_o.
Figure 5-2. An angled internal crack in a biaxially loaded panel.
Figure 5-3. Variation of normalised K_I , K_{II} and T with loading angle β in a centrally cracked plate under uniaxial load.
Figure 5-4. Variation of the biaxiality ratio with loading angle in a centrally cracked plate under biaxial uniform load for different values of the lateral load parameter λ.
Figure 5-5. Effect of T on the direction of crack growth initiation in mixed mode fracture based on the generalised maximum tangential stress criterion.
Figure 5-6. Mixed mode fracture loci based on the generalised maximum tangential stress criterion. $B=T.(\pi a)^{1/2}/K_{eff}$ and $\alpha=(2r_c/a)^{1/2}$.
Figure 5-7. Mixed mode fracture loci based on the generalised maximum tangential stress criterion. $T^*=(2\pi r_c)^{1/2}\, T/K_{If}$.
Figure 5-8. Effect of T on fracture initiation angle for different combinations of mode I and II, B is the biaxiality ratio, $\alpha=(2r_c/a)^{1/2}$.
Figure 5-9. Effect of T on fracture toughness for different combinations of mode I and II, B is the biaxiality ratio, $\alpha=(2r_c/a)^{1/2}$.
Figure 5-10. Direction of fracture initiation for the angled internal crack specimen, results obtained through experiments versus those predicted from the MTS Criterion.

Figures in Chapter 6

Figure 6-1. Effect of T-stress on fracture angle in mode II loading.
Figure 6-2. Effect of T-stress on mode II fracture toughness.
Figure 6-3. Mode II and mode I test specimens. a. Mode II shear test specimen, b. Definition for positive and negative shear in mode II loading, c. Mode I test specimen.
Figure 6-4. The mode II specimen mesh.
Figure 6-5. Normalised tangential and shear stresses around the crack tip at a distance r =0.27 mm. a. $+T$ shear specimen (Tensile loading), b. $-T$ shear specimen (Compressive loading).
Figure 6-6. $+T$ and $-T$ shear specimens after testing. a. $+T$ shear specimen (Tensile loading), b. $-T$ shear specimen (Compressive loading).
Figure 6-7. Experimental results for mode II fracture toughness.
Figure 6-8. Fracture angles for mode II test specimens.
Figure 6-9. Fracture surface for the positive T shear specimen.
Figure 6-10. Microscopic picture of the hyperbolic markings.
Figure 6-11. Fracture surface for the negative T shear specimen.
Figure 6-12. Statistical model for mode II fracture toughness in PMMA for $+T$ shear tests. Fitting parameters, K_o=1.32 and K_{min}=0.787.
Figure 6-13. Statistical model for mode II fracture toughness in PMMA for $-T$ shear tests. Fitting parameters, K_o=2.54 and K_{min}=1.43.
Figure 6-14. Statistical model for mode I fracture toughness in PMMA. Fitting parameters, K_o=1.99 and K_{min}=1.47.
Figure 6-15. Probability of mode II fracture in PMMA for the $+T$ and $-T$ shear tests predicted from probability of mode I fracture toughness results.

Figures in Chapter 7

Figure 7-1. Finite element simulation of the mode II boundary layer model showing the displacement boundary conditions along the circular boundary (T=0)
Figure 7-2. Effect of T-stress on the shape of the plastic zone near the tip of a mode II crack in small scale yielding.
Figure 7-3. Variation of tangential stress normalised with respect to the yield stress along the direction of maximum tangential stress for different values of T/σ_o (mode II boundary layer formulation).
Figure 7-4. Variation of radial stress normalised with respect to the yield stress along the direction of maximum tangential stress for different values of T/σ_o (mode II boundary layer formulation).
Figure 7-5. Relation between Q and T/σ_o in mode I for n=10. (present results compared with those of O'Dowd and Shih, 1995).
Figure 7-6. Singular term for the normalised tangential stress along the direction θ_o= −77° in mode II. HRR solution compared with boundary layer formulation with T=0.
Figure 7-7. Relation between Q and T/σ_o in mode II for n=3, 8 and 13.

Figure 7-8. Q calculated in mode II along the direction of maximum tangential stress for $\sigma_{\theta\theta}$, σ_{rr} and σ_m for n=8.
Figure 7-9. Effect of T/σ_o on the angular distribution of $\sigma_{\theta\theta}/\sigma_o$.
Figure 7-10. Effect of T/σ_o on the angular distribution of σ_{rr}/σ_o.
Figure 7-11. Effect of T/σ_o on the angular distribution of σ_m/σ_o.
Figure 7-12.Variation of the mode I constraint parameter Q_I for a centrally cracked plate at different levels of load. (Present results compared with those of O'Dowd and Shih, 1992).
Figure 7-13. Variation of the mode II constraint parameter Q_{II} for the mixed mode specimen at different levels of shear load. (Perfect connection model).
Figure 7-14. Variation of the mode II constraint parameter Q_{II} for the mixed mode specimen at different levels of shear load. (Contact model).
Figure 7-15. Variation of the mode II constraint parameter Q_{II} for the mixed mode specimen at different levels of shear load. (Pinned model).
Figure 7-16. Variation of the tangential stress $\sigma_{\theta\theta}$ normalised with respect to the yield stress σ_o along the direction of maximum $\sigma_{\theta\theta}$. (Pure shear in the perfect connection model).
Figure 7-17. Variation of the tangential stress $\sigma_{\theta\theta}$ normalised with respect to the yield stress σ_o along the direction of maximum $\sigma_{\theta\theta}$. (Pure shear in the contact model).
Figure 7-18. Variations of the angular distribution of the tangential stress $\sigma_{\theta\theta}$ normalised with respect to the yield stress σ_o. (Pure shear in the pinned model).
Figure 7-19. Effect of T/σ_o on the angular distribution of σ_m/σ_{eff}.
Figure 7-20. Effect of T/σ_o on the angular distribution of $\sigma_{r\theta}/\sigma_o$.
Figure 7-21. Effect of T/σ_o on the angular distribution of σ_{eff}/σ_o.
Figure 7-22. Influence of remote boundary T on near crack tip stresses for small scale yielding.

Figures in Chapter 8

Figure 8-1. The Q-T diagram for n=3, mode I versus mode II.
Figure 8-2. The Q-T diagram for n=13, mode I versus mode II.

NOMENCLATURE

Roman notations

A_2	Amplitude of the effect of the higher order elastic-plastic stresses
a	Crack length for edge cracks or semi crack length for internal cracks
a_{eff}	Effective crack length
a_o, b_o	Half of major and minor axes of an ellipse
B	Biaxiality ratio
E	Young's modulus
G	Strain energy release rate
G_c	Critical strain energy release rate
H	Specimen height
I_n	Constant in HRR solution for near crack tip stresses
J	J-integral
K_I	Mode I stress intensity factor
K_{II}	Mode II stress intensity factor
K_{eff}	Effective stress intensity factor
K_{IC}	Mode I plane strain fracture toughness
K_{If}	Mode I fracture toughness
K_{IIf}	Mode II fracture toughness
K_o , K_{min}	Constant parameters in Wallin's statistical model
M^e	Far field mode mixity parameter
M^p	Near field mode mixity parameter
n	Hardening coefficient
P	External point load
P_f	Cumulative probability of fracture
Q	Dimensionless constraint parameter
Q_I , Q_{II}	Mode I and mode II constraint parameters
R	Radius of the boundary layer model
r	Radial distance from the crack tip
r_c	Critical distance from the crack tip
r_p	Second estimate of the plastic zone size
r_y	First estimate of the plastic zone size
S	Strain energy density
S_c	Critical strain energy density

S_d	Distortional strain energy density
S_v	Dilatational strain energy density
T	T-stress
T^*	Nondimensionalised T-stress
$\boldsymbol{t}$	Traction vector
t	Specimen thickness
U	Elastic strain energy
$\boldsymbol{u}$	Displacement vector
u_x , u_y	Displacements in x and y directions
V	Volume
W	Specimen width
W^*	Strain energy density
x,y,z	Cartesian co-ordinates

Subscript and superscript notations

HRR	Corresponding to the HRR solution
max	Maximum value
min	Minimum value
SSY	Corresponding to the small scale yielding conditions

Greek notations

α	Dimensionless critical distance from the crack tip ($\sqrt{2r_c / a}$)
α_o	Constant in Ramberg-Osgood equation
β	Angle between the crack line and the loading direction
δ	Crack tip opening displacement
ε_{ij}	Strain tensor
$\tilde{\varepsilon}_{ij}$	Dimensionless angular functions in the HRR solution for strains
ε_o	Yield strain
Φ	Airy stress function
λ	Lateral load parameter
μ	Shear modulus
ν	Poisson's ratio
θ	Angle from the crack line
θ_o	Direction of fracture initiation relative to crack line

σ_{eff}	Effective stress
σ_f	Critical cleavage fracture stress
σ_{ij}	Stress tensor
$\tilde{\sigma}_{ij}$	Dimensionless angular functions in the HRR solution for stresses
σ_m	Mean (or hydrostatic) stress
σ_{rr}	Radial stress
$\sigma_{r\theta}$	Shear stress in polar co-ordinates
σ_{XX}, σ_{YY}	Far field tensile stresses in x and y directions
σ_{xx}, σ_{yy}, σ_{zz}	Direct stresses in Cartesian co-ordinates
σ_{xy}, σ_{yz}, σ_{zx}	Shear stresses in Cartesian co-ordinates
$\sigma_{\theta\theta}$	Tangential stress
$\sigma_{\theta\theta c}$	Critical tangential stress
σ_o	Yield stress
σ_1, σ_2, σ_3	Principal stresses

CHAPTER ONE

INTRODUCTION

1-1. THE ROLE OF GEOMETRY AND CONSTRAINT IN FRACTURE MECHANICS

The existence of flaws is inevitable in engineering structures and components. These flaws are created either by manufacturing or fabrication deficiencies and may grow during the service life of the component to become cracks. The aim of fracture mechanics is the ability to assess the likelihood of failure of a component containing such a crack.

Linear elastic fracture mechanics (LEFM) provides a basic framework to examine the integrity of materials in cracked bodies. LEFM is, however, restricted to specimens which fracture with negligible plasticity around the crack tip. Most commonly used structural materials such as those used for pressure vessels in power plants are highly ductile and undergo a large amount of plastic deformation before fracture. For such cases a development of LEFM is used: elastic-plastic fracture mechanics (EPFM).

A crack can be subjected to three different modes of loading known as mode I, mode II and mode III. Mode I refers to tensile loading in which the crack flanks tend to open. In mode II the crack is subjected to an in-plane shear load and its flanks slide without opening. Mode III corresponds to out-of-plane shear loading. A pure mode of loading rarely occurs in real components and hence cracks often experience mixed mode loading, which refers to a combination of two or three modes of loading. Because of symmetry, crack extension in mode I is expected to initiate along the line of the initial crack. A criterion for mixed mode I/II loading is more complicated than

for pure mode I because both the direction of fracture initiation and the onset of fracture must be determined.

The criteria available in LEFM and EPFM to assess the integrity of cracked components depend directly on the microscopic mechanism of fracture. Two major mechanisms of cracking in materials are brittle fracture and ductile fracture. Brittle fracture takes place without noticeable crack tip plasticity. In contrast, ductile crack growth is associated with a significant amount of energy absorption due to large scale plasticity.

The Resistance of a material to crack extension is called the fracture toughness, commonly assumed to be a material property. However, experimental studies show that the values of the fracture toughness obtained from different standard cracked specimens can be significantly different. Therefore, it is often suggested to use test specimens, such as the three point bend specimen or the compact tension specimen, which give a lower bound measure of the fracture toughness. Although using the resulting toughness ensures the safety of the cracked bodies, in practice the resistance of engineering components and structures to fracture can be considerably higher. This introduces conservatism in the failure assessment of structures.

The dependency of fracture toughness on geometry and loading conditions is normally attributed to the level of constraint around the crack tip. The fracture toughness is low for specimens having a highly constrained plastic zone around the crack tip. In such specimens less energy is absorbed by plastic deformation and more energy is made available for fracture. Conversely, the resistance to cracking is high for low constraint specimens which develop a larger plastic zone around the crack tip.

The effect of geometry and constraint in brittle and ductile fracture has received much attention in recent years, particularly in the power industry. The traditional failure assessment methods based on high constraint fracture tests can lead to costly and unnecessary inspections and repairs. To avoid excessive conservatism in the safety assessment of components, the fracture toughness should be measured using specimens having the same level of constraint as that for the defective body. However this requires appropriate parameters to quantify the crack tip constraint.

Mathematical solutions show that each component of the elastic stress in a cracked body can be represented by a series expansion. The leading term in this series expansion is singular and its magnitude is defined by a parameter called the stress intensity factor. The singular term is very large near the crack tip and drops towards the external boundary. The higher order terms which are significant in the far field are traditionally neglected near the crack tip. There is also a constant term of stress parallel to the crack called the T-stress which is independent of distance from the crack tip. The plastic stresses in a hardening material may also be shown as series expansions with the first terms being singular. In this case, a parameter called the J-integral (Rice, 1968) defines the magnitude of the singular term.

The stresses inside the plastic zone can be influenced significantly by a remote T-stress. Analytical and experimental studies by Betegon and Hancock (1991), Hancock et al (1993) and Sumpter (1993) have shown that in mode I, T can be used as a measure of constraint for contained yielding. Specimens having positive T are known to have higher constraint than those having negative T. However, the elastic T-stress is not relevant to crack problems involving large scale plasticity or fully yielded conditions. O'Dowd and Shih (1991) proposed a dimensionless parameter Q to describe the crack tip constraint for such conditions.

Classical theories of fracture mechanics assume that a single parameter such as the J-integral is sufficient to describe fully the stresses and strains near the crack tip. Larsson and Carlsson (1973) and Bilby et al. (1986) studied the crack tip stresses for several mode I specimens. They showed that for many practical geometries and loading conditions, a single parameter fracture mechanics is not accurate and a two-parameter characterisation is required. The J-T and J-Q approaches are the two major theories in the two parameter fracture mechanics.

Although substantial analytical and experimental studies have been carried out to evaluate the effects of geometry and constraint in cracked specimens, almost all of these studies are limited to pure mode I. There are many different real applications where cracked components are subjected to pure shear or combined tension and shear loading. For such components, the geometry and loading configuration may influence significantly the onset of fracture.

1-2. INTRODUCTION TO THE THESIS

The main objective of this thesis is to explore the effects of geometry and constraint for mode II and mixed mode loading in both linear elastic and elastic-plastic materials. The stresses near the crack tip are studied to evaluate appropriate parameters for describing the crack tip constraint. Methods are suggested for quantifying the constraint parameters in mixed mode loading. Experimental studies are undertaken to show the effects of geometry and loading on mode II brittle fracture.

Chapter 2 presents a detailed review of the previous work in linear elastic and elastic plastic mixed mode fracture mechanics. The two parameter characterisation and the constraint effects in pure mode I are also reviewed.

As noted earlier the higher order terms of the crack tip stresses are traditionally ignored. Because of difficulties in determining the constant coefficients of the higher order terms, it is not clear how much error is introduced by ignoring these terms. In Chapter 3 a binomial expansion is used to determine the higher order terms of stresses for an internal crack specimen subjected to pure tension. The effects of the higher order terms are investigated, both on the crack tip stresses and on the size of plastic zone along the crack line.

Despite the significance of the T-stress in describing the constraint effects, there are few methods available for determining T. Analytical methods are restricted to a limited number of simple specimens. Therefore, a simple and accurate computational method is more desirable. A new method is suggested in Chapter 4 for determining the T-stress for both mode I and mixed mode loading using finite element analysis. The variation of T is studied for a mixed mode specimen.

The effects of geometry and loading type in linear elastic mixed mode I/II fracture mechanics is quantified in Chapter 5. This is achieved by including the T-stress in a conventional mixed mode fracture criterion. The effect of T on the direction of fracture initiation and the mixed mode fracture toughness is shown.

The numerical results in Chapter 5 indicate that the maximum effect of the T-stress in brittle fracture occurs for pure mode II. The aim of Chapter 6 is to study experimentally the effect of the T-stress in shear loading and to validate the numerical

results presented for mode II in Chapter 5. A new shear specimen is designed to provide significant positive and negative values of T-stress for positive and negative shear loading. Perspex (PMMA) which is a highly brittle material at room temperature is used. The direction of fracture initiation and the mode II fracture toughness is determined from the positive and negative shear fracture tests. The microscopic features observed across the fracture surface are described for each type of the shear tests. A probability model is used to predict the distribution of the results obtained for $+T$ and $-T$ mode II fracture toughness.

The effects of geometry and constraint in mixed mode I/II loading is addressed in Chapter 7 for elastic-plastic materials. The results are shown in detail for mode II. The variation of the near crack tip stresses by a remote T-stress is studied. Single parameter and two parameter characterisation in shear loading is discussed. A Q-T diagram is evaluated to determine the mode II constraint parameter Q_{II} in terms of the T-stress for small scale yielding. The variation of Q_{II} with load is investigated for several shear specimens and is compared with that predicted by the Q-T diagram. The effect of geometry and constraint on mode II fracture initiation is discussed for both brittle fracture and ductile fracture.

Chapter 8 presents a general discussion on the important results of the thesis and finally Chapter 9 outlines the major findings of the present research followed by suggestions for potential future work.

CHAPTER TWO

LITERATURE REVIEW

2-1. INTRODUCTION

In this chapter a review of previous work in linear elastic and elastic plastic mixed mode fracture mechanics is presented. Emphasis is given to the subjects that are referred to in the forthcoming chapters.

The stresses and strains around the crack tip and the mechanisms of crack growth are described in sections 2-2 and 2-3. The major criteria suggested in the literature for predicting mixed mode fracture are reviewed in section 2-4 for linear elastic materials and in section 2-5 for elastic plastic materials. Section 2-6 reviews some methods for determining the crack tip parameters K_I, K_{II} and T. Finally the effect of crack tip constraint in fracture mechanics and major methods for quantifying the constraint are described in section 2-7.

The review is mainly confined to crack problems involving mixed mode loading. However, mode I crack problems are also described briefly in some of the sections as a background to mixed mode fracture.

2-2. STRESSES NEAR THE CRACK TIP

2-2-1. Elastic stresses and displacements

One of the first attempts for stress analysis of an elastic flawed body was by Inglis (1913) who solved the problem of an elliptical hole in a plate. Westergaard (1939)

proposed a complex variable technique to find the singular stresses around the tip of a sharp crack. Later, Williams (1957) attempted to solve the well known biharmonic elasticity equation

$$\nabla^4 \Phi = 0 \tag{2-1}$$

for a linear elastic, homogeneous and isotropic cracked body, where Φ is the Airy stress function. Williams split the stress function into an odd and an even part corresponding to symmetric and antisymmetric stress fields. He suggested a harmonic function for each part, satisfying both eq 2-1 and the stress free boundary conditions along the faces of the crack. The stresses resulting from each function could be written as eigen-series expansions

$$\sigma_{ij} = \left(\sum_{m=0}^{\infty} C_m r^{m/2} g_m(\theta) \right)_{ij} \tag{2-2}$$

where σ_{ij} is the stress tensor, r and θ are the polar co-ordinates shown in Fig 2-1, and g_m is a function of θ. The constant coefficients C_m depend on the geometry and loading configurations of the cracked body.

Three types of loading, shown in Fig 2-2 can be applied to a cracked geometry:

a) Mode I (opening mode) in which crack flanks open without any sliding.
b) Mode II (sliding or in-plane shearing mode) in which crack flanks slide normal to the line of crack front without any opening.
c) Mode III (out-of-plane shearing mode) in which crack flanks slide parallel to the line of crack front without any opening.

Any loading condition involving a combination of these three modes is called mixed mode loading. Only mixed modes I and II are studied in this thesis. The co-ordinates x, y and z shown in Fig 2-2 are the conventional Cartesian co-ordinates with the crack plane along the (x,z) plane.

Using Williams' solution, the series expansions for elastic stresses near the crack tip are written, for mode I, as

$$\sigma_{xx} = \frac{K_I}{\sqrt{2\pi r}}\cos\frac{\theta}{2}\left[1-\sin\frac{\theta}{2}\sin\frac{3\theta}{2}\right]+T+O(r^{1/2}) \quad (2\text{-}3a)$$

$$\sigma_{yy} = \frac{K_I}{\sqrt{2\pi r}}\cos\frac{\theta}{2}\left[1+\sin\frac{\theta}{2}\sin\frac{3\theta}{2}\right]+O(r^{1/2}) \quad (2\text{-}3b)$$

$$\sigma_{xy} = \frac{K_I}{\sqrt{2\pi r}}\cos\frac{\theta}{2}\sin\frac{\theta}{2}\cos\frac{3\theta}{2}+O(r^{1/2}) \quad (2\text{-}3c)$$

and for mode II as

$$\sigma_{xx} = -\frac{K_{II}}{\sqrt{2\pi r}}\sin\frac{\theta}{2}\left[2+\cos\frac{\theta}{2}\cos\frac{3\theta}{2}\right]+O(r^{1/2}) \quad (2\text{-}4a)$$

$$\sigma_{yy} = \frac{K_{II}}{\sqrt{2\pi r}}\sin\frac{\theta}{2}\cos\frac{\theta}{2}\cos\frac{3\theta}{2}+O(r^{1/2}) \quad (2\text{-}4b)$$

$$\sigma_{xy} = \frac{K_{II}}{\sqrt{2\pi r}}\cos\frac{\theta}{2}\left[1-\sin\frac{\theta}{2}\sin\frac{3\theta}{2}\right]+O(r^{1/2}) \quad (2\text{-}4c)$$

where the stresses σ_{xx}, σ_{yy} and σ_{xy} are shown in Fig 2-1. K_I and K_{II} are the mode I and mode II stress intensity factors (SIF), respectively. The stress intensity factors are functions of the applied load, the crack length and the geometry of the component. The second term in eq 2-3a, T, is a constant stress parallel to the crack. The T-stress is only due to the symmetric (mode I) component of loading and vanishes for antisymmetric (mode II) loading. The contribution of higher order terms in the series expansions are denoted by $O(r^{1/2})$ which are considered to be negligible near the crack tip.

The first term in each of eqs 2-3 and 2-4 is singular and tends toward infinity at the crack tip. The classical theories of fracture mechanics assume that the singular terms can be used to describe fully the elastic stresses near the crack tip. For mixed modes I and II, the stresses shown in eqs 2-3 and 2-4 are superimposed. The normal to the plane component of stress σ_{zz} is determined from Hooke's law as

$$\sigma_{zz} = \nu(\sigma_{xx}+\sigma_{yy}) \qquad \text{Plane strain} \qquad (2\text{-}5a)$$

$$\sigma_{zz} = 0 \qquad \text{Plane stress} \qquad (2\text{-}5b)$$

where ν is Poisson's ratio.

Displacements corresponding to the singular terms of elastic stresses are written for mode I as

$$u_x = \frac{K_I}{\mu}\sqrt{\frac{r}{2\pi}}\cos\frac{\theta}{2}\left[\frac{1}{2}(\kappa-1)-\sin^2(\frac{\theta}{2})\right] \quad (2\text{-}6a)$$

$$u_y = \frac{K_I}{\mu}\sqrt{\frac{r}{2\pi}}\sin\frac{\theta}{2}\left[\frac{1}{2}(\kappa+1)-\cos^2(\frac{\theta}{2})\right] \quad (2\text{-}6b)$$

and for mode II as

$$u_x = \frac{K_{II}}{\mu}\sqrt{\frac{r}{2\pi}}\sin\frac{\theta}{2}\left[\frac{1}{2}(\kappa+1)+\cos^2(\frac{\theta}{2})\right] \quad (2\text{-}7a)$$

$$u_y = -\frac{K_{II}}{\mu}\sqrt{\frac{r}{2\pi}}\cos\frac{\theta}{2}\left[\frac{1}{2}(\kappa-1)-\sin^2(\frac{\theta}{2})\right] \quad (2\text{-}7b)$$

where μ is the shear modulus and

$$\kappa = 3-4\nu \qquad \text{Plane strain} \quad (2\text{-}8a)$$

$$\kappa = (3-\nu)/(1+\nu) \qquad \text{Plane stress} \quad (2\text{-}8b)$$

The displacement components in x and y directions, u_x and u_y, are considered to be zero at the crack tip.

2-2-2. Plastic zone around the crack tip

Although a linear elastic solution predicts infinite stresses at the tip of a sharp crack, in practice the stresses are finite. This is because some materials yield beyond a certain level of applied stresses causing the region around the crack tip to undergo plastic deformation. Equations presented in the previous section are based on the assumption that the size of a plastic zone developing around the crack tip is so small that its effect on the elastic stresses can be neglected.

Irwin (1960) suggested a simple model for predicting the size of plastic zone ahead of the crack tip. Consider the variation of σ_{yy} along the crack line for a remotely loaded

cracked panel in a state of plane stress. The simplest yield criterion postulates that the plastic yielding occurs when the maximum principal stress exceeds the yield stress obtained from a uniaxial tensile test. According to this criterion, σ_{yy} will reach the material yield stress, σ_o, at some distance ahead of the crack tip, r_y , which can be calculated as:

$$r_y = \frac{1}{2\pi}\left(\frac{K_I}{\sigma_o}\right)^2 \tag{2-9}$$

The radius r_y can be taken as the first estimate of the extent of plastic zone. However, it was obtained based on the elastic stresses. A more accurate prediction for the plastic zone size can be determined if the stresses ahead of the crack tip are redistributed such that equilibrium is maintained. This results in a second estimate for the size of plastic zone r_p defined as

$$r_p = \frac{1}{\pi}\left(\frac{K_I}{\sigma_o}\right)^2 \tag{2-10}$$

which is twice as large as r_y , the first order estimate. The redistributed stress in the elastic region is higher than that of the purely elastic solution. In order to take into account this increase in the stress intensity factor K_I, Irwin (1960) proposed an effective crack length, a_{eff} , defined as the sum of the actual crack size a and a plastic zone correction

$$a_{eff} = a + r_y \tag{2-11}$$

Using the effective crack length a_{eff}, the validity of linear elastic stresses can be extended to circumstances where a limited amount of plasticity occurs around the crack tip. The radii r_y and r_p defined in eqs 2-9 and 2-10 are for plane stress. Irwin (1960) showed that ahead of the crack tip the plastic zone size for plane strain is one third of that for plane stress. This is because of the higher level of stress triaxiality in plane strain which constrains the spread of the plastic zone.

Solutions suggested by Irwin for the plastic zone size are solely based on the singular terms of the elastic stresses. However, more accurate estimates of plastic zone size can be obtained when the effects of higher order terms of stresses are also considered.

Dugdale (1960) suggested another approach known as the strip yield model, to obtain the extent of the plastic zone ahead of the crack for a mode I plane stress cracked geometry. He postulated that the crack can extend right through the plastic zone. The crack was assumed to be closed by a force resulting from the yield stress inside the plastic zone. The amount of yielding necessary to remove the elastic stress singularity at the crack tip could determine the size of the plastic zone. According to the Dugdale model the extent of plastic zone ahead of the crack tip for plane stress is

$$r_p = \frac{\pi}{8}\left(\frac{K_I}{\sigma_o}\right)^2 \tag{2-12}$$

When compared to eq 2-10 it will be seen that the result is very similar. Eq 2-12 is valid as long as the remote load is small compared with the yield stress σ_o. It is noted that neither of the Irwin and Dugdale models takes the effect of material work hardening into account.

2-2-3. Stresses and strains inside the plastic zone

For large scale plasticity, the elastic solution for crack tip stresses are no longer reliable and the stresses inside the plastic zone should be found using theories of plasticity. An important parameter for characterising the stresses inside the plastic zone is the *J*-integral which is described here.

J-Integral

Consider a contour Γ enclosing the crack tip which starts from an arbitrary point on the lower crack face and moves anticlockwise towards an arbitrary point on the upper crack face. The *J*-integral (Rice, 1968) is defined as a line integral along this contour

$$J = \int_{\Gamma}\left(W^* dy - \boldsymbol{t}.\frac{\partial \boldsymbol{u}}{\partial x} ds\right) \tag{2-13}$$

where x and y are the Cartesian co-ordinates, ds is a line element along the contour Γ, W^* is the density of stress working, $\boldsymbol{u}$ is the displacement vector and $\boldsymbol{t}$ is the traction vector which is the outward normal to the element ds. Rice (1968) showed that for a cracked geometry, J is constant and is independent of the path selected for the contour integral. The value of J is also the same for the near crack tip plastic and far field elastic regions of the cracked body.

Rice also showed that for a non-linear elastic solid, J is the rate of change of potential energy with respect to crack growth. For linear elastic materials, J is identical to the well known strain energy release rate G given by

$$G = -\frac{1}{t}\frac{\partial U}{\partial a} \tag{2-14}$$

where a is the crack length, t is the specimen thickness and U is the elastic strain energy of the body. Irwin (1957) showed that for purely elastic solids, there is a unique relation between the energy release rate G and the stress intensity factors. The relation between J, G and the elastic stress intensity factors can be written as

$$J = G_i = \frac{K_i^2}{E'} \qquad i=\text{I, II} \tag{2-15a}$$

for pure mode and as

$$J = G = \frac{K_I^2 + K_{II}^2}{E'} \tag{2-15b}$$

for mixed mode loading, where E' is equal to the Young's modulus E for plane stress and equal to $E/(1-\nu^2)$ for plane strain.

Pure mode I (II) loading

The elastic-plastic properties of materials are often modelled by the Ramberg-Osgood relation which is an equation for the material stress-strain curve, given by

$$\frac{\varepsilon}{\varepsilon_o} = \frac{\sigma}{\sigma_o} + \alpha_o \left(\frac{\sigma}{\sigma_o}\right)^n \tag{2-16}$$

where σ_o is the yield stress, ε_o is a fitting parameter usually taken as σ_o/E, n is the hardening coefficient and α_o is a material constant. Very near the crack tip, inside the plastic zone, where the elastic strains are negligible in comparison to the total strains, eq 2-16 can be approximated by a pure power law model: $\varepsilon/\varepsilon_o = \alpha_o (\sigma/\sigma_o)^n$.

Hutchinson (1968) and Rice and Rosengren (1968) showed that for either mode I or mode II, the stresses and strains inside the plastic zone around the tip of a crack can be

written as asymptotic series solutions for homogeneous, isotropic and non-linear materials obeying the power law model.

The first terms in these series expansions are singular and are known as the HRR (Hutchinson, Rice and Rosengren) solution

$$\frac{\sigma_{ij}}{\sigma_o} = \left(\frac{E}{\alpha_o \sigma_o{}^2 I_n} \cdot \frac{J}{r} \right)^{\frac{1}{n+1}} \tilde{\sigma}_{ij}(n,\theta) \tag{2-17}$$

$$\frac{\varepsilon_{ij}}{\sigma_o} = \frac{\alpha}{E} \left(\frac{E}{\alpha_o \sigma_o{}^2 I_n} \cdot \frac{J}{r} \right)^{\frac{n}{n+1}} \tilde{\varepsilon}_{ij}(n,\theta) \tag{2-18}$$

where r and θ are the polar co-ordinates. The dimensionless functions $\tilde{\sigma}_{ij}(n,\theta)$ and $\tilde{\varepsilon}_{ij}(n,\theta)$ which vary with θ, together with I_n depend on the hardening coefficient, n, the loading mode and the stress state (plane stress/plane strain). Values of $\tilde{\sigma}_{ij}$, $\tilde{\varepsilon}_{ij}$ and I_n have been tabulated by Shih (1983) for different values of the hardening coefficient.

Eqs 2-17 and 2-18 show that, similar to the stress intensity factors for the elastic solution, J is the characterising parameter for elastic-plastic materials and defines the amplitude of the singularity of the HRR solution. The HRR solution is valid as long as strains are infinitesimal, the deformation theory of plasticity holds and the loading is in either pure mode I or pure mode II. The higher order terms of the series expansions for stresses and strains inside the plastic zone which are ignored in the HRR solution can improve the accuracy of the results. This will be elaborated later in this chapter.

Mixed mode loading

The elastic-plastic stresses for mixed mode loading cannot be determined directly by superimposing the pure mode results. This is because of the non-linear behaviour of the material properties. To extend the HRR solution to mixed mode problems Shih (1974) introduced a near crack tip field mixity parameter, M^p as

$$M^p = \frac{2}{\pi} \tan^{-1} \left| \lim_{r \to 0} \frac{\sigma_{\theta\theta}(r, \theta = 0)}{\sigma_{r\theta}(r, \theta = 0)} \right| \tag{2-19}$$

and showed that the stresses and strains inside the plastic zone are singular and can be written as

$$\frac{\sigma_{ij}}{\sigma_o} = \left(\frac{E}{\alpha_o \sigma_o{}^2 I_n(M^p)} \cdot \frac{J}{r} \right)^{\frac{1}{n+1}} \tilde{\sigma}_{ij}(n,\theta,M^p) \tag{2-20}$$

$$\frac{\varepsilon_{ij}}{\sigma_o} = \frac{\alpha}{E} \left(\frac{E}{\alpha_o \sigma_o{}^2 I_n(M^p)} \cdot \frac{J}{r} \right)^{\frac{n}{n+1}} \tilde{\varepsilon}_{ij}(n,\theta,M^p) \tag{2-21}$$

The dimensionless functions $\tilde{\sigma}_{ij}$, $\tilde{\varepsilon}_{ij}$ and I_n are very similar to those defined for the HRR solution except that, here, they depend also on the near tip mixity parameter M^p. These functions have been given by Shih et al (1988) for different values of hardening coefficient n and mixity parameter M^p. It is seen from eq 2-20 that the magnitude of singular stresses in mixed mode loading can be written as

$$K_M^P = \left(\frac{EJ}{\alpha_o \sigma_o{}^2 I_n(M^p)} \right)^{\frac{1}{n+1}} \tag{2-22}$$

Shih (1974) showed that for small scale yielding the near field mixity parameter M^p is directly related to a far field elastic mixity parameter M^e defined as

$$M^e = \frac{2}{\pi} \tan^{-1} \left| \lim_{r \to \infty} \frac{\sigma_{\theta\theta}(r,\theta=0)}{\sigma_{r\theta}(r,\theta=0)} \right| = \frac{2}{\pi} \tan^{-1} \left| \frac{K_I}{K_{II}} \right| \tag{2-23}$$

The relation between M^e and M^p depends on the hardening coefficient. Thus, for small scale yielding the singular stresses and strains near the crack tip can be described fully by two parameters: the J-integral and the far field mixity parameter M^e which is determined from the stress intensity factors. Because the values of the J-integral in elastic and plastic regions are the same, from eqs 2-15b and 2-23 the strength of singular stresses K_M^P can be related to the mode I and mode II stress intensity factors by

$$J = \frac{K_I{}^2 + K_{II}{}^2}{E'} = \frac{\alpha \sigma_o{}^2}{E} I_n(M^p)(K_M^P)^{n+1} \tag{2-24}$$

It is noted that both the mixity parameters M^e and M^p are equal to 1 for mode I and 0 for mode II, and vary between 0 and 1 for mixed mode loading.

2-3. MECHANISMS OF CRACK GROWTH

In Section 2.2 the stresses and strains around the tip of a crack were described. When a cracked body is subjected to a critical loading conditions, the crack begins to extend. There are two important types of fracture in solids: brittle fracture and ductile fracture.

Brittle fracture is often referred to unstable crack growth or fast fracture and frequently leads to catastrophic consequences. Brittle fracture occurs in materials having low ductility that typically exhibit little plastic deformation around the crack tip. In steels, brittle fracture is associated with cleavage fracture of the grains.

The micro-mechanism of brittle fracture is widely regarded as elastic extension of atomic bonds ahead of the crack tip, up to the point of ultimate separation. In this case, the ideal fracture strength of material can be estimated by considering the force required to disconnect two atoms. From a continuum mechanics point of view, brittle fracture can be considered as a stress controlled mechanism of failure. A well known model for cleavage fracture due to Ritchie, Knott and Rice (1973) proposes that cleavage fracture occurs when the tensile stress at a critical distance r_c ahead of the crack tip exceeds a critical cleavage fracture stress σ_f where r_c and σ_f are material properties.

Ductile fracture takes place in materials susceptible to high plastic deformation. Crack growth in this case is often slow and materials near the crack tip undergo large plastic deformation prior to the initiation of crack growth. Microscopic studies suggest that there are two major mechanisms for crack growth in ductile materials: (i) void growth and coalescence, and (ii) shear band localisation and decohesion. A brief description of these mechanisms is presented here.

Engineering metallic alloys often contain impurities or second phase particles. When a ductile alloy is subjected to a certain level of tensile deformation, the inclusions are separated from the surrounding materials by either particle cracking or interface decohesion. This gives rise to microvoids which are normally located in front of the crack tip for a mode I crack geometry. Once nucleated, microvoids grow under the influence of the increasing tensile stresses. The crack grows by microvoid coalescence

when the excessive plastic strains cause localised flow or necking between the blunted crack tip and the first void ahead of it. The crack keeps advancing as the same process is repeated for the subsequent voids.

Several mathematical models have been suggested to describe the process of void growth and coalescence in metallic alloys, see for example Rice and Tracey (1969), Gurson (1977) and Rousselier et al. (1989). The main point which these models have in common is that the initiation and extension of crack growth in the mechanism of void growth are directly dependent on the magnitude of the tensile hydrostatic (mean) stress σ_m and inversely dependent on the effective stress σ_{eff} around the crack tip. The stresses σ_m and σ_{eff} are functions of the stress components and can be written in the Cartesian co-ordinates as

$$\sigma_m = \frac{1}{3}\left(\sigma_{xx} + \sigma_{yy} + \sigma_{zz}\right) \tag{2-25}$$

$$\sigma_{eff} = \frac{1}{\sqrt{2}}\sqrt{(\sigma_{xx} - \sigma_{yy})^2 + (\sigma_{yy} - \sigma_{zz})^2 + (\sigma_{zz} - \sigma_{xx})^2 + 6(\sigma_{xy}{}^2 + \sigma_{yz}{}^2 + \sigma_{zx}{}^2)} \tag{2-26}$$

Because both the mean stress and the effective stress are invariants of the stress tensor, eqs 2-25 and 2-26 can also be written for the stresses in polar co-ordinates.

The second mechanism of crack growth in ductile materials is mainly controlled by shear stresses (or strains) near the crack tip. Clayton and Knott (1976) suggest that following the formation of a microvoid around an inclusion in front of the crack tip shear deformation is localised in a band joining the crack tip to the void. Extension of the crack takes place by shear decohesion along this band when the shear strain attains a critical value.

The direction of crack growth in this mechanism is expected to be along the maximum radius of the plastic zone. This corresponds to an angle about 70° from the crack line for a mode I crack. The microstructural studies by Clayton and Knott (1976) show that following a small number of stages of crack growth, the path of crack advance tends towards the line of the initial crack. The successive change in the direction of crack growth provides a zig-zag fracture surface which is a characteristic of mode I crack growth by the mechanism of shear localisation and decohesion. The

alteration in the path of crack growth can be attributed to features of the plastic zone which is constrained and develops regions of tension, susceptible to cracking (Beachem and Yoder, 1973).

Clayton and Knott (1976) suggest that in mode I, the mechanism of shear decohesion is more likely to occur in ductile materials with low or intermediate work hardening whereas high work hardening favours the mechanism of void growth and coalescence. Although void growth and coalescence follow a significant amount of crack tip blunting, shear decohesion can takes place with little or negligible crack tip blunting.

2-4. LINEAR ELASTIC FRACTURE MECHANICS (LEFM)

The main microscopic mechanisms of crack growth were briefly outlined in Section 2-3. The identification of the mechanism of fracture is an important stage in the macroscopic analysis of crack growth. This is because the criterion which is employed to predict the onset of fracture must be consistent with the actual mechanism of crack growth.

Sections 2-4-1 and 2-4-2 present a short background about the mode I brittle fracture and a more detailed review of the mixed mode brittle fracture criteria. In these two sections the size of plastic zone is considered to be so small that fracture can be predicted based on the linear elastic stresses near the crack tip but outside the plastic zone.

2-4-1. LEFM - Mode I

Stress approach

According to the classical theories of fracture mechanics, the crack tip stresses for different specimens having similar stress intensity factors are the same. Therefore, the critical stress required for brittle fracture is attained when the stress intensity factor K_I reaches a critical value, K_{IC}.

$$K_I = K_{IC} \tag{2-27}$$

where K_{IC} is the mode I fracture toughness for the state of plane strain. The fracture toughness is often taken to be a material property and independent of the specimen geometry.

Energy approach

Crack growth in a purely elastic material is associated with two major changes in the total energy of the cracked specimen: some of the strain energy conserved around the crack tip is released, and some energy is consumed to break the atomic bonds in front of the crack. Griffith (1921) suggested that unstable crack growth takes place when the elastic strain energy available to propagate the crack exceeds the energy absorbed in creating new crack surfaces. According to this criterion, if the critical energy required for the initiation of crack growth is G_c, fracture occurs when

$$G = G_c \tag{2-28}$$

where G is the elastic strain energy release rate defined earlier in eq 2-14. The critical energy G_c is assumed to be a material property and for mode I it is directly related to the fracture toughness K_{IC}. The Griffith's criterion was originally suggested for purely elastic materials later modified to account for a limited amount of energy dissipation due to the plastic deformation around the crack tip.

2-4-2. LEFM - Mixed mode

The geometry and loading configurations in mode I are symmetric. Therefore, brittle fracture is expected to initiate in the same direction as the original crack. This is not the case for mixed mode loading where the crack tip stresses are asymmetric. A criterion for mixed mode fracture should be able to predict both the direction of crack growth and the onset of fracture.

Several criteria have been suggested by researchers for mixed mode fracture in linear elastic materials. Three well known criteria are described in this section. Reference is also given briefly to some of the others. It is common to use the angled internal crack problem as an example for theoretical and experimental verification of the criteria. In this specimen the angle between the crack line and the loading direction β can change from zero to 90° to provide different mixities of modes I and II (see Fig 2-3a). The solution for this example is also presented using some of the fracture criteria.

Maximum tangential stress (MTS) criterion

In an early attempt, Erdogan and Sih (1963) suggested two important criteria, known collectively as the maximum tensile stress (MTS) criterion for a two dimensional mixed mode crack problem. These are;

(i) The crack propagates radially along the direction of maximum tangential stress around the crack tip.

(ii) Crack propagation occurs when the magnitude of tangential stress $\sigma_{\theta\theta}$ along this direction acquires a critical value $\sigma_{\theta\theta c}$.

The singular term of the tangential stress can be written as

$$\sigma_{\theta\theta} = \frac{1}{\sqrt{2\pi r}} \cos\frac{\theta}{2}\left[K_I \cos^2\frac{\theta}{2} - \frac{3}{2} K_{II} \sin\theta \right] \tag{2-29}$$

By differentiating eq 2-29 with respect to θ and equating the result to zero, the direction for fracture initiation θ_o is found according to the MTS criterion as

$$\frac{(1-3\cos\theta_o)}{\sin\theta_o} = \frac{K_I}{K_{II}} \tag{2-30}$$

Eq 2-30 shows that θ_o is a function of the ratio between the stress intensity factors K_I and K_{II}. For pure mode II this equation becomes $1-3\cos\theta_o = 0$ and the direction of fracture initiation θ_o is $-70.53°$ for maximum $\sigma_{\theta\theta}$. The solution for eq 2-30 for the internal crack problem in terms of the crack angle β is

$$\left(\tan\frac{\theta_o}{2}\right) = \frac{1}{4}\tan\beta \pm \frac{1}{4}\sqrt{\tan^2\beta + 8} \tag{2-31}$$

Once θ_o is obtained from eq 2-30, it is replaced in eq 2-29 and fracture initiation is determined by equating $\sigma_{\theta\theta}$ to $\sigma_{\theta\theta c}$. If the critical stress $\sigma_{\theta\theta c}$ is written in terms of the mode I fracture toughness K_{IC}, the condition for fracture initiation is

$$\frac{K_I}{K_{IC}} \cos^3\frac{\theta_o}{2} - 3\frac{K_{II}}{K_{IC}} \cos^2\frac{\theta_o}{2} \sin\frac{\theta_o}{2} = 1 \tag{2-32}$$

From eq 2-32, for pure mode II, where K_I vanishes and θ_o = –70.53°, the mode II fracture toughness is 0.87 times the mode I fracture toughness. The solutions for eqs 2-31 and 2-32 are shown in Figs 2-3b and 2-3c respectively.

The results of experiments on PMMA for the internal angled cracked panel by Williams and Ewing (1972) showed a discrepancy between the fracture initiation angle obtained from experiment and those predicted by eq 2-31. The discrepancy was more considerable for small values of the crack angle β. Williams and Ewing showed that an improved correlation with test results is obtained if the effect of the T-stress is included in eq 2-31. According to their calculation which was corrected later by Finnie and Saith (1973), the direction of fracture initiation θ_o is determined for the internal angled crack problem by solving

$$\tan^2\beta - \left[\frac{1-3\cos\theta_o}{\sin\theta_o}\right]\tan\beta - \left[\frac{16\alpha\sin\frac{\theta_o}{2}}{3\tan\theta_o}\right]\left(1-\tan^2\beta\right) = 0 \qquad (2\text{-}33)$$

where α is a dimensionless parameter equal to $\sqrt{\frac{2r_c}{a}}$, a is the crack length and r_c is a critical distance from the crack tip. Eq 2-33 predicts that for β =0 the crack initiates along the direction θ_o= –90° which is more consistent with the experimental results compared with θ_o = –70.5° predicted by eq 2-31.

For r_c =0 the MTS criterion indicates that along the direction of maximum tangential stress, the shear stress vanishes and hence the tangential stress is a principal stress. Maiti and Smith (1983) showed that if the stresses are studied along a circle of radius r_c > 0, the maximum tangential stress is no longer a principal stress. They then suggested that mixed mode fracture can be predicted in brittle materials based on a maximum principal stress criterion. However, the results of their criterion were not much different from those of the MTS criterion.

McClintock (1963) extended the application of the MTS criterion from a slit to an elliptic crack. He proposed that the maximum surface tangential stress on the boundary of the elliptic crack is used as a measure of crack extension. Chang (1981a) modified this criterion and suggested that the maximum tangential stress is evaluated on a circle of critical radius, r_c around the elliptic crack tip.

Later, Chang (1981b) proposed the maximum tangential strain criterion in which the maximum tangential strain around the crack tip is employed as a measure of crack growth for both a slit and an elliptic crack. In a similar attempt, Fischer and Goldner (1981) suggested that the maximum principal strain in the vicinity of the crack tip is used to determine the propagation direction and the fracture load.

Maximum energy release rate criterion (MERR)

It is proposed in this criterion that

(i) Crack extension occurs at the crack tip in a radial direction along which the energy release rate is a maximum.

(ii) The crack extension initiates when the energy release rate reaches some critical level.

The energy release rate in mixed mode I and mode II was described by eq 2-15b for a crack propagating in its initial plane. However, the crack extension is often not co-linear for a crack subjected to either antisymmetric or asymmetric loads. In this case, it is necessary first to analyse a crack having a main branch and a propagating branch. The propagating branch is called a kinked crack, and is set at an arbitrary angle θ to find the stress intensity factors for the kinked crack. By substituting these stress intensity factors in equation 2-15b and differentiating the result with respect to θ, the condition for crack extension can be obtained from $(\partial G / \partial \theta) = 0$.

Numerous investigators have attempted to find the stress intensity factors for kinked cracks using closed form solutions, see for example Lo (1978), Bilby and Cardew (1975) and Hayashi and Nemat-Nasser (1981). Nuismer (1975) assumed that in the limit as the length of kink crack tends towards zero, the stress field at its tip must approach the stress field at the tip of the original crack, before extension begins. Making the above simple continuity assumption, he obtained the stress intensity factors for a kinked crack and then, using equation 2-15b, concluded that the greatest strain energy release rate occurs in the direction of the maximum tangential stress $\sigma_{\theta\theta}$. This implies that the energy release rate criterion for mixed mode fracture based on Nuismer's approach yields the same results as the maximum tangential stress (MTS) criterion.

Hussain et al (1974) made use of the properties of the path independent integrals around the crack tip and obtained the mixed mode strain energy release for a kinked crack. They argued that the integrals involved in Irwin's approach to obtain the energy release rate cannot be applied directly to the present problem due to the discontinuity introduced by the deflected crack extension. It was shown that the solution at the tip in the limit, as the length of the kinked crack shrinks to zero, is not the same as the solution at the tip of the original crack before propagation. According to their approach the fracture angle predicted by the maximum energy release rate criterion is slightly higher than the result of the MTS criterion.

Minimum strain energy density criterion (SED)

Sih (1973a,b and 1974) developed another criterion for mixed mode fracture in brittle materials. Consider a volume element $dV=dxdydz$ in a linear elastic material. The strain energy dW^* stored in this element is

$$dW^* = [\tfrac{1}{2E}\left(\sigma_{xx}{}^2 + \sigma_{yy}{}^2 + \sigma_{zz}{}^2\right) - \tfrac{\nu}{E}\left(\sigma_{xx}\sigma_{yy} + \sigma_{yy}\sigma_{zz} + \sigma_{zz}\sigma_{xx}\right) + \tfrac{1}{2\mu}\left(\sigma_{xy}{}^2 + \sigma_{xz}{}^2 + \sigma_{yz}{}^2\right)]dV \tag{2-34}$$

where μ is the shear modulus. By substituting the singular stresses ahead of the crack in eq 2-34, the strain energy density function dW^*/dV can be written as

$$\frac{dW^*}{dV} = \frac{S(\theta)}{r} = \frac{1}{r}\left[a_{11}K_I{}^2 + 2a_{12}K_I\,K_{II} + a_{22}K_{II}{}^2\right] \tag{2-35}$$

where S is the strain energy density factor. The coefficients in eq 2-35 are

$$a_{11} = \frac{1}{16\mu}(\kappa - \cos\theta)(1+\cos\theta) \tag{2-36a}$$

$$a_{12} = \frac{1}{16\mu}(2\cos\theta - \kappa + 1)\sin\theta \tag{2-36b}$$

$$a_{22} = \frac{1}{16\mu}[(\kappa+1)(1-\cos\theta) + (1+\cos\theta)(3\cos\theta - 1)] \tag{2-36c}$$

where κ was defined earlier in eq 2-8. Sih's strain energy density (SED) criterion suggests that:

(i) Crack propagation is postulated to initiate in the direction of minimum strain energy density

$$\frac{dS}{d\theta}=0 \quad , \quad \frac{d^2S}{d^2\theta}>0 \quad \text{at } \theta_o \tag{2-37a}$$

(ii) Crack extension initiates when the strain energy density factor along this direction attains a critical value S_c

$$S(K_I, K_{II}, \theta_o)=S_c \tag{2-37b}$$

Based on the SED criterion the fracture initiation angle θ_o is obtained for the angled crack problem as

$$2(1-2\nu)\sin(\theta_o-2\beta)-2\sin[2(\theta_o-\beta)]-\sin 2\theta_o=0 \tag{2-37c}$$

Eq 2-37c indicates that, unlike the MTS and MERR criteria which are independent of material properties, the SED criterion depends on Poisson's ratio, ν.

Later, Sih (1974) proposed that the SED criterion is valid outside a circle of radius r_c, called the core region within which SED tends towards infinity and the material and the nature of deformation may be significantly different from those on the outside. However, he did not define quantitatively the values of r_c for different materials. In this regard, Theocaris and Andrianopoulos (1982a) introduced the von Mises elastic-plastic boundary, instead of a circle of constant radius, to define the core region. They showed that the direction of crack extension for the strain energy density criterion will be independent of Poisson's ratio if the SED is evaluated along this boundary. They also suggested that the minimum radius of the plastic zone can be employed as a measure of crack extension.

Sih and MacDonald (1974) suggested that the strain energy density factor is written as the sum of two components, one due to a change in volume S_v, the other due to distortion or change in shape S_d. They showed that along the direction of minimum SED the dilatational strain energy density, S_v, is greater than that of the distortional S_d. Inversely, along the direction of maximum SED, S_d is greater than S_v and maximum yielding occurs. This implies that based on the SED criterion the crack always propagates into the elastic zone and away from the plastic region, in the case of small scale yielding.

Theocaris and Andrianopoulos (1982b) proposed their own criterion, called the T-criterion, as: (i) The crack extension occurs along the direction of maximum dilatational strain energy density, $(S_v)^{max}$. (ii) Crack growth commences when the dilatational strain energy, S_v, attains a critical value of $(S_v)_{cr}$ at a point in the vicinity of crack tip. (iii) The $(S_v)^{max}$ is evaluated along the von Mises elastic-plastic boundary or, in other words, along the contour line of constant distortional strain energy density, S_d, around the crack tip. The direction of crack extension predicted by the T-criterion for the angled internal crack problem is considerably higher than those obtained through the MTS and SED criteria, particularly for β=0° loading where the predicted angle of fracture tends towards –95°.

Yehia (1985) showed that the function S_v along the elastic plastic boundary is independent of applied load, and concluded that the T-criterion cannot be used to predict the critical applied load. Later he proposed an individual criterion, called the Y-criterion (Yehia 1991), in which the minimum distortional strain energy density along a circle of radius r_c is employed to obtain the propagation direction and fracture load.

In another attempt, Koo and Choy (1991) suggested that the maximum tangential strain energy density can be used as a measure of crack growth. They showed that the results of this criterion is located between the results of the MTS and the maximum tangential strain criteria.

Remarks on mixed mode fracture criteria

A review of the mixed mode fracture criteria shows that most of these criteria complement each other for the mode I condition and deviate from each other for cracks under combined modes. Experimental studies on the internal angled crack specimen also shows that the results for the direction of initiation of crack growth are scattered in a band which is wider for small values of the crack angle β, see for example Liu (1974), Williams and Ewing (1972), Palaniswami and Knauss (1978), and Yokobori et al (1983). Since the results of almost all of the mixed mode fracture criteria lie in this band of experimental results, it is not possible to predict which criterion is more reliable.

Among the criteria described in this section, the maximum tensile stress (MTS), maximum energy release rate (MERR) and minimum strain energy density (SED)

criteria have received more attention in the literature. However, due to simplicity and ease of use the MTS criterion has been more popular for researchers. It was noted earlier that the SED criterion depends on Poisson's ratio. This is a disadvantage which can make the SED criterion less attractive compared with the material independent criteria.

For more complicated geometries where finite element analysis is used, the MTS and SED criteria are considered to be more appropriate. This is because the tangential stress and the strain energy density are often readily available in the commercial finite element codes. The maximum energy release rate criterion is suitable to the simple geometries where the stress intensity factors are known. Nevertheless, the fracture angle predicted by this method is also, in general, close to that predicted by the MTS criterion.

2-4-3. Brittle fracture in PMMA

Mixed mode brittle fracture has also been studied experimentally by numerous researchers. Most of these studies have been conducted on PMMA which is a cheap and easily machinable polymer known for its high brittleness. Later in Chapter 6, PMMA is used to investigate brittle fracture in shear loading. Therefore, a brief review of the mechanisms of yielding in polymers and previous mixed mode experiments on PMMA is presented in this section.

Mechanisms of yielding in polymers

Industrial applications of polymers have been increasing in recent decades. It has been found that polymers could yield by two mechanisms: shear yielding and normal yielding (crazing). These mechanisms are described briefly here. More details may be found in Kinloch and Young (1983), and Williams (1984).

From a continuum mechanics point of view, shear yielding is similar to plastic flow in metals. However, because the structure of polymers consists of long molecular chains the micro-mechanism of shear yielding in polymers is different from that in metals. Shear yielding in polymeric materials occurs when the local shear stress attains a critical value and molecules slide with respect to one another. If the zone of shear yielding in polymeric cracked specimens becomes extensive the specimen can fail by

ductile fracture. However this very much depends on parameters such as the loading rate and the working temperature.

Crazing is the other type of local deformation in polymers. It arises from an interpenetrating system of microvoids. Microvoiding, which takes place in regions of high hydrostatic tension, can initiate from imperfections in the microstructure such as surface flaws or dust particles. Crazes often form normal to the direction of maximum principal stress. In addition to a band of concentrated microvoids, the craze zone contains polymer fibrils which are orientated molecular chains acting as ligaments between each two neighbouring voids. The load can be transmitted across the craze faces through the fibrils.

Crazing is an important event in brittle fracture of polymers as it precedes crack growth. Crack growth in polymers takes place along the craze zone when the tensile stress sustained by fibrils exceeds a critical value. The fracture is unstable if the subsequent fibrils are also not capable of sustaining the stresses in front of the extending crack.

Since around the tip of a crack there are regions of high hydrostatic tension and high shear stress there is a competition between the two failure mechanisms. A high hydrostatic stress favours crazing, whereas shear yielding requires large deviatoric stresses. Variables like loading rate, working temperature and specimen thickness are also significant in determining the dominant failure mechanism.

Polymethylmethacrylate (PMMA) or perspex has been extensively used by workers for fracture studies (e.g. Williams and Ewing, 1972, and Davenport and Smith, 1993). That is mainly because cracked specimens made of PMMA exhibit a brittle fracture under normal testing conditions and at room temperature. In such conditions shear yielding is confined to a very small zone around the crack tip and crazing is the dominant mechanism for crack growth initiation in PMMA.

Although micromechanisms of crack growth in PMMA have been studied extensively in the literature for mode I, very few researchers have examined it for mixed mode. Maccagno and Knott (1989) suggest that craze formation occurs along the direction of maximum tensile strain and crack growth takes place when the tensile stress along this direction attains a critical value. However, Mahajan and Ravi-chandar (1989) propose

that the direction of maximum tensile stress is a favoured path for the craze formation and the subsequent crack growth.

Bhattacharjee and Knott (1995) made use of an asymmetric four point bend specimen and presented a description of the fracture surface features and path of crack growth in PMMA. For mode II dominated fracture they observed three distinct areas across the fracture surface: a mirror zone, a misty zone and a zone with hyperbolic markings. They also noticed that the number of hyperbolic markings was increased by making the mode II component larger.

Mixed mode experiments on PMMA

Various test configurations have been designed by researchers to investigate mixed mode fracture in PMMA. Some of these test specimens are reviewed here.

A large square plate containing an angled internal crack and subjected to either uni-axial or bi-axial loading was used by Erdogan and Sih (1963) , Williams and Ewing (1972) and Ueda *et al.* (1983). They achieved different mode mixities by changing the crack angle. However, the test specimen was unable to provide a pure mode II loading when the crack is in line with the loading direction. The same difficulty is seen in bending and tensile specimens containing an angled edge crack used by Ewing *et al.* (1976). In mode II only, Erdogan and Sih (1963) substituted the far field tensile load by two skew-symmetric point loads applied at holes located near the crack edges. A similar point loading was used by Maiti and Smith (1983) for other crack angles as well.

A circular tube of PMMA containing an angled crack and subjected to pure torsion was employed by Ewing and Williams (1974a) to study mixed mode brittle fracture. Royer (1986 and 1988) designed a Y shape mixed mode specimen containing two edge cracks. By changing the angle of loading in two top branches of the specimen Royer achieved different combinations of modes I and II. A disadvantage in using specimens involving two crack tips, such as the internally cracked specimen or Y shape specimen, is that any slight discrepancy between the properties of the two crack tips may prevent simultaneous crack propagation at both tips of the crack. This can introduce inaccuracy into the test conditions.

Richard (1985), Banks-Sills and Bortman (1986), and Mahajan and Ravi-chandar (1989) made use of rather complicated configurations in which a compact tension-shear specimen was located inside a fixture. Mixed mode loading could be achieved by applying the load through a number of holes drilled in the fixture at different angles. Davenport and Smith (1993 and 1995) replaced the compact tension-shear specimen by single edge notched and single edge cracked specimens. They showed that mixed mode fracture toughness of PMMA in the notched specimens is considerably higher than in the mode I cracked specimens. Maccagno and Knott (1989) and Bhattacharjee and Knott (1995) investigated mixed mode brittle fracture in PMMA using an asymmetric four point bend specimen. They could provide different combinations of modes I and II by changing the positions of supports and loading points on the specimen.

Aside from Bhattacharjee and Knott (1995), all of the workers mentioned report that a linear elastic fracture criterion, such as the maximum tensile stress criterion, is able to predict satisfactorily the direction and the onset of crack growth in PMMA. However, the scatter of the experimental results obtained from different test specimens is considerable, particularly for mode II dominated fracture. Bhattacharjee and Knott (1995) do not present a clear reason for their results not agreeing with linear elastic MTS criterion. However, they ruled out the possible effect of the crack tip plastic deformation as a reason for this discrepancy. This is because even using the small scale yielding assumption, with different plastic hardening coefficients, they were not able to predict the experimental results. However, they suggest that the fracture toughness in PMMA is increased if the tip of the initial crack is not accurately uniform. This is because a non-uniform crack tip might give rise to local crack extensions with mode mixities different from that associated with global loading.

2-4-4. Statistical modelling of brittle fracture

In engineering analysis of a brittle cracked body it is common to assume a single value for fracture toughness. However, the results of fracture tests conducted on accurately manufactured specimens cut in the same direction from the same batch of a material often show a considerable scatter in fracture toughness. From a microscopic point of view it is well understood that the onset of crack growth in a brittle material depends largely on the distribution of inhomogenities such as voids or second phase particles around the crack tip. The scatter in the results of fracture tests could therefore

be attributed mainly to the random distribution of the inhomogenities in material. This suggests that a reliable figure for fracture toughness is obtained only if a large number of tests is carried out. Meanwhile the amount of testing can be reduced considerably provided an appropriate probabilistic analysis is performed to predict the scatter in fracture toughness data.

Based on a weakest link phenomenon, Weibull (1951) suggested a probability distribution model which has been used widely to describe scatter in fracture toughness for brittle materials. The weakest link phenomenon for brittle fracture assumes that the probability of failure equals the probability of the crack tip stress and strain fields sampling at least one critical fracture-triggering particle. A two parameter Weibull model for fracture data (Wallin, 1984) is often shown as

$$P_f = 1 - \exp\left[-\left(\frac{K_I}{K_o}\right)^m\right] \tag{2-38}$$

where P_f is the cumulative probability of fracture, m is a constant describing the magnitude of scatter, K_I is the applied stress intensity factor and K_o is a normalisation parameter corresponding to fracture toughness at 62.3% fracture probability.

However one major problem with eq (2-38) is that K_I vanishes for P_f=0, i.e. a two parameter Weibull function always predicts the minimum toughness in the distribution model, to be zero. Wallin (1984) suggested a three parameter model for the distribution of fracture data as

$$P_f = 1 - \exp\left[-\left(\frac{K_I - K_{min}}{K_o - K_{min}}\right)^m\right] \tag{2-39}$$

where K_{min} is a lower fracture toughness below which brittle fracture is unlikely. He also proposed that the theoretical value for m is constant and equal to four. Wallin (1984) used the experimental results for different steels and showed that eq (2-39) with m=4 can be employed as a reliable model to predict the distribution of fracture toughness data.

2-5. ELASTIC-PLASTIC FRACTURE MECHANICS (EPFM)

Elastic-plastic fracture mechanics (EPFM) deals with cracked specimens where a significant volume around the crack tip undergoes plastic deformation prior to initiation of fracture. For such cases, which very often happens for metallic alloys, the failure mechanism can be either the brittle fracture or the ductile failure. Brittle fracture may be preceded with or without some stages of slow crack growth. For ductile materials, final failure often occurs following numerous stages of slow crack growth. For materials having very high fracture toughness, failure can be due to plastic collapse in the uncracked ligament of the specimen with negligible amount of crack extension.

A review of the main criteria for elastic plastic crack growth is presented in Section 2-5-1 for pure mode I and in Section 2-5-2 for mixed mode loading.

2-5-1. EPFM - Mode I

Experimental studies by Wells (1961) showed that in tough materials, the crack faces often move apart and the crack tip is blunted considerably before crack extension. The maximum value of crack tip blunting was directly related to the material fracture toughness. He proposed that the failure of cracked geometries in the presence of moderate plasticity can be described by the crack tip opening displacement (CTOD) denoted by δ.

There is a direct relation between the CTOD and the J-integral. Either the J-integral or the CTOD can be used as characterising parameters in elastic-plastic fracture. For specimens failing by the mechanism of brittle fracture, the unstable fracture takes place when J (or δ) attains a critical value J_c (or δ_c) which is a material property. Because the stress field inside the plastic zone near the crack tip is described by J, the critical value J_c corresponds to the critical stress needed for initiation of crack extension in the stress controlled mechanism of brittle fracture.

In the case of ductile crack growth, J (or δ) first reaches a critical initiation value J_i (or δ_i) for which crack growth is initiated. Following a few steps of stable crack growth, the final failure occurs when J reaches J_c beyond which unstable fracture takes place. Since J_c is often significantly greater than J_i, the resistance of material to

crack growth increases after initial crack growth. This represents an important safety margin between initiation and instability of crack growth.

Incremental crack extension in ductile materials makes the analytical modelling for predicting the entire process of failure, from initiation to rupture, much more complicated than for unstable brittle fracture. The minimum strain energy density (SED) criterion, initially suggested for linear elastic mixed mode fracture, was extended to predict mode I crack growth in ductile materials. The modified SED criterion has been described by Sih and Kiefer (1979) for small scale yielding and by Sih and Madenci (1983a,b) for gross yielding problems.

Substantial work has been carried out to simulate the stable crack growth in ductile materials using a so called local approach. In this method finite element analysis is employed to simulate the extension of a damage zone in front of the crack tip resulting from the growth and coalescence of microvoids, see for example Roos et al. (1991) and Bilby et al. (1992).The simulation often requires user defined subroutines in the FE code to implement a damage model such as those referred to in Section 2-3.

2-5-2. EPFM - Mixed mode

Brittle fracture

Mixed mode specimens can fail by a mechanism of brittle fracture even in the presence of significant plasticity around the crack tip. This has been shown for example through experiments carried out by Maccagno and Knott (1991) for several steel alloys. The direction and the onset of crack growth for such cases can be predicted by using the mixed mode criteria described in section 5-4-2. However, some modifications are needed to account for the effect of crack tip plasticity.

Wang (1985) and Melin (1987) suggested modifications to the maximum energy release rate (MERR) criterion involving a small plastic region around the crack tip for mixed mode loading. Chow and Jilin (1985 and 1986) employed the maximum dilatational strain energy density criterion to predict the direction and onset of fracture in an elastic-plastic crack problem. They showed that for mode I their results are in agreement with those predicted by Sih and Madenci (1983b) using a modified minimum strain energy density (SED) criterion.

The maximum tangential stress (MTS) criterion can also be used to solve the elastic-plastic crack problem in mixed mode loading. The near field mixity parameter M^p is determined and the tangential stress is calculated using the elastic-plastic stresses given by Shih (1974), and described in Section 2-2-3. Shih showed that the crack tip plasticity has little effect on changing the direction of fracture initiation θ_o. For small scale yielding the near field elastic-plastic stresses can be related to the far field elastic stresses. In this case the onset of crack growth is determined from

$$\left(\frac{K_I}{K_{Ic}}\right)^2+\left(\frac{K_{II}}{K_{Ic}}\right)^2=\left(\frac{\tilde{\sigma}_{\theta\theta}\{n,0,1\}}{\tilde{\sigma}_{\theta\theta}\{n,\theta_o,M^p\}}\right)^{n+1}\left(\frac{I_n\{M^p\}}{I_n\{1\}}\right) \tag{2-40}$$

where the related parameters were described following eqs 2-18 and 2-19. Maccagno and Knott (1985 and 1991) showed for several steel alloys that the fracture load predicted using the elastic-plastic MTS criterion are in better agreement with the experimental results than those predicted by the linear elastic MTS criterion.

Budden (1987) made use of slip line field theory and extended the application of the elastic-plastic MTS criterion to consider the effect of the large geometry changes near the crack tip in mixed mode loading. He suggested that the direction of fracture initiation θ_o in mode II is about -81.8° which is almost the same as the angle θ_o predicted by Shih (1974) for $n=\infty$, without considering crack tip blunting effects.

Ductile failure

Almost all the finite element studies for modelling the mechanism of void growth and coalescence (the local approach) are confined to pure mode I where the path of crack extension is along the plane of the initial crack. In mixed mode loading, the damage zone or the crack growth trajectory is often subject to continuous change as the load increases. The simulation of stable crack growth in ductile materials for mixed mode loading is therefore much more complicated than that for mode I.

A transition between the micromechanisms of crack growth has been noticed by several researchers studying experimentally mixed mode failure in ductile materials. For example, Tohgo and Ishii (1992), Hallback and Nilsson (1994) and Kamat and Hirth (1996) have reported for several aluminium alloys that in mode I dominated loading their specimens failed by the mechanism of void growth whereas for mode II

dominated loading, the specimens failed by the mechanism of shear localisation. A brittle to ductile transition has also been reported by Swankie and Smith (1998) and Smith et al (1998a and 1998b) for mixed mode fracture in several steel alloys. The transition between the mechanisms of failure emphasises that in analysing crack growth for different mode mixities, different criteria need to be employed. The identification of the failure mechanisms and the determination of the transition limit which are essential in selecting appropriate crack growth criteria for each mode mixity require extensive experimental studies.

Because of difficulties mentioned above, almost all of the analytical studies for mixed mode loading in ductile materials are confined to investigation of the crack tip fields prior to any crack extension (e.g. Aoki et al, 1987, Budden and Jones, 1991, Chow and Wang, 1991, Ghoshal and Narasimham, 1994 and 1996, and Hallback, 1997).

In practice, an approximate method can be used to determine the load corresponding to the ductile failure in specimens subjected to mode II dominated loading. This method predicts the collapse load at which the effective stress in the uncracked ligament of the specimen reaches the ultimate strength of the material without considering any crack growth. This can be undertaken either for a work hardening material using FE analysis (Ayatollahi, 1996) or for a perfect plastic material (Smith et al, 1998a and 1998b) using a limit load analysis suggested by Miller (1987).

2-6. METHODS OF CALCULATING THE CRACK TIP PARAMETERS

In this section some methods for determining the stress intensity factors (SIF) and the T-stress are presented for pure mode I and mixed mode loading. For the stress intensity factors, only a brief description of the major methods which make use of the finite element analysis is outlined. The review of the available methods for calculating T-stress is presented in more detail.

2-6-1. Stress intensity factors, K_I and K_{II}

Numerous researchers have attempted to develop methods for determining the stress intensity factors for different cracked specimens. A collection of the analytical solutions can be found in Tada et al (1985). Finite element analysis can also be

employed to calculate SIFs, particularly for more complicated cracked geometries where analytical solutions are not available.

Parks (1977) suggested a virtual crack extension method which was modified later by Li et al (1985) to calculate the *J*-integral using finite element analysis. The method has been implemented in most of the commercial FE codes to enable the user to determine the *J*-integral for any cracked geometry. For pure mode I (or II), the stress intensity factor K_I (or K_{II}) can be determined directly from eq 2-15a in terms of the *J*-integral.

The preceding method is not appropriate for mixed mode loading because J is a function of both K_I and K_{II}. In this case the crack tip stresses and strains can be used to find SIFs. For example, very near the crack tip where the effects of higher order terms in eq 2-3, 2-4, 2-6 and 2-7 are negligible, K_I and K_{II} can be determined from

$$K_I = \lim_{r\to 0} \sigma_{yy}\sqrt{2\pi r} \quad , \quad K_{II} = \lim_{r\to 0} \sigma_{xy}\sqrt{2\pi r} \quad : \quad \theta = 0 \tag{2-41}$$

or

$$K_I = \lim_{r\to 0} u_y \sqrt{\frac{2\pi\mu^2}{r}} \quad , \quad K_{II} = \lim_{r\to 0} u_x \sqrt{\frac{2\pi\mu^2}{r}} \quad : \quad \theta = \pi \text{ (crack face)} \tag{2-42}$$

The accuracy of SIFs calculated from eqs 2-41 and 2-42 very much depends on the accuracy of the stresses and strains obtained from the finite element analysis.

One of the methods for improving the accuracy of the near crack tip stresses is to use appropriate elements which are able to model the singularity of the stresses and strains. Henshel and Shaw (1975) and Barsoum (1976) independently suggested a simple method to provide the necessary singularity in quadratic isoparametric elements. In this method the $1/\sqrt{r}$ singularity is achieved when the rings of mid-side nodes in the elements surrounding the crack tip are shifted to the quarter points. However, this arrangement is appropriate only for linear elastic problems where the $1/\sqrt{r}$ singularity prevails.

The *J*-integral can also be used to determine the stress intensity factors for mixed mode loading. In this method, the ratio R_k between K_I and K_{II} is calculated from the displacements along the upper and lower crack faces as

$$R_K = \frac{K_{II}}{K_I} = \frac{u_x(r_o^+) - u_x(r_o^-)}{u_y(r_o^+) - u_y(r_o^-)} \tag{2-43}$$

where r_o is a small radius from the crack tip and the signs + and – corresponds to the upper and lower faces of the crack respectively. From eq 2-15b and 2-43, the stress intensity factors are determined as

$$K_I = \sqrt{\frac{E'J}{1+R_K^2}} \quad , \quad K_{II} = R_K K_I \tag{2-44}$$

2-6-2. *T*-stress

A number of methods for obtaining T for a variety of loading conditions and geometries have been developed over the last 25 years. Some of the major methods are described below.

Larsson and Carlsson (1973) suggested that in mode I, T can be determined along the crack flanks using two elastic FE analyses, one for the actual cracked body and the other for a boundary layer model. The stress T was the average difference between σ_{xx} along the crack face in the two analyses. They did not extend their mode I method to the general mixed mode case.

A variational technique based on the theorem of minimum potential energy was used by Leevers and Radon (1983) to calculate the vector of coefficients {c} for the eigen-series expansion of the mode I stresses. By minimising the potential energy with respect to the coefficients they derived a set of equilibrium equations which could be solved to obtain {c} for a given geometry. The stress intensity factor K_I and T were taken from the first and the second terms in the vector {c}. A similar approach was employed by Ewing et al. (1976) for mixed mode I and II. In their technique {c} included the coefficients in both symmetric and antisymmetric parts of Williams' solution to account for the two modes of loading. Knesl (1995) also attempted to determine T by calculating these coefficients in mode I. He used special types of element called crack-tip hybrid elements developed through a Hellinger-Reissner principle, and could determine T by calculating the first few coefficients of {c}. All these methods require complex numerical calculations not available in commercial finite element codes.

Using the properties of path independent integrals, Cardew et al. (1984), and later Kfouri (1986) suggested a method to obtain T in mode I based on an unpublished theorem proposed by Eshelby. In this method the path independent J integral is determined for the given specimen from two elastic FE analyses. In the first analysis the specimen is subjected to the actual loading conditions. These loading conditions are added in the second analysis to an auxiliary field of stress corresponding to a semi-infinite crack in an infinite plate subjected to a point force at the crack tip in the direction of the crack line. Cardew et al. (1984), and Kfouri (1986) proposed a formula to relate T to these two values of J integral and calculated T for the given specimen. Hallback and Jonsson (1996) used a similar method but for mixed mode conditions to obtain T for a mixed mode test specimen. Path independent integrals were also employed by Olsen (1994) and Sladek et al. (1997) to compute K_I, K_{II} and T for mixed mode loading using the boundary element technique. These methods all require multiple finite element or boundary element analyses.

To determine T for mixed modes I and II, Seed and Nowell (1994) represented a crack as a continuous distribution of edge dislocations. They utilised the distributed dislocation method to derive the singular equations which were solved numerically to find stress intensity factors and T. They presented results for an inclined edge crack in a semi-infinite plate subjected to a uniform tensile load.

Sham (1991) presented values of T for a single edge notched (SEN) specimen subject to tension and pure bending, and also for a three point bend specimen. He used a second order weight function, determined through FE analysis, in conjunction with a reciprocal work integral to calculate T in mode I. Fett (1997) proposed a closed form approximation for T for a mode I rectangular cracked specimen under tension and bending. He suggested an appropriate Green's function and used the boundary collocation method to calculate the second term in the Williams' expansion.

2-7. CONSTRAINT EFFECTS IN FRACTURE MECHANICS

Experimental studies show that the fracture toughness obtained from different standard cracked specimens made of similar material are not the same. This indicates that the fracture toughness or the critical value of J for fracture initiation, J_{crit} is not merely a material property but depends also on the geometry and loading

configurations. The geometry dependency of fracture toughness can be attributed to the effect of the crack tip constraint.

It is well known that the fracture toughness is higher for cracked specimens which at fracture load exhibit a larger plastic zone around the crack tip. This is because more energy is consumed for plastic deformation and less energy remains for breaking the atomic bonds ahead of the crack tip. In contrast, in the specimens where the plastic zone is highly constrained, more energy is available for brittle fracture and hence the fracture toughness is low. For example, the fracture toughness for plane strain specimens is lower than for plane stress ones. The effect of stress triaxiality in plane strain constrains the extent of the plastic zone. In addition to the specimen thickness, there are other parameters such as the crack length or the type of loading which influence the crack tip constraint.

To obtain a rather unique result for K_{IC}, which is considered to be geometry independent, some restrictions for length parameters are recommended by fracture toughness testing procedures (e.g. ASTM, E399-90 or British Standard, BS-7448, 1991) in different fracture test specimens. For example, for the three-point bend or compact tension specimens, it is required that

$$t\ ,\ (W-a)\geq 2.5\left(\frac{K_{IC}}{\sigma_o}\right)^2 \tag{2-45}$$

where t and W are the specimen thickness and width and a is the crack depth. The size limits differ for different specimens and provide conditions necessary for J-dominance, that is conditions where the crack tip fields are described only by J. Section 2-7 reviews the necessary conditions for J-dominance, the parameters influencing the crack tip constraint and the methods available for quantifying the constraint.

2-7-1. J-dominance

Based on the classical theories of fracture mechanics, the stresses and strains around the tip of a mode I crack can be characterised by a single parameter such as K_I or J. This is true only when certain size restrictions are applied for each crack specimen (Shih and German, 1981). However, the geometry dependency of the fracture

toughness suggests that at least a second parameter is required to predict the critical conditions for crack growth in different specimens.

It is common to use a so-called boundary layer model (Rice and Tracey, 1973) to study the effect of the crack tip parameters on the stresses inside the plastic zone. In the boundary layer model (BLM) a crack is considered in a circular region so that the crack tip is placed in the centre of the region, as shown in Fig 2-4. The elastic stresses or displacements corresponding to the first term of the Williams' series expansions are applied to the boundary of the region. Material properties are considered to be elastic-plastic. To ensure the conditions necessary for small scale yielding, the magnitudes of the boundary conditions should be limited to a level at which the maximum radius of plastic zone is very small compared with the radius of the circular region. With this arrangement the stresses inside the plastic zone are in good agreement with the stresses given by the HRR solution.

Larsson and Carlsson (1973) modified this model by adding the effect of T-stress to the boundary conditions. The mode I displacements u_x and u_y along the boundary of a plane strain circle of radius R can be written for the modified boundary layer model (MBLM) as

$$u_x(R,\theta) = K_I \frac{1-\nu}{E}\sqrt{\frac{R}{2\pi}}\cos\left(\frac{\theta}{2}\right)(3-4\nu-\cos\theta)+T\frac{1-\nu^2}{E}R\cos\theta \qquad (2\text{-}46a)$$

$$u_y(R,\theta) = K_I \frac{1-\nu}{E}\sqrt{\frac{R}{2\pi}}\sin\left(\frac{\theta}{2}\right)(3-4\nu-\cos\theta)-T\frac{\nu(1+\nu)}{E}R\sin\theta \qquad (2\text{-}46b)$$

Elastic-plastic finite element analysis of the modified boundary layer model by Larsson and Carlsson (1973) showed that positive or negative values of T significantly influence the shape and size of the plastic zone around the crack tip. Rice (1974) showed that the effect of T on the CTOD or J is negligible compared with its effect on the plastic zone.

Bilby et al. (1986) took into account the effect of large deformations around the crack tip and performed elastic-plastic finite element analyses for several common mode I cracked specimens. They compared the results of their analyses with the results of a modified boundary layer model having similar K_I and T terms on the boundary. Bilby

et al. (1986) showed that the crack tip fields can be described by a single parameter such as J (or CTOD) only for specimens where the value of $T\sqrt{\pi a}/K_I$ is high.

Further studies by Betegon and Hancock (1991), Al-Ani and Hancock (1991) and Du and Hancock (1991) related the single parameter characterisation of the crack tip fields to the sign of the T-stress. They indicated that for small scale yielding J-dominance is maintained for geometries having zero or positive T. For geometries with negative T, two parameters, J and T, are needed to describe the crack tip fields. The results of the analysis carried out by Hancock and co-workers showed that the crack tip constraint is higher for bending specimens and for specimens having deep cracks. In contrast, the constraint is less for tensile specimens and for specimens containing short cracks.

2-7-2. Methods of quantifying the crack tip constraint

As noted earlier, the fracture toughness depends considerably on the crack tip constraint. The effects of constraint in mode I brittle fracture can be studied by comparing the tangential stress $\sigma_{\theta\theta}$ directly ahead of the crack tip for specimens having different geometry and loading configurations. Three major approaches for quantifying the crack tip constraint are: J-T, J-Q, and J-A_2. These approaches are described briefly here.

J-T approach

Betegon and Hancock (1991) made use of a modified boundary layer model and studied the mode I stresses inside the plastic zone. Different values of T/σ_o were considered in the boundary conditions. An elastic-plastic finite element analysis with small deformations was performed. The tangential stress $\sigma_{\theta\theta}$ along the crack line was normalised by the yield stress σ_o and the distance from the crack tip was normalised by J/σ_o . For small scale yielding with T=0, the tangential stress was close to but lower than that of the HRR solution.

Betegon and Hancock showed that by changing the value of T/σ_o on the boundary of model, the small scale yielding (with T=0) results for $\sigma_{\theta\theta}/\sigma_o$ are shifted up for positive values of T and down for negative values of T. The effects of positive and negative T on the tangential stress ahead of the crack tip are shown schematically in Fig 2-5. These curves are almost parallel, at least for the range of $2 \leq (r\sigma_o/J) \leq 5$. The

effect of negative T on reducing the tangential stress was much more than the effect of positive T on increasing the tangential stress.

The normalised tangential stress can be written as a polynomial in terms of the tangential stress corresponding to the small scale yielding solution with T=0 and the shift in the tangential stress due to the effect of T. This polynomial was shown by Betegon and Hancock (1991) for materials with a hardening coefficient n equal to 13 and ∞ as

$$\left(\frac{\sigma_{\theta\theta}}{\sigma_o}\right)_{(r,T)} = \left(\frac{\sigma_{\theta\theta}}{\sigma_o}\right)_{(r,T=0)} + 0.64\left(\frac{T}{\sigma_o}\right) - 0.4\left(\frac{T}{\sigma_o}\right)^2 \qquad n=13\,,\ \frac{T}{\sigma_o}\le 0 \qquad \text{(2-47a)}$$

$$\left(\frac{\sigma_{\theta\theta}}{\sigma_o}\right)_{(r,T)} = \left(\frac{\sigma_{\theta\theta}}{\sigma_o}\right)_{(r,T=0)} + 0.6\left(\frac{T}{\sigma_o}\right) - 0.75\left(\frac{T}{\sigma_o}\right)^2 \qquad n=\infty\,,\ \frac{T}{\sigma_o}\le 0 \qquad \text{(2-47b)}$$

Similar equations may be provided for other values of hardening coefficient. The effect of constraint in brittle fracture can be quantified using the J-T approach. The elastic T-stress is determined for the given geometry and its effect on the tangential stress is determined using equations similar to 2-47.

J-Q approach

O'Dowd and Shih (1991, 1992 and 1994) suggested a dimensionless parameter Q to determine the level of constraint around the tip of a mode I crack. They performed an elastic-plastic finite element analysis accounting for large strains to study the effect of T on the tangential stress $\sigma_{\theta\theta}$ along the crack line. For small to moderate scale yielding they used a modified boundary layer model with different values of T/σ_o in the boundary conditions and defined the constraint parameter Q as

$$Q = \frac{\sigma_{\theta\theta} - (\sigma_{\theta\theta})_{REF}}{\sigma_o} \quad \text{along } \theta = 0, \text{ at } 1 \le \frac{r\sigma_o}{J} \le 5 \qquad \text{(2-48)}$$

where $(\sigma_{\theta\theta})_{REF}$ can be either the tangential stress corresponding to the HRR solution $(\sigma_{\theta\theta})_{HRR}$ or the tangential stress determined from the small scale yielding solution $(\sigma_{\theta\theta})_{SSY}$ with T=0.

O'Dowd and Shih used eq 2-48 for different values of hardening coefficient n and suggested a number of curves to describe relations between Q and T/σ_o for mode I loading (see Fig 2-6). They could show the results as a polynomial

$$Q\left(n,\frac{T}{\sigma_o}\right)=a_1(n)\left(\frac{T}{\sigma_o}\right)+a_2(n)\left(\frac{T}{\sigma_o}\right)^2+a_3(n)\left(\frac{T}{\sigma_o}\right)^3 \qquad (2\text{-}49)$$

where a_1 to a_3 are functions of n. Ainsworth and O'Dowd (1995) simplified eq 2-49 for small scale yielding as

$$Q=\frac{T}{\sigma_o} \quad \text{if} \quad \frac{T}{\sigma_o}<0 \qquad (2\text{-}50a)$$

$$Q=\frac{T}{2\sigma_o} \quad \text{if} \quad \frac{T}{\sigma_o}>0 \qquad (2\text{-}50b)$$

Eqs 2-49 and 2-50 can be used for small to moderate scale yielding (contained yielding). For large scale yielding the crack tip constraint should be obtained in the actual specimen directly from eq 2-48. This has been done by O'Dowd and Shih (1992) for a number of standard crack specimens by using the J-Q approach.

O'Dowd and Shih (1991 and 1992) also compared the stresses obtained from a finite strain analysis and those of a small strain analysis and showed that the effect of crack tip blunting on the stresses ahead of the crack tip is significant only for $(r\sigma_o/J) \leq 1$. Therefore, a small strain analysis is sufficient to determine the constraint provided the parameter Q is calculated at a distance $(r\sigma_o/J)$ larger than 1. It is noted that for the range of $2\leq(r\sigma_o/J)\leq 5$, the value of Q is almost independent of the distance from the crack tip. However, Q is often determined at $(r\sigma_o/J)=2$. Similar to the results of the J–T approach, negative Q corresponds to specimens having negative T-stress, low crack tip constraint and high fracture toughness, and vice versa for positive Q.

J-A_2 approach

Like the Williams' solution for the elastic stresses, the stresses inside the plastic zone around the crack tip can be shown as a series expansion. The leading term in this series solution is singular and represents the HRR solution. The third approach for quantifying the constraint is to determine the higher order terms of the elastic-plastic

stresses. In this approach the conditions for J-dominance is determined by comparing the magnitude of the higher order stresses with that of the HRR solution.

Li and Wang (1986) made use of an appropriate stress function and obtained a two-term expansion for the stresses near the tip of a mode I crack for the state of plane strain. In a similar attempt, Sharma and Aravas (1991) formulated the problem in terms of stresses and displacements and proposed a method to obtain the higher order terms of the elastic-plastic series expansions for stresses, strains and displacements. They presented the results as a two-term series for both plane stress and plane strain. Xia et al (1993) derived the first four terms of the series expansions for the mode I stresses and the hardening coefficient n=3, 5, 7 and 10. They showed that some of the coefficients of the series solution depend on the others.

The series expansion for elastic-plastic stresses were also obtained by Yang et al (1993a,b) for both mode I and mode II. They indicated that for a high hardening behaviour ($n \leq 3$) the first four terms of the series solution can be described by two parameters J and A_2 where A_2 represents the amplitude of the contribution of the higher order terms. For low hardening behaviour ($n \geq 3$), J and A_2 characterise the first three terms of the series solution. The results presented by Yang et al suggest that for low hardening materials ($n \geq 3$), A_2 can be considered as a constant term which depends on the geometry and loading conditions in the specimen.

A_2 can be employed as a parameter to quantify the crack tip constraint and its effect on the brittle fracture toughness. This has been described by Chao and Ji (1995) for different crack specimens. Chao (1993) made use of the J-A_2 approach and showed that for the state of plane stress, A_2 is negligible and a single parameter such as J can describe the crack tip fields.

A critical review of three approaches

Among the three approaches mentioned in this section for quantifying the crack tip constraint, the J-T approach is the most convenient one. In this approach, the elastic T-stress is employed to predict the level of constraint. The T-stress is known for most of the standard cracked specimens with different ratios of the crack length to the specimen width. For more complicated geometries, T can be determined using a single elastic finite element analysis, as described in Chapter 4. However, the J-T approach is confined to the crack problems involving contained yielding (i.e. small to

moderate scale yielding). This is because T as an elastic term of stress loses its relevance under full plasticity. The limitations of the J-T approach have been studied by Wang (1993) and Wang and Park (1995) for several common cracked specimens.

The J-Q approach can be used for both contained yielding and full plasticity. O'Dowd and Shih (1993) and O'Dowd (1995) suggest that the relation between Q and T is independent of geometry only for contained yielding, but in fully yielded conditions the constraint parameter Q depends on the geometry and the type of loading. In this case an elastic-plastic analysis is required to find out the constraint parameter Q. In the presence of excessive crack tip blunting, the J-Q approach can also fail to determine crack tip constraint.

The J-A_2 approach provides analytical solutions to find out the effect of higher order terms of the elastic-plastic stresses. Therefore it can be considered to be more accurate than the other approaches. For example, the analytical results obtained from the J-A_2 approach show that the J-Q approach is not appropriate for materials with high hardening behaviour ($n \leq 3$) because the second term of stress is not constant and is highly dependent on the distance from the crack tip. However, the J-A_2 approach requires complicated mathematical calculations to determine the necessary parameters and functions for the three-term series solution. This makes the J-A_2 approach inappropriate for quantifying the crack tip constraint in specimens other than the conventional simple crack specimens.

2-7-3. Constraint effects in mixed mode fracture

Very little research has been carried out to study the effect of constraint in mode II and mixed mode (I/II) loading. Yang et al (1993a and b) and Chao and Yang (1996) extended the application of the J-A_2 approach to the mode II crack problems. They employed the Airy stress function and assumed antisymmetric boundary conditions to find out the higher order terms of the mode II stresses inside the plastic zone near the crack tip. They showed that for plane stress and plane strain, the higher order stresses are negligible compared with the singular term (the HRR solution for mode II). This implies that a single parameter is sufficient to describe the crack tip stresses and strains for an antisymmetric (mode II) field of deformation.

Du et al. (1991) used a modified boundary layer model to extend the application of the J-T approach to mixed mode loading. The tractions or displacements on the boundary of their model consisted of the singular terms corresponding to both mode I and mode II, and the T-stress. They studied the effect of T on the near tip stresses for different mode mixities and proposed that J-dominance in mixed mode loading is maintained for specimens having zero or positive T. In contrast, the crack tip stresses in specimens with negative T fall below the singular stresses given by Shih (1974). However, because the finite geometry specimens they studied were mode I dominated ($M^e \geq 0.82$), they could not present any results to show the effect of constraint in mode II dominated specimens.

2-7-4. Constraint effects in mode I ductile fracture

It was noted in section 2-3 that mode I ductile crack growth in metallic alloys often takes place by the micromechanism of void growth and coalescence. The mathematical models describing this mechanism show that void growth depends directly on the stress triaxiality factor that is the ratio of the mean (or hydrostatic) stress σ_m over the effective stress σ_{eff}.

O'Dowd and Shih (1991) and O'Dowd (1995) made use of a modified boundary layer model (MBLM) to study the effect of T-stress on different components of the crack tip stresses inside the plastic zone. Their study was confined to mode I and plane strain conditions. They showed that the direct stresses σ_{rr}, $\sigma_{\theta\theta}$ and σ_{zz} depend significantly on the value of T in the boundary conditions on the MBLM whereas the shear stresses do not. For a given value of T, the change in direct stress was nearly the same. Therefore, the constraint parameter Q can be determined using any component of the direct stress. This also indicates that in front of a mode I crack, the effect of crack tip constraint on the deviatoric stress is much less than its effect on the mean stress.

Using a MBLM, O'Dowd and Shih (1992) and Henry and Luxmoore (1997) investigated the effect of T on the triaxiality factor for contained yielding and also for fully yielded conditions in several mode I crack specimens. The results of their study show that the triaxiality factor in mode I specimens having a positive Q is slightly higher than the triaxiality factor obtained from the HRR solution. However, for specimens having negative Q, the triaxiality factor is significantly lower than that of

the HRR solution. The effect of Q on the triaxiality factor σ_m / σ_{eff}, suggests that Q can also be used as a constraint parameter for initiation toughness in ductile fracture.

Wu and Mai (1995) carried out experimental investigations on several mode I specimens and showed that the initiation fracture toughness in ductile materials is enhanced for specimens having negative Q. They found similar results from finite element analysis by studying the crack tip parameters for different specimens.

Experimental studies by Hancock et al. (1993) indicated that T can be used to characterise the resistance curve in ductile materials. They showed that the resistance curve for specimens having negative T is significantly higher than for specimens having zero or positive T. Burstow and Howard (1996) employed the Rousselier damage model (Rousselier et al, 1989) and simulated the initiation and growth of ductile tearing by finite element analysis. They showed that the effect of the crack tip constraint on the slope of the resistance curve is significantly more than its effect on the value of initiation fracture toughness.

CHAPTER THREE

HIGHER ORDER TERMS OF STRESSES IN AN INTERNAL CRACK PROBLEM

3-1. INTRODUCTION

It is often assumed that stresses near the tip of a crack in a linear elastic material can be described based entirely on the singular term of the Williams series expansion for the crack tip stresses. Very little research has been carried out to quantify the error resulting from ignoring the higher order terms of the series expansion. This can be due to difficulties in determining the coefficients of higher order terms for a given geometry.

In this Chapter a binomial expansion is employed to determine the first few terms of the Williams series solution for a large centrally cracked plate subjected to a uniform tensile load. It is shown that adding the higher order terms to the singular term improves the accuracy of the results for direct stresses near the crack tip along the crack line. The effect of higher order terms on the extent of the plastic zone ahead of the crack tip is also studied. Results are shown for both plane stress and plane strain conditions. The plastic zone size is determined using both the Tresca and the von Mises yield criteria. The effect of load biaxiality on the size of plastic zone is also studied.

3-2. BINOMIAL EXPANSION OF THE EXACT STRESSES

Consider an infinite plate containing an elliptical hole of major axis $2a_o$ and minor axis $2b_o$. The plate is subjected to a uniform far field tensile stress σ_{YY} parallel to the

minor axis of the ellipse (see Fig 3-1a). The stresses along the major axis have been given by Muskhelishvili (1963) as

$$\sigma_{xx} = \xi_1 - \xi_2 \qquad \sigma_{yy} = \xi_1 + \xi_2 \qquad \sigma_{xy} = 0 \tag{3-1}$$

where

$$\xi_1 = \frac{\sigma_{YY}}{2}\left[1 + \frac{2(1+\alpha)}{\beta^2 - \alpha}\right] \qquad \xi_2 = \frac{\sigma_{YY}}{2}\left[1 + \frac{\alpha^2 - 1}{\beta^2 - \alpha}\left(1 + \frac{\alpha - 1}{\beta^2 - \alpha}\cdot\frac{3\beta^2 - \alpha}{\beta^2 - \alpha}\right)\right]$$

and

$$\alpha = \frac{a_o - b_o}{a_o + b_o} \qquad \beta = \frac{x}{a_o + b_o} + \left[\left(\frac{x}{a_o + b_o}\right)^2 - \alpha\right]^{1/2}$$

σ_{xx}, σ_{yy} and σ_{xy} are the direct and shear stresses in the conventional Cartesian co-ordinates and x and y are distance from the centre of the ellipse along the major co-ordinates. If the minor axis of ellipse shrinks to zero (b_o=0), eqs 3-1 can be used to determine the stresses in a mode I cracked plate along the crack line as

$$\sigma_{xx} = \sigma_{YY}\left[\frac{r+a}{\sqrt{r(r+2a)}} - 1\right] \tag{3-2a}$$

$$\sigma_{yy} = \sigma_{YY}\left[\frac{r+a}{\sqrt{r(r+2a)}}\right] \tag{3-2b}$$

$$\sigma_{xy} = 0 \tag{3-2c}$$

where a is the semi crack length and r is distance from the crack tip along the axis x. Here the uppercase subscripts refer to remote conditions and the lower case subscripts refer to the local field equations. If equation 3.2b is rewritten as

$$\frac{\sigma_{yy}}{\sigma_{YY}} = f\left(\frac{2r}{a}\right) = \left(\frac{2r}{a}\right)^{-1/2}\left(1 + \frac{1}{2}\left(\frac{2r}{a}\right)\right)\left(1 + \frac{1}{4}\left(\frac{2r}{a}\right)\right)^{-1/2} \tag{3-3}$$

and a binomial expansion is used to expand the third term in eq 3-3, σ_{yy} can be written for $(2r/a) < 4$ as a series expansion

$$\frac{\sigma_{yy}}{\sigma_{YY}} = f\left(\frac{2r}{a}\right) = \left(\frac{2r}{a}\right)^{-\frac{1}{2}} + \left(\frac{3}{2^3}\right)\left(\frac{2r}{a}\right)^{\frac{1}{2}} - \left(\frac{5}{2^7}\right)\left(\frac{2r}{a}\right)^{\frac{3}{2}} + \left(\frac{7}{2^{10}}\right)\left(\frac{2r}{a}\right)^{\frac{5}{2}} - \left(\frac{45}{2^{15}}\right)\left(\frac{2r}{a}\right)^{\frac{7}{2}} + \left(\frac{77}{2^{18}}\right)\left(\frac{2r}{a}\right)^{\frac{9}{2}} - \cdots\cdots \qquad \frac{2r}{a} < 4 \tag{3-4}$$

and similarly for σ_{xx}:

$$\frac{\sigma_{xx}}{\sigma_{YY}} = \left(\frac{2r}{a}\right)^{-\frac{1}{2}} - 1 + \left(\frac{3}{2^3}\right)\left(\frac{2r}{a}\right)^{\frac{1}{2}} - \left(\frac{5}{2^7}\right)\left(\frac{2r}{a}\right)^{\frac{3}{2}} + \left(\frac{7}{2^{10}}\right)\left(\frac{2r}{a}\right)^{\frac{5}{2}} - \left(\frac{45}{2^{15}}\right)\left(\frac{2r}{a}\right)^{\frac{7}{2}} + \left(\frac{77}{2^{18}}\right)\left(\frac{2r}{a}\right)^{\frac{9}{2}} - \cdots\cdots \qquad \frac{2r}{a} < 4 \tag{3-5}$$

The second term in eq 3-5, independent of distance r, represents the constant stress T. According to eq 3-5, T in this problem is compressive and its magnitude is equal to the far field stress σ_{YY}.

The coefficients of equations 3-4 and 3-5 are equivalent to those of the Williams series expansions for direct stresses along the crack line for a remotely loaded large plate containing an internal crack. Since the coefficients of the series expansions are known the effects of higher order terms in the crack tip stresses can be investigated accurately. The normalised stress σ_{yy}/σ_{YY}, for each of the terms in eq 3-4 is shown in Fig 3-2 and the sum of the terms is shown in Fig 3-3. As shown in Fig 3-3 the accuracy of σ_{yy} is considerably improved when only a few higher order terms are added to the singular term. Fig 3-4 indicates how non-singular terms, particularly T, improve the value of σ_{xx}. Results for series expansion solution have been compared in Figs 3-3 and 3-4 with the exact solution expressed by eqs 3-2.

3-3. PLASTIC ZONE SIZE

Almost all of the mathematical models suggested in the literature for the plastic zone size around the crack tip take into account only the singular stresses. In this section, a more accurate prediction for the extent of the plastic zone along the crack line is obtained by adding the non-singular terms of stresses shown in eqs 3-4 and 3-5. In addition to the normal-to-the-crack load σ_{YY}, a remote lateral load $\sigma_{XX} = \lambda\sigma_{YY}$ is also considered where λ is the lateral load parameter. The extent of the plastic zone is determined for both plane stress and plane strain conditions using both von Mises and Tresca yield criteria. For simplicity, no hardening effect is considered and the size of plastic zone is determined based on the elastic stresses. Therefore, the results are more appropriate for small scale yielding.

Consider an internal crack in an infinite plate subjected to biaxial loading as shown in Fig 3-1b. The lateral load parameter λ is assumed to be between 0 and 1. The lateral load σ_{XX} is in line with the crack and is only added as a constant term in eqs 3-2a and 3-5. Therefore, the in-plane stresses in the plate can be written as

$$\sigma_{yy} = \sigma_{YY} \cdot f\left(\frac{2r}{a}\right) \tag{3-6}$$

$$\sigma_{xx} = \sigma_{YY}\left[f\left(\frac{2r}{a}\right) + (\lambda - 1)\right] \tag{3-7}$$

$$\sigma_{xy} = 0 \tag{3-8}$$

where $f(2r/a)$ is the right hand side of eq 3-3 for the exact solution or eq 3–4 for the series expansion solution. Eq 3-7 can also be written as

$$\sigma_{xx} = \sigma_{yy} + \sigma_{YY}(\lambda - 1) \tag{3-9}$$

The through-thickness stress σ_{zz} is zero for plane stress and can be found from Hooke's law for plane strain as $\sigma_{zz} = \nu(\sigma_{xx} + \sigma_{yy})$. Therefore

$$\sigma_{zz} = 0 \qquad \text{Plane stress} \tag{3-10a}$$

$$\sigma_{zz} = \nu\sigma_{YY}\left[2f\left(\frac{2r}{a}\right) + (\lambda - 1)\right] \qquad \text{Plane strain} \tag{3-10b}$$

where z is normal to the plane of the plate direction and ν is Poisson's ratio. It should be noted that σ_{xx}, σ_{yy} and σ_{zz} are principal stresses along the crack line. Because in linear elastic fracture mechanics, the extent of the plastic zone is assumed to be limited to a very small distance from the crack tip, the yielding conditions are studied here for a plastic zone r_y not greater than the arbitrarily small value of $a/4$.

3-3-1. Plastic zone size-Tresca yield criterion

According to the Tresca yield criterion, an element of material yields when the difference between the maximum principal stress σ_{max} and the minimum principal stress σ_{min} is equal to the yield stress σ_o, i.e. $(\sigma_{max} - \sigma_{min}) = \sigma_o$. It can be seen from eq 3-9 or Fig 3-4 that for $0 \le \lambda \le 1$ and $(2r/a) \le 0.5$, σ_{xx} is always positive and σ_{yy} is equal to or greater than σ_{xx}. This is valid for any number of terms in the series expansions described by eqs 3-4 and 3-5.

Therefore, for plane stress (σ_{zz} =0), σ_{yy} and σ_{zz} are the maximum and minimum principal stresses. Using eqs 3-6 and 3-10a, the extent of the plastic zone along the crack line r_y can be found from the Tresca yield criterion using

$$\frac{\sigma_{YY}}{\sigma_\circ} = \frac{1}{f(2r_y/a)} \qquad \text{Plane stress} \qquad (3\text{-}11)$$

For plane strain the sign of σ_{xx} depends on r, λ and ν. For example in single-axial loading (λ=0), σ_{xx} is positive only for $(2r/a) \leq 0.33$. In biaxial loading if λ=0.5 or 1, σ_{xx} is positive even up to $(2r/a)$ =1 (this is based on ν=0.3). In these cases the extent of yielding zone is determined as

$$\frac{\sigma_{YY}}{\sigma_\circ} = \frac{1}{(1-2\nu)f(2r_y/a) - \nu(\lambda-1)} \qquad \text{Plane strain} \qquad (3\text{-}12)$$

3-3-2. Plastic zone size- von Mises yield criterion

According to the von Mises criterion, yielding occurs when

$$\sqrt{(\sigma_1-\sigma_2)^2+(\sigma_2-\sigma_3)^2+(\sigma_3-\sigma_1)^2} = \sqrt{2}\sigma_\circ \qquad (3\text{-}13)$$

where σ_1 to σ_3 are the principal stresses. If equations 3-6, 3-7 and 3-10 are replaced in eq 3-13, the plastic zone size can be determined from

$$\frac{\sigma_{YY}}{\sigma_\circ} = \frac{2}{\sqrt{\left(2f(2r_y/a)+(\lambda-1)\right)^2+3(\lambda-1)^2}} \qquad \text{Plane stress} \qquad (3\text{-}14)$$

for plane stress and

$$\frac{\sigma_{YY}}{\sigma_\circ} = \frac{2}{\sqrt{\left(2(1-2\nu)f(2r_y/a)+(\lambda-1)(1-2\nu)\right)^2+3(\lambda-1)^2}} \qquad \text{Plane strain} \qquad (3\text{-}15)$$

for plane strain. Because the von Mises yield criterion is independent of the sign and magnitude of stresses, the yielding conditions can be determined for any distance from the crack tip. However, to comply with the restrictions of LEFM the results are shown here only for small values of plastic zone size.

Equations 3.11, 3-12, 3-14 and 3-15 can be used to determine the external loads required for providing a plastic zone of radius r_y. The effect of non-singular terms of stresses on the extent of the plastic zone can be studied by adding the higher order terms of series expansions of stresses shown by eqs 3-4 and 3-5. The exact solution for the plastic zone size is found if the exact solution for stresses expressed in eqs 3-3 is employed.

Figs 3-5 to 3-8 show the variation of plastic zone size r_y normalised with respect to one quarter of the crack length $a/2$ for different external loads σ_{YY}. The results are shown for both uniaxial and biaxial loading. For biaxial loading the lateral load parameter λ is 0.5 . Figs 3-5 and 3-6 indicate the results for plane stress with Tresca and von Mises yield criteria, respectively. Similar results are shown in Figs 3-7 and 3-8 for plane strain.

3-4. DISCUSSION

3-4-1. Higher order terms of stresses

The first six terms of the series expansion for σ_{yy}/σ_{YY} described by eq 3-4 are shown in Fig 3–2. It is observed that very near the crack tip, say $2r/a < 0.2$, σ_{yy} is dominated by the singular term and the other terms are negligible. However, further away from the crack tip the second term represents a significant fraction of the total stress σ_{yy}. Fig 3-3 shows that the two-term solution is in considerably better agreement with the exact solution than the singular solution. For instance, at a distance $r = \frac{a}{4}$ (or $\frac{2r}{a}=0.5$) from the crack tip, the results of the singular-term, two-term and exact solutions for σ_{yy}/σ_{YY} are 1.41, 1.68 and 1.67, respectively. Hence an error of 16% is accepted if only the singular term is considered. This error reduces to 0.6% for a two-term solution. Fig 3-2 and 3-3 show that apart from the second term, the other higher order terms are negligible near the crack tip.

Williams (1957) showed that for any cracked geometry the elastic stresses around the crack tip can be expressed as infinite eigen-series expansions. The sign and magnitude of the coefficients in these series expansions depend on the geometry and loading configurations of the specimen. Classical theories of linear elastic fracture mechanics

assume that crack growth in brittle materials initiates when the singular term of the series expansion for the opening stress ahead of the crack tip attains a critical value. The microstructural studies of brittle fracture show that the critical stress corresponding to the initiation of crack growth should be investigated at a critical distance r_c from the crack tip. However, the results of the present study show that further away from the crack tip the second term in eq 3-4 can be significant compared with the singular term. This implies that a singular term based analysis for mode I cracked specimens is likely to lead to an inaccuracy in predicting the fracture load. In other words, because the second term of Williams series solution for σ_{yy} varies for different geometries, mode I fracture toughness in linear elastic materials can be a function of the geometry and the type of loading in specimens. It can be suggested from eq 3-4 and Fig 3-3 that specimens having a positive second-term exhibit a lower fracture toughness than specimens having a negative second-term.

Figs 3-2 and 3-3 show that for higher values of $2r/a$, the significance of the second term is increased in comparison with the singular term. Since the critical radius r_c is assumed to be independent of crack length, the normalised critical distance $2r_c/a$ is higher for shorter cracks. Therefore it is expected that the effect of the second term on fracture toughness is more significant for small cracks.

Fig 3-4 displays the sum of the first few terms of the series expansion for σ_{xx} described by eq 3-5. It is seen that the difference between the singular term and the exact solution is significant even very near the crack tip. This difference is considerably reduced if the T-term is added to the singular term and vanishes if the second non-singular term is also included. For example, at a distance $r = \frac{a}{4}$ (or $\frac{2r}{a} = 0.5$) from the crack tip, a singular term solution has an error of 62% whereas this error decreases to 22% when the T-term is taken into account. A solution in uding the first three terms leads to an error of almost zero.

It should be noted that in this section the plastic zone around the crack tip is assumed to be so small that crack growth can be described entirely based on the elastic stresses. In this case, the effect of σ_{xx} on mode I fracture toughness is considered to be negligible in a stress controlled mechanism of fracture. Therefore, ignoring the higher order terms of series expansion for σ_{xx} is likely to have no influence on mode I fracture toughness. However, this is not the case for mixed mode brittle fracture. It is

shown in Chapter 5 that for mode II dominated loading even for a purely elastic material the higher order terms in σ_{xx}, in particular the T-term, can have a considerable effect on fracture toughness.

For small scale yielding conditions, the opening stress σ_{yy} inside the plastic zone ahead of the crack tip depends on the values of both σ_{xx} and σ_{yy} in the elastic area surrounding the plastic zone. This implies that ignoring the higher order terms of the Williams series expansions can lead to inaccurate results for the stresses inside the plastic zone. The significant effect of T-stress on the crack tip stresses has been shown by researchers for small scale yielding, see for example Betegon and Hancock (1991). The results of present study show that the $\sqrt{r}$ terms in the series expansions for both σ_{xx} and σ_{yy} can be significant and hence can influence considerably the stresses inside the plastic zone. However, the effect of the other higher order terms are negligible as they have almost no influence on elastic stresses near the crack tip.

3-4-2. Effect of higher order terms on the plastic zone size

Figs 3-5 to 3-8 show the effect of higher order terms of the series expansion for stresses σ_{xx} and σ_{yy} on the extent of plastic zone ahead of the crack tip. The normalised plastic zone size $2r_y/a$ is displayed in terms of the normalised external load σ_{YY}/σ_o for plane strain in Figs 3-5 and 3-6 and for plane stress in Figs 3-7 and 3-8. The results are studied for each case using both Tresca and von Mises yield criteria.

It is seen from these figures that for very small scale yielding e.g. $r_y<a/40$ ($2r_y/a$ <0.05), a singular term solution is sufficient to estimate the extent of the plastic zone. However the effect of the higher order terms are significant for larger amounts of plasticity. In almost all of the cases the results of a series expansion solution are considerably improved when T is added to the singular terms. It is observed th T has a more significant effect on improving the singular term solution than the $\sqrt{r}$ terms. However in all of the cases the series expansion results are in very good agreement with those of exact solution, when both T and $\sqrt{r}$ terms are added to the singular terms.

It can be seen by comparing Figs 3-5 and 3-6 with Figs 3-7 and 3-8 that for a given external load, the spread of plasticity in plane stress is higher than that in plane strain.

As described in Section 2-2-2 the lower level of plasticity in plane strain is due to the higher level of stress triaxiality around the crack tip.

The important point observed from Figs 3-7a and b is that in the case of plane stress when the Tresca yield criterion is employed, neither T nor the biaxiality of loading have any effect on the plastic zone size. This is because in small scale yielding σ_{yy} and σ_{zz} are always the largest and smallest values of principal stresses respectively, if $0 \leq \sigma_{XX} \leq \sigma_{YY}$ and $0 \leq \lambda \leq 1$. Hence, σ_{xx} which includes T and the lateral load effect does not have any contribution in the yielding of materials when the Tresca yield criterion is employed.

It has been shown by other workers (e.g. Larsson and Carlsson, 1973) that the T-stress has a significant effect on the extent of plastic zone. However, all of those studies are based on the von Mises yield criterion. The results of present study show that the effect of T on the plastic zone size depends also on the yield criteria used.

The influence of the higher order terms of the crack tip stresses on the plastic zone size has also been studied by Edmunds and Willis (1977). They used a matched expansion technique to obtain the near crack tip stresses inside the plastic zone in terms of the far field series expansion of the elastic stresses. Edmunds and Willis determined the extent the plastic zone in front of the crack tip for the internal crack specimen using the Dugdale (1960) yielding model. They compared the results of one-, two- and three-term expansion with those of the exact solution and showed that the plastic zone size predicted from the Dugdale model is considerably more accurate when the effect of the higher order stresses is taken into account.

3-5. CONCLUDING REMARKS

1) A binomial expansion can be used to determine the coefficients of Williams' series expansion for direct stresses along the crack line in a centrally cracked large plate.

2) It was shown that the higher order terms of a series expansion of stress are not negligible near the crack tip. For the normal-to-the-crack stress σ_{yy}, the accuracy of results is significantly improved if the $\sqrt{r}$ term is added to the singular term. For the parallel-to-the-crack stress σ_{xx}, the T-stress improves considerably the accuracy of the results. The discrepancy between the exact solution and the series expansion solution

for σ_{xx} almost vanishes near the crack tip when the $\sqrt{r}$ term is also added to the first two terms.

3) It was shown that the higher order terms have also a significant effect on the accuracy of the size of plastic zone ahead of the crack tip calculated using the series expansion. The extent of plastic zone was determined using the Tresca and von Mises yield criteria and for both plane stress and plane strain conditions. In all the cases the results obtained using the exact solution were in very good agreement with those predicted from the series expansion solution if the T-term and $\sqrt{r}$ terms are also considered together with the singular terms.

4) The results of the present study showed that in plane stress if the Tresca yield criterion is used, the T-term has no influence on the size of plastic zone ahead of the crack tip. This implies that the effect of higher order terms on the plastic zone size can depend on the yield criterion employed.

CHAPTER FOUR

METHODS FOR CALCULATING *T*-STRESS IN MODE I AND MIXED MODE PROBLEMS

4-1. INTRODUCTION

It was shown in Chapter 3 that in mode I, the higher order terms of William's series solution can have a considerable effect on describing the crack tip elastic stresses and on the size of plastic zone ahead of the crack tip. However, because of difficulties in determining the higher order terms for various cracked geometries, it is common in engineering analyses to ignore their effect. It is well established for small scale yielding that among the higher order terms, the *T*-term has the most influence on the plastic zone size and the stresses inside the plastic zone.

There are some analytical and numerical methods to determine T for cracked specimens. However, a review of the literature (Chapter 2) indicates that most of the methods are confined to simple geometries and loading configurations. As a more general solution, finite element (FE) analysis can be used to obtain T for any geometry and loading configurations.

This Chapter explores methods of calculating T directly from finite element a lysis. It is shown that for mode I more reliable results with less mesh refinement can be achieved if crack flank displacements are used rather than crack flank stresses. Methods are also suggested for calculating T for any mixed mode I/II loading without having to calculate stress intensity factors. It is shown that there is good agreement between the results from the proposed methods and analytical results.

The T-stress is determined for a test configuration designed to investigate brittle and ductile fracture in mixed mode loading. It is shown that in shear loading of a cracked specimen T vanishes only when a truly antisymmetric field of deformation is provided. However this rarely happens in practice and the presence of T in shear is often inevitable. It is shown that for some cases the magnitude of T in shear is much more than that for tension. The effect of crack length is also investigated.

4-2. MIXED MODE CRACK TIP STRESSES

It was outlined in Section 2-2-1 that the in-plane linear elastic stresses around the tip of a crack can be described by symmetric and antisymmetric fields, called mode I and mode II respectively. The stresses for each of the fields can be written as an eigen series expansion (Williams, 1957). Near the tip of the crack, where the higher order terms of the series expansion are negligible, stresses for mixed mode are

$$\sigma_{xx} = \frac{K_I}{\sqrt{2\pi r}}\cos\frac{\theta}{2}\left[1-\sin\frac{\theta}{2}\sin\frac{3\theta}{2}\right]+T-\frac{K_{II}}{\sqrt{2\pi r}}\sin\frac{\theta}{2}\left[2+\cos\frac{\theta}{2}\cos\frac{3\theta}{2}\right]+O(r^{1/2}) \quad (4\text{-}1a)$$

$$\sigma_{yy} = \frac{K_I}{\sqrt{2\pi r}}\cos\frac{\theta}{2}\left[1+\sin\frac{\theta}{2}\sin\frac{3\theta}{2}\right]+\frac{K_{II}}{\sqrt{2\pi r}}\sin\frac{\theta}{2}\cos\frac{\theta}{2}\cos\frac{3\theta}{2}+O(r^{1/2}) \quad (4\text{-}1b)$$

$$\sigma_{xy} = \frac{K_I}{\sqrt{2\pi r}}\cos\frac{\theta}{2}\sin\frac{\theta}{2}\cos\frac{3\theta}{2}+\frac{K_{II}}{\sqrt{2\pi r}}\cos\frac{\theta}{2}\left[1-\sin\frac{\theta}{2}\sin\frac{3\theta}{2}\right]+O(r^{1/2}) \quad (4\text{-}1c)$$

where K_I and K_{II} are the mode I and mode II stress intensity factors (SIF) and r, θ, x and y are co-ordinates in conventional polar and Cartesian systems with the crack tip at the origin. The effects of the higher order terms of series expansions are shown by $O(r^{1/2})$. The term T, a constant stress parallel to the crack, is only due to a symmetric component of loading and vanishes for pure mode II. To normalise the effect of T relative to the stress intensity factor in mode I, Leevers and Radon(1983) proposed a dimensionless parameter called the biaxiality ratio B, where

$$B = \frac{T\sqrt{\pi a}}{K_I} \quad (4\text{-}2)$$

and a is the crack length. Equation (4-2) can be extended to mixed mode as

$$B = \frac{T\sqrt{\pi a}}{K_{eff}} \tag{4-3}$$

where the effective stress intensity factor K_{eff} is defined as

$$K_{eff} = \sqrt{K_I^2 + K_{II}^2} \tag{4-4}$$

Despite the significance of T in describing the near crack tip stresses, few methods are available for calculating T, particularly for mixed mode. A review of the current major methods for determining T in two dimensional problems was presented in Section 2-6-2.

4-3. DETERMINING T USING FINITE ELEMENT ANALYSIS

Most of the methods described in Section 2-6-2 are in practice confined to simple geometries and loading configurations. The remaining methods either need multiple analyses or require a specific formulation not available in many finite element codes. Therefore, it is preferable to determine T using a single standard elastic finite element analysis. Below, methods that can be used in finite element analysis, are developed. These methods can be used for any geometry and loading configuration and do not rely on special purpose numerical procedures.

4-3-1. Mode I

For pure mode I the singular term due to K_{II} vanishes in eqs 4-1. Therefore, near the tip of a crack, where higher order terms can be considered to be negligible, eq 4-1a shows that σ_{xx} comprises of the singular term and T. This implies that T can be determined along any direction where the singular term of σ_{xx} vanishes or can be set to zero by superposing with a fraction of σ_{yy} . This corresponds to diffe t angular positions around the crack tip. For example;

- Along $\theta = 0$: $T = \sigma_{xx} - \sigma_{yy}$ (4-5.a)
- Along $\theta = -\pi$ or $+\pi$: $T = \sigma_{xx}$ (4-5.b)
- Along $\theta = -\pi/3$ or $+\pi/3$: $T = \sigma_{xx} - (\sigma_{yy})/3$ (4-5.c)
- Along $\theta = -\pi/2$ or $+\pi/2$: $T = \sigma_{xx} - (\sigma_{yy})/3$ (4-5.d)
- Along $\theta = -2\pi/3$ or $+2\pi/3$: $T = \sigma_{xx} - \sigma_{yy}$ (4-5.e)

Since eq 4-5.b uses one stress component it is convenient to use this equation. In theory eq 4-5.b should provide T within a reasonable distance from the crack tip. But in practice it is seen that FE results are not acceptable unless a large number of elements are used to simulate the crack tip zone, see for example Kardomateas et al. (1993) and Sherry et al. (1995).

An improved method of obtaining the T stress without recourse to much mesh refinement is presented here. This method uses the displacements along the crack faces. Due to traction free boundary conditions along the crack faces, Hooke's law can be written for small strains as

$$\sigma_{xx} = E' \varepsilon_{xx} = E' \frac{du_x}{dx} \tag{4-6}$$

where ε_{xx} and u_x are the strain and displacement respectively parallel-to-the-crack and E' is defined as

$$E' = \begin{cases} E & \text{Plane stress} \\ \dfrac{E}{1-\nu^2} & \text{Plane strain} \end{cases} \tag{4-7}$$

where E is Young's modulus and ν is Poisson's ratio.

For $\theta = -\pi$ or $+\pi$ the singular term of σ_{xx} vanishes and hence near the crack tip, σ_{xx} in eq 4-6 can be represented by T alone

$$T = E' \frac{du_x}{dx} \tag{4-8.a}$$

Since the left hand side of eq 4-8.a is constant, the slope du_x/dx can be replaced by $\frac{u_x(x) - u_x(0)}{x}$ where $u_x(0)$ denotes u_x at the crack tip. Therefore T can be written as

$$T = E' \cdot \frac{u_x(x) - u_x(0)}{x} \tag{4-8.b}$$

This indicates that using either u_x or its slope along the crack faces, T can be determined directly from FE results.

4-3-2. Mixed mode I/II

Eq 4-1a shows that for mixed mode loading, along any radial direction from the crack tip, there is a singular term due to either mode I or mode II or both. The methods described for mode I are not therefore suitable for mixed mode I/II loading. For example, along the crack line in front of the crack tip the singular term of σ_{xx} vanishes for mode II but not for mode I. However, T can be obtained if the appropriate singular terms are subtracted from σ_{xx}. Although, this requires further calculations to determine the stress intensity factors. Also, the consistency and accuracy of the results in this method depend considerably on the accuracy of the stress intensity factors.

The T-stress however can be found without using stress intensity factors when the symmetric properties of mode I and antisymmetric properties of Mode II for direct stresses are used. The stresses in one half of the cracked specimen are added to those of the other half. The mode II stresses vanish and mode I stresses are doubled. Consequently any of the following equations can be used to determine T directly from finite element results along the crack faces

$$T = \left(\sigma_{xx} - \sigma_{yy}\right)_{\theta=0} \tag{4-9.a}$$

$$T = \frac{1}{2}\left[\left(\sigma_{xx}\right)_{\theta=-\pi} + \left(\sigma_{xx}\right)_{\theta=\pi}\right] \tag{4-9.b}$$

$$T = \frac{1}{2}\left[\left(\sigma_{xx} - \frac{\sigma_{yy}}{3}\right)_{\theta=-\frac{\pi}{3}} + \left(\sigma_{xx} - \frac{\sigma_{yy}}{3}\right)_{\theta=\frac{\pi}{3}}\right] \tag{4-9.c}$$

$$T = \frac{1}{2}\left[\left(\sigma_{xx} - \frac{\sigma_{yy}}{3}\right)_{\theta=-\frac{\pi}{2}} + \left(\sigma_{xx} - \frac{\sigma_{yy}}{3}\right)_{\theta=\frac{\pi}{2}}\right] \tag{4-9.d}$$

$$T = \frac{1}{2}\left[\left(\sigma_{xx} - \sigma_{yy}\right)_{\theta=-\frac{2\pi}{3}} + \left(\sigma_{xx} - \sigma_{yy}\right)_{\theta=\frac{2\pi}{3}}\right] \tag{4-9.e}$$

Similar to mode I, it is convenient to use eq 4-9.b as it uses only one component of stress.

The displacement approach described earlier can also be employed to determine T in mixed mode loading. Using eq 4-6 for both the upper and the lower edges of the crack, and summing the results, T can be expressed as

$$T = \frac{1}{2} E' \left(\left(\frac{du_x}{dx} \right)_{\theta=-\pi} + \left(\frac{du_x}{dx} \right)_{\theta=\pi} \right) \tag{4-10}$$

Based on the displacements alone, T can be expressed as

$$T = \frac{1}{2x} E' \left[u_x(x,-\pi) + u_x(x,\pi) \right] \tag{4-11}$$

Since the path independent integral J for mixed mode loading is usually available from the FE analysis, and using the expression $K_{eff} = \sqrt{JE'}$, the biaxiality ratio B for mixed mode conditions is

$$B = T\sqrt{\frac{\pi a}{JE'}} \tag{4-12}$$

Eq 4-12 together with any of eqs 4-9 to 4-11 can be used to determine B without having to calculate separately K_I and K_{II}.

4-4. FINITE ELEMENT RESULTS

In this section the stress and displacement methods for mode I and mixed mode conditions are used to determine T from finite element analysis for a number of cracked specimens. The results of the two methods are compared. The analytical results for these specimens are used to verify the accuracy of the results obtained from the displacement method.

4-4-1. Mode I

Finite element analyses using ABAQUS (1997) were employed to determine T for mode I using the stress and displacement methods described earlier. Two standard test specimens were examined: the single edge notched (SEN) and double edge notched (DEN) specimens shown in Fig 4-1. For the SEN specimen the crack length a to width W ratio was 0.4 and for the DEN specimen a/W was 0.2 . Due to symmetry, only one half of the SEN and one quarter of the DEN specimens were considered. As shown in Fig 4-2, in the crack tip region 12 rows of elements were used where each row had 17 eight-noded plane strain elements in the radial direction. A square root singularity in the stress/strain field was produced at the crack tip by using quarter

point scaling between the circumferential rows of nodes surrounding the crack tip. The specimens were subjected to a uniform tensile far field stress σ_{far}.

The stress and the displacement methods, using eqs 4-5.b and 4-8.b, were used to determine T for distances x behind the crack tip and along the crack face. Figs 4-3 and 4-4 show the results obtained for the SEN and DEN specimens respectively where T is normalised with respect to the far field stress σ_{far}, and the distance x is normalised with respect to the crack length a. The magnitude of T is determined from the constant part of the results. For large negative values of x/a the higher order terms become noticeable, while for small negative x/a the crack tip singularity affects the results. The results from both specimens show that the stress method does not provide a constant value for T.

Similar analyses were carried out for different crack depth ratios. Fig 4-5 shows the results for T/σ_{far} calculated from the displacement method for the SEN and DEN specimens, compared with those obtained by Kfouri (1986).

4-4-2. Mixed mode I/II

To verify the methods described earlier for mixed mode conditions, T was calculated for an inclined edge crack in a large square plate for which an analytical solution for T exists. The plate was subjected to a uniform far field tensile stress σ_{far} as shown in Fig 4-6. The angle between σ_{far} and the crack direction was denoted by β, such that when β equals 0^o mode II conditions apply and when β equals 90^o mode I conditions apply. The model had 28 rows of elements in the circumferential direction each containing 20 eight-noded plane strain elements.

The T-stress was calculated using both the stress method (eq 4-9 b and the displacement method (eq 4-11) for different crack angles β. Results for $\beta = 70^o$ are shown in Fig 4-7 and compared with the analytical results from Seed and Nowell (1994). It is seen that both the stress and displacement methods give results that compare well with the analytical results, but only just behind the crack tip for $x/a > -0.04$. The displacement method provides better results over a larger distance. Results for T calculated from FE results from the displacement method for different crack angles are compared in Fig 4-8 with analytical results from Seed and Nowell (1994). There is very good agreement between the results.

4-5. APPLICATION TO A MIXED MODE TEST FIXTURE

Davenport and Smith (1993) designed a tension-shear specimen to study mixed mode failure in both brittle and ductile materials. This test apparatus was later modified by Swankie (1999) to allow fracture testing of larger crack specimens. In the present section, first the details of finite element modelling of the modified test apparatus are described. Next, the displacement method (eq 4-11) used in the previous section for mixed mode loading is employed to calculate T in the specimen for different combinations of tensile and shear loads. Both the effect of loading configuration and the effect of crack length on T are investigated. Although the contribution of T in shear loading of cracked specimens has been assumed to be zero in previous studies, it is shown that a considerable value of T can be present in the shear loading of specimens.

4-5-1. Finite element modelling

The modified test apparatus is shown in Fig 4-9a and consists of a single edge notched (SEN) specimen in a two-part fixture. The SEN specimen of width 20 mm, thickness 20 mm and length 160 mm is inserted inside the fixture such that the specimen is completely surrounded by the fixture. The distance between the corresponding loading holes in the two parts of fixture is about 330 mm. The maximum thickness of the fixture is 65 mm. The position of the SEN specimen inside the fixture is shown in Fig 4-9b. The specimen is held in the fixture through four location pins. Loads are applied to the fixture via the loading holes. The positions of loading holes on the fixture are selected such that the SEN specimen can be subjected to different mode mixities from pure tension ($\beta=90^{o}$) to pure shear ($\beta=0^{o}$) as shown in Figure 4-9b.

Because of the space needed for inserting the specimen, the thickness is not uniform in the fixture. However for simplicity, a 2D finite element analysis with uniform thickness for both the specimen and the fixture was considered. It is considered that the uniform thickness model provides an adequate finite element simulation of the specimen and fixture. This is because change in the stiffness of the fixture (due to varied thickness) has no significant effect on the load which is transferred from the fixture to the cracked specimen. It is noted that a 2D finite element analysis is significantly less costly than a 3D analysis.

Three different models were used to simulate the connection between the fixture and specimen as shown schematically in Fig 4-10. The reason for using three models was to understand the influence of the connection on the values of T determined from FE analysis.

For all models the basic finite element mesh was the same. Fig 4-11 shows the FE mesh for the SEN specimen. A total of 1120 eight noded plane strain elements were used for the specimen. The FE mesh for the fixture which consists of 152 eight noded plane strain elements is shown in Fig 4-12. The rectangular section shown in the middle of the fixture in Fig 4.12 represents the location of the SEN specimen relative to the fixture. In all three FE models the meshes representing the specimen and fixture were overlaid although different methods were used to connect the specimen and fixture meshes together. Further details of the precise differences between the models are described below.

1) Perfect connection model:

   In this model the nodal points along the external boundary of the specimen are tied to the corresponding nodes along the rectangular boundary in the middle of the two parts of the fixture (the bold line in Fig 4-12). The connection is shown as broken line in Fig 4-10a. The fixture and the specimen in the perfect connection model can be considered as a single unit but with different material properties.

2) Pinned model:

   In this model the specimen is connected to the two parts of the fixture only through the location pins shown in Fig 4-9. The pin connection is simulated by tying the appropriate nodes in the specimen and the fixture which are shown in Figs 4-11a and 4-12. The external boundary of the specimen in the pinned model an freely deform without any contact with the fixture.

3) Contact model:

   In the real test apparatus, the specimen is inserted inside the rebates available in the middle of the two parts of the fixture. Therefore, the external boundary of the specimen is in contact with the boundaries of these rebates. The specimen is also connected to the fixture through the location pins. For mode I dominated conditions (β near 90°), the load is transferred to the specimen mainly through the

location pins, whereas in mode II dominated conditions (β near 0°), the specimen is subjected predominantly to the contact forces transferring from the surfaces of the rebates in the fixture. The connection between the specimen and the fixture in the contact model is simulated by modifying the pinned model such that in addition to the connection through the location pins, contact surfaces are considered between the external boundary of the specimen and the boundary of the rebates in the two parts of the fixture (shown by bold line in Fig 4-12). Contact elements were interposed between the jig and the specimen with a coefficient of friction of 0.5 to represent dry steel on dry steel in the Coulomb friction model.

While the real loading configuration is best simulated by the contact model, the perfect connection model was used initially for simplicity. However, as described later, only the pinned model provides a pure antisymmetric stress field for the SEN specimen in mode II loading.

In the finite element analyses Young's modulus and Poisson's ratio for the specimen were 210 GPa and 0.3, respectively. Young's modulus for the fixture was considered to be three times that for the SEN specimen to account for additional thickness of the fixture. In the perfect connection model, Young's modulus for the rectangular section in the middle of the fixture was a small number. This allows the specimen to deform with its real stiffness and independent of the highly stiff fixture which is perfectly connected to the specimen. The crack depth to the specimen width ratio was 0.5 in the first set of analyses. A load of 60 kN was applied at different loading angles: $\beta = 0^{\circ}$, 22.5°, 45°, 67.5°, and 90°.

4-5-2. Effect of loading configuration

The biaxiality ratio B was calculated for the three models using eqs 4-11 an 4-12. Fig 4-13 shows the results for different loading angles. Although it is expected that both K_I and B are zero for antisymmetric loading (pure mode II), it is seen that for $\beta = 0$ (pure shear) B is zero only for the pinned model. For both the perfect connection and contact models there is therefore a large value of T-stress for pure shear loading.

For the perfect connection model with the fixture and specimen as a single unit B always increases with decreasing loading angle β. For loading the specimen only through the location holes (pinned model) a similar result is obtained with B

increasing with decreasing loading angle. However, in pure shear B is zero, while for the perfect connection model, in pure shear a positive B was obtained. In contrast to the perfect connection and pinned models, the contact model yielded decreasing B with decreasing loading angle. In pure shear B is negative indicating a major contribution occurring as a result of the contact forces on the edges of the specimen. It is seen in Fig 4-13 that in the contact model the magnitude of B for mode II is much higher than that for mode I. In mode I ($\beta = 90^{\circ}$), although the load in the contact model is mainly transferred to the specimen through the location pins, B is slightly less than that for the pinned model. This is due to the effect of contact forces which constrain the rotation of the specimen inside the fixture.

4-5-3. Influence of crack length for mixed mode

To investigate the effect of crack depth on T for mixed mode loading, similar analyses were carried out for a number of crack depth to specimen width ratios. Fig 4-14 shows the variation of B versus loading angle for the pinned model for a/W= 0.1, 0.5 and 0.7. Since the antisymmetric loading is retained when the length of the crack is changed, B in mode II vanishes for all the cases. Table 4-1 shows that the results obtained here for B in mode I are in good agreement with those presented by Sham (1991) for SEN specimens with the same crack lengths subjected to a uniform tensile load. It is seen that B is increased by increasing the crack length.

The effect of crack length on B for the contact model is shown in Fig 4-15 for a/W= 0.1, 0.3, 0.5, 0.6, 0.7 and 0.8 . In all the cases a considerable change in B is obtained by moving from mode I to mode II. The maximum discrepancy between the values of B for different crack lengths is observed for β=45°. As expected, in mode I the value of B is increased by increasing the crack depth. A similar trend is seen for other loading angles except for mode II where B decreases for deeper cracks. Th hange in B with increasing crack depth in mode I and mode II is shown in Fig 4-16.

The results obtained for the biaxiality ratio B for different loading angles β are shown in Table 4-2 for the three models with a/W =0.1, 0.5 and 0.7.

4-6. DISCUSSION

4-6-1. Stress method versus displacement method

Finite element results for T/σ_{far} shown in Figs 4-3 and 4-4 for two different mode I cracked specimens were obtained using both the stress and the displacement methods. Near the crack tip ($x/a<0.02$) the results are influenced by the numerical errors normally expected from FE results in highly stressed zones. At distances far from the crack tip, the effect of higher order terms in Williams' series expansion are significant. The results for T are strongly influenced by these factors very near the crack tip and very far away from the crack tip, and will depend on the geometry, loading and more importantly the suitability of the method used to determine T. Therefore, T must be determined from a region where T is a constant. Figs 4-3 and 4-4 show that for identical meshes the stress method does not provide a constant value for T/σ_{far}. Similar difficulties in using the stress method have also been observed by Kardomateas et al. (1993) and Sherry et al. (1995). Each report that considerable mesh refinement is required to achieve accurate results using the stress method. This argument also applies for the stress method suggested in Section 4-3-2 for mixed mode loading.

For the stress method, the finite element analysis calculates the stresses on the nodal points along the crack faces from extrapolation of the stresses at the integration points of the corresponding elements. Since the singular term vanishes only along the crack face and not at the integration points, extrapolation introduces numerical errors. The error is particularly noticeable close to the crack tip. However in the displacement method this error is considerably reduced as σ_{xx} (or T) can be directly calculated from the displacements of the nodal points along the crack face.

4-6-2. T in the present mixed mode specimen

The displacement method suggested for mixed mode loading was used to determine T in a mixed mode test specimen. Three models were used for simulation of the test conditions. All three models could be subjected to different combinations of mode I and mode II from pure tension to pure shear. Although eq 2-4a shows that T vanishes for pure mode II, it was found that for pure shear loading of the specimen in the

perfect connection and contact models there was a large constant term of stress parallel to the crack.

To describe this constant term of stress, reference should be made to Williams' series solution for stresses in cracked bodies. According to his solution, T always vanishes for antisymmetric fields of deformation (described here as ideal mode II). For the perfect connection and contact models of the mixed mode test fixture such a field is not provided when the SEN specimen is subjected to shear loading, even though K_I vanishes. This implies that in shear loading for these models, only the T term from eqs 2-3 is present in conjunction with mode II stresses expressed in eqs 2-4. Ideal mode II conditions can be achieved, for instance, in a symmetric cracked specimen with the crack as line of symmetry when forces of the same magnitude but of opposite sign are applied parallel to the crack and at symmetric points (see Fig 4-17).

The SEN specimen in the pinned model is an example of ideal mode II in shear loading if the diameter of the location pins is considered to be very small. Antisymmetry in this specimen is maintained even if the crack length is changed. This can be seen in Fig 4-14 where B vanishes for different crack lengths when β reduces to zero. However, since it is very unlikely that an ideal mode II occurs in real applications, the presence of T for shear loading of a cracked body must be considered inevitable. The results obtained here show that the magnitude of T in shear loading is very much dependent on the type and position of loading.

A number of other test specimens have been designed to investigate mixed mode fracture. A critical review of some of these specimens has been presented by Richard (1989). The results of the present research suggest that because of the potential effect of T on mode II and mixed mode fracture toughness, the magnitude of T in shear loading of mixed mode specimens should also be evaluated.

4-7. CONCLUDING REMARKS

1) In mode I, T can be obtained by direct use of the displacement u_x (or the slope of u_x in x direction) along the crack flanks. The displacement method gives more reliable results with less mesh refinement for T in comparison with that of the stress method.

2) T can also be determined in mixed mode problems using the stresses or displacements along the two faces of the crack without having to calculate stress intensity factors. This can be done if the contribution of mode II direct stresses (or displacements) are eliminated first by superposition of the stresses (or displacements) along the two faces of the crack.

3) A single edge notched specimen subjected to different loading conditions and different combinations of modes I and II loading was investigated. It was shown that for shear loading of the specimen a significant T-stress can be obtained except when the loading is purely antisymmetric.

4) Finite element analysis of the mixed mode specimen showed that for the real loading conditions, the magnitude of the biaxiality ratio B in mode II is much higher than that for mode I loading. In this case, the biaxiality ratio in mode II decreases with increasing crack length, while for mode I B increases with increasing crack length.

CHAPTER FIVE

A GENERALISED MTS CRITERION

5-1. INTRODUCTION

Several criteria were described in Section 2-4-2 for predicting brittle fracture in specimens subjected to mixed mode loading. The conventional maximum tangential stress (MTS) criterion proposed by Erdogan and Sih (1963) assumes that stress intensity factors K_I and K_{II} are sufficient to predict the direction and the onset of crack growth in a linear elastic mixed mode specimen. This is based on the assumption that the higher order terms in the series expansion for the tangential stress $\sigma_{\theta\theta}$ around the crack tip are always negligible compared with the singular term.

In Chapter 4, the finite element analyses of a mixed mode specimen revealed that, the T-term can be significant and hence modify the crack tip stresses depending on the loading configuration. The significance of the T-stress is shown for another specimen in this Chapter where the crack tip parameters K_I , K_{II} and T are studied for a large plate containing an angled internal crack and subjected to either uniaxial or biaxial loads. Different combinations of modes I and II are achieved in the specimen when the crack angle is altered. It is shown that for some crack angles the stre s around the crack tip are dominated by T. Therefore, the conventional MTS criterion which ignores the effect of T in mixed mode fracture is not suitable for fracture studies in such specimens.

A generalised MTS criterion is presented in this Chapter to investigate mixed mode fracture for linear elastic and brittle materials where the size of the plastic zone around the crack tip is negligible relative to the size of the crack. Therefore the elastic stresses

are sufficient to study the crack propagation. The generalised criterion takes into account the effects of both the singular term and the T term in the tangential stress around the crack tip. Using this criterion, the direction and the onset of fracture initiation can be predicted for mixed mode cracked specimens with any combination of the crack tip parameters K_I , K_{II} and T. It is shown that positive T reduces the fracture toughness in mixed mode loading and negative T increases it. The effect of T on the angle of initiation of crack growth is also discussed.

5-2. MIXED MODE CRACK TIP PARAMETERS

The series expansions for the elastic stresses around the crack tip described in Section 4-2 can be rewritten in the polar co-ordinates for any homogeneous and isotropic body as

$$\sigma_{rr} = \frac{1}{\sqrt{2\pi r}}\cos\frac{\theta}{2}\left[K_I(1+\sin^2\frac{\theta}{2}) + K_{II}(\frac{3}{2}\sin\theta - 2\tan\frac{\theta}{2})\right] + T\cos^2\theta + O(r^{1/2}) \quad (5\text{-}1)$$

$$\sigma_{\theta\theta} = \frac{1}{\sqrt{2\pi r}}\cos\frac{\theta}{2}\left[K_I\cos^2\frac{\theta}{2} - \frac{3}{2}K_{II}\sin\theta\right] + T\sin^2\theta + O(r^{1/2}) \quad (5\text{-}2)$$

$$\sigma_{r\theta} = \frac{1}{2\sqrt{2\pi r}}\cos\frac{\theta}{2}\left[K_I\sin\theta + K_{II}(3\cos\theta - 1)\right] - T\sin\theta\cos\theta + O(r^{1/2}) \quad (5\text{-}3)$$

where σ_{rr}, $\sigma_{\theta\theta}$ and $\sigma_{r\theta}$ are the polar stresses shown in Fig 2-1. The higher order terms $O(r^{1/2})$ can be considered to be negligible near the crack tip. It is seen that T has a contribution to all three stress components in polar co-ordinates, unlike in Cartesian co-ordinates. The crack tip parameters K_I, K_{II}, and T depend on the geometry and loading configurations and can vary considerably for different specimens.

It is well known that crack growth in brittle materials initiates from the boundary of a very small process zone surrounding the crack tip. This implies that fo xample, crack growth in mode I initiates when the tangential stress $\sigma_{\theta\theta}$ at a critical radius r_c in front of the crack tip attains a critical value $(\sigma_{\theta\theta})_c$. The parameters r_c and $(\sigma_{\theta\theta})_c$ are material properties which are assumed to be independent of the geometry of specimen and loading configuration. A similar concept can also be used for the maximum tangential stress (MTS) criterion in mixed mode loading. Using this approach, the direction of fracture initiation and the onset of crack growth should be investigated at the critical radius r_c from the crack tip and not at the crack tip where r =0.

At the critical distance r_c where the contributions of the higher order terms $O(r^{1/2})$ in eq 5-2 can be ignored, the singular term is finite and the T-stress can be a significant fraction of the tangential stress (see Fig 5-1). For pure mode I, the T-term vanishes in the expansion for the tangential stress in front of the crack tip along the crack line (θ =0). Therefore, the effect of T on the mode I fracture toughness can be neglected for linear elastic materials. However, in mixed mode where the crack growth is not in the same plane as the initial crack, T has a contribution to the tangential stress along the direction of initiation of crack growth and hence influences the mixed mode fracture toughness. However, this influence is significant only for specimens where the T-term is not negligible compared to the singular term in eq 5-2. One appropriate parameter which can be used to quantify this fraction is the biaxiality ratio B described in Section 4-2:

$$B = \frac{T\sqrt{\pi a}}{K_{eff}} \qquad K_{eff} = \sqrt{K_I{}^2 + K_{II}{}^2} \tag{5-4}$$

In the next section the crack tip parameters K_I, K_{II}, T and B are studied for the angled internal crack specimen. This is a specimen which has been used frequently by researchers for mixed mode fracture experiments. It is shown that for certain conditions in the specimen, the parameter T dominates in characterising the crack tip stresses and hence the fracture toughness.

5-3. ANGLED INTERNAL CRACK SPECIMEN

Consider a plate containing an internal crack of length $2a$ which is angled to the edges of the plate (see Fig 5-2a). The plate is subjected to uniform far field stresses, σ in the vertical direction and $\lambda\sigma$ in the horizontal direction, where λ is the lateral load ratio. The crack makes an angle β with the vertical direction. By changing β different combinations of modes I and II can be achieved.

If the crack length is very small compared with the edges of the plate, a closed form solution can be found for K_I, K_{II}, and T. This can be achieved by considering another large plate inside the initial one, such that the edges of the secondary plate are parallel or normal to the crack as shown in Fig 5-2b. Using the statical equilibrium relations the far field stresses on the boundary of the secondary plate are

$$\sigma_X = \sigma(\cos^2\beta + \lambda\sin^2\beta) \tag{5-5}$$

$$\sigma_Y = \sigma(\lambda \cos^2 \beta + \sin^2 \beta) \tag{5-6}$$

$$\sigma_{XY} = \sigma(1-\lambda)\cos\beta \sin\beta \tag{5-7}$$

where σ_X, σ_Y and σ_{XY} are shown in Fig 5-2c. The stress intensity factors are known for the secondary plate as

$$K_I = \sigma_Y \sqrt{\pi a} = \sigma\sqrt{\pi a}(\lambda \cos^2 \beta + \sin^2 \beta) \tag{5-8a}$$

$$K_{II} = \sigma_{XY} \sqrt{\pi a} = \sigma\sqrt{\pi a}(1-\lambda)\cos\beta \sin\beta \tag{5-8b}$$

As described in Section 3-2, T is

$$T_x = \sigma_X - \sigma_Y = \sigma(1-\lambda)\cos 2\beta \tag{5-9}$$

The stress intensity factors K_I and K_{II} obtained for the secondary plate are equivalent to those of the primary plate. The subscript x emphasises that T_x is in the direction of x axis in the local co-ordinates shown in Fig 5-2a. The biaxiality ratio B can be written for this specimen as

$$B = \frac{(1-\lambda)\cos 2\beta}{\sqrt{\lambda^2 \cos^2 \beta + \sin^2 \beta}} \tag{5-10}$$

Eqs 5-8 to 5-10 show that for $\lambda \neq 0$, either $\beta = 0^\circ$ or 90° correspond to pure mode I. Pure mode II can be achieved for example when $\beta = 45^\circ$ and $\lambda = -1$ in which case $T_x = B = 0$. For equal biaxial tension ($\lambda = 1$), K_{II} and T vanish and $K_I = \sigma\sqrt{\pi a}$ for any angle β.

Although theoretically the biaxially loaded plate is more suitable for providing a complete range of mixed modes I and II, there are some difficulties in using the plate for experimental studies. For example, it is not suitable for a conventional uniaxial tensile testing machine as a special apparatus is required to apply the biaxia ad. The specimen may also fail due to buckling when subjected to lateral compression ($\lambda < 0$). Therefore, the uniaxially loaded plate has been used more in mixed mode experiments. For the uniaxially loaded specimen where $\lambda = 0$ eqs 5-8 to 5-10 are written as

$$K_I = \sigma\sqrt{\pi a} \sin^2 \beta \tag{5-11}$$

$$K_{II} = \sigma\sqrt{\pi a} \cos\beta \sin\beta \tag{5-12}$$

$$T_x = \sigma \cos 2\beta \tag{5-13}$$

$$B = \frac{\cos 2\beta}{\sin \beta} \tag{5-14}$$

Fig 5-3 shows the angular (β) variations of stress intensity factors normalised with respect to $\sigma\sqrt{\pi a}$ and T normalised with respect to σ. For β =90°, pure mode I is obtained, but for β=0° both the mode I and mode II stress intensity factors vanish and T is the only non-vanishing term of the series expansions of the stresses. This implies that for small values of β where the singular terms of stresses at the critical distance r_c diminish, the fracture event is dominated by T. Fig 5-3 and eqs 5-11 and 5-12 show that pure mode II cannot be obtained in the angled internal crack specimen when loaded uniaxially.

As described earlier, the magnitude of T relative to that of stress intensity factors can be expressed using the biaxiality ratio B. Fig 5-4 displays the variation of the biaxiality ratio B versus, the crack angle β in the biaxially loaded specimen for different values of the lateral load ratio λ = –1, –0.5, 0, 0.5 and 1. For the uniaxially loaded specimen (λ=0), when β approaches zero B tends to infinity because the stress intensity factors tend towards zero. The results of other values of the lateral load ratio λ show that B can vary considerably, depending on the loading conditions.

This section studied a specimen which has a considerable value of B in mixed mode loading. Similar conditions were also observed for the mixed mode configuration described in Section 4-5. Ignoring the effect of T in fracture studies of such specimens can introduce an inaccuracy in life assessment of the cracked engineering components. In the next section a generalised MTS criterion is described which takes into account the effect of T in mixed mode fracture of linear elastic specimens.

5-4. *K-T* FORMULATION FOR THE MTS CRITERION

The maximum tangential stress criterion suggests that in a brittle material crack propagation initiates along the direction θ_o which corresponds to the maximum tangential stress around the crack tip. The angle θ_o can be found from

$$\frac{\partial \sigma_{\theta\theta}}{\partial \theta} = 0 \qquad \Rightarrow \qquad \theta = \theta_o \tag{5-15}$$

Retaining both the singular terms and the T-term in the series expansions for $\sigma_{\theta\theta}$, and using eqs 5-2 and 5-15, θ_o is determined by solving

$$[K_I \sin\theta_o + K_{II}(3\cos\theta_o - 1)] - \gamma \sin\frac{\theta_o}{2}\cos\theta_o = 0 \tag{5-16}$$

where

$$\gamma = \tfrac{16}{3} T\sqrt{2\pi r_c} \tag{5-17}$$

If the critical radius from the crack tip is presented in the dimensionless form of $\alpha = \sqrt{\frac{2r_c}{a}}$, the parameter γ can also be written in terms of B as

$$\gamma = \tfrac{16}{3} B\alpha K_{eff} \tag{5-18}$$

where a is the crack length and the effective stress intensity factor K_{eff} and the biaxiality ratio B were described earlier by eq 5-4.

Once the direction of initiation of fracture θ_o is found from eq 5-16, it is replaced in eq 5-2 to determine the conditions for the onset of crack propagation. This gives

$$\sqrt{2\pi r_c}(\sigma_{\theta\theta})_c = \cos\tfrac{\theta_o}{2}\left[K_I \cos^2\tfrac{\theta_o}{2} - \tfrac{3}{2} K_{II}\sin\theta_o\right] + \sqrt{2\pi r_c}\, T\sin^2\theta_o \tag{5-19}$$

where $(\sigma_{\theta\theta})_c$ is the critical value of the tangential stress at the critical radius r_c. For pure mode I where both K_{II} and θ_o are equal to zero and K_I can be replaced by the mode I fracture toughness K_{If}, eq 5-19 reduces to

$$\sqrt{2\pi r_c}\,\sigma_{\theta\theta_c} = K_{If} \tag{5-20}$$

Introducing eq 5-20 into eq 5-19, the onset of crack extension can be found from

$$\cos\tfrac{\theta_o}{2}\left[K_I \cos^2\tfrac{\theta_o}{2} - \tfrac{3}{2} K_{II}\sin\theta_o\right] = -T\sqrt{2\pi r_c}\sin^2\theta_o + K_{If} \tag{5-21}$$

or in terms of B from

$$\cos\tfrac{\theta_o}{2}\left[K_I \cos^2\tfrac{\theta_o}{2} - \tfrac{3}{2} K_{II}\sin\theta_o\right] = -B\alpha K_{eff}\sin^2\theta_o + K_{If} \tag{5-22}$$

Eqs 5-16, 5-21 and 5-22 describe a generalised MTS criterion where mixed mode fracture is predicted for any geometry for which K_I, K_{II}, and T are known. The solution for these equations is not as straight forward as those presented by Erdogan and Sih (1963) for the conventional MTS criterion. The closed form solution used here to solve the equations is described in detail in Appendix A5. The results are presented in Figs 5-5 and 5-6 where the effect of T is represented by a dimensionless parameter $B\alpha$.

Fig 5-5 shows the effect of $B\alpha$ on the angle of fracture initiation θ_o for different values of mixity parameter M^e given by

$$M^e = \frac{2}{\pi}\tan^{-1}\left(\frac{K_I}{K_{II}}\right) \tag{5-23}$$

M^e is 1 for pure mode I and 0 for pure mode II. As shown in Fig 5-5 the angle between the direction of fracture initiation and the crack line increases for positive values of $B\alpha$ and decreases for negative values of $B\alpha$.

The fracture loci are shown in Fig 5-6 for different values of $B\alpha$. It is observed that fracture toughness in mixed mode is enhanced for negative values of $B\alpha$ and lessens for positive values of $B\alpha$. The results for $B\alpha$=0 in Figs 5-5 and 5-6 correspond to the solution of the conventional MTS criterion proposed by Erdogan and Sih (1963). Fig 5-7 shows an alternative solution to eq 5-22 where fracture loci are presented for different values of a dimensionless parameter T^* given by

$$T^* = \frac{T\sqrt{2\pi r_c}}{K_{If}} \tag{5-24}$$

The effect of positive and negative $B\alpha$ on the direction of fracture initiation and the fracture toughness have been compared for different values of K_I/K_{II} in Fi 5-8 and 5-9.

5-5. DISCUSSION

5-5-1. Angled crack specimen

Section 5-3 investigated the crack tip parameters for the angled crack specimen. It was shown that the values of K_I, K_{II}, T and B change considerably depending on the crack

angle and the lateral load ratio λ. Fig 5-4 showed that the biaxiality ratio B, in particular, can have a wide range of values. For cases with high values of B, the crack tip stresses at the critical distance r_c, are dominated by the T-term in eqs 5-1, 5-2 and 5-3. As a result, the onset of crack propagation in such cases is influenced considerably by T.

As described earlier in Section 2-4-2, Williams and Ewing (1972) studied the particular case of the angled internal crack specimen subjected to uniaxial loading (λ=0). They took into account the effect of T in the crack tip stresses and predicted the direction of initiation of fracture and the onset of crack growth using the MTS criterion for different values of the crack angle β. According to their calculation which was corrected later by Finnie and Saith (1973), the direction of initiation of fracture θ_o varies from zero for β=90° to -90° for β=0° whereas the conventional MTS criterion proposed by Erdogan and Sih (1963) suggests $-70.5° \leq \theta_o \leq 0°$.

Williams and Ewing (1972) and Finnie and Saith (1973) showed that the direction of fracture initiation obtained through experiments on the angled internal crack specimens of PMMA are in better agreement with those predicted by eq 2-33 than those calculated from the conventional MTS criterion, see Fig 5-10. This implies that the conventional MTS criterion might predict inaccurate results for crack growth in some mixed mode specimens.

5-5-2. Generalised MTS criterion

Although the results presented by Williams and Ewing (1972) shows that T can influence the mixed mode fracture, there are two major restrictions. Firstly their solution can be used only for the angled internal crack specimen where closed form solutions for K_I, K_{II}, and T are simply obtained. There are numerous mi ed mode specimens designed by researchers to study brittle fracture in mixed mode I/II loading. Because the crack tip parameters can vary considerably for different specimens, only a comprehensive solution such as the one suggested in Section 5-4 is able to explore the effect of T for any mixed mode geometry. Secondly, as shown in Fig 5-3, pure mode II cannot be achieved in the angled crack specimen. This implies that the solution presented by Williams and Ewing (1972) is not able to predict any possible T-stress effect in mode II fracture. Even for the biaxially loaded angled crack specimen in which pure mode II can be obtained when λ=-1 and β = 45°, a similar

restriction is observed. This is because for this loading configuration T always vanishes and hence has no influence on the fracture event (see Fig 5-4).

The solution method presented in Section 5-4 is a generalised MTS criterion which takes into account the effect of T and can be used for any mixed mode geometry and loading configuration. The results of the generalised method are shown in Figs 5-5 to 5-7. To use the fracture diagrams shown in these figures, first the crack tip parameters K_I, K_{II}, and T need to be determined for the given specimen. These parameters are then used to calculate the biaxiality ratio B and the mixity parameter M^e. The stress intensity factors may be obtained from handbooks (e.g. Tada *et al.*, 1985) for simple geometries or can be determined through FE analysis by using the methods described in Section 2-6-1 for more complicated problems. The T-stress can also be calculated from FE analysis utilising either the stress method or the displacement method described in Section 4-3-2 for mixed mode loading. The parameter $\alpha = \sqrt{\frac{2r_c}{a}}$ is determined from the crack length a and the critical distance r_c which is a material property. Using the calculated values of $B\alpha$ and M^e, the direction of initiation of crack growth θ_o is predicted from Fig 5-5 for the given specimen. The same data can be used to find the onset of fracture using either Fig 5-6 or Fig 5-7. However in this case the mode I fracture toughness K_{If} must also be known.

Fig 5-5 displays the effect of T on the angle of fracture initiation for a linear elastic material. While T has no influence on the angle of crack propagation θ_o in mode I, its effect is increased by making the contribution of mode II larger. It is seen that, in general, the angle between the initial crack line and the direction of fracture initiation increases for positive values of T and decreases for negative values of T. For instance, according to Fig 5-4, for the angled internal crack specimen subjected to uniaxial loading (λ=0) T is positive when $0° \leq \beta \leq 45°$ and hence the experimental resu ts for the magnitude of θ_o are expected to be higher than those predicted by the conventional MTS criterion. The opposite is expected for $45° \leq \beta \leq 90°$. This is corroborated by the experimental results presented by Williams and Ewing (1972) for PMMA, although they did not explore the change in the sign of T and its effect on θ_o (see Fig 5-10).

The effect of T on the mixed mode fracture toughness was shown in Figs 5-6 and 5-7. It can be seen that the mode I fracture toughness K_{If} (horizontal axis) is independent of T but when the mode II contribution is increased, T influences the onset of crack

growth. The maximum effect of T on fracture toughness is for pure mode II. It is seen that except for pure mode I, negative values of T enhances and positive values of T lessens the fracture toughness.

As discussed earlier the effect of T on θ_o and the onset of crack propagation is not the same for different combinations of modes I and II. This can also be seen in Figs 5-8 and 5-9. Fig 5-8 shows that when $K_I > K_{II}$, the increase in θ_o due to a positive value of $B\alpha$ is more than the decrease in θ_o due to negative $B\alpha$ of the same magnitude, and vice versa for $K_I < K_{II}$. Similarly from the change in the slope of the curves in Fig 5-9 it can be concluded that when $K_I > K_{II}$, the effect of positive $B\alpha$ on decreasing fracture toughness ratio K_{eff}/K_I, is more than the effect of negative $B\alpha$ of the same magnitude on increasing the fracture toughness. This is opposite when $K_I < K_{II}$.

5-6. CONCLUDING REMARKS

1) The results obtained through the conventional MTS criterion are not accurate for specimens where the stresses around the crack tip are influenced significantly by T.

2) A generalised MTS criterion has been presented for linear elastic and brittle materials in which the effects of both the singular term and the T-term in the tangential stress are included. Using this criterion, mixed mode brittle fracture can be predicted in any specimen for which the crack tip parameters K_I, K_{II} and T are known.

3) It was shown that negative values of T increase the mixed mode fracture toughness whereas positive values of T reduce the mixed mode fracture toughness.

4) The angle between the crack line and the direction of initiation of fracture increases in specimens with positive T and decreases in specimens with negative T.

5) The effect of T on mixed mode fracture depends also on the radius of the critical zone around the crack tip.

CHAPTER SIX

EXPERIMENTAL STUDY OF *T*-STRESS EFFECTS IN MODE II

6-1. INTRODUCTION

The computational studies in Chapter 4 showed that there are circumstances where large amounts of positive or negative T can be present in the shear loading of cracked specimens. The generalised maximum tangential stress criterion developed in Chapter 5 predicted that T can influence considerably mixed mode fracture in brittle materials. The main objective of this Chapter is to investigate experimentally the effect of T on mode II fracture toughness.

The generalised MTS criterion is formulated for pure mode II where the effects of both the singular term and T in the crack tip stresses are included. A failure diagram is then developed in which mode II fracture toughness can be found for different values of T. For the experiments, PMMA shear specimens, which are able to generate significant values of positive or negative T in mode II, are used. Finite element analysis is carried out to obtain T for the specimen using the displacement method given in Chapter 4 for mixed mode loading. Fracture tests are conducted using the PMMA specimens, and the effect of T on mode II fracture toughness is d ermined experimentally. The fracture surfaces are also studied for different loading conditions. A brief description of different features observed on the fracture surface is presented for each case. A probability analysis is carried out to obtain a suitable function for predicting the distribution of the experimental results.

6-2. THEORY

The generalised MTS criterion described in detail in Chapter 5, is briefly presented in this Section for pure mode II. As shown in Chapter 4, there are real loading conditions where, for pure shear, a significant T-stress is present. For such cases the tangential stress around the crack tip, which includes T, can be written as

$$\sigma_{\theta\theta} = \frac{3K_{II}}{2\sqrt{2\pi r}}\cos\frac{\theta}{2}\sin\theta + T\sin^2\theta + O(r^{1/2}) \tag{6-1}$$

The effect of the higher order terms $O(r^{1/2})$ can be neglected near the crack tip where crack growth initiates. According to the maximum tangential stress criterion, the direction of maximum tangential stress θ_o can be obtained when the hoop stress is differentiated with respect to θ, so that

$$\frac{\partial\sigma_{\theta\theta}}{\partial\theta} = K_{II}\left(3\cos\theta_o - 1 - \tfrac{16}{3}B.\alpha.\sin\frac{\theta_o}{2}\cos\theta_o\right) = 0 \tag{6-2}$$

where

$$\alpha = \sqrt{\frac{2r_c}{a}} \qquad \text{and} \qquad B = \frac{T\sqrt{\pi a}}{K_{II}} \tag{6-2a}$$

B is the biaxiality ratio, r_c is the critical distance from the crack tip and a is the crack length. Eq 6-2 was solved numerically to find out the direction of crack growth for different values of $B\alpha$. The results are shown in Fig 6-1.

According to the MTS criterion, crack growth occurs when the tangential stress attains a critical value $\sigma_{\theta\theta\,c}$. This is a material property and is assumed to be independent of mode mixity. At a load corresponding to mode II fracture, eq 6-1 is replaced by

$$\sigma_{\theta\theta c} = \frac{3K_{IIf}}{2\sqrt{2\pi r_c}}\cos\frac{\theta_o}{2}\sin\theta_o + T\sin^2\theta_o \tag{6-3}$$

where K_{IIf} is the mode II fracture toughness. As described in Section 5-4, the critical tangential stress $\sigma_{\theta\theta c}$ can be written in terms of the mode I fracture toughness K_{If} as

$$\sigma_{\theta\theta c} = \frac{K_{If}}{\sqrt{2\pi r_c}} \tag{6-4}$$

If the angle θ_o determined for a given $B\alpha$ from eq 6-2 and the critical stress $\sigma_{\theta\theta\,c}$ defined by eq 6-4 are replaced in eq 6-3, the mode II fracture toughness K_{IIf} can be found in terms of K_{If} and $B\alpha$ as

$$\frac{K_{IIf}}{K_{If}} = \frac{1}{B.\alpha.\sin^2\theta_o - \frac{3}{2}\sin\theta_o \cos\frac{\theta_o}{2}} \tag{6-5}$$

Fig 6-2 shows the calculated variation of the normalised mode II fracture toughness with $B\alpha$.

It is worth pointing out that the conventional MTS criterion, which corresponds to $B\alpha$=0, predicts that for mode II, the direction of maximum hoop stress is -70.6° and K_{IIf}=0.87K_{If} (Erdogan and Sih, 1963).

6-3. EXPERIMENTS

6-3-1. Material

PMMA is known to behave in a brittle fashion both in mode I and mode II (Williams, 1984). This material was selected as the test material for this study. Specimens were machined from a cast Perspex sheet of 20mm thickness. According to the manufacturer, the PMMA had a molecular weight of $M_w = 10^6$ g/mol. An earlier study by Davenport (1993) determined the basic material properties where, Young's modulus = 2800 MPa, Poisson's ratio = 0.38, yield stress = 45 MPa and ultimate stress = 75 MPa. All the specimens were cut from one sheet of material and with the same orientation for the loading axis to reduce possible orientation effects on material properties associated with the manufacturing process.

6-3-2. Specimens

Mode II and mode I specimens, as shown in Fig 6-3, were machined from the perspex sheet. To produce the crack in the specimens, a slit of almost 9 mm length was introduced using a fret saw of 0.35 mm thickness. By pushing a razor blade for another 1 mm inside the slit a sharp tip was produced to make the total crack length around 10 mm. In this case the remaining ligament was about 10 mm (a/W=0.5). Due to occasional kinking of the razor blade, it was difficult to produce a straight tip in

some specimens. Those specimens with a kinked initial crack were discarded. For the rest of specimens, the length and width of the initial slit and the total crack were measured from a magnified picture of the crack using an optical microscope. The dimensions of each crack which are described by parameters a_1, a_2, d_1 and d_2 as shown in Figs 6-3d, are given in Tables 6-1 to 6-3. The small gap between the two faces of the crack prevents any crack closure due to possible minor inaccuracy in manufacturing the specimens.

Care was taken for the mode II specimens to keep the centre of the loading holes along the crack plane. This helped to make sure that the external load had no component normal to the crack and the ligament was subjected to pure shear. A high ratio of cross section area to length L was considered in designing the mode II specimen to prevent possible buckling when subjected to a compressive load.

It is useful to be reminded that the conventional elastic crack tip stresses for mode II given in eq 2-4 are related to a positive shear loading shown in Fig 6-3b. In this case the direction of positive θ is counter-clockwise. However the same equations for the crack tip stresses can be used for a negative shear loading provided a clockwise direction is considered for positive θ, as shown in Fig 6-3b. Tensile and compressive loads on the mode II specimen shown in Fig 6-3a correspond to positive and negative shear loads, respectively. This implies that according to the MTS criterion, and with the definition of positive direction for θ, it is expected that crack growth would occur in the lower part of the specimen for tensile loading and in the upper part of the specimen in compressive loading. It should be noted that the appropriate direction for θ is used for all the results presented in this Chapter for the mode II shear specimens.

6-3-3. Finite Element Analysis

The mode II specimen was simulated using the finite element code ABAQUS. The specimen was considered to be linear elastic with the Young's modulus and Poisson's ratio given in Section 6-3-1. The mesh design is shown in Fig 6-4. The crack tip zone consisted of 30 rings of elements where each ring had 36 eight-noded plane strain elements circumferentially. A quarter point scaling was used between the circumferential rows of nodes surrounding the crack tip to produce a square root singularity in the strain field at the crack tip. The boundary conditions and the loading

point are shown in Fig 6-4. The specimen was subjected to compressive and tensile reference loads of the same magnitude 5 kN.

The J-integral was obtained from ABAQUS, which uses the modified virtual crack extension method proposed by Li *et al.* (1985). The J-integral for both cases of tensile and compressive loading was equal to 2027 N/m . Apart from the first contour, the J-integral was path independent for the remaining 30 contours surrounding the crack tip. T was determined by using the displacement method described in Section 4-4-2 for mixed mode loading. The values of T-stress for compressive loading was -28 MPa and for tensile loading was +28 MPa. From J and T and eq 6-2a the biaxiality ratio B was determined to be as +2 for tensile load and -2 for compressive load. It is worth pointing out that unlike J and T, the magnitude of the biaxiality ratio B is independent of the magnitude of load.

If the mode II stress intensity factor K_{II} is written as $K_{II}=Y.P$ where P is the load applied whether compressive or tensile and Y is a geometry factor then from the results of finite element analysis Y is determined as

$$Y=\frac{K_{II}}{P}=\frac{\sqrt{E'J}}{P}=499.6\ \mathrm{m}^{-3/2} \tag{6-6}$$

With reference to the sign of the T-stress, in the present analysis the mode II specimen is called a $+T$ shear specimen for tensile loading and a $-T$ shear specimen for compressive loading. Figs 6-5a and 6-5b show the angular variation of the tangential and shear stresses for the $+T$ and $-T$ shear specimens, respectively at r =0.27 mm. The stresses in these figures are normalised with respect to the product P/ta where t is the specimen thickness. The reason for choosing this distance is discussed in Section 6-4-3.

6-3-4. Test method

Tests were carried out at room temperature (20°C) using a Shimadzu Autograph universal testing machine of 10 kN capacity. Tests were carried out under displacement controlled loading at 0.5 mm/min. A total of ten mode I tests, ten $+T$ shear tests and ten $-T$ shear tests were conducted. The peak load at fracture and the corresponding displacement were recorded by a data processing unit attached to the

machine. The load-displacement results were also plotted using an *x/y* chart recorder. All the specimens exhibited a linear load-displacement diagram prior to fracture, confirming the linear elastic behaviour of the material.

For mode II tests, none of the compressively loaded *-T* shear specimens failed due to buckling. Visual inspection showed that the crack faces did not come into contact with each other and remained parallel in both tensile and compressive tests. For compressive tests some parts of the specimens shattered. Therefore it was necessary to use a glass guard in front of the specimen for safety reasons. After testing, the fracture initiation angles for the shear specimens were measured from the magnified picture of each broken specimen. However, for some of the specimens the fracture initiation angles varied slightly along the crack front. Therefore the fracture angle was measured along the centre line of the surface at mid-thickness. For mode I specimens, fracture took place along the direction $\theta_o = 0$ and the variation in the direction of fracture was negligible.

Photographs of the *+T* and *-T* shear specimens after fracture are shown in Fig 6-6. It can be seen that the plane of fracture in the *+T* specimen is slightly curved in front of the crack across the ligament, whereas the curvature of the fracture plane across the ligament in the *-T* specimen is considerable. The plane of fracture was flat for all of the mode I specimens.

6-3-5. Experimental results

The measured fracture loads and the fracture angles are shown in Table 6-1 for the *+T* shear specimens and in Table 6-2 for the *-T* shear specimens. Fracture toughness values were calculated from $K_{IIf} = Y.P_{cr}$ and using eq 6-6.

Table 6-3 shows the results for mode I tests. Fracture toughness values were calculated using

$$K_{If} = \frac{P_{cr}}{t\sqrt{W}} f\left(\frac{a}{W}\right) \tag{6-7}$$

where the geometry factor $f\left(\frac{a}{W}\right)$ is given by Tada *et al.* (1985) for single edge notched tensile specimens,

$$f\left(\frac{a}{W}\right)=\frac{\sqrt{2\tan\frac{\pi a}{2W}}}{\cos\frac{\pi a}{2W}}\left[0.752+2.02\left(\frac{a}{W}\right)+0.37\left(1-\sin\frac{\pi a}{2W}\right)^3\right] \quad (6\text{-}8)$$

where t is the specimen thickness. Fracture load, mode I fracture toughness K_{If} and the corresponding mode II fracture toughness (K_{IIf} =0.87K_{If} based on the conventional MTS criterion) are shown in Table 6-3 for mode I tests. Chao and Zhang (1997) have shown that at room temperature, the size of plastic zone in PMMA in front of the crack tip at fracture load is much less than the critical distance r_c. This implies that the plasticity effects around the crack tip are negligible and the use of linear elastic stresses for predicting the onset of crack growth is justified. Eq 5-2 shows that in mode I, T has no effect on the elastic hoop stress in front of the crack tip. Therefore the mode I fracture toughness obtained here for PMMA can be considered to be independent of T if a fracture criterion based on the critical tensile stress is used. This implies that the mode II fracture toughness calculated here from mode I tests can be attributed to T=0 shear tests.

Figure 6-7 shows the mode II fracture toughness data for the +T shear tests, the -T shear tests and the calculated mode II toughness from the mode I tests. Also shown in this figure are the mean values of the results for each case. The fracture initiation angle of the crack growth for mode II tests and the corresponding average values are shown in Fig 6-8.

Fig 6-9 shows a schematic picture of the fracture surface from a +T shear specimen. This was representative of the fracture surface of all the +T shear specimens. The fracture surface was slightly curved and consisted of three distinct zones: a mirror area, an area with ridge markings and an area with hyperbolic features. A m oscopic picture of the hyperbolic features is shown in Fig 6-10a. It is described in detail later (Section 6-4-4) that each hyperbolic marking can be related to a local secondary crack growth initiated from the pole of the hyperbola. Fig 6-10b shows a magnified picture of the hyperbolic markings, where the nucleation point and the radial growth of the secondary crack can be seen clearly.

The fracture surface for the -T shear specimen is shown schematically in Fig 6-11. In this case the fracture surface was considerably curved and consisted of a strip of mirror zone in the middle of the surface and two bands of long ridge markings at the sides of the mirrored area.

6-3-6. Statistical distribution of K_{IIf} data

As discussed in Chapter 2, according to a general statistical model suggested by Weibull (1951), Wallin (1984) proposed a description for the probability of brittle fracture. In general the micromechanism of brittle fracture in PMMA for mode I was found to be similar to that for mode II, therefore a similar model is used here to investigate the statistical description of the fracture toughness data in the present mode I and mode II experiments.

Wallin's probability function for mode I is

$$P_f = 1 - \exp\left[-\left(\frac{K_{If} - K_{\min}}{K_o - K_{\min}}\right)^4\right] \tag{6-9a}$$

An extension of this function can be written for mode II as

$$P_f = 1 - \exp\left[-\left(\frac{K_{IIf} - K_{\min}}{K_o - K_{\min}}\right)^4\right] \tag{6-9b}$$

where P_f is the probability of fracture, K_{min} and K_o are variables which can be found by fitting the model to the experimental data obtained for mode I or mode I fracture toughness. The variable K_o is equal to K_{IIf} corresponding to a 63.2% fracture probability. The experimental values of fracture toughness given in Tables 5-1 to 5-3 are arranged in ascending order. The probability of fracture P_f is obtained from

$$P_f = \frac{i}{N+1} \qquad i = 1,2,\ldots..,N \tag{6-10}$$

where N is the total number of experiments.

A non-linear regression technique was used to fit the non-linear model shown by eq 6-9 to the experimental data. The technique seeks the values of the parameters K_{min} and K_o that minimise the sum of the squared differences between the values of the observed and predicted values of the dependent variable P_f and gives the best fit between the model and the data.

The scientific graphing software SigmaPlot which utilises this technique, was employed to fit the mode I and mode II fracture toughness data to eqs 6-9a and 6-9b. Results for parameters K_{min} and K_o are displayed in Table 6-4. Figs 6-12a to 6-14a show the predicted functions together with the experimental data for three cases: $+T$ shear tests, $-T$ shear tests and mode I tests.

Eqs 6-9a and 6-9b can be rewritten as

$$\left[\mathrm{Ln}\left(\frac{1}{1-P_f}\right)\right]^{1/4} = \frac{K_{If} - K_{\min}}{K_o - K_{\min}} \qquad (6\text{-}11a)$$

and

$$\left[\mathrm{Ln}\left(\frac{1}{1-P_f}\right)\right]^{1/4} = \frac{K_{IIf} - K_{\min}}{K_o - K_{\min}} \qquad (6\text{-}11b)$$

If $g(P_f)$ represents the function of P_f shown on the left side of eqs 6-11 and the fracture toughness results K_{If} (or K_{IIf}) are plotted versus $g(P_f)$, the distribution function is linear. In this case K_{min} and K_o can be obtained directly from K_{If} (or K_{IIf}) corresponding to $g(P_f)$=0 and 1, respectively. Figs 6-12b to 6-14b show the distribution functions determined based on eqs 6-11a and 6-11b for the three sets of results described earlier.

6-4. DISCUSSION

6-4-1. Effect of T in mode II fracture- Theory

Erdogan and Sih (1963) suggested a single parameter maximum tensile stress criterion based on the singular term of the crack tip stresses. According to this criterion, mode II fracture occurs at an angle of -70.6° relative to the crack plane and the mode II fracture toughness is equal to 0.87 times the mode I fracture toughness.

Earlier, a two parameter (K_{II} and T) MTS criterion was developed for mode II loading where the contribution of both the mode II singular stresses and the T-stress were considered. A dimensionless parameter $B\alpha$ was used to show the effect of T on mode II fracture. Figs 6-1 and 6-2 show that T can have a considerable effect on fracture angle and fracture toughness in mode II. It is seen from Fig 6-1 that the angle between the crack line and the direction of the initiation of crack growth increases by positive values of T and decreases by negative values of T. For example, there is a difference of 27° for the crack growth direction where $B\alpha$ =-0.6 and $B\alpha$ =+0.6 . The results displayed in Figs 6-1 and 6-2 can also be shown by following polynomial functions

$$\theta_o = -69.84 - 22.43\,(B.\alpha) + 11.32\,(B.\alpha)^2 + 0.5668\,(B.\alpha)^3 \tag{6-12}$$

$$\frac{K_{IIf}}{K_{If}} = 0.871 - 0.687\,(B.\alpha) + 0.388\,(B.\alpha)^2 - 0.091\,(B.\alpha)^3 \tag{6-13}$$

The coefficients in eqs 6-12 and 6-13 were determined by fitting a third order polynomial to the curves shown in Figs 6-1 and 6-2. Fig 6-2 shows that negative values of $B\alpha$ makes the mode II fracture toughness larger whereas positive values of $B\alpha$ lessens the mode II fracture toughness. For instance, the mode II fracture toughness for $B\alpha$ =-0.5 is more than twice that for $B\alpha$ =+0.5. It is seen from Figs 6-1 and 6-2 that the effect of a negative $B\alpha$ on fracture angle and fracture toughness is considerably more than that for a positive $B\alpha$. For example, the ratios of the fracture initiation angles and the fracture toughness with and without the T-stress are

$$\frac{\theta_{o(B.\alpha=0)} - \theta_{o(B.\alpha=-0.5)}}{\theta_{o(B.\alpha=0)}} = 0.21 \qquad \frac{\theta_{o(B.\alpha+0.5)} - \theta_{o(B.\alpha=0)}}{\theta_{o(B.\alpha=0)}} = 0.1$$

$$\frac{K_{II(B.\alpha=-0.5)} - K_{II(B.\alpha=0)}}{K_{II(B.\alpha=0)}} = 0.53 \qquad \frac{K_{II(B.\alpha=0)} - K_{II(B.\alpha+0.5)}}{K_{II(B.\alpha=0)}} = 0.29 \tag{6-14}$$

6-4-2. Effect of T in mode II fracture- Experiments

To verify experimentally the effect of T, a mode II specimen of PMMA was designed which could provide large values of positive and negative T for different types of shear loading. Mode I fracture tests were also carried out to predict the mode II fracture toughness based on the conventional (T=0) MTS criterion where K_{IIf} = $0.87K_{If}$. The results for mode I fracture toughness are shown in Table 6-3. The

average value for the mode I fracture toughness was 1.95 MPa$\sqrt{m}$ which is in good agreement with 1.87 MPa$\sqrt{m}$ given by Maccagno and Knott (1988).

The direction of the initiation of crack growth for the shear specimens are shown in Fig 6-8. The average value for the $+T$ specimens was -78.6^{o} and for the $-T$ specimen was -55.2^{o} with a difference of 23.4^{o}. The scatter in the results for the $-T$ specimens is slightly more than that of the $+T$ specimens.

The mode II fracture toughness obtained from the $+T$ shear specimens, $-T$ shear specimens and that calculated from mode I specimens are shown in Fig 6-7. The average values of K_{IIf} for these cases were 1.27, 2.43 and 1.69 (=0.87*1.95) MPa$\sqrt{m}$ respectively. Although the results of the FE analysis show that for the same magnitude of load, the stress intensity factor for both $+T$ and $-T$ shear specimens are identical, the average of K_{IIf} for the $-T$ specimens is almost twice the average of K_{IIf} for the $+T$ specimens. This clearly indicates that an MTS criterion solely based on the singular terms of the crack tip stresses can introduce a considerable error in predicting mode II fracture toughness.

Williams and Ewing (1972 and 1974b) and Finnie and Saith (1973) analysed the angled internal crack problem and showed that an improved MTS criterion, which accounts for the effect of T, provides a better agreement with the results of experiments conducted on PMMA. However, because the angled internal crack problem fails to provide pure shear, their results could not reveal the possible effect of T on mode II fracture of brittle materials. The common assumption that T always vanishes in mode II, which results from William's (1957) solution for the crack tip stresses, is another factor for reasons why workers have not investigated the effect of T in mode II fracture. But it was shown in Chapter 4 that in mode II, T vanishes only for purely antisymmetric loading and that T can be considerable in some actical cases in the shear loading of cracked bodies.

It should be noted that Banks-Sills and Arcan (1986) and Banks-Sills and Bortman (1986) also attempted to consider the effect of the higher order stress terms in the mixed mode specimen they had designed. However their solution method only accounted for the $\frac{1}{\sqrt{r}}$ and $\sqrt{r}$ terms and T was omitted in their analyses.

As shown in Tables 6-1 and 6-2 the average values for the normalised mode II fracture toughness K_{IIf}/K_{If} for the $+T$ and $-T$ shear specimens were 0.65 and 1.25 respectively. Fig 6-2 shows that these two values for K_{IIf}/K_{If}, correspond to a $B\alpha$ of 0.4 and -0.43, respectively. From the FE results, B for the $+T$ and $-T$ specimens, is equal to +2 and -2. This indicates that α is almost constant and equal to 0.2 for the positive and negative T-stress conditions. Therefore the radius of process zone r_c can be predicted for PMMA using eq 6-2a

$$r_c = \alpha^2 . \frac{a}{2} = 0.2 \text{ mm} \tag{6-15}$$

The critical distance r_c calculated here based on the results of the mode II fracture toughness can be used to predict the direction of fracture initiation θ_o from eq 6-12. The results can then be compared with the value of the angle θ_o determined experimentally for the positive and negative T shear specimens. For r_c=0.2 mm and Bα=+0.4, the angle θ_o is found as -77° for the $+T$ shear specimen while for r_c=0.2 mm and Bα= -0.4, the angle θ_o is found as -54.1° for the $-T$ shear specimen. Fig 6-8 shows that the predicted values of θ_o are in good agreement with those measured from experiment.

6-4-3. Mechanism of crack growth

Earlier, finite element analyses revealed the angular distribution of the tangential and shear stresses around the crack tip. The results for normalised stresses are shown in Figs 6-4 and 6-5 for the $+T$ and the $-T$ shear specimens, respectively. It can be seen that the maximum tangential stress $\sigma_{\theta\theta}$ and the maximum magnitude of shear stress $|\sigma_{r\theta}|$ occurs at about -75° and -10° respectively for the $+T$ shear specimen and around -55° and +10° respectively for the $-T$ shear specimen. Figs 6-4 and 6-5 show that for the same load, the maximum value of tangential stress $\sigma_{\theta\theta}$ in the $+T$ sp men is considerably higher than that for the $-T$ specimen. It is also observed that varying T from positive to negative values changes the direction of maximum magnitude of shear stress $|\sigma_{r\theta}|$ from the negative into positive sectors of θ.

The normalised stresses shown in Figs 6-4 and 6-5 were obtained along a fixed distance of 0.27 mm from the crack tip. This distance corresponds to the radius of the nearest ring of nodal points in the FE model which corresponds to the estimated

process zone radius r_c=0.2 mm. A difference of 0.07 mm has only a negligible effect on the angles of the maximum $\sigma_{\theta\theta}$ and the maximum $|\sigma_{r\theta}|$.

As described earlier in Section 2-4-3, two main mechanisms of yielding in PMMA are shear yielding and crazing. Shear yielding is favoured by deviatoric component of the stress tensor and is expected to occur in the direction of maximum shear stress. In contrast, crazing is anticipated to take place in the sector of high hydrostatic tension. In a set of mixed mode tests on PMMA, Mahajan and Ravi-chandar (1989) observed that the craze formation and the subsequent crack growth occurred along the direction of maximum tensile stress around the crack tip. The present study shows that the directions of the maximum $\sigma_{\theta\theta}$ obtained from FE analysis for both of the shear specimens are in good agreement with the directions of initiation of crack growth observed in the experiments. This also confirms that crack growth in this study is preceded by crazing and not shear yielding.

6-4-4. Fractography of the fracture surfaces

Fractography of different polymers has been studied extensively in the literature. This can be due to the large variety of features which can be observed on fracture surface for different test conditions. However almost all of the studies are confined to mode I fracture. A review of the studies for amorphous thermoplastics and in particular for PMMA has been presented by Doll (1988). Bhattacharjee and Knott (1995) carried out a number of mixed mode tests for PMMA at a low rate of loading. They explored the fracture surface for the specimens fractured in different combinations of modes I and II. For mode II they observed three distinct areas: a mirror region, a misty region and a region with hyperbolic markings.

In this section different features observed across the fracture surface for tl resent $+T$ and $-T$ shear specimens are described and briefly discussed.

+T shear specimens

It was shown in Fig 6-6 that the fracture plane for the $+T$ shear specimens is nearly normal to the original crack. Although the plane is not precisely flat, its curvature is negligible. As shown in Fig 6-9c the fracture surface can be divided into three areas: a mirror area, a strip of ridges next to the crack front and a zone of hyperbolic signs surrounding the mirror area.

The mirror area initiates from the middle section of the original crack front (portion *aa* indicated in Fig 6-9c) and extends to the central zone of the fracture surface. As described earlier brittle crack growth in PMMA is often preceded by crazing which results from microstructural void growth around the crack tip. Since void growth takes place in a region of high hydrostatic tension, it is expected that crazing and crack growth initiate from the mid-thickness of the specimen, which is known for high stress triaxiality, and extend rapidly towards the free surfaces of the specimen (surfaces *B-C-B* in Fig 6-9c). This zone of primary crack growth is observed as a mirror area on the fracture surface. The points located outside the mirror area are subjected to this primary crack growth after a short time lag. The position of the mirror area also depends on the positions of initial flaws or the fracture-triggering particles in front of the crack edge. It was observed that in some specimens the mirror area was shifted slightly from the symmetry line of the surface.

The area of ridge markings occurs next to the edge of the original crack. The ridges are inclined such that at one end they tend towards the central part of crack tip (points *a* shown in Fig 6-9) and at the other end they tend towards the two lateral surfaces (surfaces *B*). The ridges closer to the surfaces *B* are longer than those near the points *a*. However the strip of the ridge markings is limited to a small band next to the crack front.

It is proposed that once primary crack growth commences from the mirror area, the points locating outside this area are subjected to two waves of crack extension: one from the primary crack growth of the mirror area and one from the edge of the initial crack. If the planes of the approaching cracks are not exactly the same, such as that for slightly curved surfaces, the intersecting stress fields form a local sharp edge which is observed as a ridge on the fracture surface (see Fig 6-9d). This is corroborat y the angles at which ridges are inclined. It is clear that the points which are closer to the lateral surfaces *B* have more time before being subjected to the primary crack growth. This allows more extension for the local crack front leading to an increase in the length of the ridges. Nevertheless, because the overall curvature of the fracture surface is negligible, the two extending cracks join together shortly and make an identical plane. Therefore the strip of ridges is confined to a narrow band next to the edge of the original crack.

The area of hyperbolic features is observed in the zone surrounding the central mirror area as shown in Fig 6-9c. A detailed description of the formation of these markings has been given by Doll (1988). A similar argument can be employed for the present mode II test specimen.

Once primary crack growth commences, secondary cracks will be initiated from local imperfections locating along the path of the advancing crack. The secondary cracks are initiated almost immediately after the primary crack and tend to extend uniformly as a circular crack front. Intersection of the primary crack extension with the secondary cracks forms the hyperbolic markings across the fracture surface. The direction of the symmetry line for each hyperbola, which tends towards the middle part of the initial crack front, gives support to the present argument. Microscopic pictures of the hyperbolic features were shown in Fig 6-10a and 6-10b. The radial extension of secondary cracks from the nucleation points can be seen clearly in Fig 6-10b.

-T shear specimens

Fig 6-6 shows that the fracture surface for this specimens is considerably curved such that the crack path which was initiated at an angle around -55° becomes parallel to the loading direction. The fracture surface, shown schematically in Fig 6-11, exhibits two main areas: A band of mirror zone at middle of the surface and two strips of long ridges at the sides of the mirror area.

The mirror band is seen in the middle part of the specimen which extends all along the fracture surface. As described earlier, crazing and cracking is initiated from middle part of the initial crack front where the stress triaxiality is high. The propagating crack extends as a mirror strip without any marking.

As described for the $+T$ shear specimen, intersection of the primary crack growth with the local crack extension from the local crack front generates the ridges shown in Figs 6-11b and 6-11c . The ridges extend in two strips on the sides of the central mirror area. The height of ridges near the edge of the initial crack is higher than those observed for the $+T$ shear specimens. This could be due to the significant curvature on the fracture surface which causes higher interference between the two intersecting waves of crack growth. However, the height of the ridges decreases considerably

when the curved fracture surface becomes almost flat, further away from the edge of the initial crack.

No hyperbolic markings are seen on the fracture faces of the -T shear specimens. This might suggest that formation of the secondary cracks from imperfections are more likely to take place when the fracture surface is flat or has negligible curvature. In that case a certain number of inclusions remain in the path of a unidirectionally propagating crack and more chance of initiating secondary cracks occurs.

It was observed that for some of the -T specimens, besides the normal ridge markings, a number of more elevated hill shaped features was observed next to the initial crack edge. This can be due mainly to an unevenness of the crack edge resulting from the inaccuracy of the specimen manufacture in the manufacturing process.

6-4-5. Statistical modelling

As described earlier in Section 2-4-4, Wallin (1984) made use of a three parameter Weibull function and proposed a model for cleavage fracture toughness data. He showed that the distribution of K_{If} for different steels can be predicted by this model with a slope parameter m=4. The mode II fracture toughness data obtained from the +T and -T shear tests and those predicted from the mode I tests were fitted using the same statistical model. It was found that a total of 10 experimental results was sufficient to fit the two-parameter model to the fracture toughness data.

Results for the parameters K_o and K_{min} for three sets of experiments are shown in Table 6-4. Figs 6-12 to 6-14 also show that the distribution functions obtained using this model are in good agreement with both mode I and mode II fracture toughness data for PMMA. It can be seen from Figs 6-12 and 6-13 that although T ffects considerably the mean value of the mode II fracture toughness, the statistical model can still be used for the results of both +T and -T shear tests. However the ratio K_o /K_{min} in the distribution function for the -T shear tests is more than that for +T shear tests, representing more scatter in the results of the -T shear tests.

The statistical models suggested in the literature for predicting the distribution of brittle fracture data investigate mainly the micromechanism of cleavage fracture and mode I loading. The models are often based on a weakest link argument which

assumes that failure takes place when at least one fracture-triggering particle is sampled. It is known that the micro-mechanism of brittle fracture in steels is different from that in PMMA. However both mechanisms of cleavage fracture and crazing are similar in that the crack growth occurs when the stress at a critical distance attains a critical value. Therefore, the statistical models suggested based on the weakest link argument and used widely for cleavage fracture is able to predict the distribution of fracture toughness data in PMMA.

The general mechanism of initiation of crack growth in modes I and II is the same. The major difference between mode I and mode II brittle fracture is the angle at which the crack tip is expected to sample the critical fracture-triggering particles. Therefore, the effect of loading mode on the statistical model for brittle fracture can be considered to be negligible. However, the scatter in the results for the direction of initiation of crack growth for mode II tests can be expected to be higher than that for mode I. This is because crack growth in mode I (unlike in mode II) is self-similar and occurs along the plane of symmetry.

Figs 6-7, 6-12 and 6-13 show that the scatter in the fracture toughness results for the $-T$ shear tests is slightly higher than that for the $+T$ shear tests. This can be attributed to the effects of constraint along the direction of initiation of crack growth. For the $+T$ shear specimens which exhibit higher constraint, both the singular term and the T-term in the tangential stress along the direction of initiation of fracture are tensile. Whereas for the $-T$ shear specimens, the T-stress has a compressive effect along the normal to the direction of fracture initiation. This implies that there is a competition between an opening stress due to the singular term of the tangential stress and a compressive stress due to the effect of T. Hence more scatter can be expected in the fracture toughness results for the $-T$ shear tests.

The distribution of the fracture toughness results for the $+T$ and $-T$ shear tests in PMMA can be predicted using the results of the mode I fracture toughness tests. As shown in Table 6-3, the fitting parameters in Wallin's model are K_o= 1.99 MPa$\sqrt{m}$ and K_{min}= 1.47 MPa$\sqrt{m}$ for the mode I fracture toughness results. From the estimated critical distance r_c=0.2 mm and the calculated values of B, the parameter $B\alpha$ is −0.4 for the $+T$ shear specimens and -0.4 for the $-T$ shear specimens. Using either eq 6-13 or Fig 6-2 the ratio K_{IIf}/K_{If} is determined for the $+T$ and $-T$ shear specimens as 0.653 and 1.214 respectively. This ratio can be used to predict the fitting parameters K_o and

K_{min} for mode II fracture toughness results from those determined earlier for mode I tests.

$$K_o\left[K_{IIf},(+T)\right]=0.653K_o\left[K_{If}\right]=1.3\ \text{MPa}\sqrt{\text{m}} \quad (6\text{-}16a)$$

$$K_{\min}\left[K_{IIf},(+T)\right]=0.653K_{\min}\left[K_{If}\right]=0.961\ \text{MPa}\sqrt{\text{m}} \quad (6\text{-}16b)$$

$$K_o\left[K_{IIf},(-T)\right]=1.214K_o\left[K_{If}\right]=2.42\ \text{MPa}\sqrt{\text{m}} \quad (6\text{-}17a)$$

$$K_{\min}\left[K_{IIf},(-T)\right]=1.214K_{\min}\left[K_{If}\right]=1.79\ \text{MPa}\sqrt{\text{m}} \quad (6\text{-}17b)$$

The values of predicted K_o and K_{min} are replaced in eq 6-9b and the probability of mode II fracture in PMMA is predicted for each set of shear tests from the probability of mode I fracture. The results are shown in Fig 6-15. It is seen from Fig 6-15 that the distribution functions for mode II fracture toughness predicted from that determined for mode I test results are in good agreement with the experimental results for both the $+T$ and $-T$ shear tests. However, the predicted function for the $-T$ shear tests is slightly conservative.

The results of the present study show that if $B\alpha$ is known for a shear specimen, not only can the mode II fracture toughness be determined from mode I fracture toughness K_{If}, but also a reliable probability function for mode II test results can be predicted by using the probability function for mode I fracture results.

6-5. CONCLUDING REMARKS

1) A failure diagram in terms of K_{II} and T was obtained for mode II using the MTS criterion. The diagram suggests that the effect of T can be significant in linear elastic mode II fracture.

2) A shear specimen was designed to study brittle fracture in mode II for different shear loading conditions. The finite element analysis showed that, depending on the loading conditions, the specimen could provide a considerable positive or negative T in conjunction with the singular terms of stresses.

3) Shear tests were carried out on PMMA using the proposed specimen. The results of experiments showed that the mode II fracture toughness in the $-T$ shear specimen is significantly higher than that in the $+T$ shear specimen. The direction of crack growth initiation is also considerably changed for the two loading conditions.

4) It was shown that the mode II fracture toughness and the direction of crack growth initiation predicted using the failure diagram are in good agreement with the experimental results obtained from the $+T$ and $-T$ shear tests.

5) The fractography of the specimens showed that the features observed across the fracture surface in the $+T$ shear specimens are considerably different from those observed in the $-T$ shear specimens.

6) A statistical function based on the Weibull probability model was used to predict the distribution of fracture toughness results. It was shown that the function which has already been used widely for cleavage fracture in steels can also be employed to predict the results of brittle fracture in PMMA for both $+T$ and $-T$ shear tests.

CHAPTER SEVEN

EFFECTS OF GEOMETRY AND CONSTRAINT IN MIXED MODE LOADING

7-1. INTRODUCTION

It was shown in previous chapters that the magnitude of the T-stress can be significant in cracked specimens subjected to mixed mode loading. By taking the T-stress into account, a generalised maximum tangential stress (MTS) criterion in terms of the parameters K and T was suggested for linear elastic mixed mode fracture. The significant effect of the T-stress on the mode II fracture toughness was also shown experimentally for a typical brittle material. However, all of these previous studies have been based on linear elastic fracture mechanics.

For metallic components, an often significant volume of material around the crack tip undergoes plastic deformation prior to crack growth. Therefore, elastic-plastic stress and strain fields should be employed to study fracture conditions. Metals with lower ductility fail in a brittle manner by cleavage fracture of the grains. Conversely, for highly ductile materials failure is often associated with slow crack growth and a significant amount of plastic deformation. Two major mechanisms of duc le crack growth in metallic alloys are the mechanism of void growth and coalescence, and the mechanism of shear localisation and decohesion.

As described in Section 2-7-2, the effects of geometry and loading conditions in mode I fracture can be quantified by a dimensionless constraint parameter Q. The parameter Q describes the difference between the actual near crack tip stresses and the stresses obtained from the HRR solution. For small scale yielding where the maximum radius of the plastic zone is small compared to the relevant lengths in the cracked specimen,

the constraint parameter Q can be obtained in terms of the remote elastic T-stress. O'Dowd and Shih (1992) have used a so-called boundary layer formulation to obtain the relation between Q and T for several hardening coefficients in mode I. They have also shown that Q can be used as a constraint parameter for both brittle fracture and ductile fracture where this is a result of the mechanism of void growth.

Although substantial work has been carried out to show that the far-field elastic T-stress has a significant influence on the near crack tip stresses, almost all of these investigations have been confined to pure mode I. In this chapter, a boundary layer formulation is described and a method for determining the constraint parameter Q is presented for mixed mode loading. The effect of the T-stress on different crack tip parameters is studied and a Q-T diagram is obtained for mode II. Finite element analysis is also carried out to calculate the constraint parameter Q for several shear specimens and the results are compared with those predicted by the Q-T diagram. The influence of the T-stress on both mode II brittle fracture and mode II ductile fracture is also discussed. For ductile fracture the T-stress effect is studied for both the mechanism of void growth and coalescence, and the mechanism of shear localisation.

7-2. QUANTIFYING Q FOR MIXED MODE PROBLEMS

In this section, the modified boundary layer formulation and a method for quantifying the constraint parameter Q are described for mixed mode loading.

7.2.1. Boundary layer formulation

The boundary layer formulation described in section 2-7-1 for pure mode I can be used to simulate the small scale yielding conditions for a mixed mode crack. A circular region containing an edge crack is considered such that the crack tip placed on the centre of the circle. Elastic-plastic material properties are used. The traction or displacements corresponding to the elastic mixed mode fields are applied along the circular boundary. To comply with the requirements for small scale yielding an appropriate magnitude for the boundary conditions is chosen such that the maximum radius for the plastic zone around the crack tip remains very small compared with the radius of the circle.

If singular terms alone define the boundary conditions, the stresses inside the plastic zone are expected to be consistent with the singular stresses presented by Shih (1974) and described in Section 2-2-3, for mixed mode loading. The boundary layer formulation can also be modified to include the T-stress in the boundary conditions. For the state of plane strain, these boundary conditions are

$$u_x(\theta) = K_I \frac{1-\nu}{E}\sqrt{\frac{R}{2\pi}}\cos\frac{\theta}{2}\left[(1-2\nu)-\sin^2\left(\frac{\theta}{2}\right)\right]+ K_{II}\frac{1-\nu}{E}\sqrt{\frac{R}{2\pi}}\sin\frac{\theta}{2}\left[2(1+\nu)+\cos^2\left(\frac{\theta}{2}\right)\right]+T\frac{1-\nu^2}{E}R\cos\theta \tag{7-1a}$$

$$u_y(\theta) = K_I \frac{1-\nu}{E}\sqrt{\frac{R}{2\pi}}\sin\frac{\theta}{2}\left[2(1+\nu)-\cos^2\left(\frac{\theta}{2}\right)\right] -K_{II}\frac{1-\nu}{E}\sqrt{\frac{R}{2\pi}}\cos\frac{\theta}{2}\left[(1-2\nu)-\sin^2\left(\frac{\theta}{2}\right)\right]-T\frac{\nu(1+\nu)}{E}R\sin\theta \tag{7-1b}$$

where u_x and u_y are the displacement components in x and y directions, and R is the radius of the circle.

Unlike the pure mode I case, where due to symmetry only one half of the model can be simulated, a mixed mode boundary layer formulation should be modelled using the full circular region.

7-2-2. Determination of the constraint parameter Q

In Section 2-7-2 the dimensionless parameter Q was introduced to quantify the crack tip constraint in pure mode I. This was achieved by evaluation of the stresses ahead of the crack tip along the crack line where fracture initiation is expected to o ur. The mode I constraint parameter Q_I corresponding to brittle fracture is determined as

$$Q_I = \frac{\sigma_{\theta\theta}-(\sigma_{\theta\theta})_{REF}}{\sigma_o} \quad \text{along } \theta = 0 \text{ for } 1 \le \frac{r\sigma_o}{J} \le 5 \tag{7-2}$$

where σ_o is the yield stress, $\sigma_{\theta\theta}$ is the actual tangential stress and $(\sigma_{\theta\theta})_{REF}$ is either the HRR solution for mode I or the boundary layer solution for small scale yielding with T=0. A similar formulation can be used to determine $Q_{I,II}$ for mixed mode loading.

However, in this case, brittle fracture no longer takes place along the crack line. If the maximum tangential stress (MTS) criterion is adopted for predicting the direction of fracture initiation, the crack tip constraint should be studied along the direction of maximum tangential stress θ_o around the crack tip. Therefore, the constraint parameter in brittle fracture for mixed mode loading $Q_{I/II}$ can be determined from

$$Q_{I/II} = \frac{\sigma_{\theta\theta} - (\sigma_{\theta\theta})_{REF}}{\sigma_o} \quad \text{at } \theta = \theta_o \quad \text{for } , 1 \le \frac{r\sigma_o}{J} \le 5 \tag{7-3}$$

where here $(\sigma_{\theta\theta})_{REF}$ is either the singular solution for $\sigma_{\theta\theta}$ given by Shih (1974) or the mixed mode boundary layer solution for small scale yielding (T=0) with the appropriate combination of the mode I and mode II components of the displacements along the circular boundary of the model.

Shih (1974) has shown that the direction of maximum tangential stress θ_o depends on both the mode mixity and the material properties. Therefore, the method of determining Q in mixed mode (or even in pure mode II) is more complicated than that for pure mode I. This is described in more detail later in Section 7-3-2. Because of the large amount of computational effort required to evaluate Q for mixed mode loading, the remaining parts of this chapter are confined to pure mode II. However, the same methodology can be employed for mixed mode.

7-3. CONSTRAINT EFFECTS IN MODE II BRITTLE FRACTURE

In this section the constraint near the tip of a mode II crack is studied. A relation between T and Q is obtained using a modified boundary layer formulation. The variation in Q is also determined for several pure shear specimens and is compared with those predicted by the Q-T diagram.

7-3-1. Finite element modelling for boundary layer formulation

An appropriate boundary layer formulation was used in the finite element code ABAQUS (1997) to study the near crack tip stresses in mode II loading. The finite element mesh for the boundary layer model of radius 200mm is shown in Fig 7-1. Thirty rings of elements were considered where each ring consisted of 35 eight-noded plane strain elements in the circumferential direction. The density of nodal points was

biased towards the crack tip such that the length of the elements in the first ring next to the crack tip was $5.5*10^{-7}$ times the radius of the boundary layer model. The Ramberg-Osgood equation with n=8 and α_o=1.4 was used for the plastic material properties. Young's modulus, Poisson's ratio and the yield stress were 214 GPa, 0.3 and 400 MPa respectively. These material properties which are related to A508 steel were determined from a standard tensile test carried out by Davenport (1993).

The mode I stress intensity factor K_I was set to zero in eqs 7-1a and 7-1b and the resulting displacement components were applied along the circular boundary. Three sets of finite element analyses with T>0, T=0 and T<0 were carried out to study the effect of the T-stress on the shape and size of the plastic zone near the tip of a mode II crack. The plastic zone represents the region where the effective stress σ_{eff} exceeds the yield stress σ_o and hence undergoes plastic deformation. It is noted that the normal-to-the-crack component of displacement u_y is much less than the parallel-to-the-crack component of displacement u_x in pure mode II. This is shown in Fig 7-1 for T=0.

The size of plastic zones obtained from the three analyses and normalised with respect to $(K_{II}/\sigma_o)^2$ are seen in Figs 7-2a to 7-2e for T/σ_o =+0.4, +0.2, 0, -0.2 and -0.4, respectively. As expected, Fig 7-2c shows that the plastic zone in mode II for the case of T=0 is symmetric with respect to the crack line. It is seen from Figs 7-2a, 7-2b, 7-2d and 7-2e that the plastic zone is no longer symmetric when T takes a non-zero value. The significant effect of T-stress on the shape of the plastic zone suggests that the elastic-plastic fields near the tip of a mode II crack can change considerably for different values of T.

7-3-2. *T*-stress effect on mode II crack tip stresses

The finite element model described in the previous section was employed to study the effect of T on the near crack tip stresses in a mode II boundary layer formulation with small scale yielding conditions. The mode II stress intensity factor K_{II} and three values of T/σ_o =-1, T/σ_o =0 and T/σ_o = +1 were considered by applying the associated elastic displacements along the circular boundary of the model. The parameters K_{II} and T were applied incrementally with a fixed ratio of T/K_{II} throughout each analysis. To keep the size of the plastic zone very small compared with the radius of the circular boundary R , the stress intensity factor K_{II} was considered to be 53 MPa$\sqrt{m}$. In this case the maximum radius for the plastic zone was less than 0.06 of R.

To study the T-stress effects relevant to brittle fracture, the maximum tangential stress criterion was adopted and the stresses evaluated along the direction of maximum tangential stress θ_o. The material properties were the same as those described in the previous section.

For the analysis with T/σ_o =0, the angle θ_o was equal to -76° and was independent of the magnitude of load. Because θ_o was not necessarily in line with one of the radial sets of nodes in the finite element mesh, the stresses along this direction had to be determined by a cubic interpolation between adjacent nodes. For the other two analyses where $T/\sigma_o \neq 0$, the maximum tangential stress angle θ_o changed with the magnitude of T/σ_o on the boundary. Therefore, the numerical interpolation had to be redone separately for each increment. The extremes for θ_o were -84.6° for T/σ_o =-1 and -64.9° for T/σ_o =+1. The stages described above show that the computational work needed to calculate the crack tip constraint for mode II (and similarly for mixed mode) is much more than that for pure mode I.

The stresses calculated along θ_o were normalised with respect to the yield stress σ_o and were plotted versus the normalised distance $r\sigma_o/J$ from the crack tip. With this normalisation it was observed that the results for T/σ_o =0 obtained for each component of stress were the same irrespective of the load.

Fig 7-3 and 7-4 show normalised $\sigma_{\theta\theta}$ and σ_{rr} obtained along the direction θ_o for different values of T/σ_o. It is seen that T can influence significantly the stresses near the crack tip. Both $\sigma_{\theta\theta}$ and σ_{rr} are increased by positive values of T/σ_o and decreased by negative values of T/σ_o. All of the curves for each component of stress are almost parallel between $1 \leq (r\sigma_o/J) \leq 5$. This implies that the stress corresponding t given value of T/σ_o can be predicted if the small scale yielding solution with T=0 is shifted up or down by an appropriate amount.

7-3-3. Relation between T and Q in mode II

It is known in mode I that Q can be predicted from the elastic T-stress at least for small scale yielding. In this section Q is first found in terms of T using a mode I boundary layer formulation and the results are compared with those presented by

other workers so as to validate the computational method used here. Next, a mode II boundary layer formulation is used to find Q in terms of T/σ_o for pure shear.

Mode I - validation

To validate the finite element procedure used here for computing Q in mode II, the boundary layer model was first subjected to the pure mode I boundary conditions. Three analyses were carried out with T/σ_o = -1, 0 and +1. Linear elastic-power law hardening material properties with n=10, ν=0.3 and ε_o=1/300 (where $\varepsilon_o = \sigma_o/E$) were used. The constraint parameter Q_I was calculated from eq 7-2 at $r = 2J/\sigma_o$ for different values of T/σ_o on the circular boundary. The tangential stress $\sigma_{\theta\theta}$ obtained from the boundary layer formulation with T=0 was considered for $(\sigma_{\theta\theta})_{\text{REF}}$. Fig 7-5 shows that the results of the present analysis for Q_I versus T/σ_o are in good agreement with those given by O'Dowd and Shih (1994).

Mode II

Just as for eq 7-2, the constraint parameter in a mode II crack problem Q_{II} is calculated from

$$Q_{II} = \frac{\sigma_{\theta\theta} - (\sigma_{\theta\theta})_{REF}}{\sigma_o} \quad \text{along } \theta = \theta_o \text{ , at } 1 \le \frac{r\sigma_o}{J} \le 5 \tag{7-4}$$

where $(\sigma_{\theta\theta})_{\text{REF}}$ can be obtained either from the HRR solution for mode II or from a mode II boundary layer formulation with T=0. The HRR solution for $\sigma_{\theta\theta}$ in mode II is rewritten as

$$\frac{\sigma_{\theta\theta}}{\sigma_o} = \left(\frac{1}{\alpha_o \varepsilon_o (I_n)_{II}}\right)^{\frac{1}{n+1}} \left(\frac{r\sigma_o}{J}\right)^{\frac{-1}{n+1}} \left(\tilde{\sigma}_{ij}(n,\theta)\right)_{II} \tag{7-5}$$

where the subscript II for I_n and $\tilde{\sigma}_{\theta\theta}$ indicates that the mode II values of these functions should be used. The analytical results presented by Shih (1974) show that for n=8, the direction of maximum tangential stress in mode II is about -77°. If the tables of Symington et al. (1988) are employed to determine $(I_n)_{II}$ and $\left(\tilde{\sigma}_{\theta\theta}(\theta,n)\right)_{II}$ for θ_o= -77° and n=8, the results of eq 7-5 is simplified to

$$\frac{\sigma_{\theta\theta}}{\sigma_o} = (2.01)\left(\frac{r\sigma_o}{J}\right)^{-1/9} \tag{7-6}$$

Fig 7-6 shows the results of eq 7-6 together with those obtained from the mode II boundary layer formulation with T=0, described earlier. It is seen that the difference between the two curves is negligible and hence either of them can be used for calculating Q_{II}. In this study $(\sigma_{\theta\theta})_{BLM,T=0}$ is employed as the reference stress.

Small strain finite element analysis was performed for three hardening coefficients n=3, 8 and 13. The other material properties were the same as those given in Section 7-3-1. The tangential stress $\sigma_{\theta\theta}$ was calculated at the end of each load increment along the direction of maximum tangential stress θ_o, which varied with increasing load. The variation of the angle θ_o with T/σ_o is shown in Table 7-1. The mode II constraint parameter Q_{II} was calculated using eq 7-4 at the distance r=2J/σ_o from the crack tip.

Fig 7-7 and Table 7-2 show the relation between Q_{II} and T/σ_o for mode II loading with small scale yielding conditions for n=3, 8 and 13. It is seen that Q_{II} is positive for positive values of T/σ_o and negative for negative values of T/σ_o. The absolute value of Q_{II} is also higher for materials having a lower plastic hardening coefficient n.

To study the effect of T-stress in mode I, previous work has shown that either the radial stress or the mean stress may be used, either calculation providing similar results. Therefore, two equations similar to eq 7-4 will be used to evaluate the corresponding Q_{II} parameters.

$$(Q_{II})_{rr} = \frac{\sigma_{rr} - (\sigma_{rr})_{BLM,T=0}}{\sigma_o} \quad \text{along } \theta = \theta_o \text{, at } 1 \le \frac{r\sigma_o}{J} \le 5 \tag{7-7}$$

$$(Q_{II})_{m} = \frac{\sigma_{m} - (\sigma_{m})_{BLM,T=0}}{\sigma_o} \quad \text{along } \theta = \theta_o \text{, at } 1 \le \frac{r\sigma_o}{J} \le 5 \tag{7-8}$$

where $(Q_{II})_{rr}$ and $(Q_{II})_m$ are the difference field for the radial and mean stresses. Because the crack tip stresses are used to study for the effect on mode II brittle fracture, $(Q_{II})_{rr}$ and $(Q_{II})_m$ are also calculated along the direction of maximum tangential stress θ_o.

Eq 7-7 and 7-8 were calculated at the distance $r=2J/\sigma_o$ from the crack tip for $n=8$ and for different values of T/σ_o . Fig 7-8 shows the results obtained for $(Q_{II})_{rr}$ and $(Q_{II})_m$ together with those obtained earlier for the tangential stress $(Q_{II})_{\theta\theta}$. It is seen that the results have a similar trend and the maximum difference between $(Q_{II})_{\theta\theta}$ and $(Q_{II})_m$, which occurs at $T/\sigma_o=-1$, is less than 0.1 .

Figs 7-9a, 7-10a and 7-11a show the effect of T/σ_o on the angular distributions of the stresses $\sigma_{\theta\theta}$, σ_{rr} and σ_m normalised with respect to the yield stress σ_o and calculated at the distance $r=2J/\sigma_o$ from the crack tip. Figs 7-9b, 7-10b and 7-11b show the difference between these components of stress for different values of T/σ_o and those obtained for $T/\sigma_o=0$.

7-3-4. Variation of Q in mode II crack geometries

In real specimens, the variation of the constraint parameter Q with load can be determined directly from the near crack tip stresses using finite element results. Alternatively, the Q parameter can be predicted from a Q-T diagram using the value of the T-stress corresponding to the load. In this section the variation of Q with applied load is obtained for several mode I and mode II specimens. The results of the mode I analysis are used to validate the calculation method. The finite element results for Q are used to study the extent of validity of the results obtained from the Q-T diagram.

Mode I - validation

The variation of the constraint parameter Q is first calculated for a mode I crack specimen and the results are compared with those presented by other researchers. This can be used for validation of the procedure employed here to determine the variations of Q with load in mode II crack geometries.

A crack of length 20 mm was considered in a 200 mm by 200 mm square plate. A linear elastic-power law hardening material model with $n=10$ and $\varepsilon_o=1/300$ was used as before. The yield stress, Young's modulus and Poisson s ratio were 400 MPa, 120 GPa and 0.3, respectively. The specimen was plane strain and was subjected to a remote uniform load normal to the crack line. The load was increased until a large plastic zone extended from the crack tip towards the boundary of the specimen. Finite element analysis was employed to calculate the constraint parameter Q from eq 7-2 at the end of several load increments throughout the analysis. Fig 7-12 shows the

variation of Q versus $\log(J/a\sigma_o)$ where a is half the crack length. It is seen that the results obtained here are in good agreement with those presented by O'Dowd and Shih (1992) for a similar crack problem.

Mode II - Shear loading of the mixed mode specimen

A mixed mode test specimen (Fig 4-9) consisting of a single edge notched (SEN) specimen and a fixture was described in detail in Section 4-5. Different mode mixity from pure mode I to pure mode II could be achieved in the SEN specimen by changing the angular position of the tensile load applied to the fixture. Three models were suggested to simulate the connection between the SEN specimen and the fixture: (i) contact model, (ii) pinned model and (iii) perfect connection model.

In this section the three models are subjected only to pure shear and with a crack length to specimen width ratio a/W in the SEN specimen of 0.5. The finite element simulation, which was described in detail in Section 4-5, is not repeated here.

Two finite element analyses are carried out for each model. In the first analysis, where Q_{II} is determined from a full field solution, the fixture has linear elastic material properties with E=500 GPa and ν=0.3 . The SEN specimen is considered to be elastic-plastic with material properties given in Section 7-3-1 for A508 steel. The shear load is increased beyond the load at which full plasticity takes place in front of the crack tip in the SEN specimen. The constraint parameter Q_{II} is calculated at $r=2J/\sigma_o$ along the direction of maximum tangential stress at different load increments throughout the analysis.

In the second finite element analysis, both the fixture and the SEN specimen are linear elastic. An arbitrary shear load P_s is applied to the specimen and the relation between the T-stress and P_s is obtained as

$$T = Y_s . P_s \tag{7-9}$$

where Y_s is a constant factor depending on the type of connection between the fixture and the SEN specimen. The T-stress is then determined at the same loads used to calculate Q_{II} in the first FE analysis. These values of T are employed to determine Q_{II} from Fig 7-7 according to the Q-T diagram for n=8.

The constant factor Y_s was found as 0.53, 4.3 and 0 MPa/kN for the perfect connection model, the contact model and the pinned model, respectively. Fig 7-13 shows the results for Q_{II} obtained from the full field solution compared with those determined from the Q-T diagram for the perfect connection model. Similar results are shown in Figs 7-14 and 7-15 for the contact and pinned models. It is seen in these figures that the results of the two approaches are in good agreement only for small scale yielding ($\log(J/a\sigma_o)$ <-3.5). As the load is increased, the difference between the results becomes significant. For loads higher than those to cause full plasticity, the value of Q_{II} drops significantly for increasing load.

Figs 7-16 to 7-18 display the variation of the tangential stress $\sigma_{\theta\theta}$ normalised with respect to the yield stress σ_o obtained from the first FE analysis with the elastic-plastic SEN specimen. Figs 7-16 and 7-17 show the variations of $\sigma_{\theta\theta}/\sigma_o$ along the direction of maximum tangential stress θ_o for the perfect connection and the contact models, respectively. The change in the angular distribution of $\sigma_{\theta\theta}/\sigma_o$ at $r=2J/\sigma_o$ from the crack tip is shown in Fig 7-18 for the pinned model. These results will be discussed later in Section 7-5-3.

7-4. CONSTRAINT EFFECTS IN INITIATION OF MODE II DUCTILE FRACTURE

Two major microscopic mechanisms of ductile tearing in metallic alloys were described earlier in Section 2-3. In this section, the crack tip fields are evaluated from a mode II boundary layer formulation to study the possible effects of the T-stress on the initiation of ductile fracture in the shear loading of cracked specimens.

7-4-1. Mechanism of void growth and coalescence

The void growth in ductile metallic alloys takes place when the inclusions and impurities near the crack tip are separated from the surrounding materials due to local tensile deformation. The initiation of ductile tearing is associated with excessive void growth and coalescence between the crack tip and the void nearest to the crack tip. Mathematical models such as those suggested by Rice and Tracey (1969) and Rousselier (1989) show that the mechanism of void growth and coalescence is mainly dependent on the ratio of mean stress σ_m to the effective stress σ_{eff} given by

$$\frac{\sigma_m}{\sigma_{eff}} = \frac{(\sigma_{xx}+\sigma_{yy}+\sigma_{zz})/3}{\sqrt{\frac{1}{2}\left[(\sigma_{xx}-\sigma_{yy})^2+(\sigma_{yy}-\sigma_{zz})^2+(\sigma_{zz}-\sigma_{xx})^2+6(\sigma_{xy}{}^2+\sigma_{yz}{}^2+\sigma_{zx}{}^2)\right]}} \quad (7\text{-}10)$$

It is expected that the crack growth in specimens failing by the void growth mechanism initiates along the direction of maximum σ_m/σ_{eff}. For pure mode I, this direction corresponds to θ=0 i.e. ahead of the crack tip along the crack line.

The mode II boundary layer formulation described in Section 7-31 is employed here to determine the direction of maximum σ_m/σ_{eff} in shear loading. The T-stress on the remote boundary is also changed and its effect on σ_m/σ_{eff} is studied along this direction. Results are shown in Fig 7-19a and 7-19b. It can be seen from Fig 7-19a that the angle θ for the maximum σ_m/σ_{eff} is about -110° for T/σ_o=0. This angle increases and decreases slightly for positive and negative values of T/σ_o, respectively. Fig 7-19b shows the angular distribution of σ_m/σ_{eff} obtained for different values of T/σ_o subtracted by σ_m/σ_{eff} corresponding to the boundary layer formulation with T/σ_o=0. It is seen that the T-stress has a significant influence on σ_m/σ_{eff}, particularly for $-120° \le \theta_o \le 120°$. This will be discussed in more detail later.

7-4-2. Mechanism of shear decohesion

In this mechanism shear bands are formed between the tip of the crack and microvoids near the crack tip. Ductile tearing initiates when the shear deformation is localised and decohesion takes place along the shear band. The shear decohesion mechanism is expected to occur in a region of high shear deformation around the crack tip.

To determine the possible directions of crack growth by this mechanism for a mode II crack problem; two parameters, the shear stress $\sigma_{r\theta}$ and the effective stress σ_{eff}, are studied around the crack tip. The mode II boundary layer formulation is used to investigate the effects of the T-stress on these parameters.

Fig 7-20a and 7-21a show the angular functions of the shear stress and the effective stress normalised with respect to the yield stress for different values of T/σ_o. The results are for $r=2J/\sigma_o$. Both functions are a maximum at about θ=0 ahead of the crack tip along the crack line. The effect of T/σ_o on the directions of maximum shear stress and maximum effective stress is negligible.

Figs 7-20b and 7-21b display the difference fields for these parameters, obtained by subtracting the results of small scale yielding with T=0 from those for the boundary layer formulation with different values of T/σ_o. It is seen from these figures that ahead of the crack tip, where shear decohesion is expected to take place, the T-stress has little effect on the shear stress and the effective stress.

7-5. DISCUSSION

7-5-1. Boundary layer formulation

Shih (1974) has shown for an elastic-plastic mixed mode crack problem, the singular stresses near the crack tip can be described fully by two parameters: the J-integral and the near crack tip mixity parameter M^p given by

$$M^p = \frac{2}{\pi}\tan^{-1}\left|\lim_{r\to 0}\frac{\sigma_{\theta\theta}(r,\theta=0)}{\sigma_{r\theta}(r,\theta=0)}\right| \tag{7-11}$$

For small scale yielding the far field elastic stresses are also characterised by two parameters: K_I and K_{II} or alternatively J and the far field mixity parameter M^e given by

$$M^e = \frac{2}{\pi}\tan^{-1}\left|\lim_{r\to \infty}\frac{\sigma_{\theta\theta}(r,\theta=0)}{\sigma_{r\theta}(r,\theta=0)}\right| = \frac{2}{\pi}\tan^{-1}\left|\frac{K_I}{K_{II}}\right| \tag{7-12}$$

According to Shih (1974), there is a unique relation between M^e and M^p in terms of the hardening coefficient n. For hardening materials (n>1), M^p is always larger than M^e. Although the mixity parameters are not the same near and far from the crack tip, the singular stresses inside the plastic zone are always identical for different geometries having similar elastic stress intensity factors K_I and K_{II} in the elastic far field. These singular stresses can be determined by a boundary layer formulation (with T=0) having the same material properties and stress intensity factors as those of the actual geometry.

It is important to note that the results obtained from the actual geometry and those of the boundary layer formulation are not consistent once small scale yielding conditions are exceeded. This restriction is more significant for mixed mode than for pure mode

I. In pure mode I excessive plastic deformation influences mainly the higher order terms and not the singular terms of the near crack tip stresses, whereas in mixed mode loading it also affects the near field mode mixity parameter M^P and hence the singular stresses. This implies that for moderate or large scale yielding in mixed mode problems, the method described for determining $Q_{I/II}$ using eq 7-3 is not accurate as the difference between the tangential stresses in this equation contains a contribution from the singular term.

7-5-2. Plastic zone in mode II

The effect of the T-stress on the shape of the plastic zone was first studied by Larsson and Carlsson (1973) for mode I. According to their results, the maximum radius of the plastic zone $(r_p)_{max}$ is enlarged by a compressive T-stress. Also the symmetric lobes of the plastic zone rotate forward. The opposite occurs for a positive T-stress: the plastic zone is contracted and rotates backwards.

Fig 7-2 shows the T-stress effect on the mode II plastic zone. For T=0, the plastic zone is symmetric with respect to the crack line and the maximum radius $(r_p)_{max}$ is along θ =0 (see Fig 7-2c). The plastic zone also contains two parts: a larger front part and a smaller rear part. The T-stress which makes the shape of the mode II plastic zone shape asymmetric, influences both the front and the rear parts of the plastic zone. A positive T causes the direction of $(r_p)_{max}$ in the front part to rotate downwards. This rotation increases for larger values of T/σ_o. The rear part of the plastic zone is also influenced by the T-stress. The lower section in the rear part is enlarged by a positive T whereas the upper section is contracted.

The effect of negative T on the shape of the plastic zone is opposite to the effect of positive T. A comparison between Figs 7-2a and 7-2e (or Figs 7-2b and 7-2d) indicates that the mode II plastic zone for a positive value of T is a mirror image of that for a negative value of T.

7-5-3. Effect of constraint for brittle fracture

The influence of the T-stress on the mode II brittle fracture was described in Section 7-3. To compare the results obtained in this study for mode II with those obtained by

other workers for mode I a short review of the previous findings for constraint effects on mode I brittle fracture is presented here.

Larsson and Carlsson (1973) carried out a number of finite element analyses for different mode I specimens and showed that for similar values of stress singularity, the near crack tip stresses inside the plastic zone can be significantly different. Betegon and Hancock (1991) attributed this discrepancy to the crack tip constraint. They used a mode I boundary layer formulation and showed that the near field stresses can be predicted by the HRR solution only for specimens having a highly constrained plastic zone. Betegon and Hancock also showed that the crack tip constraint is high for specimens having a positive T and is low for specimens having a negative T. They suggested a two parameter (J-T) characterisation for mode I crack tip fields.

O'Dowd and Shih (1991) argued that a J-T formulation is confined to small scale yielding because the elastic term T has no relevance to the fully plastic conditions. They suggested a J-Q approach to describe fully the crack tip fields in mode I loading and showed for several cracked specimens that the J-Q approach can be used even beyond small scale yielding.

J-dominance in mode II

Maccagno and Knott (1991) studied experimentally brittle fracture in several steel specimens subjected to mixed mode loading. They suggested that the maximum tangential stress (MTS) criterion can be used for predicting the direction and the onset of brittle crack growth in mixed mode specimens, even in the presence of plastic deformation around the crack tip. However, this conclusion assumes the pure antisymmetric loading for mode II used in their work, and may not be valid for more general cases of mixed mode loading.

Fig 7-3 shows that for a given hardening coefficient n, the effect of a remote T on the tangential stress $\sigma_{\theta\theta}$ along the direction of maximum tangential stress θ_o is independent of $r\sigma_o/J$ for $1 \leq r\sigma_o/J \leq 5$. The tangential stress is increased by positive T/σ_o and decreased by negative T/σ_o. It is seen that for mode II, unlike for pure mode I, positive T/σ_o can increase significantly the tangential stress.

According to Betegon and Hancock (1991), *J*-dominance in pure mode I can be attributed to geometries having zero or positive *T*. A similar phenomenon has been suggested for mixed mode loading by Du et al (1991) who have studied the effect of the *T*-stress on the near crack tip stresses for a limited number of mode I and mode II mixities. However, the results of the present study show that at least for pure mode II both positive *T* and negative *T* can provide a significant discrepancy between the crack tip stresses and the mode II HRR stresses. This implies that along the direction of maximum tangential stress in mode II, *J*-dominance is attributed only to geometries having zero (or negligible) *T*.

Mode II constraint parameter Q_{II}

To determine the mode II constraint parameter Q_{II}, the crack tip stresses were subtracted by the singular stresses obtained from a mode II boundary layer formulation with T=0. Fig 7-6 shows that the singular stress obtained from this method are in very good agreement with those of the mode II HRR solution. This agreement is better for mode II than for mode I. The numerical results by Betegon and Hancock (1991) show that the mode I HRR stresses are noticeably higher than those of the boundary layer formulation.

Fig 7-3 shows that the tangential stresses for different values of T/σ_o are parallel between $r\sigma_o/J$=1 and $r\sigma_o/J$=5. Therefore, Q_{II} can be calculated at any point between these two limits. The mode I studies by O'Dowd and Shih (1991) show that the finite element results obtained from a large strain analysis are consistent with those of a small strain analysis except for $r\sigma_o/J \leq 1$. Hence, it is more convenient to use a small strain analysis and take the results further away from the crack tip (say $r\sigma_o/J$ =2) where the effect of the large strains are negligible. Unfortunately no similar data was found in the literature for large strain effects in mode II and so the same effect was assumed here, the stresses being always evaluated at $r\sigma_o/J$=2.

Fig 7-7 shows that for positive values of T/σ_o, Q_{II} is increased by reducing the hardening coefficient n, which is similar to mode I results (O'Dowd and Shih, 1994) shown earlier in Fig 2-6. For negative values of T/σ_o, Q_{II} is increased for larger values of n which is in contrast with mode I results. It is well known that for n=1, that is for the linear elastic material properties, the *T*-stress in mode I has no effect on the tangential stress in front of the crack tip (θ = 0). Therefore, the mode I constraint parameter Q_I should vanish for n=1. The results presented by O'Dowd and Shih

(1994) for T/σ_o <0 disagree with this argument. Hence, it is suggested that the mode I Q-T diagram can be inaccurate for low values of the hardening coefficients n. For mode II, the direction of fracture initiation θ_o for brittle materials is about -70° (±20° depending on T and n) and the T-stress always influences the tangential stress along this direction, even for a linear elastic material.

Fig 7-8 shows that the constraint parameter calculated for the tangential stress $(Q_{II})_{\theta\theta}$ is in good agreement with that computed for the mean (hydrostatic) stress $(Q_{II})_m$. This implies that along the direction of maximum tangential stress, Q_{II} can be considered as a hydrostatic state of stress influencing mainly the direct stresses. The maximum discrepancy between $(Q_{II})_{\theta\theta}$ and $(Q_{II})_m$ is 0.1 which is related to T/σ_o =-1. A similar figure has been given by O'Dowd and Shih (1994) for the maximum difference between the same parameters in mode I. The effect of T on the crack tip stresses is not confined to the direction of maximum tangential stress θ_o. This is shown for example in Figs 7-9 and 7-11 where the significant effect of the T-stress can be seen for the whole range of -100°≤ θ≤+100°.

Finite geometry shear specimens

The boundary layer formulation assumes that the geometry of the specimen is so large that the crack tip stresses are insensitive to the finite geometry effects. This assumption is no longer applicable for real specimens when the extent of the plastic zone around the crack tip becomes considerable. The accuracy of the constraint parameter Q calculated from the Q-T diagram using the boundary layer formulation can be studied individually for each cracked specimen. The evolution of Q due to increasing external load is determined from the full field solution using finite element analysis and are compared with variations of Q computed from the Q-T diagram.

This has been carried out here for a mixed mode specimen subjected to pure shear with three different connection models. The results are shown in Figs 7-13 to 7-15. It was shown in Chapter 4 that in mode II the T-stress is positive for the perfect connection model, negative for the contact model and zero for the pinned model. A similar trend can be seen in Figs 7-13 to 7-15 for Q_{II} calculated based on the Q-T diagram when the shear load is not high (for instance when $\log(J/a\sigma_o)$<-3.5). The results of the full field solution are in good agreement with those of the Q-T diagram but only up to $\log(J/a\sigma_o)$=-3.25 for the perfect connection model, $\log(J/a\sigma_o)$=-3.5 for

the contact model and $\log(J/a\sigma_o)$=-2.2 for the pinned model. Beyond these limits the discrepancy between the results of two methods becomes significant.

The results of the full field solution indicate that Q_{II} decreases rapidly at higher loads for all three models. This is mainly due to the excessive plastic deformation leading to the relief of constraint around the crack tip. It is observed from Figs 7-13 to 7-15 that the extent of agreement between the results of the full field solution and those of the Q-T diagram and also the onset of the drop in the results of the full field solution vary significantly for different mode II specimens. A similar finding has been reported by O'Dowd and Shih (1992) from the finite element analysis of several mode I specimens.

7-5-4. The effect of constraint for ductile fracture

Figs 7-19 to 7-21 show the effect of the T-stress on some of the characterising parameters in the mode II ductile fracture. For the mechanism of void growth and coalescence, which depends mainly on the ratio of the mean stress to the effective stress σ_m/σ_{eff}, the direction of the maximum σ_m/σ_{eff} varies with T/σ_o within $-120°\leq\theta\leq+120°$ (see Fig 7-19a). Between these two limits σ_m/σ_{eff} is influenced significantly by T/σ_o. In contrast, Figs 7-20a and 7-21a show that T/σ_o has very little effect on the directions of the maximum shear stress and the maximum effective stress which are two important parameter in the mechanism of shear localisation and decohesion. Also the magnitudes of the shear stress and the effective stress are almost insensitive to T/σ_o along these directions.

It should be noted that the magnitudes of the difference fields corresponding to $\sigma_{r\theta}/\sigma_o$ and σ_{eff}/σ_o depend on the normalised distance $r\sigma_o/J$ from the crack tip. However, the angular functions of these parameters and the related difference fields (shown in Figs 7-20b and 7-21b) are not changed significantly by distance. The results shown in Figs 7-20 and 7-21 are calculated at $r=2J/\sigma_o$ from the crack tip to show only the typical distributions of the stresses and the corresponding T-stress effects.

Fig 7-22 compares the effect of T/σ_o on the difference fields related to the shear stress along θ = 0° and σ_m/σ_{eff} along θ =-100°. It is observed that in mode II, T can significantly influence σ_m/σ_{eff} and hence fracture initiation by the mechanism of void

growth. Conversely, $\sigma_{r\theta}/\sigma_o$ as a characterising parameter for fracture initiation by the mechanism of shear decohesion is almost insensitive to T.

It is worth noting that the results shown in Fig 7-22 can be used to understand the T-stress effects only for the initiation stage of ductile fracture. To study the effects of geometry and constraint on the resistance curve associated with the ductile crack growth in shear, an appropriate model should be used to simulate the incremental crack growth beyond the initiation stage.

7-6. CONCLUDING REMARKS

1) A mode II boundary layer formulation was used to study the effect of the remote T-stress on the near crack tip stresses for small scale yielding.

2) It was shown that T has a considerable influence on the shape of the plastic zone around the crack tip in mode II. The shape of the plastic zone for positive T is a mirror image about the crack line of that for negative T of the same magnitude.

3) Along the direction of maximum tangential stress the radial and tangential stresses are increased for positive values of T and decreased for negative values of T. Therefore, a single parameter is not sufficient to describe fully the near crack tip stresses in mode II.

4) The mode II constraint parameter Q_{II} was determined in terms of T/σ_o for small scale yielding. It can be expected that the mode II fracture toughness in brittle materials increases for shear specimens having a negative T-stress and decreases for those having a positive T-stress. The comparison of the results of Q_{II} calculated for both the tangential stress and the mean stress show that Q_{II} can be ısidered as a hydrostatic state of stress in the shear loading of cracked specimens.

5) Q_{II} was calculated for three shear specimens using both the full field solution and the Q-T diagram. The results of the Q-T diagram were in agreement with those of the full field solution for small scale yielding but not for moderate or large scale yielding.

6) It was shown that in mode II, the effect of the T-stress on the initiation of the ductile crack growth can be significant for the mechanism of void growth and coalescence and negligible for the mechanism of shear localisation and decohesion.

CHAPTER EIGHT

GENERAL DISCUSSION

8-1. INTRODUCTION

The results of the theoretical and experimental studies carried out in this research have already been discussed separately in the preceding chapters. The aim of this chapter is to present a general discussion to integrate the major findings of the thesis and to describe in more detail some of the results not discussed before.

The significance of the higher order terms of stresses, in particular the T-stress, for describing the crack tip stresses are discussed. The difference between antisymmetric loading and general shear loading is elaborated. The maximum tangential stress (MTS) criterion is compared with the generalised MTS criterion. It is shown that the results of the MTS criterion are not always a conservative prediction for mixed mode fracture.

The results of the previous mode II fracture tests on brittle materials are compared with the results obtained in this research. It is shown that the previous results can be used only for limited practical loading conditions. The effect of the T-stress on the crack tip stresses inside the plastic zone is discussed. It is shown that the T-stress effect in mode II can be very different for the three mechanisms of fracture: brittle fracture, ductile fracture by the mechanism of void growth and ductile fracture by the mechanism of shear decohesion.

8-2. HIGHER ORDER TERMS OF STRESS

In Chapter 3 a series expansion was derived for the elastic stresses near the crack tip in an internally cracked plate. It was shown that the higher order terms of stress are considerable ahead of the crack tip for both σ_{xx} and σ_{yy}. Figs 3-3 and 3-4 show that among these terms the most significant ones are the second term ($r^{1/2}$ term) for σ_{yy} and the second and third terms (T and $r^{1/2}$ terms) for σ_{xx}.

Chao and Zhang (1997) proposed a two-term criterion for mode I brittle fracture and in linear elastic materials. They took into account both the singular term and the $r^{1/2}$ term in σ_{yy} and predicted the onset of crack propagation for a stress-controlled mechanism of fracture. Chao and Zhang showed that the mode I fracture toughness can vary for brittle materials depending on the geometry and the type of loading.

It can be suggested from the results shown in Fig 3-3 that a two-term fracture criterion is considerably more accurate than a single term, at least for the internal crack specimen. The influence of the second term of the series expansion for σ_{yy} in a stress controlled fracture criterion depends on the crack length and the critical radius r_c from the crack tip. A three-term fracture criterion is not expected to be more accurate as Fig 3-3 shows that the third term is negligible near the crack tip. It is noted that the T-term and the $r^{1/2}$ term of the series expansion for σ_{xx} has no influence on fracture toughness in the stress controlled criterion suggested by Chao and Zhang. However, these terms can affect the fracture toughness in a strain-controlled two-term (or three-term) fracture criterion where the opening strain ε_{yy} depends on σ_{xx} because of Hooke's law effects.

The higher order terms of stress can influence considerably the size of the plastic zone in front of the crack tip r_p. It is seen from Figs 3-5 to 3-8 that the plastic zone size predicted from a two term solution (singular term and T term) is generally more accurate than that of the singular term alone. However, Fig 3-7 shows that the effect of the T-term on the plastic zone size depends also on the yield criterion used. For plane stress T has no influence on r_p if the Tresca yield criterion is used. Figs 3-5 to 3-8 show that a three-term approximation for the plastic zone size ($r^{-1/2}$, T, $r^{1/2}$ terms) gives a very good agreement with the exact solution.

A mixed mode fracture criterion by Theocaris and Andrianopoulos (1982a) suggests that fracture in brittle materials occurs when the minimum radius of the plastic zone $(r_p)_m$ around the crack tip attains a critical value. For a mode I crack the minimum radius of plastic zone $(r_p)_m$ is along the crack line in front of the crack tip. Therefore, the higher order terms of stress can influence significantly the fracture toughness in the internal crack specimen, if the criterion suggested by Theocaris and Andrianopoulos (1982a) is used.

It is concluded that a two parameter approach to the characterisation of fracture is more accurate than a single parameter approach, such as the use of the stress intensity factor alone. Indeed, there are circumstances where a single parameter approach will give unacceptably inaccurate results.

8-3. *T*-STRESS IN MIXED MODE LOADING

Despite the significance of the higher order terms of stress, in particular the *T*-stress, they are often ignored in the fracture studies of components. This is mainly due to the computational difficulties for determining the constant coefficients of the series solution which can vary noticeably for different specimens. For example, in comparison with the number of methods to evaluate the stress intensity factor, few methods are known for determining the *T*-stress, particularly in mixed mode loading. Among the methods available for calculating *T*, analytical methods can be used only for simple geometries. Most of the computational methods either require a specific formulation not available in the standard finite element codes or require more than one finite element analysis.

The displacement method described in Section 4-3 is a simple method which can be used to determine *T* for any geometry. Fig 4-8 shows that the finite element results obtained from this method are in good agreement with the analytical results even for the more complicated case of mixed mode loading. The displacement method was used to study the variations of *T* in the mixed mode test specimen shown in Fig 4-9. Fig 4-13 shows that the biaxiality ratio *B*, the dimensionless equivalent to *T*, can change significantly from mode I to mode II. However, its variation depends largely on the loading configuration, represented here by the three connection models between the fixture and the SEN specimen. The maximum variation is seen for the contact model.

An important result which is observed from Fig 4-13 is the presence of the T-stress in mode II loading. It is commonly assumed that T vanishes for mode II. This assumption is mainly due to the series solution presented by Williams (1957) for the crack tip stresses. Let us recall the definitions of mode I and mode II loading. In pure mode I, the crack flanks open without any sliding whereas in pure mode II crack flanks slide without any opening. To provide the conditions necessary for mode II, Williams (1957) assumed an antisymmetric stress field and derived series expansions for stresses and displacements near the crack tip. The Williams' solution for σ_{xx} in mode II shows that T always vanishes for antisymmetric loading. This is in agreement with the results of the pinned model as shown in Fig 4-13. However, it has been shown in this research that there are practical loading conditions where the crack flanks slide without opening (pure mode II) but where an antisymmetric loading does not exist. For these loading conditions, such as the shear loading of the perfect connection and the contact models, there can be a significant T-stress in mode II as shown in Fig 4-13. It is interesting to note that for these two models the magnitude of the biaxiality ratio B in mode II is much more than in mode I. For example, for the contact model the biaxiality ratio in mode II is 7 times that of mode I. The variation of B in mixed mode depends directly on the type of loading, represented here by the connection models.

It can therefore be concluded that the antisymmetric loading is a specific state of general shear loading in which T=0. In the Williams solution for mode II (eq 2-4), both σ_{xx} and σ_{yy} near the crack tip are antisymmetric relative to the crack line, that is the sum of stress at any two symmetric points $(x_o , +y_o)$ and $(x_o , -y_o)$ is zero. But in the general shear loading only σ_{yy} is antisymmetric and the sum of σ_{xx} at any two symmetric points is a constant which is independent of distance from the crack tip and quantitatively is equal to $2T$. However, the other terms of the series solutions for the crack tip stresses in the general shear loading are similar to those presented by Williams for the antisymmetric loading.

8-4. *K-T* FORMULATION FOR LINEAR ELASTIC MIXED MODE FRACTURE

As discussed earlier, the effect of T on the mode I fracture toughness is negligible for a linear elastic material failing by a fracture mechanism controlled by tensile stress.

This is because the T-stress has no influence on the opening stress ahead of the crack tip. However, for mixed mode loading where the direction of fracture initiation θ_o makes an angle with the initial crack, T can affect the tangential stress along θ_o. The generalised maximum tangential stress criterion suggested in Chapter 5 shows that the effect of T on both the direction of fracture initiation and the fracture toughness can be significant (Figs 5-5 to 5-7).

It is important to note that the mixed mode fracture toughness obtained from the conventional MTS criterion (T=0) is not always a conservative prediction because a positive T reduces the fracture toughness as shown in Fig 5-6. In contrast, the results of the conventional MTS criterion can be too conservative when T is highly negative. Figs 5-5 to 5-7 show that the magnitude of the T-stress effect in mixed mode fracture depends on two parameters B and α. The dimensionless biaxiality ratio B represents the ratio of T relative to the stress intensity factor and depends only on the geometry and loading conditions. The parameter α is a dimensionless measure of the radius of the process zone r_c.

Even for very brittle metallic materials, there is a so-called process zone around the crack tip in which materials undergo plastic deformation, large strains and damage. Because of material damage, the stresses inside the process zone are finite and hence the maximum stress often takes place along the boundary of the process zone along the direction of fracture initiation. Therefore, the critical tangential stress for fracture is normally studied at a critical distance r_c from the crack tip which represents the radius of the process zone. The critical distance r_c is often assumed to be a material property and to depend on parameters such as the working temperature, the composition of the material and the environmental factors. Determination of r_c normally requires a mixed experimental and computational technique and a large number of tests. An example of such techniques was described in Chapter 6 for determining r_c for PMMA.

It is seen from Figs 5-5 to 5-7 that the effect of T in mixed mode fracture depends on the size of process zone: the T-stress effect increases for materials having a larger process zone. The direction of fracture initiation θ_o in the conventional MTS criterion (T=0) is independent of material properties and depends only on the mode mixity. This is not the case for the generalised MTS criterion where θ_o is also a function of r_c and can vary for different materials.

In the formulation used in Chapter 5 to quantify the effect of T in mixed mode fracture, the radius of the process zone along the direction of crack growth r_c was assumed to be constant and independent of the mode mixity and the loading conditions. This is firstly because using a mode mixity dependent r_c makes the solution method much more complicated and secondly because there is very little information in the literature about the real size of the process zone for different materials.

8-5. BRITTLE FRACTURE IN MODE II

Figs 5-6 and 5-7 show that the effect of T on the mixed mode fracture toughness is a maximum for pure mode II loading. Therefore, two sets of shear fracture tests were carried out to investigate experimentally the significance of the T-stress effects in mode II for real specimens.

The specimen shown in Fig 6-3a has the following advantages. First, the specimen can provide a significant magnitude of T for both positive and negative shear loading. Secondly, the magnitudes of T, K_I and B are similar for the same magnitudes of positive and negative shear loads. Hence, the same design can be used for both $+T$ and $-T$ shear tests and the relative effect of T on the mode II fracture toughness can be observed directly from the fracture load. Figs 6-7 and 6-8 display the difference between the results of fracture tests for the positive T and the negative T shear tests. The difference can be seen distinctly in the direction of fracture initiation (Figs 6-6 and 6-8) and in the mode II fracture toughness (Fig 6-7).

Mixed mode brittle fracture has been studied by many researchers for different materials. They have often attempted to design test specimens capable of producing symmetric loading for mode I and antisymmetric loading for mode II (*e.g.* Richard, 1981 and Banks-Sills and Bortman, 1986). For pure mode II, Banks-Sills *et al.*(1983), and Banks-Sills and Arcan (1983, 1986) have carried out substantial photoelasticity studies to show that their specimen provides an antisymmetric field of deformation near the crack tip. Similarly, Jones and Chisholm (1975) and Chisholm and Jones (1977) designed a shear specimen to give antisymmetric loading for pure mode II. However, as described earlier in Section 8-3, antisymmetric loading is a specific type of shear loading where in addition to K_I, the T-stress also vanishes. Furthermore, ideal

antisymmetric loading rarely occurs for real engineering components and in practice a considerable value of T-stress can be present for mode II loading, see also Ayatollahi *et al.* (1996 and 1998a). This suggests most of the experimental results presented in the literature for mode II brittle fracture can be used only for a limited set of real applications where the crack tip is subjected to conditions very close to antisymmetric loading.

8-6. CONSTRAINT EFFECTS IN MODE II

8-6-1. Brittle fracture

In materials having some ductility, the crack tip process zone is normally surrounded completely by the plastic zone. In this case, the conditions for brittle fracture should be determined from the elastic-plastic stresses along the boundary of the process zone. However, brittle fracture in these materials often takes place when the plastic zone is still contained by a large elastic volume. Therefore, the remote elastic stresses including the T-stress influence the size and shape of the plastic zone around the crack tip and the stresses inside the plastic zone.

Fig 7-2 shows that a remote T-stress changes appreciably the crack tip plastic zone in mode II. The change in the size of the plastic zone is the same for positive and negative values of T with similar magnitudes. This is not the case in mode I where a positive T decreases the maximum radius of the plastic zone and a negative T increases it. Fig 7-2 also shows that the effect of a positive T on the shape of the plastic zone is exactly opposite to the effect of a negative T.

The conditions necessary for J-dominance, where the crack tip stresses can be described fully by J using the HRR solution, have been studied by different researchers for mode I. Bilby et al. (1986) show that stresses inside the plastic zone can be considerably lower than those of the HRR solution for some standard fracture test specimens. They used a boundary layer formulation and showed that the tangential stress ahead of the crack tip decreases significantly for negative T and increases slightly for positive T. Betegon and Hancock (1991) complemented these studies and proposed that J-dominance or a single parameter characterisation in mode I crack problems corresponds to specimens having positive or zero T whereas a two-parameter characterisation is required for specimens having negative T.

The results of the present research indicate that the conditions for *J*-dominance in mode II are not the same as in mode I, in particular when T is positive. Fig 7-3 shows that the tangential stress $\sigma_{\theta\theta}$ along the direction of maximum tangential stress θ_o in mode II increases considerably with positive T whereas in mode I the effect of positive T on the tangential stress ahead of the crack tip is negligible. However, for both mode I and mode II the tangential stress decreases significantly by negative T. It can therefore be concluded that *J*-dominance in mode II is confined to specimens in which T is zero. For specimens having a non-zero T-stress, two-parameter characterisations must be used.

As described in Section 2-7, Yang et al (1993a and 1993b) and Chao and Ji (1995) proposed a two parameter approach based on J and A_2 to characterise fully the crack tip stresses in mode I. In this approach the higher order terms of stress within the plastic zone are determined analytically and the effect of the important terms is represented by A_2. Yang et al (1993a and 1993b) and Chao and Yang (1996) also studied the application of the J-A_2 approach for mode II loading. They showed that the effect of the higher order terms in mode II is always negligible and a single parameter approach is sufficient for describing the crack tip stresses. However, it should be noted the J-A_2 approach proposed by Yang et al and Chao and Yang for mode II is based on the assumption that the deformation field near the crack tip is always antisymmetric. Therefore, the results of their approach are correct only for specific shear specimens, subjected to antisymmetric loading.

Both the J-T and J-Q approaches described in Section 2-7-2 for mode I were used in Section 7-3-4 to determine the crack tip constraint for three different shear specimens. The mode II constraint parameter Q_{II} was calculated for each specimen using the stresses obtained from finite element analysis and was compared with that predicted from the Q-T diagram. The normalised tangential stresses $\sigma_{\theta\theta}$ along the direction of maximum tangential stress θ_o are shown in Fig 7-16 for the perfect connection model and in Fig 7-17 for the contact model. The tangential stresses are calculated at different load increments.

For the perfect connection model (Fig 7-16) the tangential stress initially increases until a load corresponding to $\log(J/a\sigma_o)$=-3.67 and then decreases significantly below the small scale yielding solution with T=0 (or the HRR solution). The stresses are

almost parallel for $1 \leq r\sigma_o/J \leq 5$, although at higher levels of load ($\log(J/a\sigma_o) > -2.75$) the stress curves diverge slightly. The change in the stress curves can also be predicted by the results shown in Fig 7-13. Since the T-stress is positive in the perfect connection model, the constraint parameter Q_{II} calculated using the Q-T diagram increases as shown by the solid line in Fig 7-13. However, the Q-T diagram, obtained for small scale yielding, does not give accurate results for moderate to large scale yielding. Therefore, the J-T approach cannot be used beyond $\log(J/a\sigma_o) = -3.67$ where the tangential stress begins to reduce due to excessive plastic deformation and loss of constraint. The stresses are still parallel up to full plasticity, that is $\log(J/a\sigma_o) = -2.75$, implying that the J-Q approach is valid for larger extents of plastic deformation. However, for loads higher than that corresponding to full plasticity, the stress curves diverge gradually and the J-Q approach is not suitable to describe the crack tip stresses.

Fig 7-17 shows that for the contact model the tangential stress is always below the HRR solution. The stresses are parallel between $1 \leq r\sigma_o/J \leq 5$ up to $\log(J/a\sigma_o) = -3.49$ and diverge considerably beyond it. It is seen from Fig 7-14 that again the J-T approach is valid for small scale yielding, the J-Q approach can be used up to full plasticity and that a two-parameter characterisation is no longer applicable beyond the full plasticity.

Fig 7-18 shows that for the pinned model the change in the tangential stresses is negligible up to $\log(J/a\sigma_o) = -2.5$. This is in agreement with the results predicted by the J-T approach (Fig 7-15) because in this model the T-stress is zero due to antisymmetric loading. However, the constraint parameter Q_{II} decreases due to excessive plastic deformation and a loss of constraint for loads higher than that to cause full plasticity, that is $\log(J/a\sigma_o) = -1.97$.

Figs 7-13 to 7-15 show that the extent of validity of the J-T approach and the J-Q approach depends significantly on the geometry and loading conditions, represented here by different connection models between the SEN specimen and the fixture. For example, the J-T approach can be used for the pinned model up to $\log(J/a\sigma_o) = -2.5$ whereas for the perfect connection and contact models, the J-T approach is confined to $\log(J/a\sigma_o) < -3.5$. A comparison between Figs 7-16 and 7-17 shows that the applicability of the J-Q approach is more limited for the contact model is than for the perfect connection model.

The *J-T* approach was also used by Du et al (1991) to study the effect of *T* on the crack tip stresses in mixed mode loading. They suggested that *J*-dominance in mixed mode loading is related to specimens having a positive or zero *T*-stress. However, this cannot be seen directly from their results, at least for pure mode II, because they did not show the complete results for the effect of positive *T* on the tangential stress near the crack tip. Furthermore, all of the mixed mode specimens studied by Du et al are mode I dominated ($M^e \geq 0.82$) and they do not show any practical specimens where there is a significant *T*-stress in mode II dominated loading conditions.

As described in Section 7-3-2, the calculation of the constraint parameter *Q* for mixed mode or pure mode II is much more laborious than for pure mode I. This is mainly because the direction of initiation of brittle fracture in mixed mode is not the same as the initial crack line and changes with increasing load. Therefore, the *Q-T* diagram was calculated in this research only for pure mode II.

For mixed mode loading, the *Q-T* diagram may be derived using the same approach as for pure mode II loading, provided the extent of plastic deformation is confined to small scale yielding (see section 7-2-2). This is because, for large scale yielding, the near field mode mixity M^p is not uniquely related to the far field mode mixity M^e (see Shih, 1974). However, it is likely that the results of the *Q-T* diagram for mixed mode lies between the two extremes related to the *Q-T* diagrams for mode I and mode II. The *Q-T* diagram is shown for both mode I and mode II in Fig 8-1 for n=3 and in Fig 8-2 for n=13. Fig 8-1 shows that for materials with high work hardening (small n) mode mixity has little effect on *Q* in specimens having negative *T*. In contrast, Fig 8-2 shows that for materials with low work hardening (large n) the effect of mode mixity on *Q* is not significant for specimens having positive *T*. These arguments cannot be extended to moderate or large scale yielding situations.

8-6-2. Ductile fracture

The two major mechanisms of ductile crack growth in metallic alloys were described earlier in section 2-3. Theoretical models such as those suggested by Rice and Tracey (1969) and Rousselier et al (1989) show that the ratio of the mean stress over the effective stress σ_m/σ_{eff} is the main characterising parameter for the mechanism of void growth and coalescence. The shear stress $\sigma_{r\theta}$ or the effective stress σ_{eff} can be

considered to be the main parameters in the mechanism of shear band localisation and decohesion.

Fig 7-19 shows that for mode II, fracture initiation by the mechanism of void growth is more likely to occur at an angle θ of about -100° where σ_m/σ_{eff} is maximum. Along this direction the effect of a remote T on σ_m/σ_{eff} near the crack tip is significant for both positive and negative T. The angular functions of $\sigma_{r\theta}/\sigma_o$ and σ_{eff}/σ_o around the tip of a mode II crack are shown in Figs 7-20 and 7-21. Both the shear stress and the effective stress are a maximum directly ahead of the crack tip. Along this direction these stresses are almost independent of the remote T-stress.

The effects of the T-stress on $\sigma_{r\theta}/\sigma_o$ along θ=0° and σ_m/σ_{eff} along θ=-100° are compared in Fig 7-22. As described earlier, in addition to J, a second parameter such as T or Q is needed to characterise fully the crack tip stresses for shear loading. It was shown in this research that T and Q, known also as constraint parameters, can vary significantly for different specimens depending on the geometry and loading conditions. The significant effect of T on σ_m/σ_{eff} displayed in Fig 7-22 shows that the initiation of crack growth can vary considerably for different shear specimens failing by the mechanism of void growth and coalescence. In contrast, the initiation fracture toughness in shear specimens failing by the mechanism of shear decohesion is expected to be independent of geometry and loading conditions.

A few researchers have attempted to study experimentally mixed mode crack growth in ductile materials. Almost all of them have reported that the microscopic mechanism of fracture is not the same for mode I and mode II. For example, Tohgo and Ishii (1992), Hallback and Nilsson (1994) and Kamat and Hirth (1996) carried out many experiments on several aluminium alloys and showed that mixed mode specimens failed by the mechanism of void growth and coalescence in mode I and by the mechanism of shear decohesion in mode II. A similar observation has been reported by Swankie (1999) for A508 pressure vessel steel. Experimental and analytical investigations by Wu and Mai (1995) and Hancock et al (1993) for various mode I specimens show that ductile crack growth depends significantly on the geometry and loading conditions of the cracked specimen. These researchers have suggested that the effect of geometry in mode I ductile failure by the mechanism of void growth can be quantified by the constraint parameters T or Q.

Swankie (1999) has recently undertaken numerous mixed mode fracture tests on A508 steel for specimens of different crack length, width and thickness. He shows that in mode II all of the specimens fail by the mechanism of shear decohesion. The results of his pure shear tests show that the effect of geometry on the resistance curve in mode II is negligible. This is in agreement with theoretical findings in the present research which suggest that the mechanism of shear decohesion is almost independent of the geometry and loading conditions in shear specimens.

Mixed mode experiments on ductile metallic alloys often involve a transition from the mechanism of void growth in mode I dominated loading to the mechanism of shear decohesion in mode II dominated loading. The mode mixity corresponding to the transition point varies for different specimens and depends on the material properties. For example, Clayton and Knott (1976) suggest that ductile materials with low or intermediate work hardening are more susceptible to failure by the mechanism of shear decohesion. Therefore, the effects of geometry and constraint in mixed mode ductile fracture which depend on the failure mechanism can vary significantly for different materials as long as there is a competition between the two mechanisms of void growth and shear decohesion.

It can therefore be concluded that the effect of the T-stress in mode II fracture depends on whether the specimen fails by brittle or ductile fracture. For brittle fracture, both positive and negative values of T influence the onset of crack extension. For ductile fracture, the significance of the T-stress depends on the mechanism of crack growth. The T-stress has a negligible effect on fracture initiation where crack growth occurs by the mechanism of shear band localisation and decohesion. Conversely, the effect of the T-stress on the initiation fracture toughness is significant in ductile materials failing by the mechanism of void growth and coalescence.

CHAPTER NINE

CONCLUSIONS AND RECOMMENDATIONS FOR FUTURE WORK

9-1. GENERAL CONCLUSIONS

Concluding remarks have already been outlined at the end of each of the preceding chapters. In this section the major findings of the present thesis are reiterated.

1. A binomial expansion has been used to determine the series solution for the stresses ahead of the crack tip in a mode I internal crack specimen. It was shown that the second term ($\sqrt{r}$ term) in σ_{yy} and the second and third terms (T-term and $\sqrt{r}$ term) in σ_{xx} are not negligible near the crack tip. These terms have a significant effect on the accuracy of the size of the plastic zone in front of the crack tip. It was shown that the magnitude of the effect of the T-stress on the size of the plastic zone can depend largely on the yield criterion used.

2. Simple methods were suggested to determine the T-stress using finite element analysis for any mode I, mode II or mixed mode situation. It was shown that more accurate results with less mesh refinement can be achieved if the crack flank displacements are used to calculate T, instead of the crack flank stresses.

3. It was revealed that, the T-stress is zero in mode II only for purely antisymmetric loading. There are real loading conditions where a significant T-stress is obtained in pure mode II loading.

4. The conventional maximum tangential stress (MTS) criterion has been modified to account for the effect of the T-stress in mixed mode fracture in linear elastic

materials. It was shown that the angle between the crack line and the direction of fracture initiation increases for positive values of T and decreases for negative values of T.

5. The mixed mode fracture toughness predicted by the conventional MTS criterion is not always conservative because the fracture toughness is reduced in mixed mode specimens having a positive T. Conversely, The results of the conventional MTS criterion can be too conservative for specimens having a highly negative T.

6. According to the generalised MTS criterion (K-T formulation), the T-stress effect in mixed mode fracture of linear elastic materials is a maximum for pure mode II and can be considered to be zero for pure mode I.

7. A shear fracture test specimen was designed to investigate experimentally the effects of positive and negative T in mode II fracture of PMMA. The experimental results showed that T has a significant effect on both the direction of fracture initiation and the fracture toughness. The results of the shear tests were in good agreement with those predicted by the generalised MTS criterion. The results of the shear fracture tests showed that the path of crack growth and the features observed across the fracture surface are considerably different for positive T and negative T shear specimens.

8. The effect of a remote T-stress on the plastic zone near the crack tip has been studied in mode II for small scale yielding by using a mode II boundary layer formulation. The shape of plastic zone was influenced significantly by T. The shape of the plastic zone for positive and negative T of the same magnitude were mirror images about the crack line.

9. The results of the boundary layer formulation showed that the tangential stress along the direction of maximum tangential stress was increased by positive T and decreased by negative T. The effect of T on the tangential stress was significant for both positive and negative T. Therefore, J-dominance in mode II is confined to antisymmetric loading for which T=0. For shear specimens having a non-zero T-stress, at least two parameters are needed to characterise fully the crack tip stresses.

10. A Q-T diagram was obtained to determine the mode II constraint parameter Q_{II} in terms of T/σ_o for shear specimens failing by brittle fracture in small scale yielding. The Q-T diagram showed that the magnitude of Q_{II} decreases for materials having a higher work hardening coefficient.

11. Elastic-plastic finite element analysis of three shear specimens showed that the near crack tip tangential stresses can be predicted for contained yielding using a two-parameter characterisation approach. The J-T approach can be used for small scale yielding and the J-Q approach can be used up to full plasticity.

12. The initiation of the ductile crack growth in mode II is influenced significantly by T for the mechanism of void growth and coalescence and is insensitive to T for the mechanism of shear localisation and decohesion.

9-2. POTENTIAL FUTURE WORK

To extend the results obtained from the theoretical and experimental studies carried out in this research, it is suggested that:

1. Using finite element analysis, the variation of the T-stress should be studied further for other mixed mode specimens. The effect of the crack length on the T-stress should be investigated to find out the relationship between T and the crack length for mixed mode loading.

2. The shear fracture experiments on PMMA need to be carried out for similar specimens with different crack lengths to investigate experimentally the effect of the crack length on the mode II fracture toughness in linear elastic materials.

3. The Q-T diagram which was presented in Section 7-3-3 for pure mode II, need to be obtained for mixed mode loading with several different mode mixities using the method outlined in Section 7-2-2.

4. The constraint parameters T and Q studied in this thesis for mode II can be implemented into a failure assessment diagram such as R6 (Milne et al., 1988) to account for the effect of geometry and loading conditions in pure shear failure of engineering components.

5. Shear fracture tests similar to those carried out on PMMA should be undertaken for a metallic alloy which fails by cleavage fracture in mode II with limited plastic deformation around the crack tip . The results of these tests can be used to validate the theoretical results obtained in Chapter 7 for the geometry and constraint effects in the mode II brittle fracture described by T or Q_{II}.

6. Similar shear tests are necessary to investigate experimentally if the initiation fracture toughness is insensitive to geometry and loading conditions for ductile materials failing by the mechanism of shear decohesion in mode II.

REFERENCES

ABAQUS, V 5.7 (1997). *User's Manual.* Hibbitt, Karlsson and Sorensen Inc, Providence, Rhode Island.

Ainsworth, R.A. and O'Dowd, N.P. (1995) Constraint in the failure assessment diagram approach for fracture assessment. *Journal of Pressure Vessel Technology.* **117**, 260-267.

Al-Ani, A.M. and Hancock, J.W. (1991). *J*-dominance of short cracks in tension and bending. *Journal of the Mechanics and Physics of Solids.* **39**, No 1, 23-43.

Aoki, A., Kishimoto, T., Yoshida and Sakata, M. (1987). A finite element study of the near crack tip deformation of a ductile material under mixed mode loading. *Journal of the Mechanics and Physics of Solids.* **35** (4), 431-455.

ASTM E399-90 (1990). Plane strain fracture toughness testing of metallic materials. Vol 3.01. American Society for Testing and Materials. Philadelphia. 487-511.

Ayatollahi, M.R. (1996). Mixed mode ductile fracture. *Internal report*, Department of Mechanical Engineering, University of Bristol, Bristol, UK.

Ayatollahi, M.R., Pavier, M.J. and Smith, D.J. (1996). On mixed mode loading of a single edge notched specimen. *International Journal of Fracture.* **82**, R61-R66.

Ayatollahi M.R., Smith D.J. and Pavier M.J. (1997) Displacement based approach to obtain *T*-stress using finite element analysis, *Proceedings of ASME-PVP Conference*, Atlanta, GA, Volume 346, pp 149-154.

Ayatollahi M.R., Smith D.J. and Pavier M.J. (1998a) A method for calculating *T*-stress for mixed mode problems, *Key Engineering Materials*, **145**, pp 83-88.

Ayatollahi M.R., Pavier M.J. and Smith D.J. (1998b) Determination of *T*-stress from finite element analysis for mode I and mixed mode I/II loading, *International Journal of Fracture* , accepted for publication.

Banks-Sills. L. and Arcan, M. (1983). An edge-cracked mode II fracture specimen. *Experimental Mechanics.* **40**, 257-261.

Banks-Sills. L. and Arcan, M. (1986). A compact mode II fracture specimen. *Fracture Mechanics: Seventeenth Volume, ASTM STP 905.* J.H. Underwood, R. Chait, C.W. Smith D.P. Wilhelm, W.A. Andrews and J.C. Newman, Eds., ASTM, Philadelphia, PA, 347-363.

Banks-Sills. L. , Arcan, M. and Bui, H.D. (1983). Toward a pure shear specimen for K_{IIC} determination. *International Journal of Fracture.* **22**, R9-R13.

Banks-Sills. L. and Bortman, Y. (1986). A mixed-mode fracture specimen: analysis and testing. *International Journal of Fracture.* **30**, 181-201.

Barsoum, R.S. (1976). On the use of isoparametric finite elements in linear fracture mechanics. *International Journal for Numerical Methods in Engineering.* 10, 25-37.

Beachem, C.D. and Yoder, G.R. (1973). Elastic-plastic fracture by homogeneous microvoid coalescence tearing along alternating shear plans. *Metallurgical Transactions.* **4** (4) , 1145-1153.

Betegon, C. and Hancock, J.W. (1991). Two-parameter characterization of elastic-plastic crack-tip fields. *Journal of Applied Mechanics.* **58**, 104-110.

Bhattacharjee, D. and Knott, J.F. (1995). Effect of mixed mode I and II loading on the fracture surface of polymethyl methacrylate (PMMA). *International Journal of Fracture.* **72**, 359-381.

Bilby, B.A. and Cardew, G.E. (1975). The crack with a kinked tip. International Journal of Fracture. **11**, 708-712.

Bilby, B.A., Cardew, G.E., Goldthorpe, M.R. and Howard, I.C. (1986) A finite element investigation of the effect of specimen geometry on the fields of stress and strain at the tips of stationary cracks. *Size Effect in Fracture.* IMechE, UK, 37-46.

Bilby, B.A., Howard, I.C. and Li, Z.H. (1992). Prediction of the first spinning cylinder test using ductile damage theory. *Fatigue and Fracture of Engineering Materials and Structures.* **16** (1), 1-20.

BS-7448 (1991) Methods for determination of K_{IC}, critical CTOD and critical J values of metallic materials. *British Standard*, London, UK.

Budden, P.J. (1987). The stress field near a blunting crack tip under mixed modes 1 and 2. *Journal of the Mechanics and Physics of Solids.* **35** (4), 458-478.

Budden, P.J. and Jones, M.R. (1991). A ductile fracture model in mixed modes 1 and 2. *Fatigue and Fracture of Engineering Materials and Structures.* **14** (4), 469-482.

Burstow, M.C. and Howard, I.C. (1996). Predicting the effects of crack tip constraint on material resistance curve using ductile damage theory. *Fatigue and Fracture of Engineering Materials and Structures*, **19** (4), 461-474.

Cardew, G.E. ,Goldthorpe, M.R. , Howard, I.C. and Kfouri, A.P. (1984). On the elastic T-term. *Fundamentals of Deformation and Fracture.* (Edited by B.A.

Bilby, K.J. Miller and J.R. Willis), Cambridge University Press, Cambridge, UK, 465-476.

Chang K.J. (1981a). Further studies of the maximum stress criterion on the angled crack problem. *Engineering Fracture Mechanics.***14**, 125-142

Chang K.J. (1981b). On the maximum strain criterion-A new approach to the angled crack problem. *Engineering Fracture mechanics.* **14**, 107-124

Chao, Y.J. (1993). On a single parameter controlled fracture of solids under plane stress conditions. *International Journal of Fracture.* **62**, R7-R10.

Chao, Y. J. and Ji, W. (1995). Cleavage fracture quantified by J and A_2. *Constraint Effects in Fracture, Theory and Applications, ASTM STP 1244*, Ed. M. Kirk and A. Bakker, Philadelphia, PA, 3-20.

Chao, Y. J. and Zhang, X.H. (1997). Constraint effect in brittle fracture. *Fatigue and fracture Mechanics: 27th Symposium, ASTM STP 1296,* R.S. Piascik, J. C. Newman, and D.E. Dowling, Eds, American Society for Testing and Materials, 41-60.

Chao, Y.J. and Yang, S. (1996). Higher order crack tip fields and its implication for fracture of solids under mode II conditions. *Engineering Fracture Mechanics.* **55** (5), 777-794.

Chisholm, D.B. and Jones, D.L. (1977). An analytical and experimental analysis of a practical mode II fracture test specimen. *Experimental Mechanics.* **17**, 7-13.

Chow C.L. and Jilin XU. (1985). Mixed mode ductile fracture using the strain energy density criterion. *International Journal of Fracture.* **28**, 17-28

Chow C.L. and Jilin XU. (1986). Response: Discussion of Mixed mode ductile fracture using the strain energy density criterion by E.E. Gdoutos. *International Journal of Fracture.* **30**, R59-R62.

Clayton, J.Q. and Knott, J.F. (1976). Observations of fibrous fracture modes in a prestrained low-alloy steel. *Metal Science*, **10**, 63-71.

Chow, C.L. and Wang J. (1991) A continuum damage mechanics model for crack initiation in mixed mode ductile fracture. *International Journal of Fracture.* **47**, 145-160.

Davenport, J.C.W. (1993). Mixed mode elastic-plastic fracture, *PhD thesis*, Department of Mechanical Engineering, University of Bristol, Bristol, UK.

Davenport, J.C.W. and Smith, D.J. (1993). A study of superimposed fracture modes I, II, III on PMMA. *Fatigue and Fracture of Engineering Materials and Structures.* **16** (10) 1125-1133.

Davenport, J.C.W. and Smith, D.J. (1995). The influence of plasticity and geometry on the mixed mode fracture of PMMA. *Constraint Effects in Fracture, Theory and Applications, ASTM STP 1244*, Ed. M. Kirk and A. Bakker, Philadelphia, PA, 344-360.

Doll, W. (1989). Fractography and failure mechanisms of amorphous thermoplastics. *Fractography and Failure Mechanisms of Polymers and Composites.* A.C. Roulin-Moloney Ed., Elsvier Science Publishers LTD, Essex, England.

Du, Z.Z., Betegon, C. and Hancock, J.W. (1991). *J* dominance in mixed mode loading. *International Journal of Fracture.* **52**, 191-206.

Du, Z.Z. and Hancock, J.W. (1991). The effect of non-singular stresses on crack-tip constraint. *Journal of the Mechanics and Physics of Solids.* **39** (4), 555-567.

Dugdale D.S. (1960). Yielding in steel sheets containing slits. *Journal of the Mechanics and Physics of Solids.* **8**, 100-104.

Edmunds, T.M. and Willis, J.R. (1977). Matched asymptotic expansions in nonlinear fracture mechanics-III. In plane loading of an elastic-perfectly plastic symmetric specimen. *Journal of the Mechanics and Physics of Solids.* **25**, 423-455.

Erdogan, F. and Sih, G.C. (1963). On the crack extension in plates under plane loading and transverse shear. *Journal of Basic Engineering, Transactions of ASME.* **85**, 525-527.

Ewing, P.D, Swedlow, J.L. and Williams, J.G. (1976). Further results on the angled crack problem. *International Journal of Fracture.* **12**, 85-93.

Ewing, P.D. and Williams, J.G. (1974a). The fracture of spherical shells under pressure and circular tubes with angled cracks in torsion. *International Journal of Fracture.* **10**, No 4, 537-544.

Ewing, P.D. and Williams, J.G. (1974b). Further observations on the angled crack problem. *International Journal of Fracture.* **10**, 135.

Fett, T. (1997). A Green's function for *T*-stress in an edge-cracked rectangular plate. *Engineering Fracture Mechanics.* **57**, No 4, 365-373.

Finnie, I. and Saith, A. (1973). A note on the angled crack problem and the directional stability of cracks. *International Journal of Fracture.* **9**, 484-486.

Fischer K.-F. and Goldner H. (1981). On the formulation of principal strain criterion in crack fracture mechanics. *International Journal of Fracture.* **17**, R3-R6

Ghosal, A.K. and Narasimhan, R., (1994). A finite element analysis of mixed mode fracture initiation by ductile failure mechanisms, *Journal of the Mechanics and Physics of Solids*, **42**, 6, 953-978

Ghosal, A.K. and Narasimhan, R., (1996). Numerical simulations of hole growth and ductile fracture initiation under mixed-mode loading. *International Journal of Fracture*. 77, 281-304.

Griffith A.A. (1921). The phenomena of rupture and flow in solids" *Philosophical Transactions Royal Society*. London, **A221**, 163-197.

Gurson A.L. (1977). Continuum theory of ductile rupture by void nucleation and growth: Part 1-Yield criteria and flow rules for porous ductile media. *Journal of Engineering Materials and Technology*. **99**, 2-15

Haefele, P.M. and Lee, J.D. (1995). The constant stress term. *Engineering Fracture Mechanics*. **50**, No 5 6, 869-882.

Hallback, N. (1997). The influence of finite geometry and material properties on mixed-mode I/II fracture of aluminium. *International Journal of Fracture*. **87**, 151-188.

Hallback, N. and Jonsson, N. (1996). *T*-stress evaluations of mixed mode I/II fracture specimens and *T*-effects on mixed mode failure of aluminium. *International Journal of Fracture*. **76**, 141-168.

Hallback, N., and Nilsson, F., (1994). Mixed-mode fracture behaviour of an aluminium alloy, *Journal of the Mechanics and Physics of Solids*, **42**, 9, 1345-1374

Hancock, J.W., Reuter, W.G. and Parks, D.M. (1993). Constraint and toughness parameterized by T. *Constraint Effects in Fracture, ASTM STP 1171.* (Edited by E.M. Hackett, K.-H. Schwalbe and R.H. Dodds), American Society for Testing and Materials, Philadelphia, 21-40.

Hayashi, K. and Nemat-Nasser, S. (1981). Energy-release rate and crack kinking under combined loading. *Journal of Applied Mechanics*. **48**, 520-524.

Henry, B.S. and Luxmoore, A.R. (1997). The stress triaxiality constraint and the Q-values as a ductile fracture parameter. *Engineering Fracture Mechanics*. **57** (4), 375-390.

Henshell, R.D. and Shaw, K.G. (1975). Crack tip elements are unnecessary. *International Journal for Numerical Methods in Engineering*. **9**, 495-509.

Hussain M.A., Pu S.L. and Underwood J. (1974). Strain energy release rate for a crack under combined mode I and Mode II. *Fracture Analysis, ASTM STP 560.* American Society for Testing and Materials, Philadelphia, 2-28

Hutchinson J.W. (1968). Singular behaviour at the end of a tensile crack tip in a hardening material. *Journal of the Mechanics and Physics of Solids.* **16,** 13-31

Inglis C.E. (1913). Stresses in a plate due to presence of cracks and sharp corners. *Transaction of the Institute of Naval Architects.* **55** 219-241.

Irwin G.R. (1957). Analysis of stresses and strains near the end of a crack traversing a plate. *Journal of Applied Mechanics.* **24,** 361-364.

Irwin G.R. (1960). Plastic zone near a crack and fracture toughness. *Proceedings of the seventh Sagamore Ordnance Materials Conference,* Vol 4, 63-78, New York, Syracuse University.

Jones, D.L. and Chisholm, D.B. (1975). An investigation of the edge-sliding mode in fracture mechanics. *Engineering Fracture Mechanics.* **7,** 261-270.

Kamat, S.V. and Hirth, J.P., (1996). Mixed mode I/II fracture toughness of 2034 aluminium alloys, *Acta Mater.*, **44,** 1, 201-208.

Kardomateas, G.A., Carlson, R.L., Soediono, A.H and Schrage, D.P. (1993). Near tip stress and strain fields for short elastic cracks. *International Journal of Fracture.* **62,** 219-232.

Kfouri, A.P. (1986). Some evaluations of elastic *T*-term using Eshelby's method. *International Journal of Fracture.* **30,** 301-315.

Kilnoch, A.J. and Young, R.J. (1983). Fracture behaviour of polymers. *Elsvier Applied Science Publishers Ltd.* Barking, England.

Kirk, M.T., Koppenhoefer, K.C. and Shih, C.F. (1993). Effect of constraint on specimen dimensions needed to obtain structurally relevant toughness measures. *Constraint Effects in Fracture, ASTM STP 1171,* (Edited by E.M. Hackett, K.-H. Schwalbe and R.H. Dodds), American Society for Testing and Materials, Philadelphia, 79-103.

Knesl, Z. (1995). Evaluation of the elastic *T*-stress using a hybrid finite element approach. *International Journal of Fracture.* **70,** R9-R14.

Koo J.M. and Choy Y.S. (1991). A new mixed mode fracture criterion: Maximum tangential strain energy density criterion. *Engineering Fracture Mechanics.* **39** (3), 443-449.

Larsson, S.G. and Carlsson, A.J. (1973). Influence of non-singular stress terms and specimen geometry on small-scale yielding at crack tips in elastic-plastic materials. *Journal of the Mechanics and Physics of Solids.* **21,** 263-277.

Leevers, P.S. and Radon, J.C. (1982). Inherent stress biaxiality in various fracture specimen geometries. *International Journal of Fracture.* **19,** 311-325.

Li, F.Z., Shih, C.F. and Needleman, A. (1985). A comparison of methods for calculating energy release rate. *Engineering Fracture Mechanics.* **21**, 405-421.

Li, Y. and Wang, Z. (1986). Higher order asymptotic field of tensile plane strain nonlinear crack problems. *Scientia Sinica (Series A).* **29**, 941-955.

Liu, A.F. (1974). Crack growth and failure of aluminum plate under in-plane shear. *AIAA Journal.* **12**, 180-185.

Lo, K.K. (1978). Analysis of branched cracks. *Journal of Applied Mechanics.* **45**, 797-802.

Maccagno T.M. and Knott J.F. (1985). Brittle fracture under mixed mode I and II loading. *International Journal of Fracture.* **29**, R49-R57

Maccagno, T.M. and Knott, J.F. (1989). The fracture behaviour of PMMA in mixed modes I and II. *Engineering Fracture Mechanics.* **34**, No 1, 65-86.

Maccagno T.M. and Knott J.F. (1991). The low temperature brittle fracture behaviour of steel in mixed mode I and II. *Engineering Fracture Mechanics.* **38**, (2/3), 111-128

McClintock F.A. (1963). Discussion: On the crack extension in plates under plane loading and transverse shear, by: Erdogan F. and Sih G.C. *Journal of Basic Engineering, Transactions of ASME.* **85**, 525-527

Mahajan, R.V. and Ravi-Chandar, K. (1989). An experimental investigation of mixed-mode fracture. *International Journal of Fracture.* **41**, 235-252.

Maiti, S.K. and Smith, R.A. (1983). Theoretical and experimental studies on the extension of cracks subjected to concentrated loading near their faces to compare the criteria for mixed mode brittle fracture. *Journal of the Mechanics and Physics of Solids.* **31** (5), 389-403.

Melin, S. (1987). Fracture from a straight crack subjected to mixed mode loading. *International Journal of Fracture.* **32**, 257-263.

Miller, A.G., (1988). Review of limit loads of structures containing defects, *International Journal of Pressure Vessels & Piping*, **32**, 197-328

Milne, I, Ainsworth, R.A., Dowling, A.R. and Stewart, A.T. (1988). Assessment of the integrity of structures containing defects. *International Journal of Pressure Vessels & Piping.* **32**, 3-104.

Muskhelishvili N.I. (1963). Some basic problems of the mathematical theory of elasticity, Noordhoff.

Nuismer R.J. (1975). An energy release rate criterion for mixed mode fracture. *International Journal of Fracture.* **11**, 245-250

O'Dowd, N.P. (1995). Applications of two parameter approaches in elastic-plastic fracture mechanics. *Engineering Fracture Mechanics.* **52** (3), 445-465.

O'Dowd, N.P. and Shih, F.C. (1991). Family of crack-tip fields characterized by a triaxiality parameter -I. Structure of field. *Journal of the Mechanics and Physics of Solids*, **39** (8), 989-1015.

O'Dowd, N.P. and Shih, F.C. (1992). Family of crack-tip fields characterized by a triaxiality parameter -II. Fracture applications. *Journal of the Mechanics and Physics of Solids.* **40** (5), 939-963.

O'Dowd, N.P. and Shih, F.C. (1994). Two-parameter fracture mechanics: theory and applications. *Fracture Mechanics 24th Volume, ASTM STP 1207*, J.D. Landes, D.E. McCabe, and J.A.M. Boulet, Eds., American Society of Testing and Materials, Philadelphia, 21-47.

Olsen, P.C. (1994). Determining the stress intensity factors K_I, K_{II} and the T-term via the conservation laws using the boundary element methods. *Engineering Fracture Mechanics.* **49**, No 1, 49-60.

Palaniswamy, K. and Knauss, W.G. (1978). On the problem of crack extension in brittle solids under general loading. Mechanics Today (ed. S. Nemat-Nasser) New York, Pergamon Press, 87-148.

Parks, D.M. (1977). The virtual crack extension method for nonlinear material behaviour. *Computer Methods in Applied Mechanics and Engineering*, **12**, 353-364.

Rice J.R. (1968). A path independent integral and the approximate analysis of strain concentration by notches and cracks. *Journal of Applied Mechanics.* **35**. 379-386

Rice J.R. (1974). Limitations to the small scale yielding approximation for crack tip plasticity. *Journal of the Mechanics and Physics of Solids.* **22**, 17-26.

Rice J.R. and Rosengren G.F. (1968). Plane strain deformation near a crack tip in a power-law hardening material. *Journal of the Mechanics and Physics of Solids.* **16**, 1-12

Rice J.R. and Tracey D.M. (1969). On the ductile enlargement of voids in triaxial stress fields. *Journal of the Mechanics and Physics of Solids.* **17**, 201-217

Rice J.R. and Tracey D.M. (1973). Computational fracture mechanics. *Numerical and Computer Methods in Structural Mechanics.* ed S.J. Fenves, N. Perrone, A.R. Robinson and W.C. Schnobrich. Academic Press, New York, NY, 585-623.

Richard, H.A. (1981). A new shear specimen. *International Journal of Fracture.* **17,** R105-R107.

Richard, H.A. (1985). Fracture predictions for cracks exposed to superimposed normal and shear stresses, *VDI-Forschundsheft.* **631,** VDI-Verlag, Dusseldorf.

Richard, H.A. (1989). Specimens for investigating biaxial fracture and fatigue processes. *Biaxial and Multiaxial Fatigue* (Edited by M.W. Brown and K.J. Miller) Mechanical Engineering Publications, London. 217-229.

Ritchie R.O., Knott J.F. and Rice J.R. (1973). On the relationship between critical stress and fracture toughness in mild steel. *Journal of the Mechanics and Physics of Solids.* **21,** 395-410

Roos, E., Seidenfuss, M., Kramer, D., Krolop, S., Eisele, U. and Hindenlang, U. (1991). Application and evaluation of different numerical methods for determining crack resistance curves. *Nuclear Engineering and Design.* **130,** 297-308.

Rousselier G., Devaux J.C., Mottet G. and Devesa G. (1989). A methodology for ductile fracture analysis based on damage mechanics: An illustration of a local approach of fracture. *Non-linear Fracture Mechanics: Volume II-Elastic Plastic Fracture, ASTM STP 995,* American Society for Testing and Materials, Philadelphia, 332-354

Royer, J. (1986). A specimen geometry for plane mixed modes. *Engineering Fracture Mechanics.* **23** (4) 363-375.

Royer, J. (1988). Study of pure and mixed-mode fracture of a brittle material. *Experimental Mechanics.* **45,** 382-387.

Seed, G.M. and Nowell, D. (1994). Use of the distributed dislocation method to determine the *T*-stress. *Fatigue and Fracture of Engineering Materials and Structures.* **17** (5) 605-618.

Sham, T.-L. (1991). The determination of the elastic *T*-term using higher order weight functions. *International Journal of Fracture.* **48,** 81-102.

Sharma, S.M. and Aravas, N. (1991). Determination of higher order terms in asymptotic elastoplastic crack tip solutions. *Journal of the Mechanics and Physics of Solids.* **39** (8). 1043-1072.

Sherry, A.H., France, C.C. and Goldthorpe, M.R. (1995). Compendium of *T*-stress solutions for two and three dimensional cracked geometries. *Fatigue and Fracture of Engineering Materials and Structures.* **18,** No. 1, 141-155.

Shih C.F. (1974). Small-scale yielding analysis of mixed mode plane strain problems. *Fracture Analysis, ASME STP 560*, American Society for Testing and Materials, Philadelphia, 187-210

Shih, C.F. (1983). Tables of Hutchinson-Rice-Rosengren singular field quantities. Technical report. Materials Research Laboratory, Brown University, Providence, RI.

Shih, C.F. and German, M.D. (1981). Requirements for a one parameter characterization of crack tip fields by the HRR singularity. *International Journal of Fracture.* **17** (1), 27-43.

Sih G.C. (1973a). Methods of analysis and solutions of crack problems. *Mechanics of Fracture, Vol. 1, Ed G.C. Sih*, Noordhoff, Leiden

Sih G.C. (1973b). Some basic problems in fracture mechanics and new concepts. *Engineering Fracture Mechanics.* **5**, 365-377

Sih G.C. (1974). Strain energy density factor applied to mixed mode crack problems. *International Journal of Fracture.* **10**, 305 321

Sih G.C. and Kiefer B.V. (1979). Non-linear response of solids due to crack growth and plastic deformation. *Non-linear and Dynamic Fracture Mechanics,* (Edited by Perrone N. and Atluri S.N.), ASME applied Mechanics Division. **35**, 136-156

Sih G.C. and MacDonald B. (1974). Fracture mechanics applied to engineering problems - strain energy density fracture criterion. *Engineering fracture Mechanics.* **6**, 361-386

Sih G.C. and Madenci E. (1983a). Fracture initiation under gross yielding: Strain energy density criterion. *Engineering Fracture mechanics*, **18** (3), 667-677

Sih G.C. and Madenci E. (1983b). Crack growth resistance characterised by the strain energy density function. *Engineering Fracture Mechanic.* **18** (6), 1159-1171

Sladek, J. , Sladek, V. and Fedelinski, P. (1997). Contour integrals for mixed-mode crack analysis: effect of nonsingular terms. *Theoretical and Applied Fracture Mechanics.* **27**, 115-127.

Smith, D.J. , Swankie, T.D., Ayatollahi, M.R. and Pavier, M.J. (1998a). Brittle and ductile failure under mixed mode loading. *Proceedings of the 12th European Conference on Fracture (ECF12)*, Sheffield, UK, Vol 2, 661-666.

Smith D.J., Ayatollahi, M.R., Davenport, J.C.W. and Swankie, T.D. (1998b). Mixed mode brittle and ductile fracture of a high strength rotor steel at room temperature. *International Journal of Fracture*, Submitted for publication.

Sorem, W.A., Dodds, R.H. and Rolfe, S.T. (1991). Effects of crack depth on elastic plastic fracture toughness. *International Journal of Fracture*, **47**, 105-126.

Sumpter, J.D.S. (1993). An experimental investigation of the T stress approach. *Constraint Effects in Fracture, ASTM STP 1171.* (Edited by E.M. Hackett, K.-H. Schwalbe and R.H. Dodds), American Society for Testing and Materials, Philadelphia, 492-502.

Swankie, T.D. (1999). The role of shear and constraint in mixed mode brittle and ductile fracture. *PhD Dissertation (in preparation),* University of Bristol, Bristol, UK

Swankie, T.D. and Smith, D.J. (1998). Low temperature mixed mode fracture of a pressure vessel steel subject to prior loading. *Engineering Fracture Mechanics.* Accepted for publication.

Symington, M., Shih, C.F. and Ortiz, M. (1988). Tables of plane strain mixed-mode plastic crack tip fields. *Technical report MRG/DMR-8714665/1.* Materials Research Group, Brown University, Providence, RI.

Tada, H., Paris, P.C. and Irwin, G.R. (1985). The stress analysis of cracks handbook. (2nd Edition). *Paris Publications Inc.,* St. Louis, USA.

Theocaris, P.S. and Andrianopoulos, N.P. (1982a). The Mises elastic-plastic boundary as the core region in fracture mechanics. *Engineering Fracture Mechanics.* **16** (3), 425-432

Theocaris, P.S. and Andrianopoulos, N.P. (1982b). A modified strain energy density criterion to crack propagation. *Journal of Applied Mechanics.* **49**, 81-86

Tohgo, K. and Ishii, H., (1992). Elastic-plastic fracture toughness test under mixed mode I-II loading. *Engineering Fracture Mechanics.* **41**, 4, 529-540

Ueda, Y. , Ikeda, K. , Yao, T. and Aoki, M. (1983). Characteristics of brittle fracture under general combined modes including those under bi-axial tensile loads. *Engineering Fracture Mechanics.* **18**, No 6, 1131-1158.

Wallin, K. (1984). The scatter in K_{IC}-results. *Engineering Fracture Mechanics.* **19**, (6), 1085-1093.

Wang M-H. (1985). A theory for the mixed energy release rate. *Engineering Fracture Mechanics.* **22** (4), 661-671

Wang, Y.Y. (1993). On the two-parameter characterization of elastic-plastic crack front fields in surface-cracked plates. *Constraint Effects in Fracture, ASTM STP 1171.* (Edited by E.M. Hackett, K.-H. Schwalbe and R.H. Dodds), American Society for Testing and Materials, Philadelphia, 120-138.

Wang, Y.Y. and Parks, D.M. (1995). Limits of J-T characterization of elastic-plastic crack-tip fields. *Constraint Effects in Fracture, Theory and Applications, ASTM STP 1244*, Ed. M. Kirk and A. Bakker. American Society for Testing and Materials. Philadelphia, PA, 43-67.

Wells, A.A. (1961). Unstable crack propagation in Metals: cleavage and fast fracture. *Proceedings of the Crack Symposium*, Vol 1, Paper 84, Cranfield, UK.

Westergaard H.M. (1939). Bearing pressures and cracks. *Journal of Applied Mechanics*. **61**, A49-A53

Williams, J.G. (1983). Fracture mechanics of polymers. *Ellis Horwood Ltd.* Chichester, England.

Williams, J.G. and Ewing, P.D. (1972). Fracture under complex stress - the angled crack problem. *International Journal of Fracture*, **8**, 441-446.

Williams, M.L. (1957). On the stress distribution at the base of a stationary crack. *Journal of Applied Mechanics*. **24**, 109-114.

Wu, S.X. and Mai, Y.W. (1995). Two-parameter (J-Q) fracture characterization of ductile tearing. *Fracture Mechanics: 26th Volume, ASTM STP 1256.* W.G. Reuter, J.H. Underwood and J.C. Newman Jr., Eds., American Society for Testing and Materials, Philadelphia, 43-53.

Xia, L., Wang, T.C. and Shih, C.F. (1993). Higher order analysis of crack tip fields in elastic power-law hardening materials. *Journal of the Mechanics and Physics of Solids*. **41** (4), 665-687.

Yang, S., Chao, Y.J. and Sutton, M.S. (1993a) Complete theoretical analysis for higher order asymptotic terms and the HRR zone at a crack tip for mode I and mode II loading of a hardening material. *Acta Mechanica*. 98, 79-98.

Yang, S., Chao, Y.J. and Sutton, M.S. (1993b). Higher order asymptotic crack tip fields in a power-law hardening material. *Engineering Fracture Mechanics*. **45** (1), 1-20.

Yehia N.A.B. (1985). On the use of T-Criterion in fracture mechanics. *Engineering Fracture Mechanics*. **22**, (2), 189-199

Yehia N.A.B. (1991). Distortional strain energy density criterion: The Y-Criterion. *Engineering Fracture Mechanics*. **39**, (3), 477-485

Yokobori, T., Yokobori, A.T., Sato, K., and Omotami, M., (1983). The effects of ferrite grain size on fracture of low carbon steels under mixed modes I and II. *Engineering Fracture Mechanics*, **17**, 187-210

Appendix A5

Generalised MTS Criterion - Solution Method

A5-1. Direction of fracture initiation

Eq 5-16 can be written as

$$\frac{K_I}{\sqrt{K_I^2 + K_{II}^2}} + \frac{aK_{II}}{\sqrt{K_I^2 + K_{II}^2}} = b \tag{A5-1}$$

where the coefficients a and b are

$$a = \frac{3\cos\theta_o - 1}{\sin\theta_o} \qquad b = \frac{8}{3} B\alpha \frac{\cos\theta_o}{\cos\frac{\theta_o}{2}}$$

If $z = \frac{K_{II}}{K_I}$ then eq A5-1 can be written as

$$\frac{1}{\sqrt{1+z^2}} + \frac{a}{\sqrt{\frac{1+z^2}{z^2}}} = b \tag{A5-2}$$

or

$$(a^2 - b^2)\, z^2 + 2az + (1 - b^2) = 0$$

which gives

$$z = \frac{K_{II}}{K_I} = \frac{-a \pm b\sqrt{a^2 - b^2 + 1}}{a^2 - b^2} \tag{A5-3}$$

Numerical results suggest that only the negative sign in the numerator of eq A5-3 is acceptable, because the direction of fracture initiation θ_o must be between –90° and 0°. Therefore the mode mixity parameter $M^e = \frac{2}{\pi}\, tan^{-1}\left(\frac{K_I}{K_{II}}\right)$ can be written as

$$M^e = \frac{2}{\pi}\tan^{-1}\left[\frac{a^2 - b^2}{-a - b\sqrt{a^2 - b^2 + 1}}\right] \tag{A5-4}$$

Recalling that a and b are functions of θ_o, eq A5-4 provides a closed form solution for the direction of fracture initiation in mixed mode fracture. Eq A5-4 gives the ratio of K_I/K_{II} required for a given fracture initiation angle θ_o. The results were shown in Fig 5-5.

A5-2. Onset of fracture, *K-B* formulation

Eq 5-22 can be written as

$$\frac{K_I}{\sqrt{K_I{}^2 + K_{II}{}^2}} + \frac{cK_{II}}{\sqrt{K_I{}^2 + K_{II}{}^2}} + \frac{d}{\sqrt{K_I{}^2 + K_{II}{}^2}} = e \qquad \text{(A5-5)}$$

where the coefficients c, d and e are

$$c = -3\tan\frac{\theta_o}{2} \qquad d = -\frac{K_{If}}{\cos^3\frac{\theta_o}{2}} \qquad e = -4B\alpha\tan\frac{\theta_o}{2}\sin\frac{\theta_o}{2}$$

Eq A5-5 can be shown in terms of z as

$$\frac{1}{\sqrt{1+z^2}} + \frac{c}{\sqrt{1+\frac{1}{z^2}}} + \frac{\frac{d}{K_I}}{\sqrt{1+z^2}} = e \qquad \text{(A5-6)}$$

Recalling that $\frac{d}{K_I} = -\frac{K_{If}}{K_I\cos^3\frac{\theta_o}{2}}$, eq A5-6 gives

$$\frac{K_I}{K_{If}} = \frac{1}{\cos^3\frac{\theta_o}{2}\left(1+cz-e\sqrt{1+z^2}\right)} \qquad \text{(A5-7)}$$

and from $K_{II} = zK_I$

$$\frac{K_{II}}{K_{If}} = \frac{z}{\cos^3\frac{\theta_o}{2}\left(1+cz-e\sqrt{1+z^2}\right)} \qquad \text{(A5-8)}$$

Once z is found from eq A5-3 for a given θ_o, the values of $\frac{K_I}{K_{If}}$ and $\frac{K_{II}}{K_{If}}$ can be determined using eqs A5-7 and A5-8 for the corresponding z and θ_o. The results then are plotted in the diagrams of $\frac{K_I}{K_{If}}$ versus $\frac{K_{II}}{K_{If}}$ for different values of $B\alpha$ (see Fig 5–6).

A5-3. Onset of fracture, *K-T* formulation

Eq 5-16 may be rewritten as

$$K_I = -K_{II}\frac{3\cos\theta_o - 1}{\sin\theta_o} + \tfrac{8}{3}T\sqrt{2\pi r_c}\frac{\cos\theta_o}{\cos\frac{\theta_o}{2}} \tag{A5-9}$$

If eq A5-9 is replaced in eq 5-21 gives

$$g_2 K_{II} = g_1 T\sqrt{2\pi r_c} - K_{If} \tag{A5-10}$$

where

$$g_1 = \tfrac{8}{3}\cos\theta_o\cos^2\frac{\theta}{2} + \sin^2\theta_o \qquad \text{and} \qquad g_2 = \frac{3\cos\theta_o - 1}{\sin\theta_o}\cos^3\frac{\theta_o}{2} + \tfrac{3}{2}\cos\frac{\theta_o}{2}\sin\theta_o$$

Eq A5-10 can also be shown as

$$\frac{K_{II}}{K_{If}} = \frac{g_1}{g_2}\frac{T\sqrt{2\pi r_c}}{K_{If}} - \frac{1}{g_2} \tag{A5-11}$$

and from eq A5-9

$$\frac{K_I}{K_{If}} = \left(-\frac{g_1}{g_2}\frac{3\cos\theta_o - 1}{\sin\theta_o} + \tfrac{8}{3}\frac{\cos\theta_o}{\cos\frac{\theta}{2}}\right)\frac{T\sqrt{2\pi r_c}}{K_{If}} - \frac{1}{g_2}\frac{3\cos\theta_o - 1}{\sin\theta_o} \tag{A5-12}$$

Eqs A5-11 and A5-12 are used to determine the fracture loci $\frac{K_I}{K_{If}}$ versus $\frac{K_{II}}{K_{If}}$ for different values of $\frac{T\sqrt{2\pi r_c}}{K_{If}}$ where the results were shown in Fig 5-7.

	a/W =0.1	a/W =0.5	a/W =0.7
B, FE analysis	-0.44	-0.15	0.213
B, Sham (1991)	-0.464	-0.153	0.21

Table 4-1. Mode I results for the biaxiality ratio B, for the single edge notched specimen.

Loading angle, β (degrees)	Connection	B (a/W=0.1)	B (a/W=0.5)	B (a/W=0.7)
0 (mode II)	Pinned	0	0	0
22.5	Pinned	-0.35	-0.098	0.177
45	Pinned	-0.422	-0.135	0.205
67.5	Pinned	-0.433	-0.146	0.211
90 (mode I)	Pinned	-0.44	-0.15	0.213
0 (mode II)	Contact	-1.32	-1.54	-1.89
22.5	Contact	-1.7	-1.39	-0.913
45	Contact	-1.85	-0.837	-0.325
67.5	Contact	-1.42	-0.471	-0.054
90 (mode I)	Contact	-0.434	-0.22	-0.004
0 (mode II)	Perfect	0.93	0.59	0.78
22.5	Perfect	-0.045	0.104	0.015
45	Perfect	-0.051	0.006	-0.031
67.5	Perfect	-0.12	-0.038	-0.048
90 (mode I)	Perfect	-0.14	-0.053	-0.053

Table 4-2. The biaxiality ratio B, for the three connection models with different crack length ratios.

Specimen	Loading (T/C)	d_1	d_2	a_1	$a_{1+}\,a_2$	δ_{cr}(mm)	P_{cr}(N)	K_{IIf}(MPa$\sqrt{}$mm)	K_{IIf}(MPa$\sqrt{}$m)	Fracture Angle
M2t-2	Tensile	0.51	0.48	9.23	9.54	1.05	2410	36.63	1.16	-82
M2T2	Tensile	0.42	0.52	9.13	9.94	1.1	2615	39.75	1.26	-77
M2T3	Tensile	0.48	0.47	9.28	10	1.14	2595	39.44	1.25	-78
M2T4	Tensile	0.49	0.46	9.23	9.84	1.18	2860	43.47	1.37	-77
M2T5	Tensile	0.51	0.47	9.00	9.84	1.15	2835	43.09	1.36	-80
M2T6	Tensile	0.57	0.53	9.27	10.09	0.99	2175	33.06	1.05	-80
M2T7	Tensile	0.46	0.50	8.77	9.68	1.05	2535	38.53	1.22	-77
M2T9	Tensile	0.52	0.51	8.52	10.01	1.26	2880	43.78	1.38	-80
M2T11	Tensile	0.54	0.54	8.44	9.9	1.30	2990	45.45	1.43	-77
M2T12	Tensile	0.54	0.55	8.67	9.98	1.12	2550	38.76	1.23	-78
Average							**2647**	**40.16**	**1.27**	**-78.6**

Table 6-1. Results for the $+T$ shear test specimens.

Specimen	Loading (T/C)	d_1	d_2	a_1	$a_{1+}\, a_2$	δ_{cr}(mm)	P_{cr}(N)	K_{IIf}(MPa√mm)	K_{IIf}(MPa√m)	Fracture Angle
M2c-1	Compressive	0.47	0.47	9.25	9.75	1.8	5340	81.17	2.57	-52
M2c-2	Compressive	0.53	0.55	9.12	10.16	1.71	5000	76	2.4	-60
M2C1	Compressive	0.51	0.48	9.42	10.10	1.79	5180	78.74	2.5	-56
M2C2	Compressive	0.55	0.54	9.74	10.52	1.55	4555	69.24	2.19	-52
M2C3	Compressive	0.52	0.52	9.29	10.30	1.51	4190	63.69	2.01	-53
M2C4	Compressive	0.53	0.58	8.94	10.18	1.55	4635	70.45	2.23	-54
M2C6	Compressive	0.44	0.44	9.03	9.95	1.73	4920	74.78	2.36	-58
M2C8	Compressive	0.52	0.51	8.18	10.01	2.05	5710	86.79	2.74	-56
M2C9	Compressive	0.55	0.52	8.34	10.00	1.97	5560	84.51	2.67	-56
M2C10	Compressive	0.53	0.55	8.30	10.00	1.9	5500	83.6	2.64	-55
Average							**5065**	**76.84**	**2.43**	**-55.2**

Table 6-2. Results for the -*T* shear test specimens.

Specimen	Loading	d_1	d_2	a_1	$a_{1+}\ a_2$	δ_{cr}(mm)	P_{cr}(N)	K_{If}(MPa√mm)	K_{If}(MPa√m)	$K_{IIf}=0.87*K_{If}$ (MPa√m)
M1-1	Mode I	0.62	0.62	7.84	10.08	0.54	1670	66.09	2.09	1.81
M2-2	Mode I	0.67	0.7	8.42	10.01	0.51	1585	62.61	1.98	1.71
M2-3	Mode I	0.63	0.64	8.21	10.17	0.49	1540	61.03	1.93	1.67
M2-4	Mode I	0.61	0.67	8.06	9.96	0.5	1610	63.56	2.01	1.74
M2-5	Mode I	0.56	0.52	8.36	9.5	0.6	1710	67.67	2.14	1.85
M2-6	Mode I	0.59	0.59	7.91	10.12	0.49	1490	58.82	1.86	1.61
M2-7	Mode I	0.53	0.54	8.16	10.02	0.5	1585	62.61	1.98	1.71
M2-8	Mode I	0.63	0.61	8.45	9.66	0.47	1475	58.19	1.84	1.59
M2-9	Mode I	0.54	0.57	9.14	11.26	0.47	1450	57.24	1.81	1.57
M2-10	Mode I	0.7	0.7	8.16	10.61	0.51	1495	59.13	1.87	1.62
Average							**1561**	**61.66**	**1.95**	**1.69**

Table 6-3. Results for the mode I test specimens.

	+T shear tests		-T shear tests		Mode I tests	
	K_o	K_{min}	K_o	K_{min}	K_o	K_{min}
Fitted values (MPa$\sqrt{m}$)	1.32	0.787	2.54	1.43	1.99	1.47

Table 6-4. Results for fitting parameters in the Wallin's model used for probability analysis of the mode I and mode II fracture toughness results.

T/σ_o	θ_o (n=3) degrees	θ_o (n=8) degrees	θ_o (n=13) degrees
1	-65.6	-65	-68.6
0.8	-67.1	-68.4	-71.2
0.6	-68.7	-71.3	-73.5
0.4	-70.5	-73.4	-75.2
0.2	-72	-74.9	-76.4
0	-72.4	-76	-78
-0.2	-70.75	-76.9	-79.4
-0.4	-73.3	-78.4	-81.3
-0.6	-75.7	-80.4	-82.6
-0.8	-77.9	-82.6	-84.1
-1	-79.9	-84.6	-86.1

Table 7-1. The variation of the direction of maximum tangential stress θ_o in mode II versus T/σ_o for n=3, 8 and 13.

T/σ_o	$Q_{II}(n=3)$	$Q_{II}(n=8)$	$Q_{II}(n=13)$
1	0.643	0.439	0.399
0.8	0.541	0.354	0.319
0.6	0.422	0.256	0.232
0.4	0.287	0.161	0.153
0.2	0.133	0.079	0.076
0	0	0	0
-0.2	-0.141	-0.084	-0.084
-0.4	-0.33	-0.177	-0.169
-0.6	-0.522	-0.293	-0.269
-0.8	-0.7	-0.419	-0.384
-1	-0.868	-0.545	-0.502

Table 7-2. The mode II constraint parameter Q_{II}, calculated along the direction of maximum tangential stress, versus T/σ_o for n=3, 8 and 13.

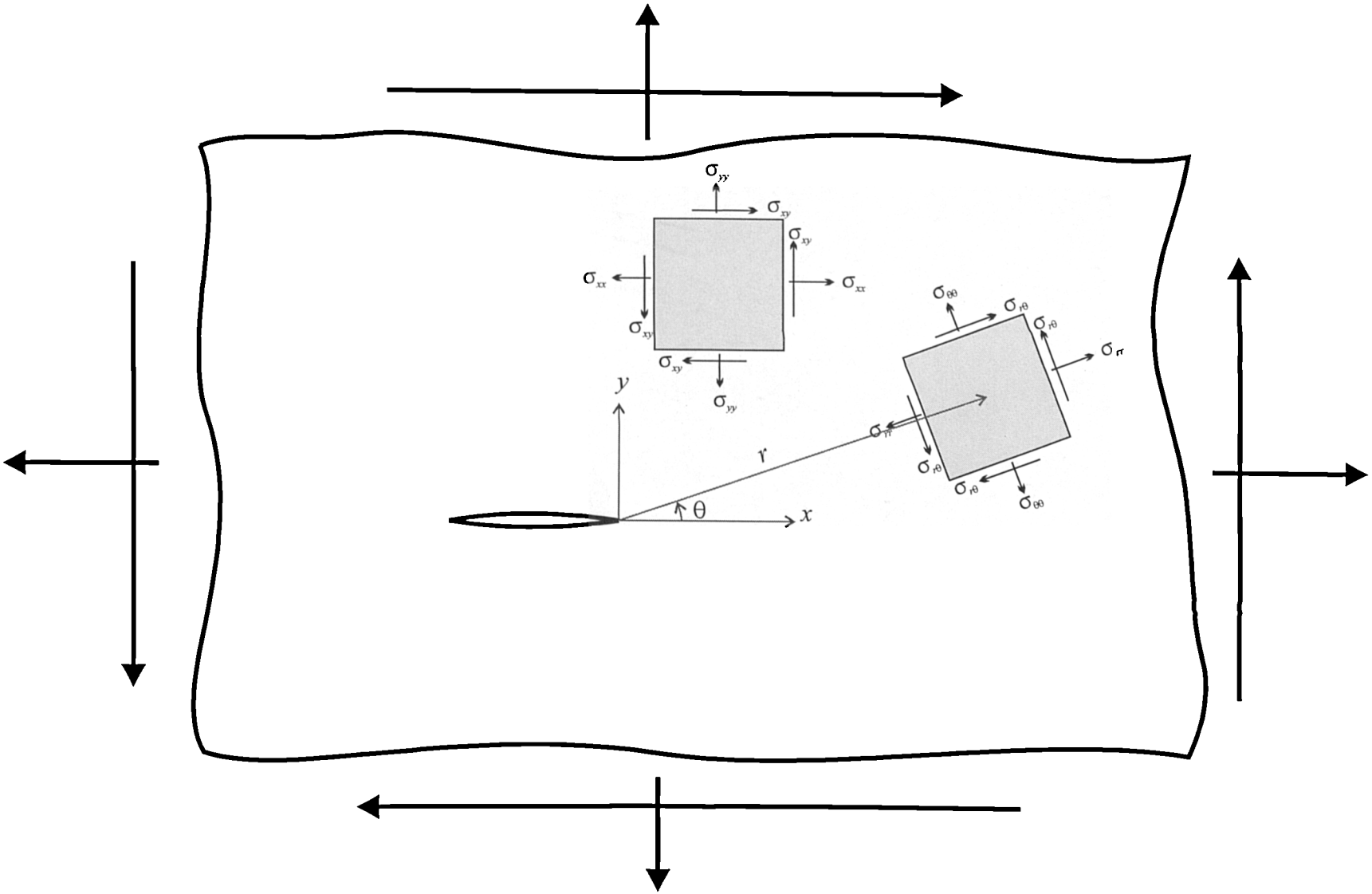

Figure 2-1. Crack tip coordinates and stresses in the Cartesian and polar coordinate systems.

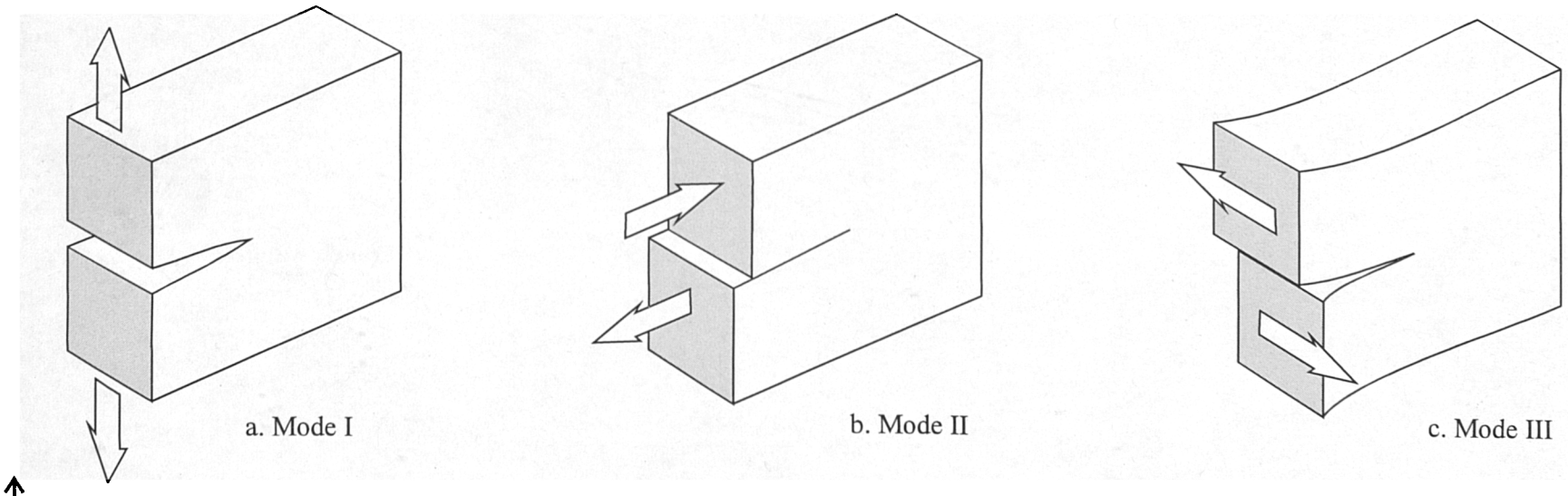

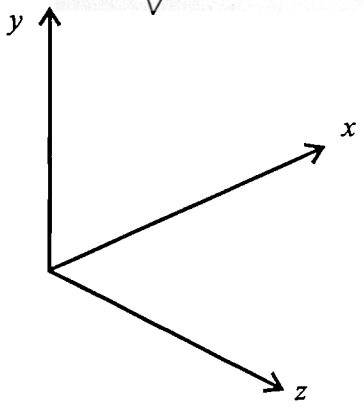

Figure 2-2. Three modes of loading in cracked specimens.

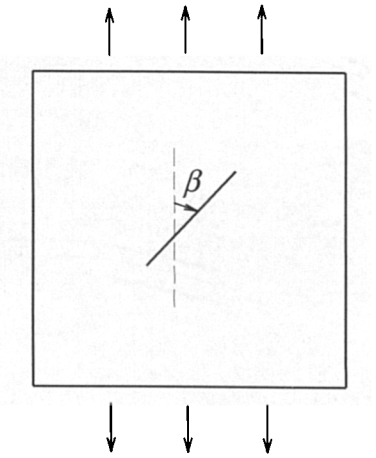

a. Angled crack in a large panel.

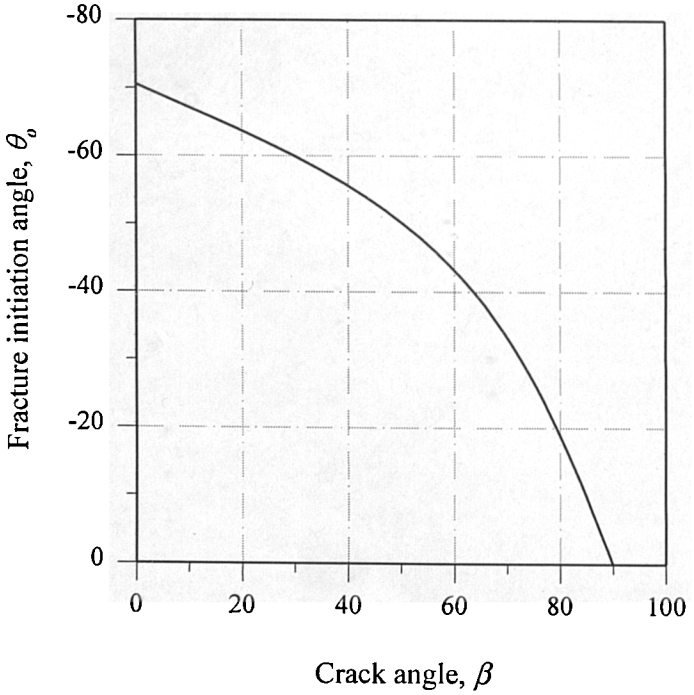

b. Direction of fracture initiation.

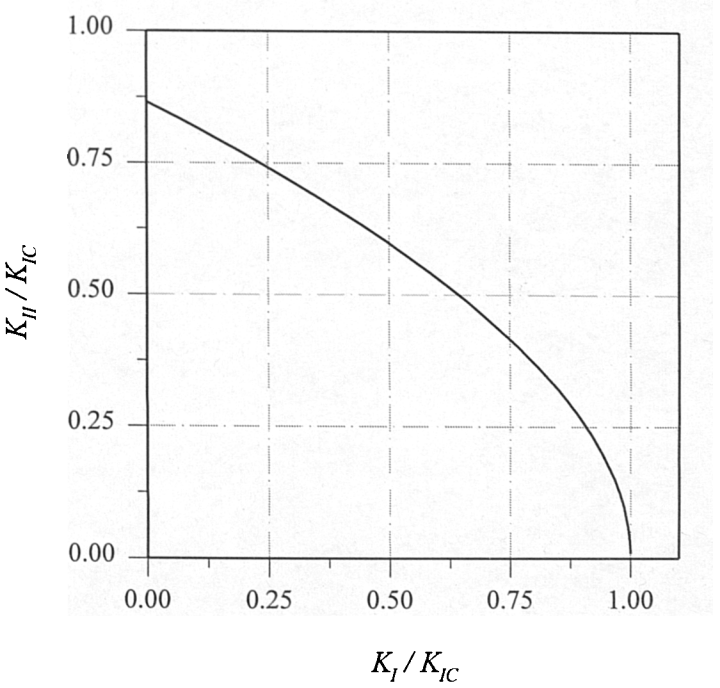

c. Onset of crack growth.

Figure 2-3. Mixed mode fracture in the angled internal crack specimen predicted based on the MTS criterion.

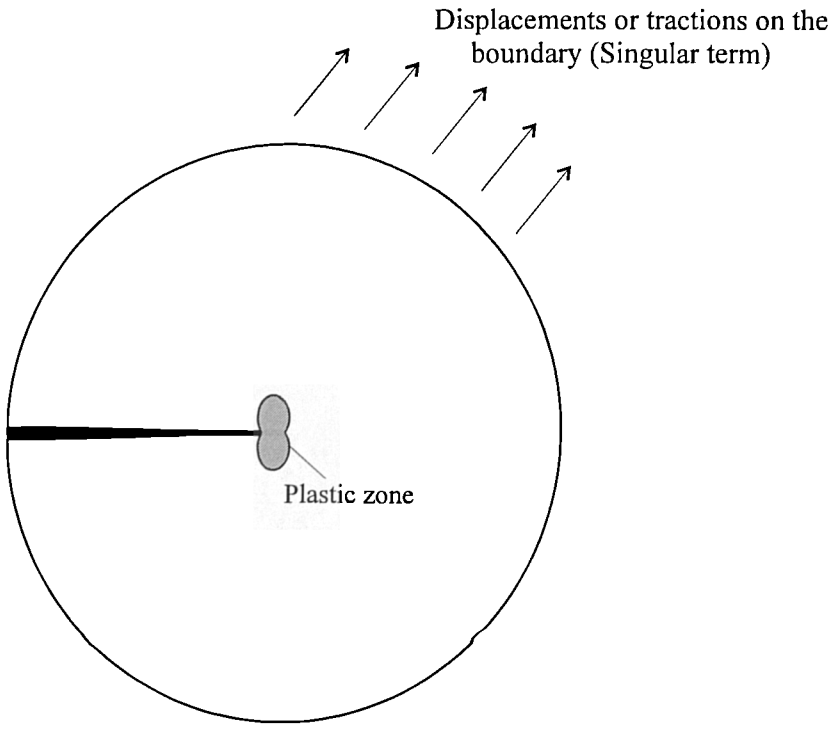

Figure 2-4. Boundary layer model to simulate small scale yielding in a finite element model.

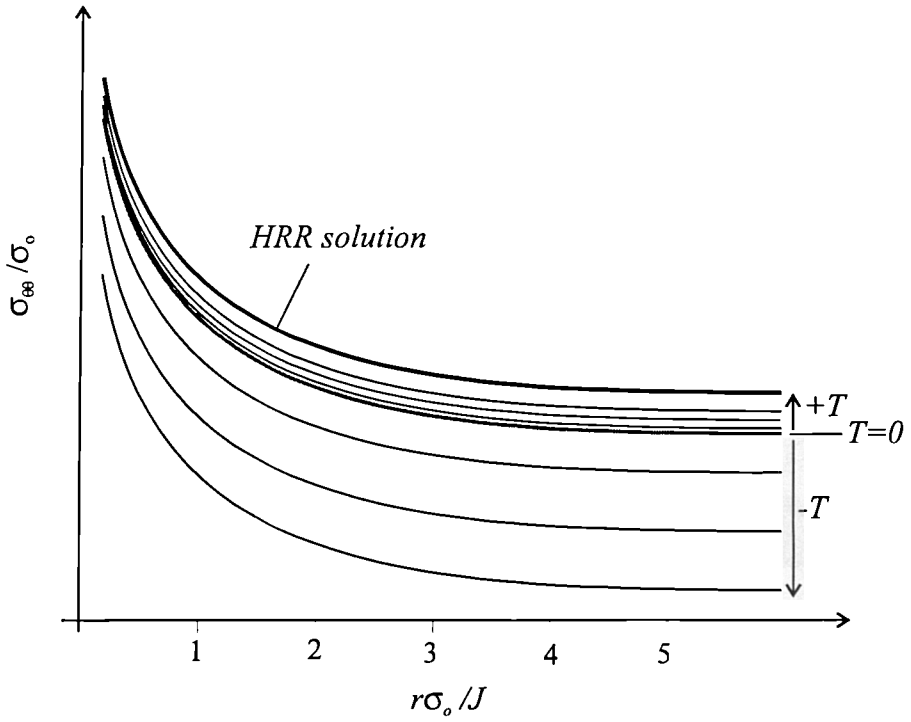

Figure 2-5. Effect of positive and negative T on the tangential stress ahead of the crack tip in a modified boundary layer model (Mode I).

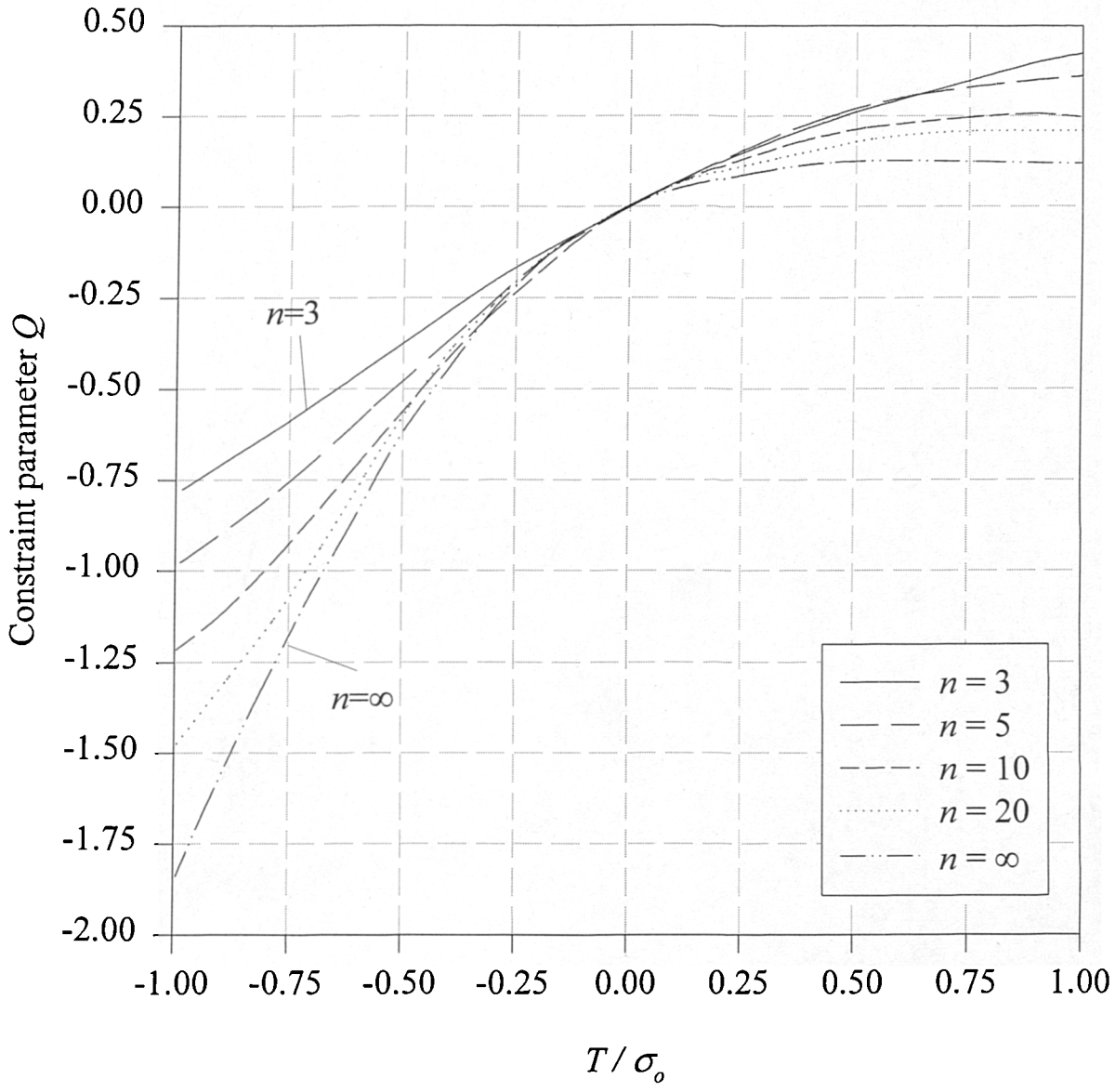

Figure 2-6. The constraint parameter Q versus T/σ_o for different values of hardening coefficient n. (O'Dowd and Shih, 1995)

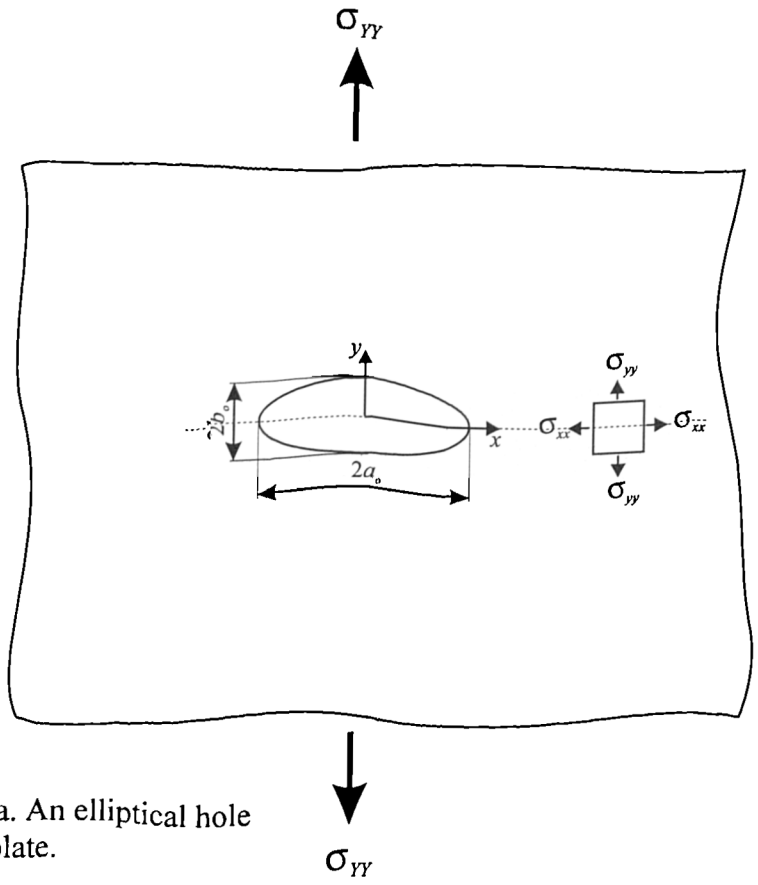

Figure 3-1a. An elliptical hole in a large plate.

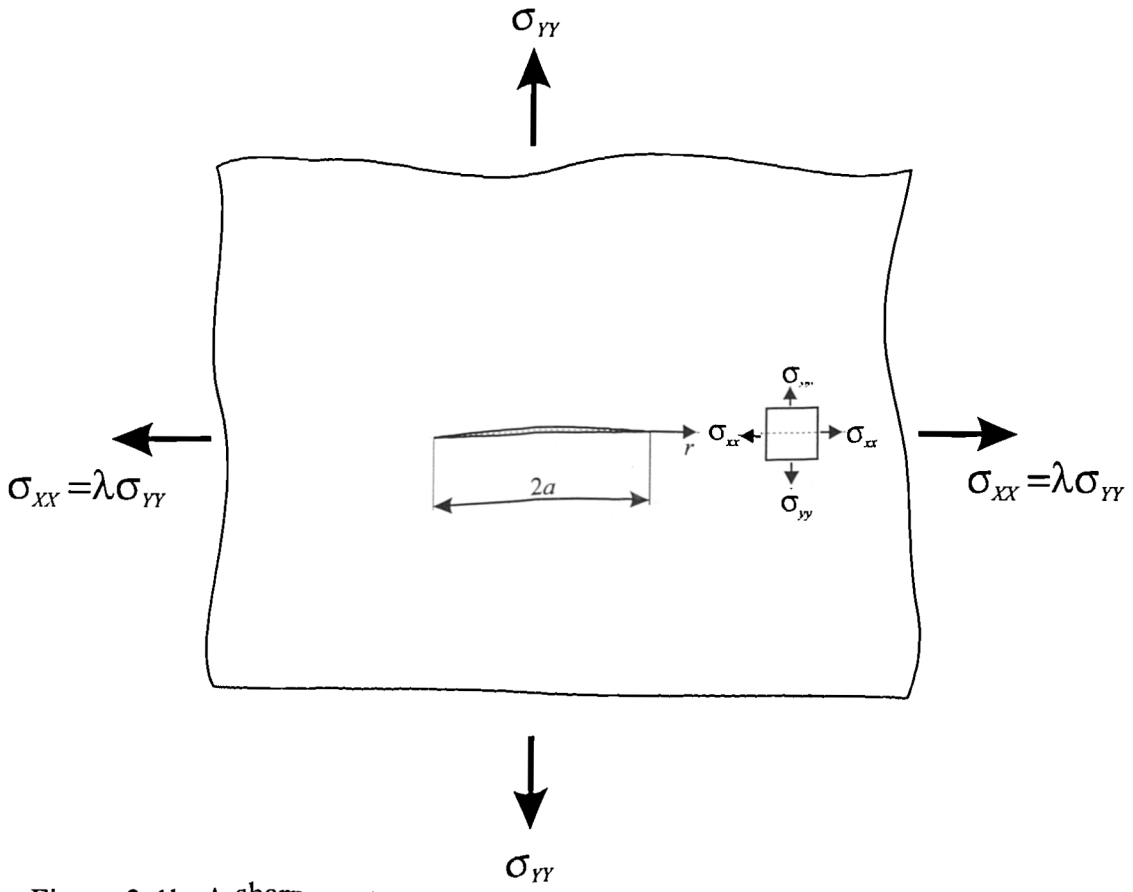

Figure 3-1b. A sharp crack in a large plate.

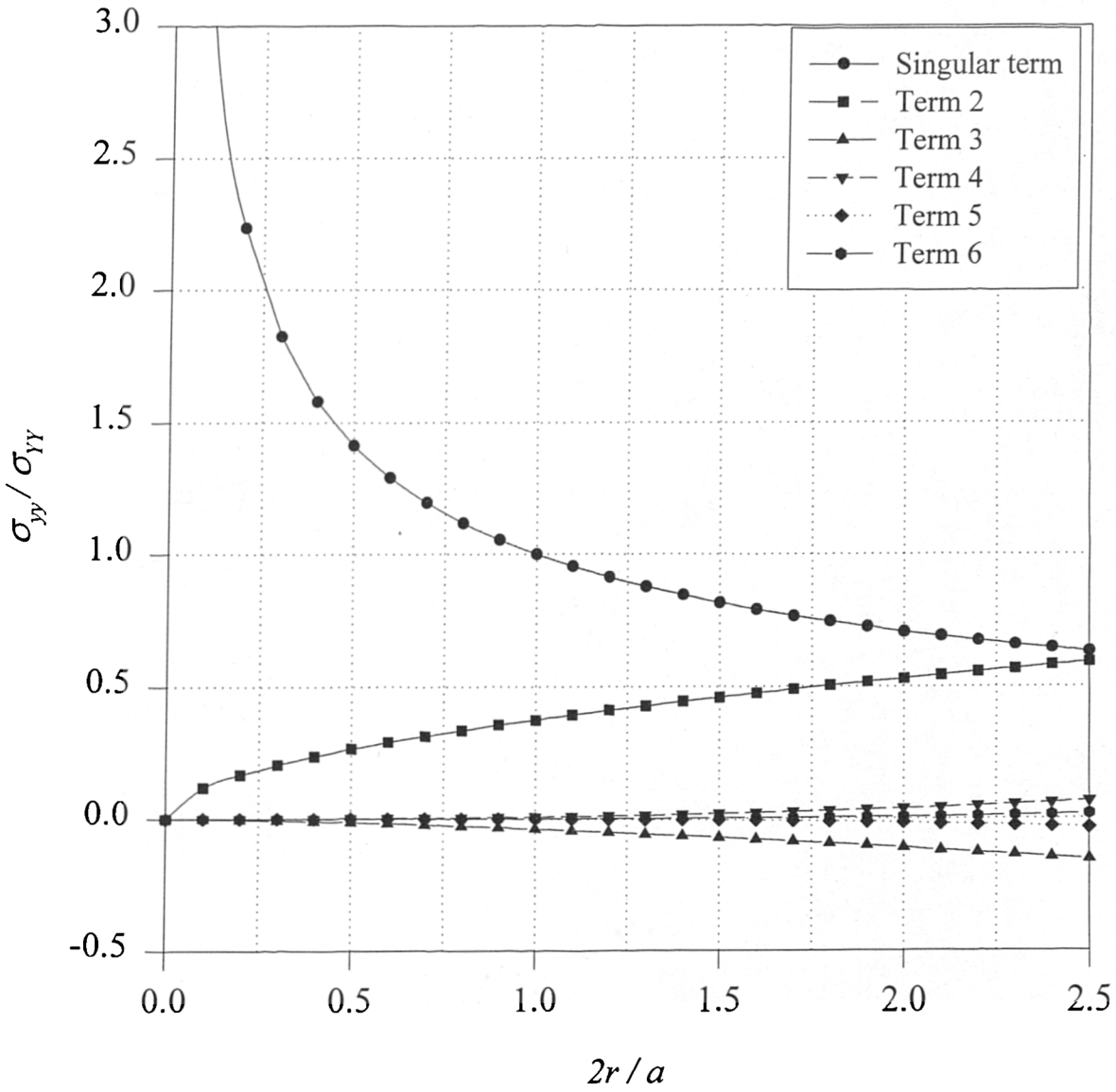

Figure 3-2. First 6 terms in series expansion for σ_{yy}.
(Internal crack in a large plate)

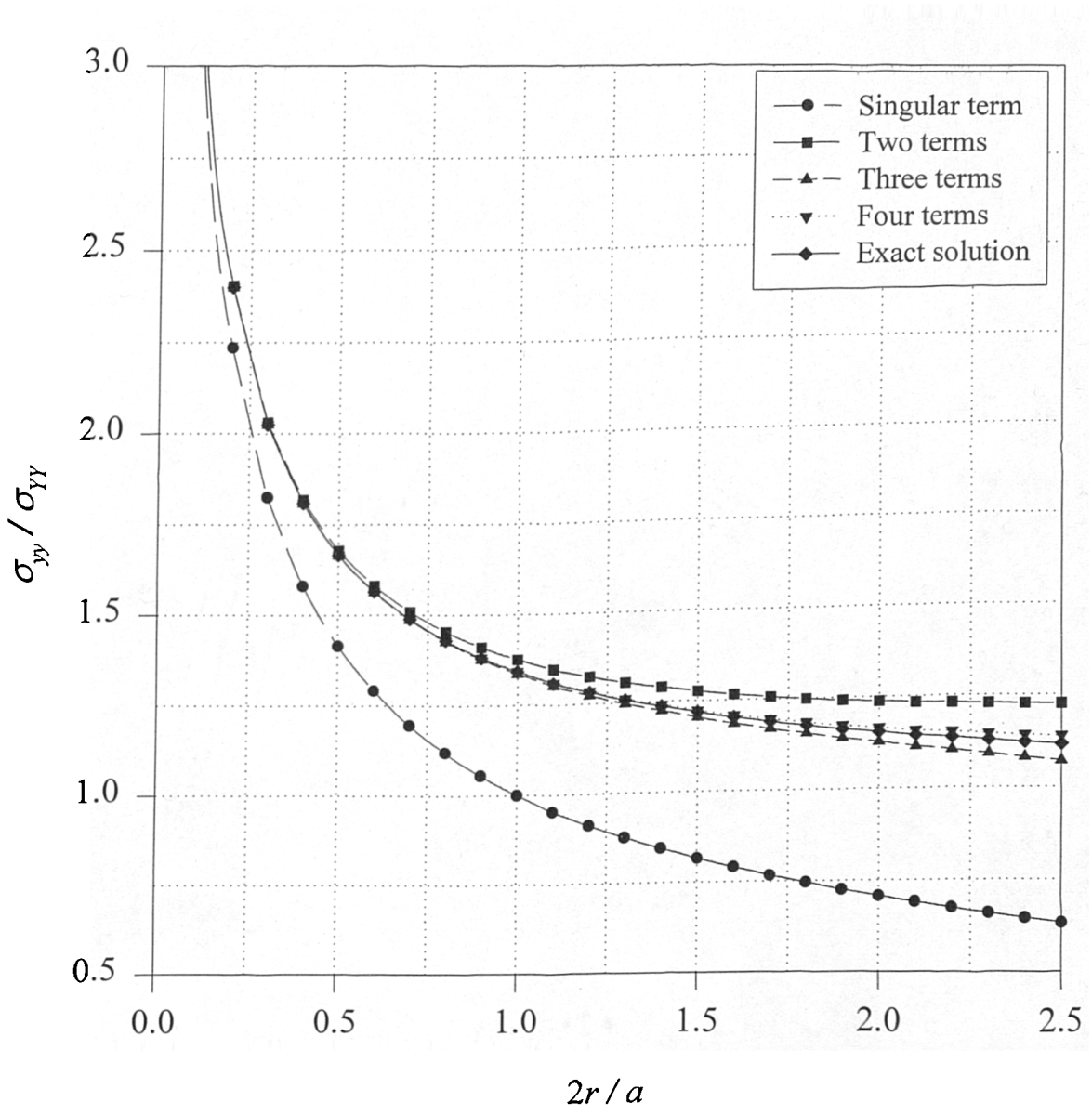

Figure 3-3. Effects of the higher order terms on improving the results for normalised σ_{yy}. (Internal crack in a large plate)

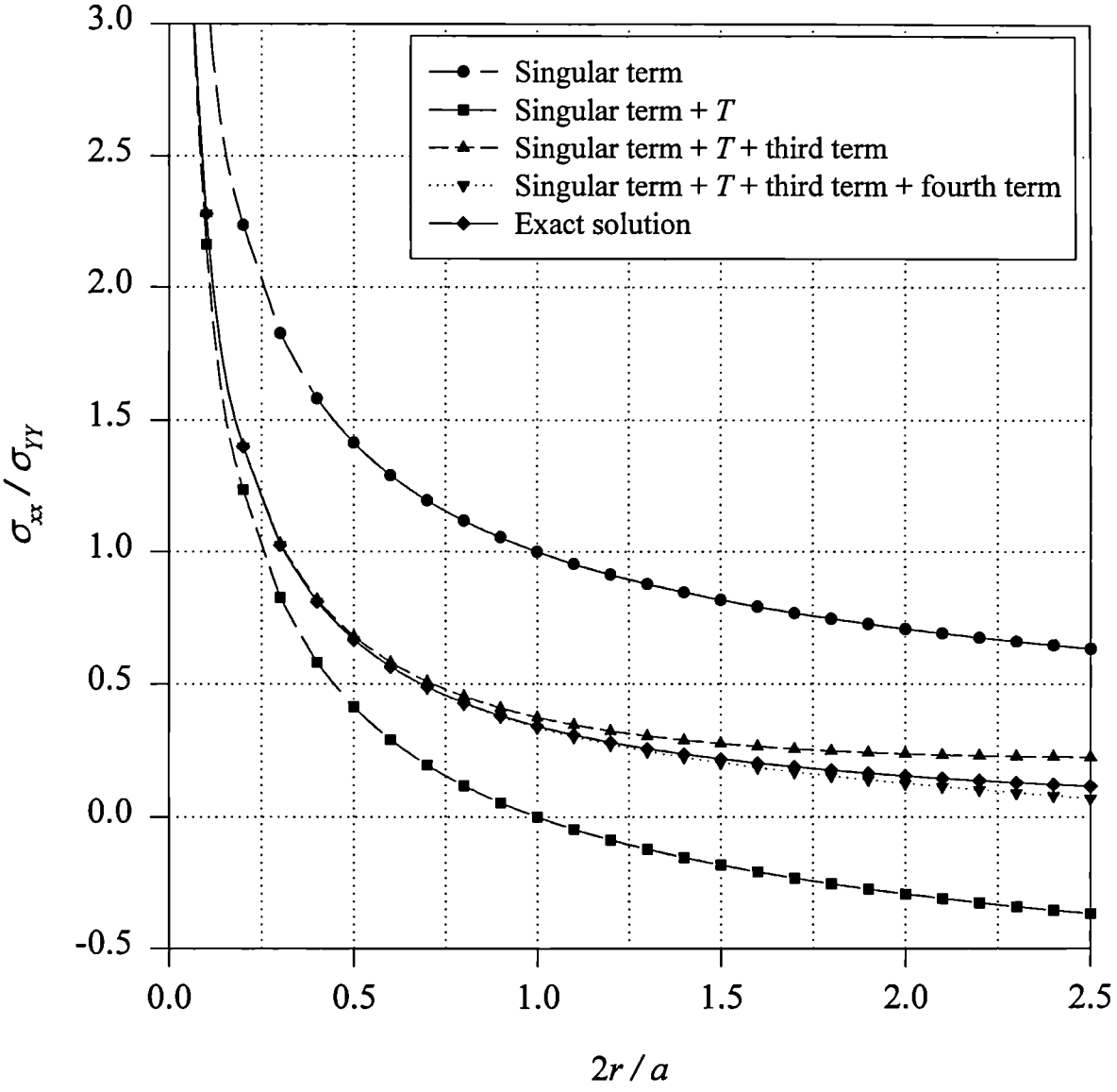

Figure 3-4. Effects of the higher order terms on improving the results for normalised σ_{xx}. (Internal crack in a large plate)

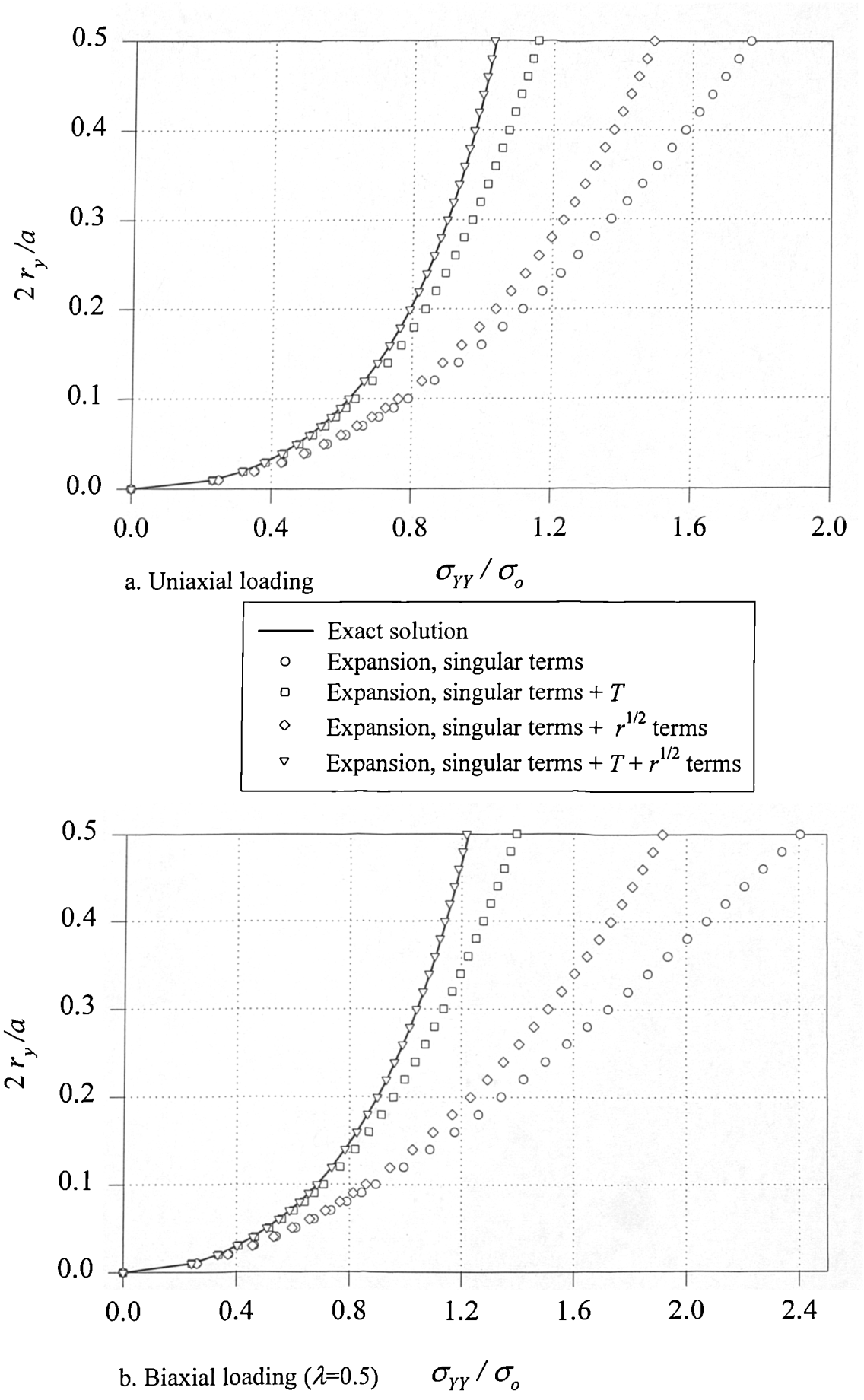

Figure 3-5. Plastic zone size along the crack line versus external load. Plane strain, Tresca yield criterion

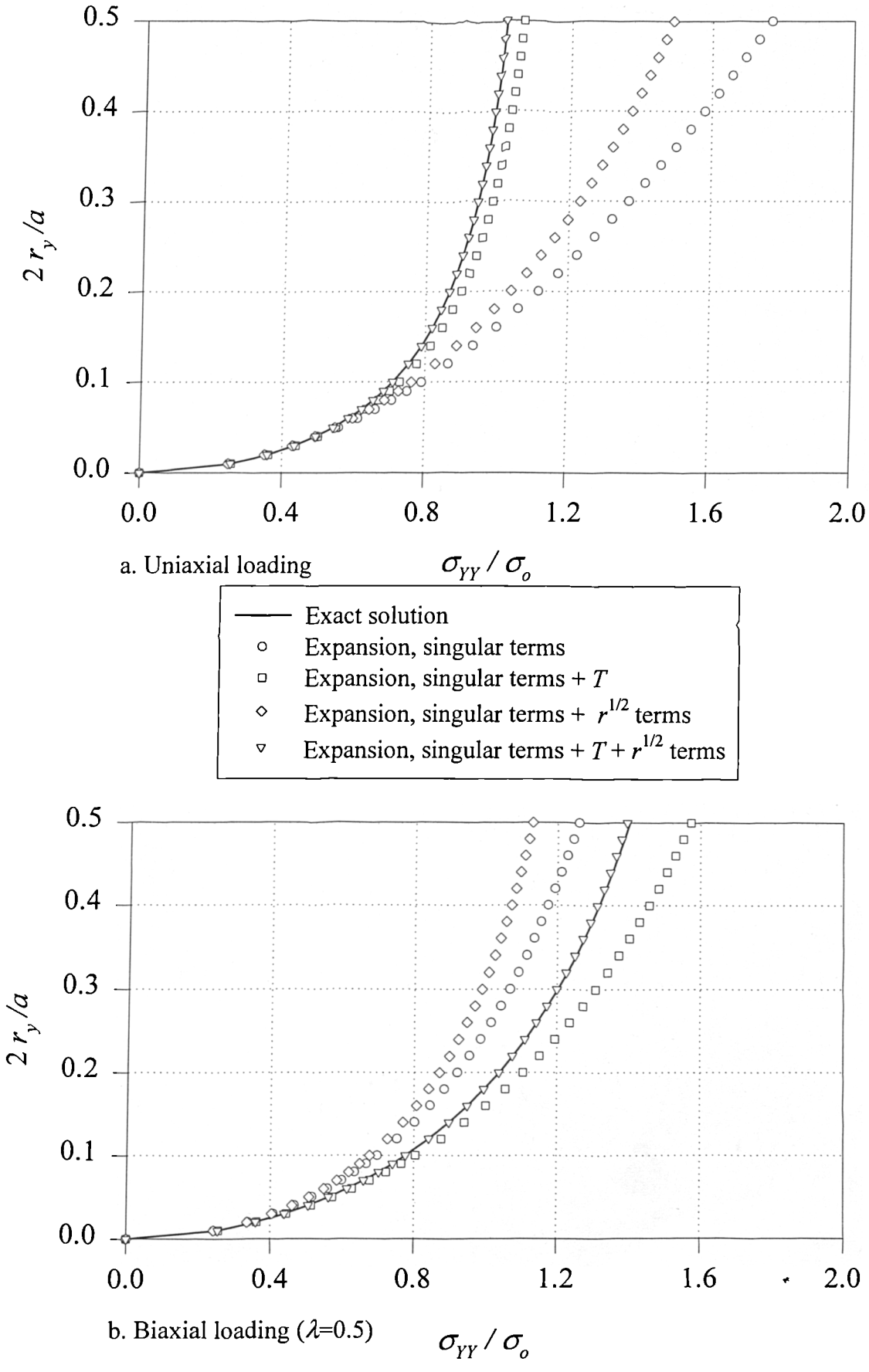

Figure 3-6. Plastic zone size along the crack line versus external load. Plane strain, von Mises yield criterion

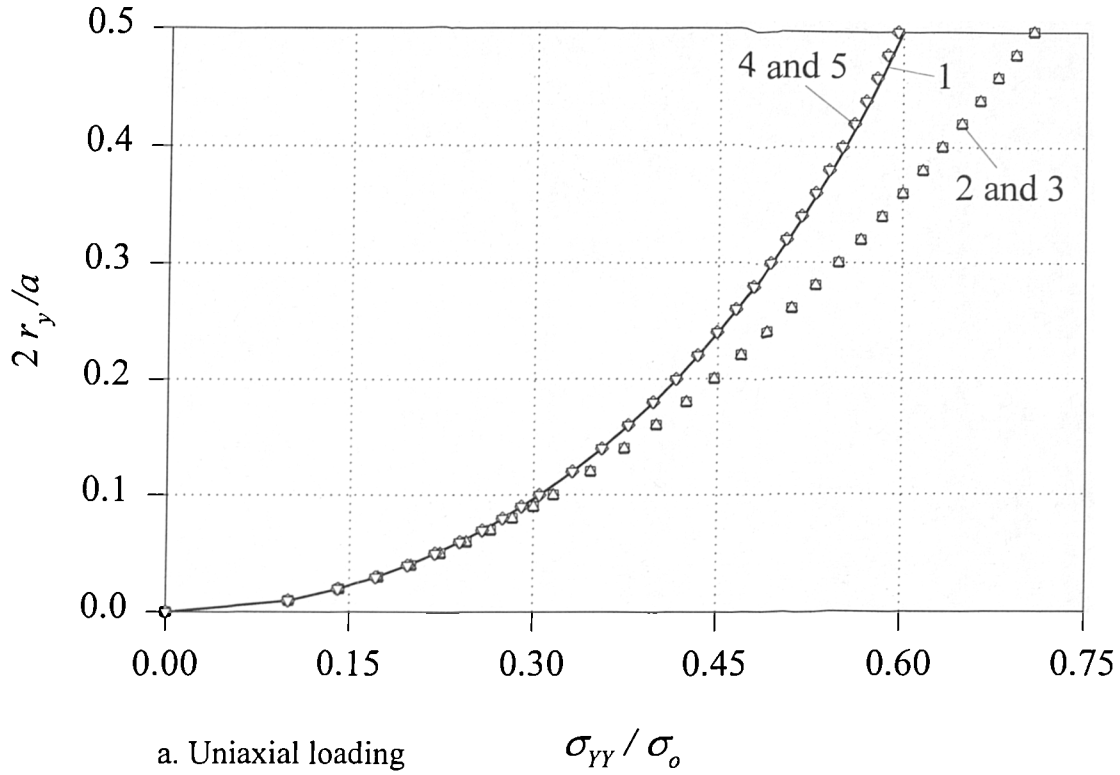

a. Uniaxial loading

1. Exact solution
2. Expansion, singular terms
3. Expansion, singular terms + T
4. Expansion, singular terms + $r^{1/2}$ terms
5. Expansion, singular terms + $T + r^{1/2}$ terms

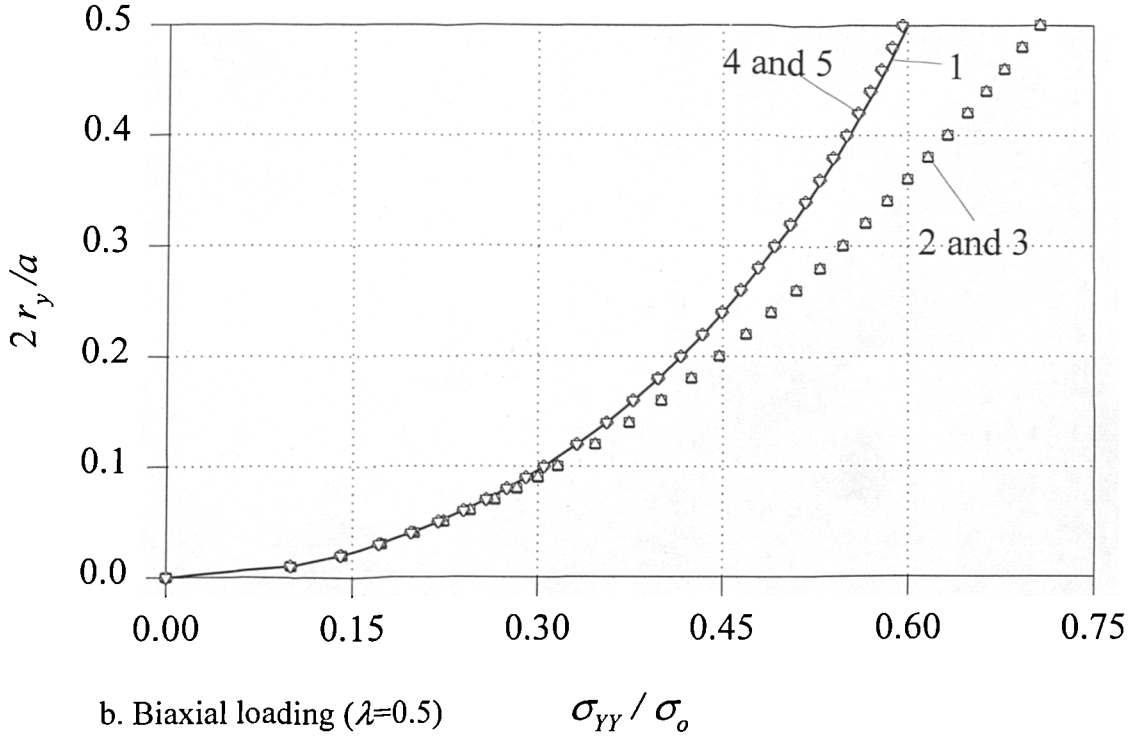

b. Biaxial loading (λ=0.5)

Figure 3-7. Plastic zone size along the crack line versus external load. Plane stress, Tresca yield criterion

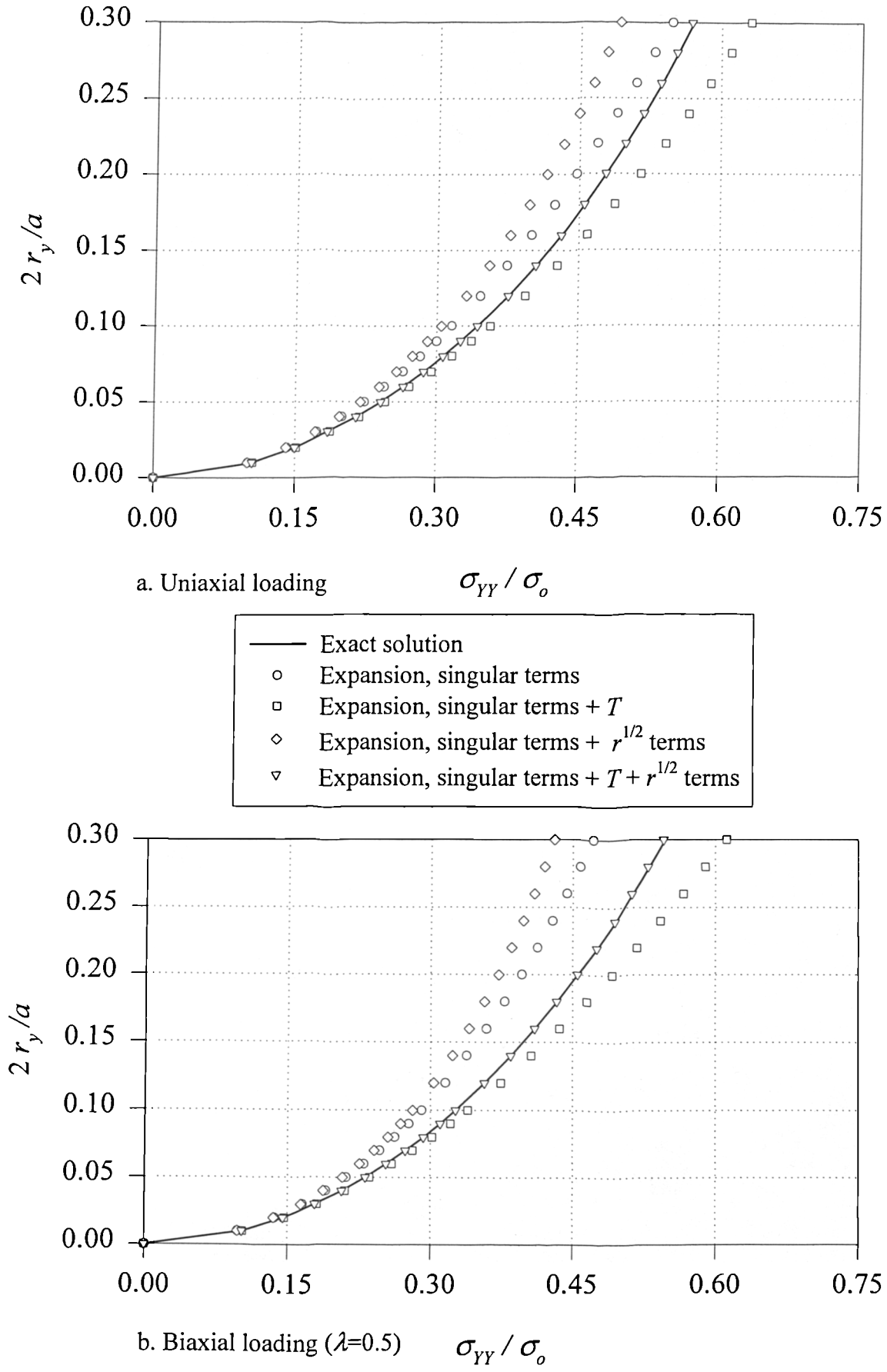

Figure 3-8. Plastic zone size along the crack line versus external load.
Plane stress, von Mises yield criterion

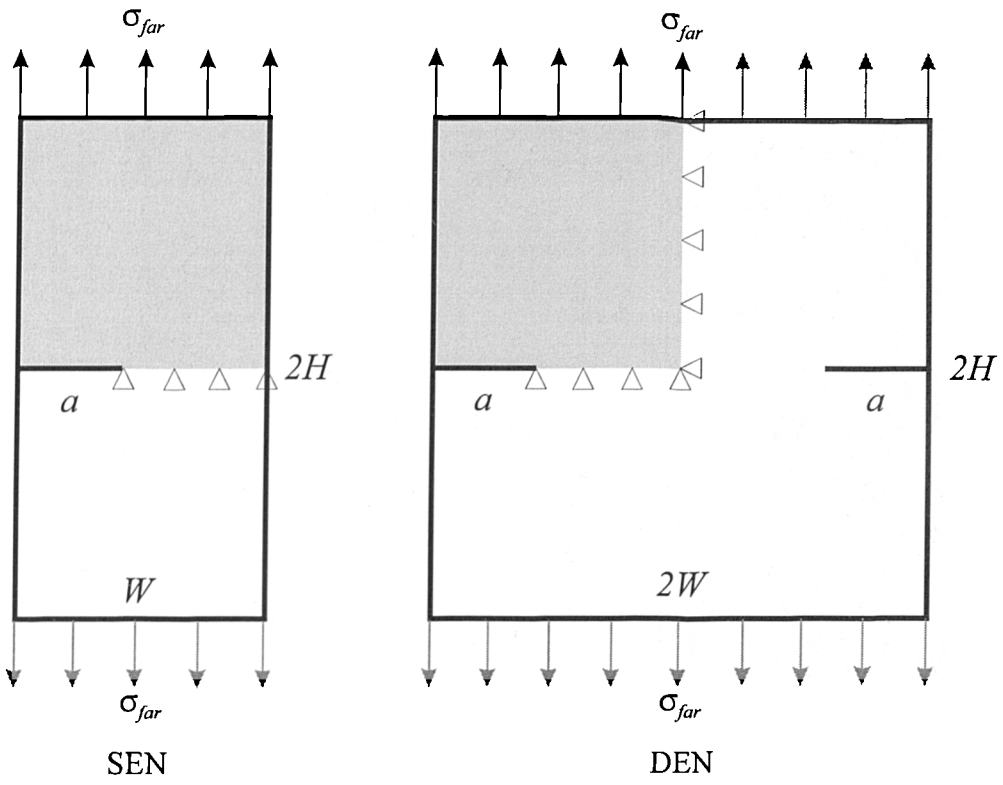

Figure 4-1. Single edge notched (SEN) and double edge notched (DEN) specimens.

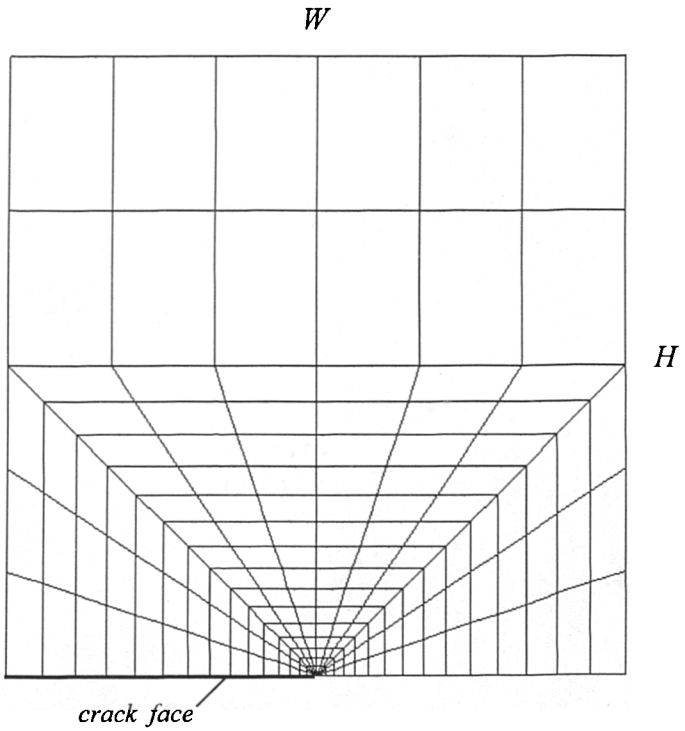

Figure 4-2. Mesh pattern for one half of the SEN specimen and one quarter of the DEN specimen.

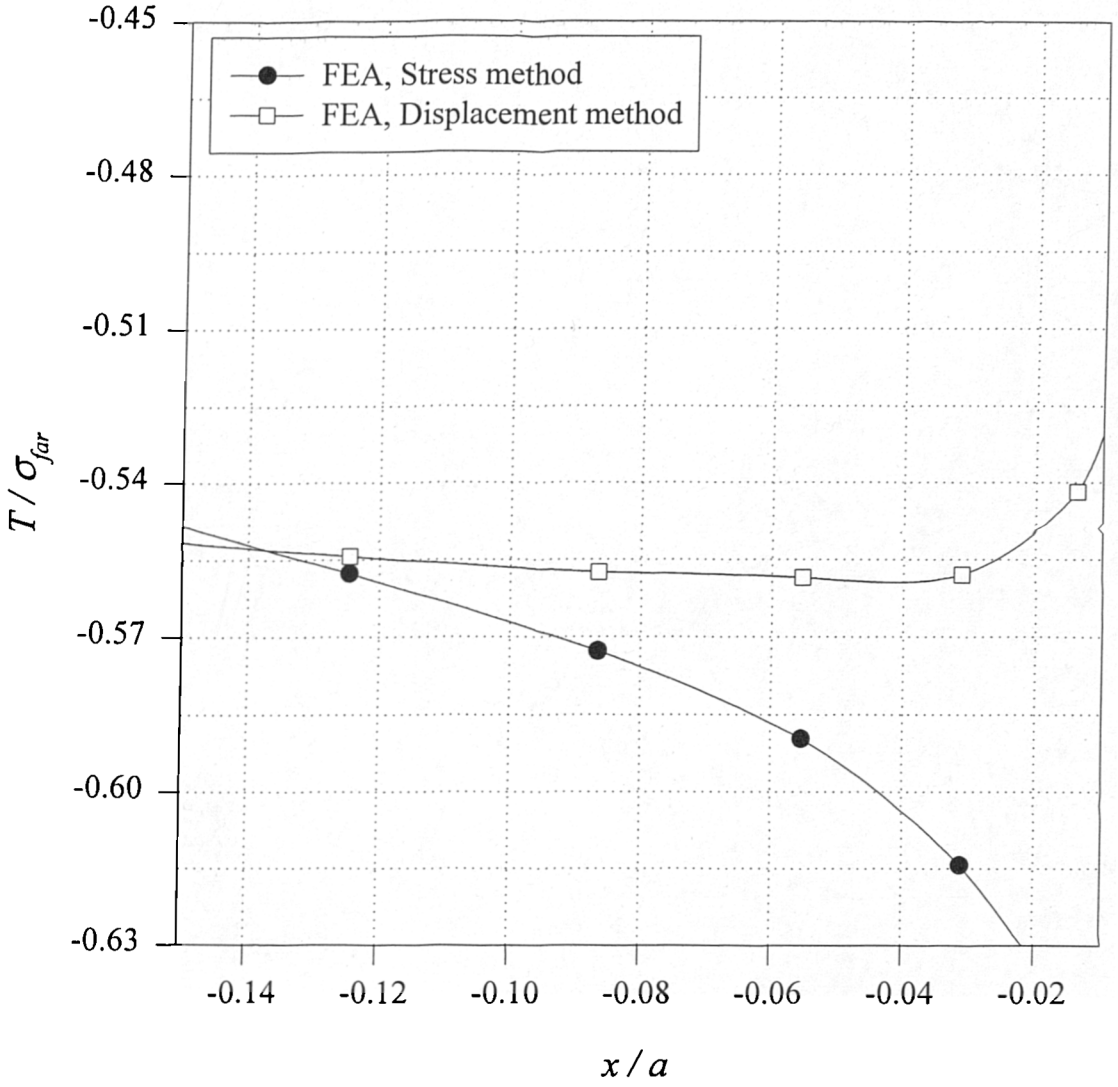

Figure 4-3. Normalised T in a single edge notched specimen of a/W=0.4 .

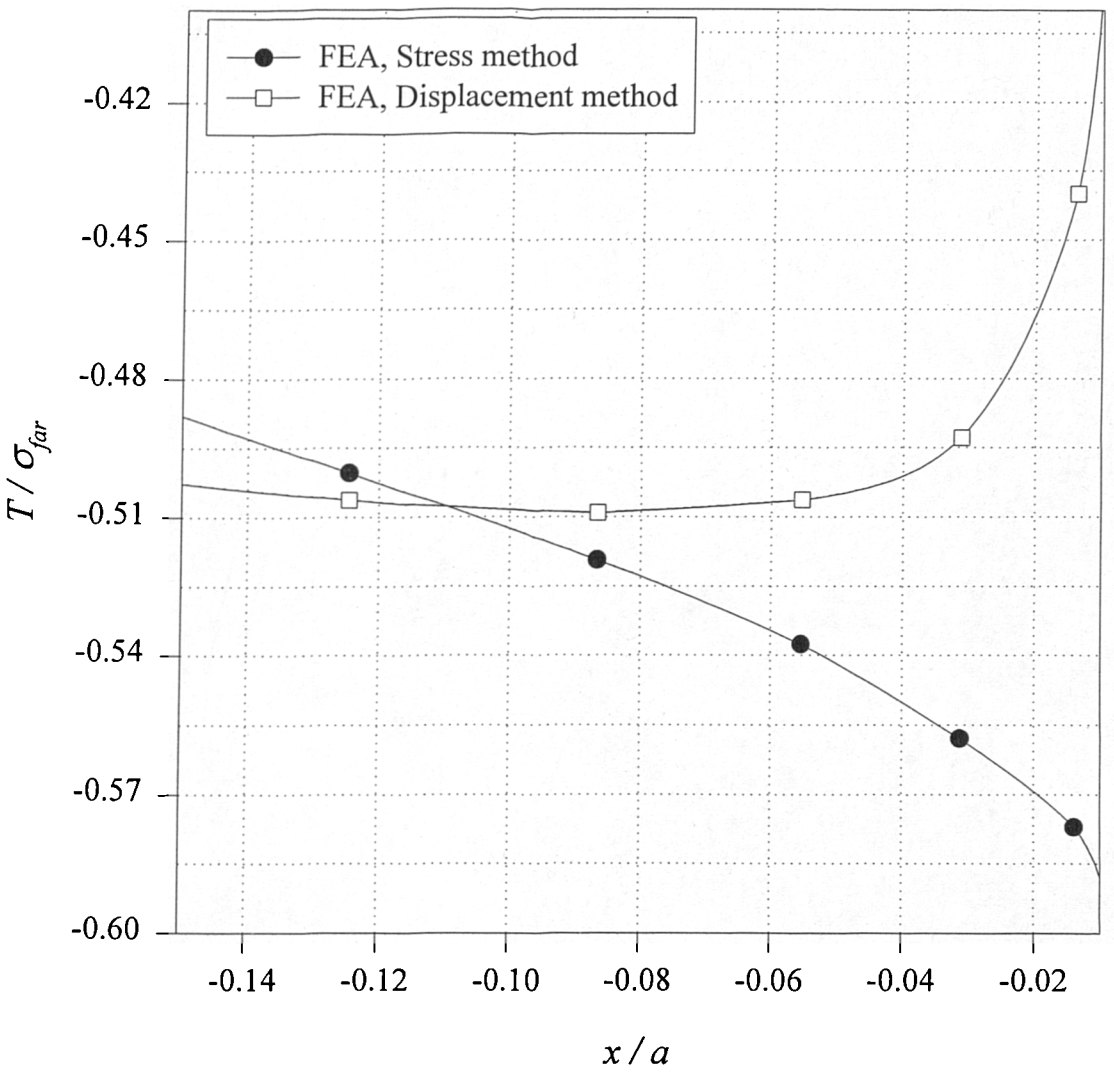

Figure 4-4. Normalised T in a double edge notched specimen of a/W=0.2 .

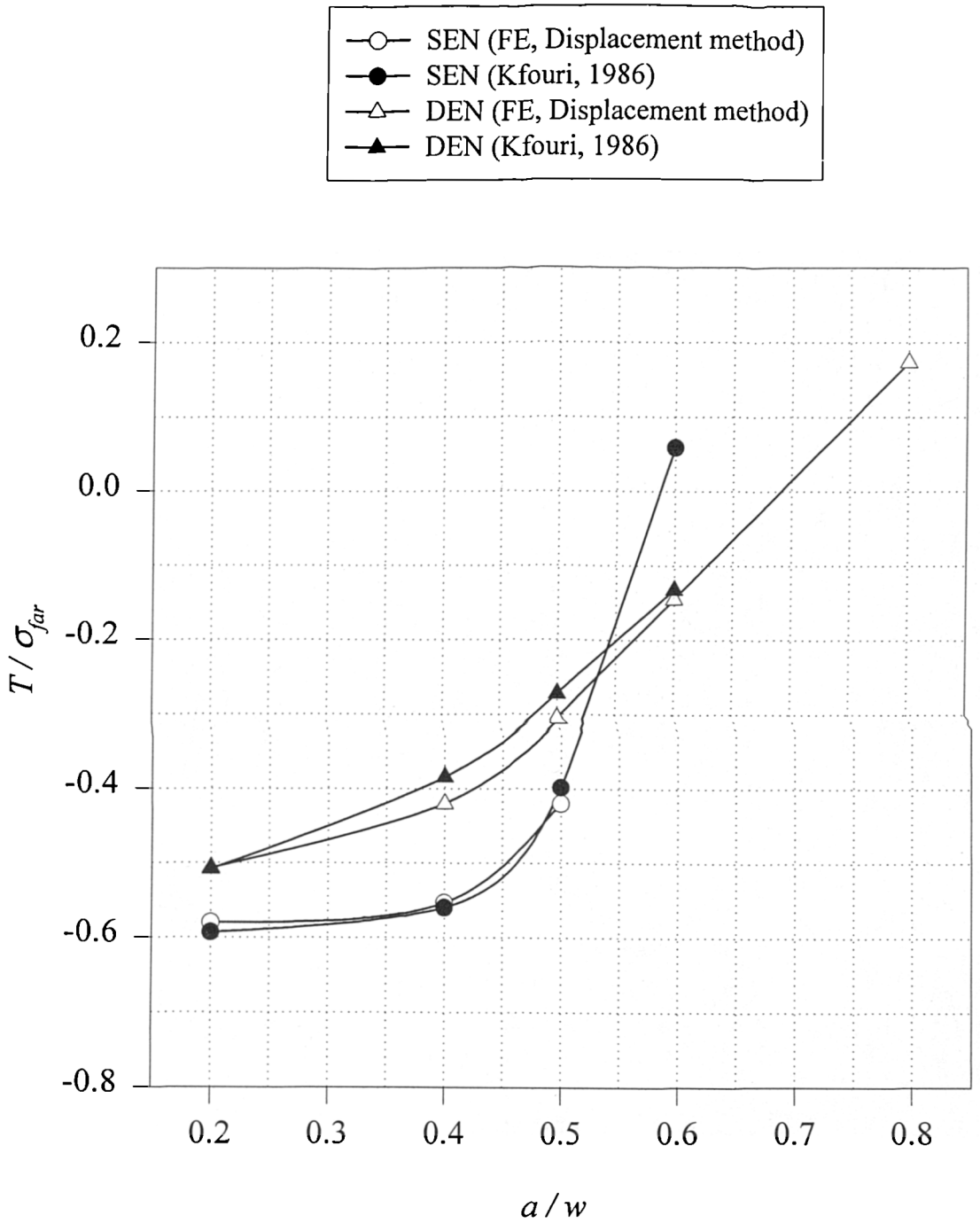

Figure 4-5. *T*-stress determined using the displacement method, compared with results calculated by Kfouri(1986) for SEN and DEN specimens of different crack length.

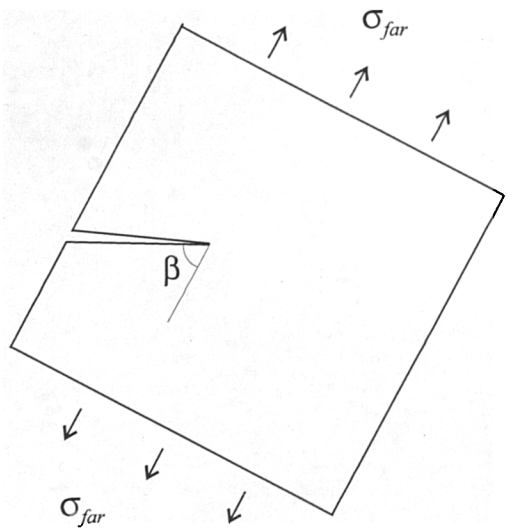

Figure 4-6. An inclined edge crack in a large square plate subjected to a uniform tensile load.

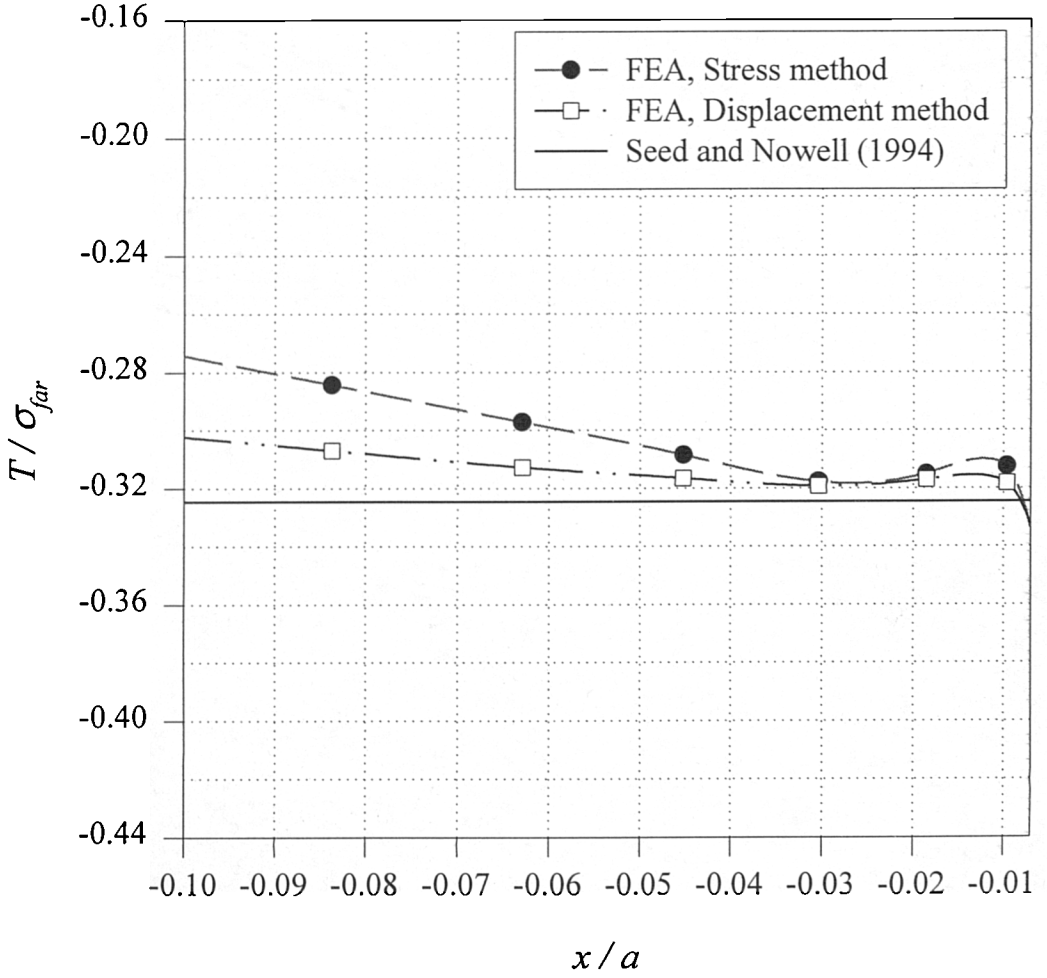

Figure 4-7. Normalised T in an angled edge crack in a large square plate (loading angle $\beta = 70^{o}$) .

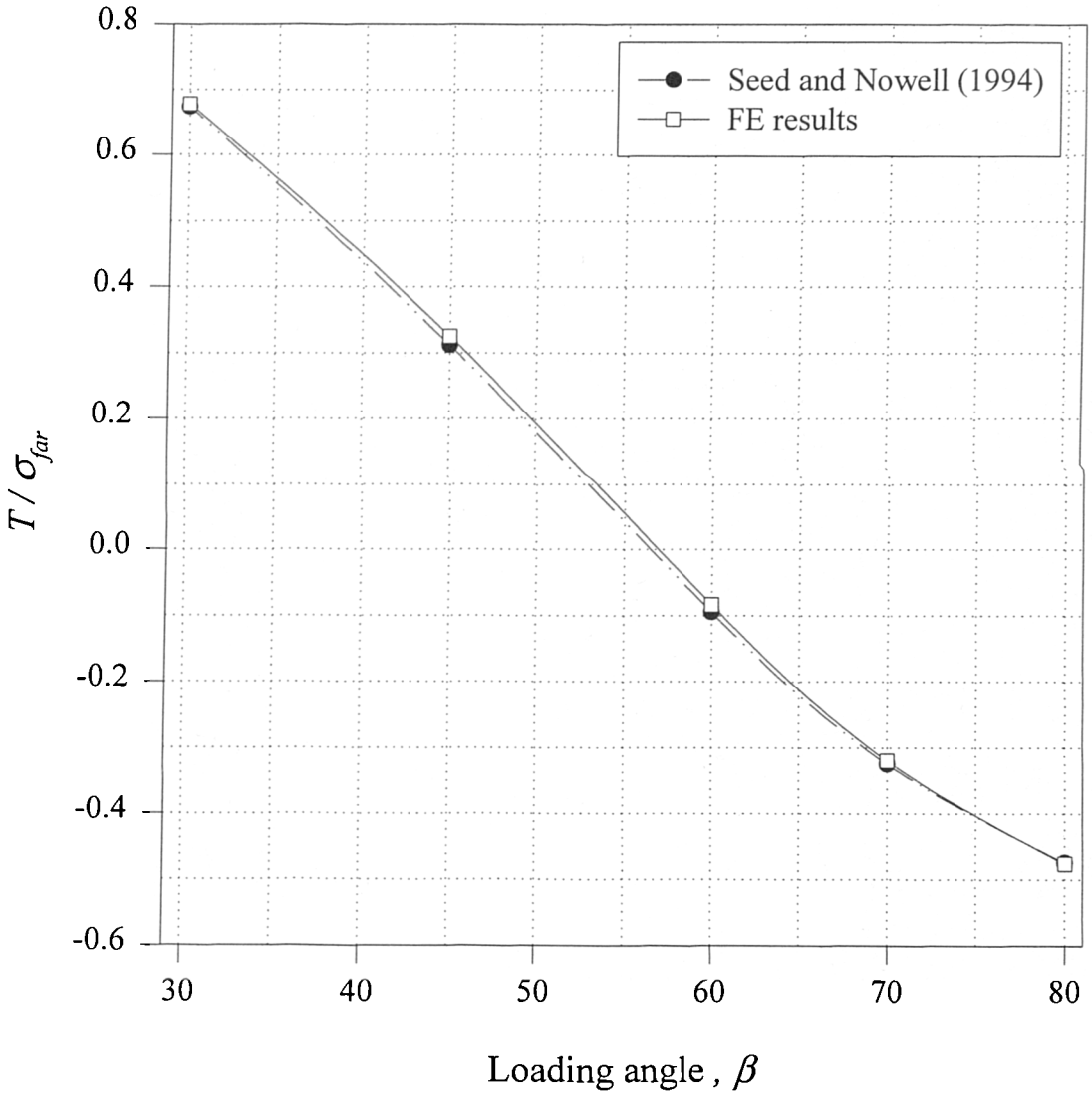

Figure 4-8. Normalised T for different loading angles, FE results compared with those presented by Seed and Nowell (1994).

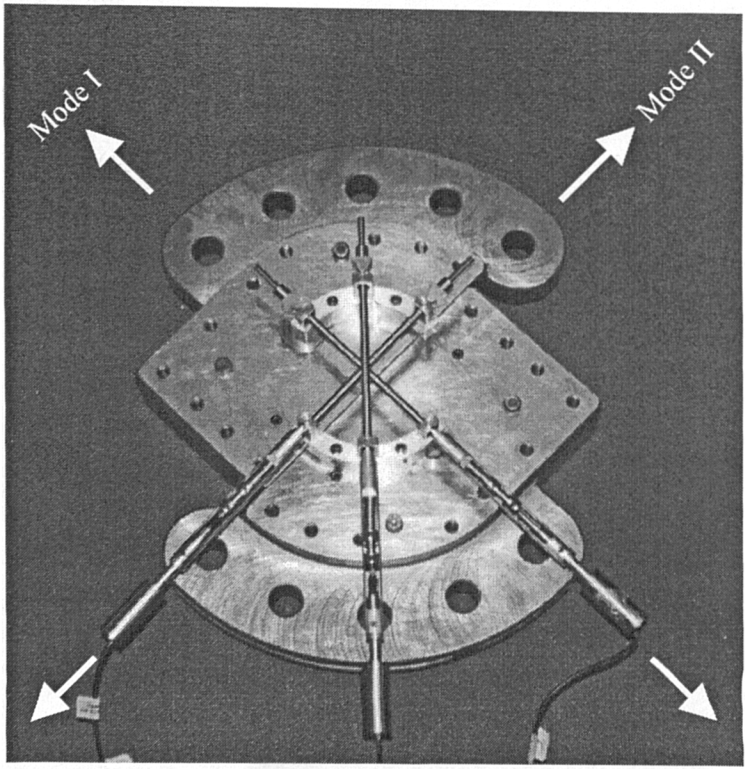

a

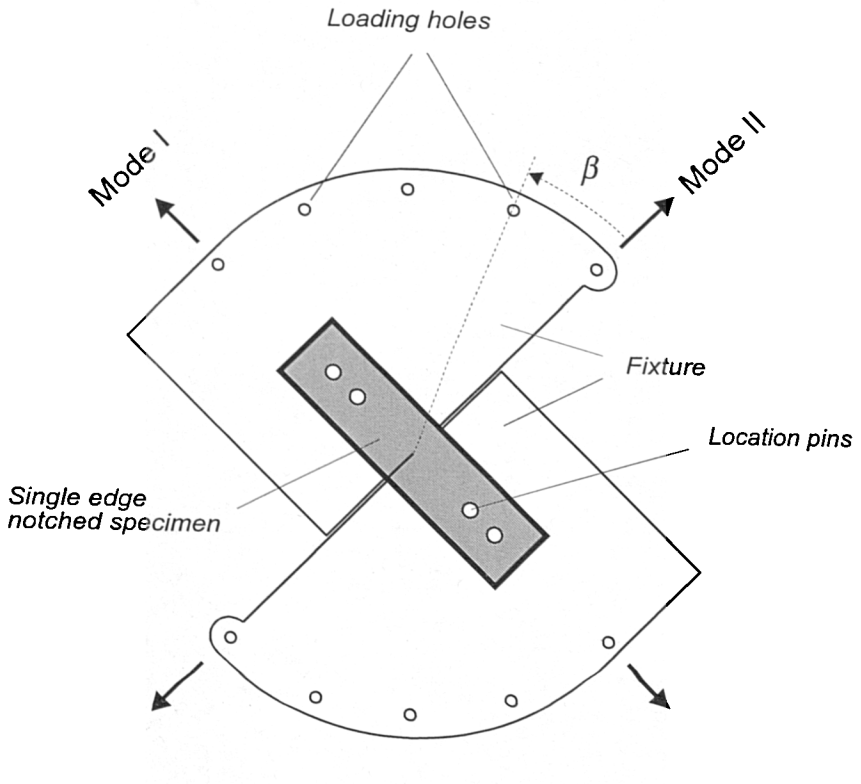

b

Figure 4-9. Test apparatus designed for mixed mode fracture tests. (Swankie, 1999)

a) Perfect connection model:
Specimen and Fixture as a single unit.
Link: Perfect connection.

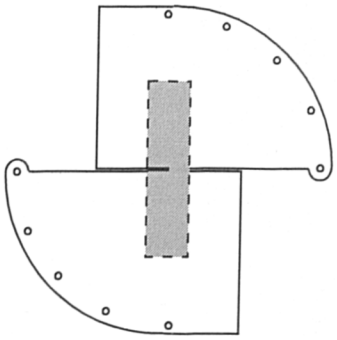

b) Pinned model:
Specimen and Fixture are two individual units.
Link: Only through location pins.

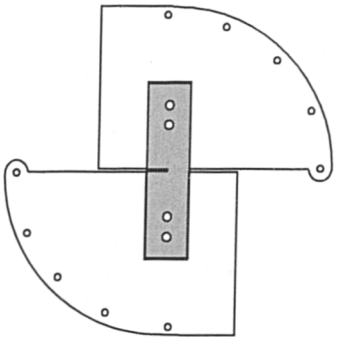

c) Contact model:
Specimen and Fixture are two individual units.
Link: Location pins plus contact elements between the two units.

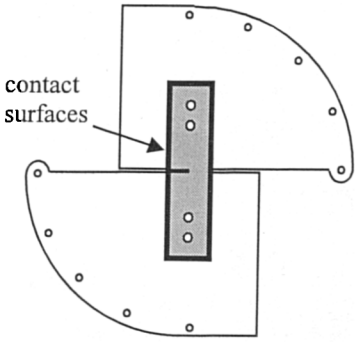

Figure 4-10. Three models used to simulate the link between the specimen and the fixture.

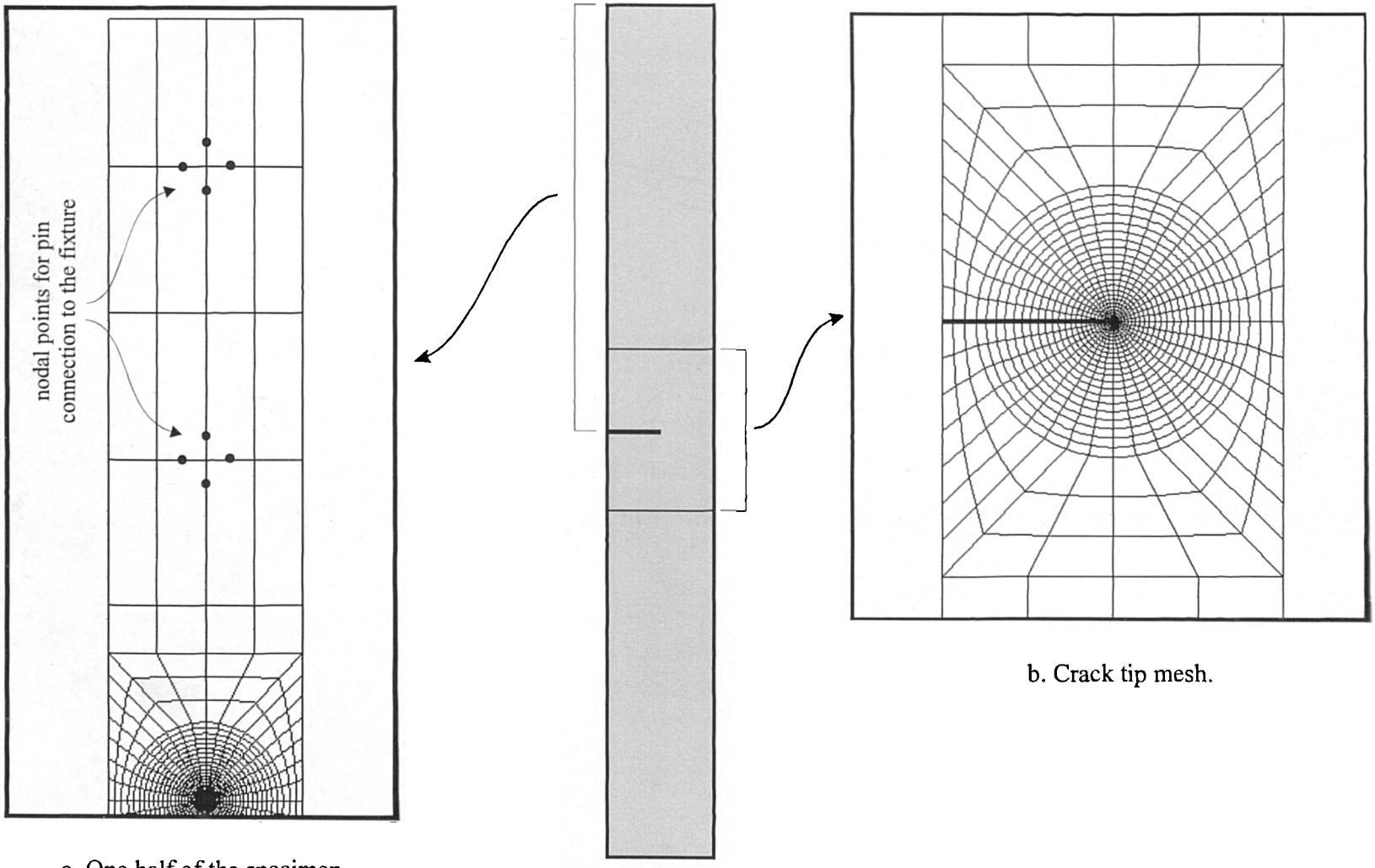

a. One half of the specimen.

b. Crack tip mesh.

Figure 4-11. Finite element mesh for
the SEN specimen.

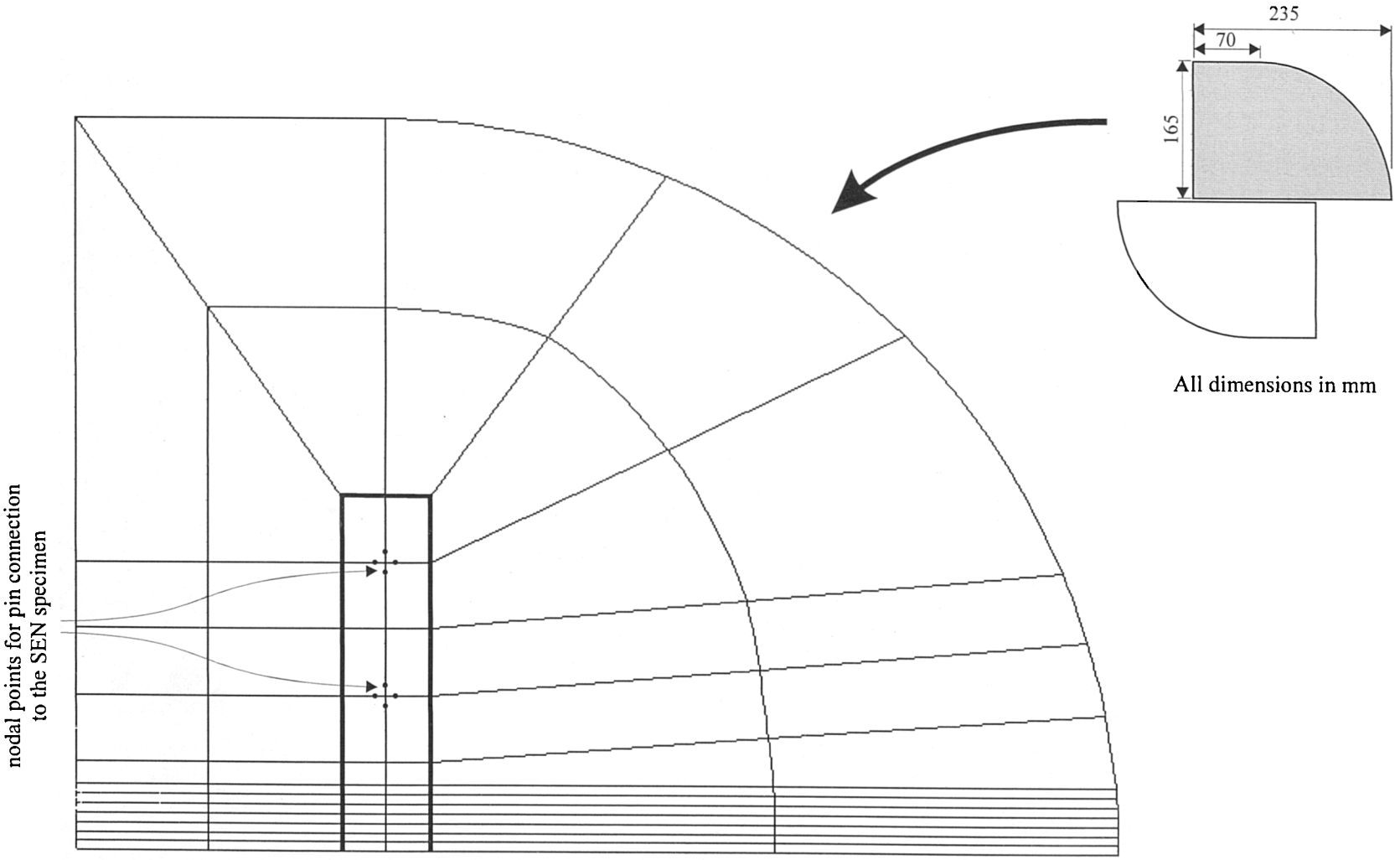

Figure 4-12. Finite element mesh for one half of the fixture.

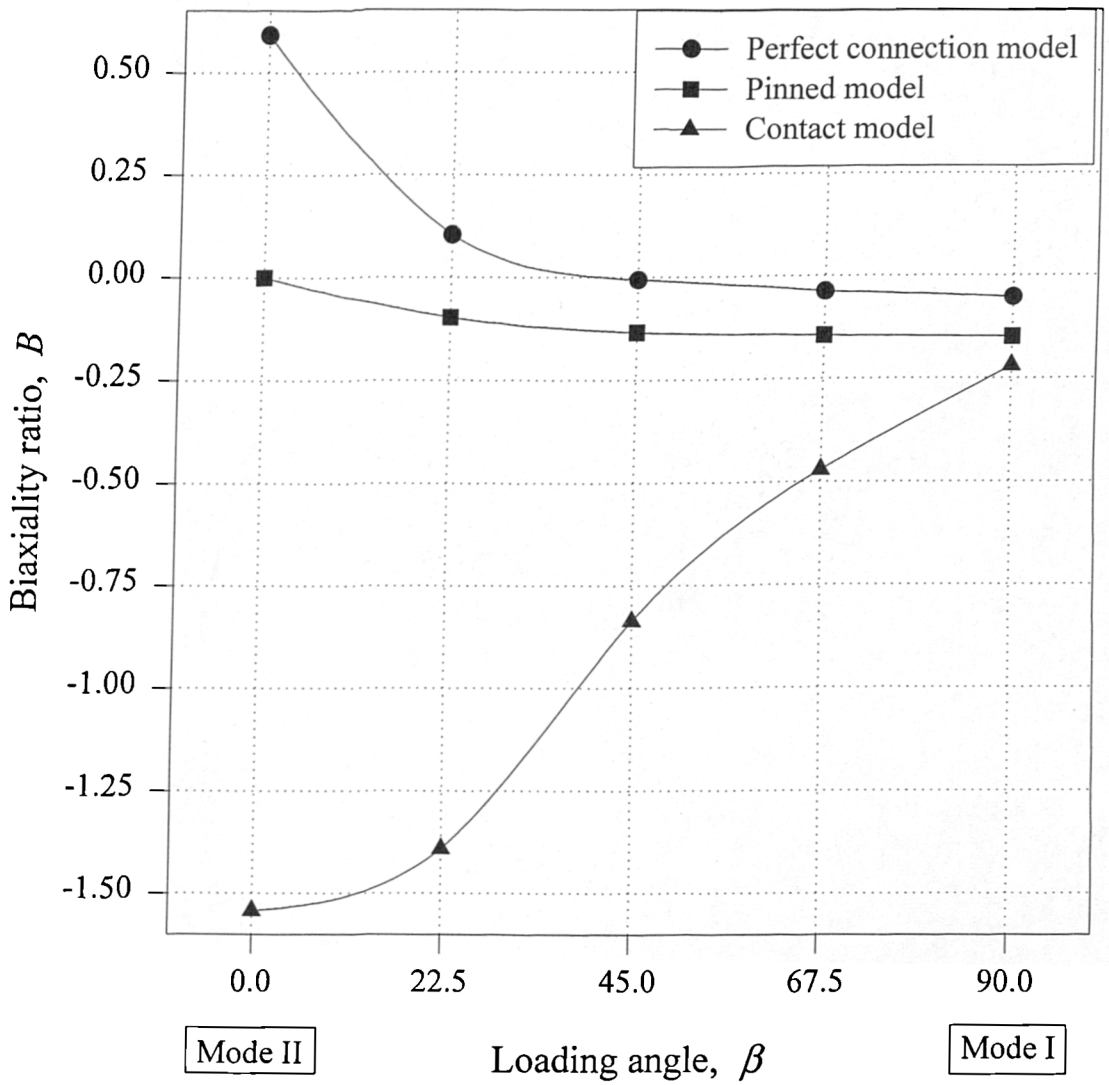

Figure 4-13. Biaxiality ratio in the mixed-mode test rig for crack depth to specimen width ratio (a/W) of 0.5.

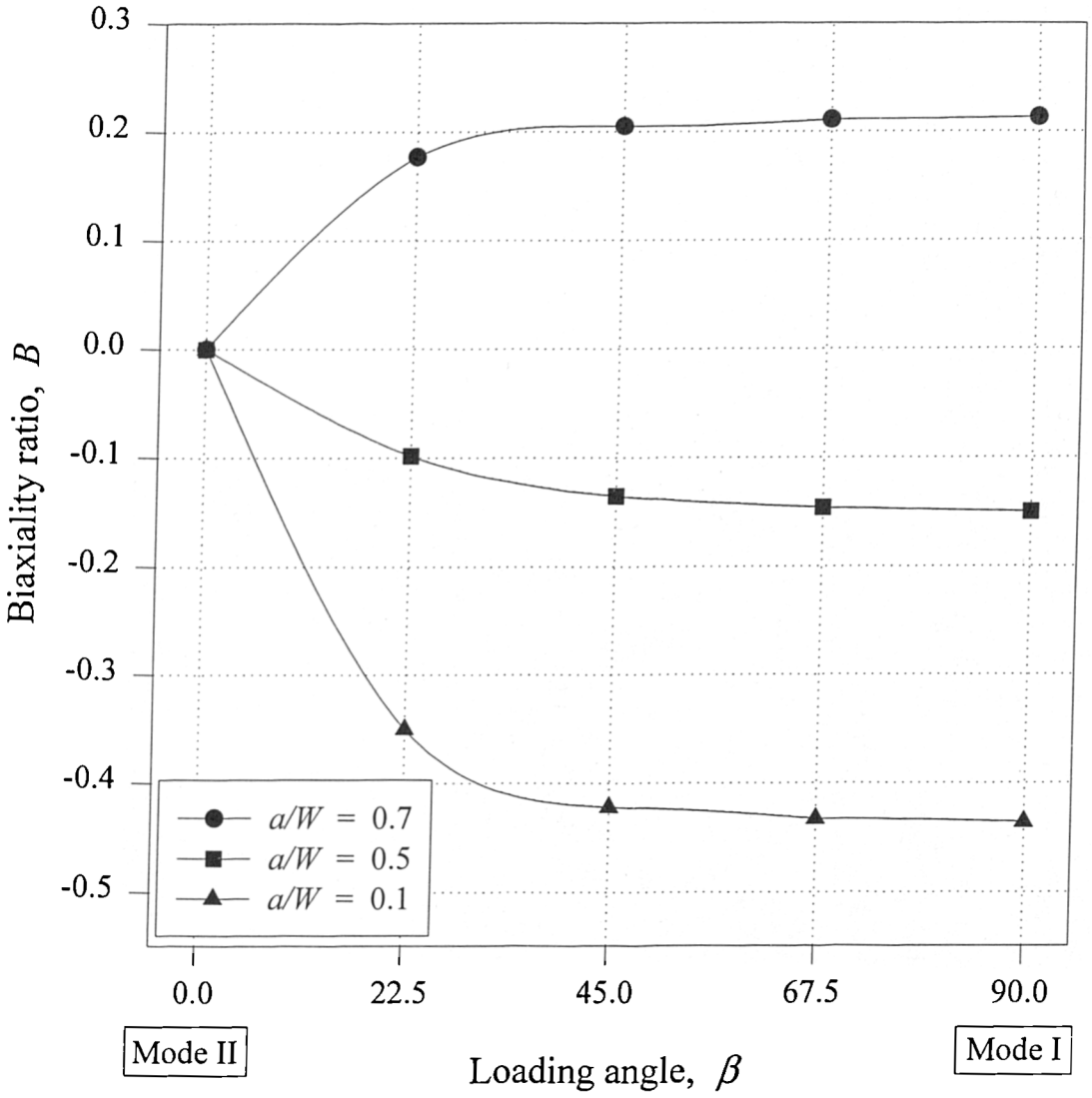

Figure 4-14. Biaxiality ratio for the mixed-mode test rig in the case of pin loading alone (pinned model) for crack depth to specimen width ratios (a/W) of: 0.1, 0.5 and 0.7 .

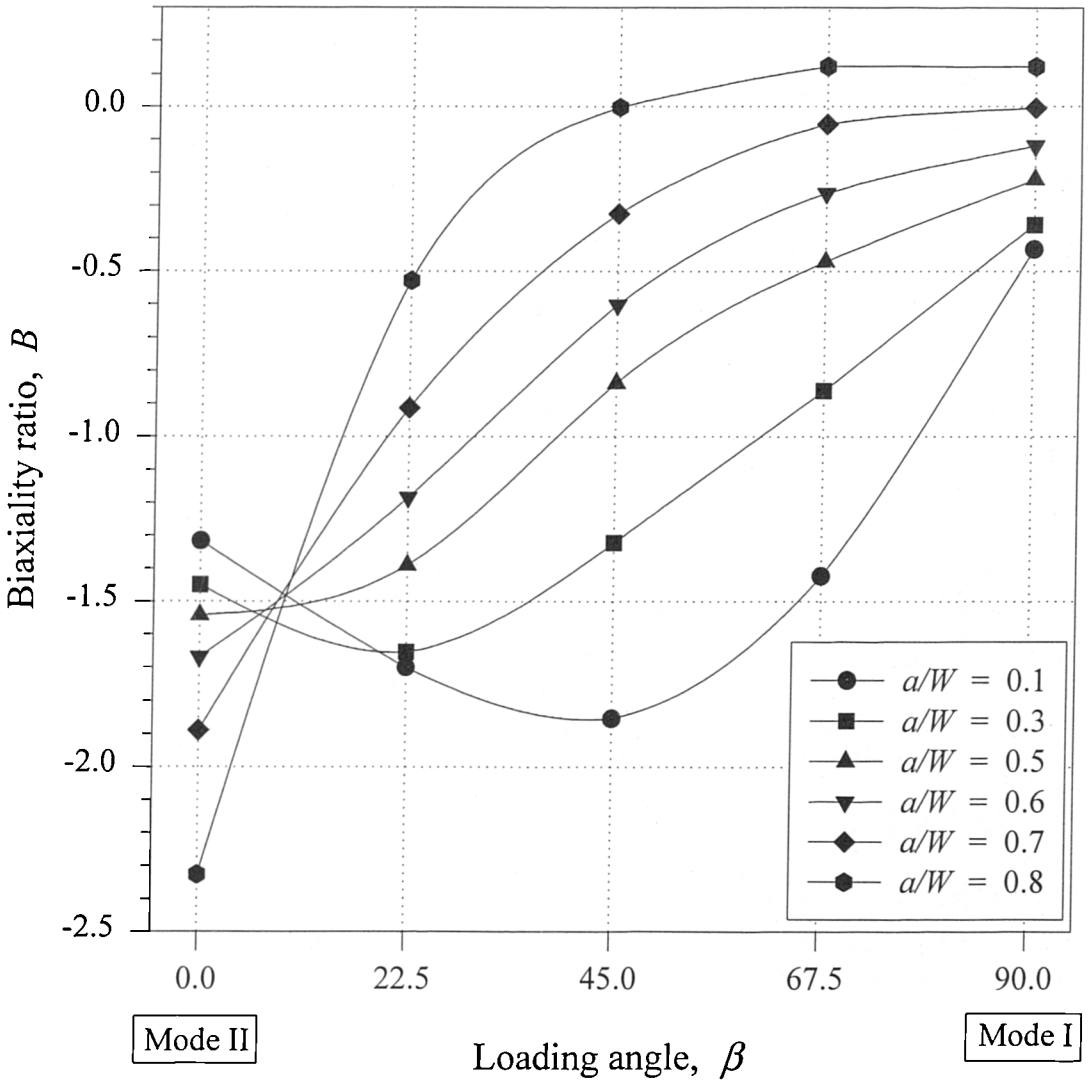

Figure 4-15. Biaxiality ratio for the mixed-mode test rig in the case of pin loading plus contact elements (contact model) for different crack depth to specimen width ratios (a/W).

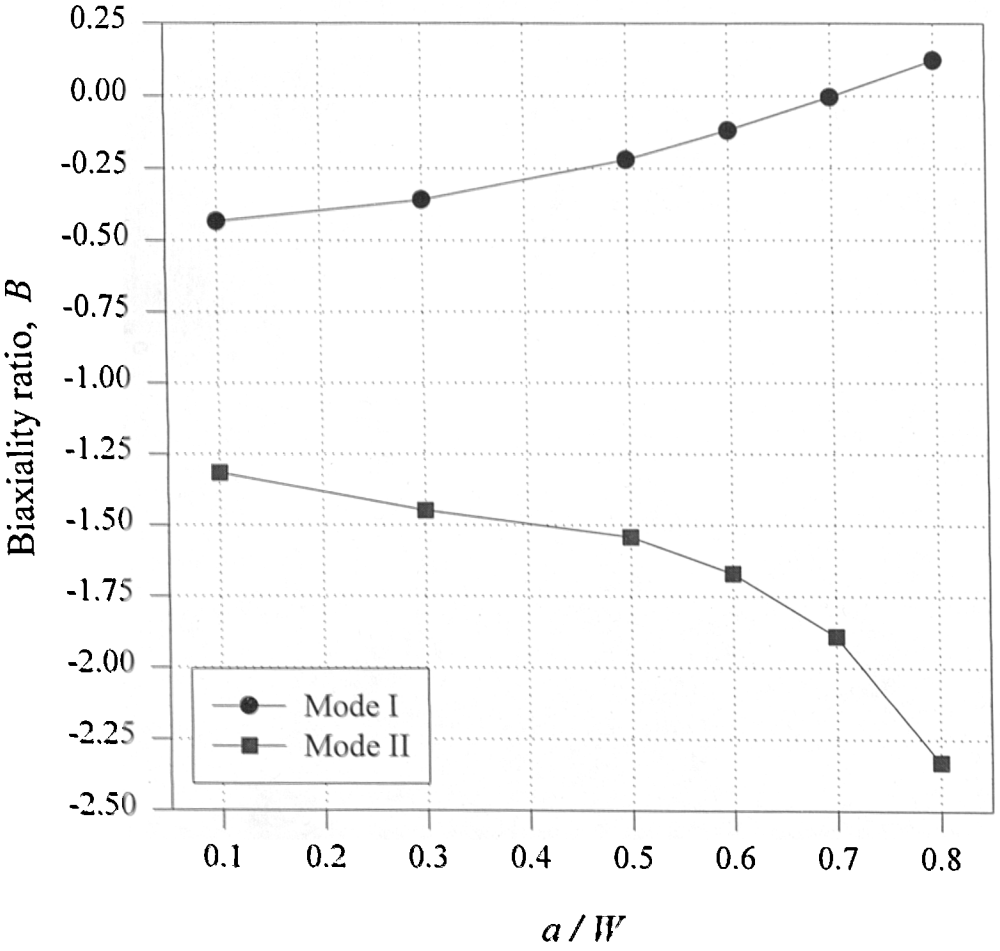

Figure 4-16. Variation of biaxiality ratio with respect to crack length to specimen width (a/W) for modes I and II in the contact model.

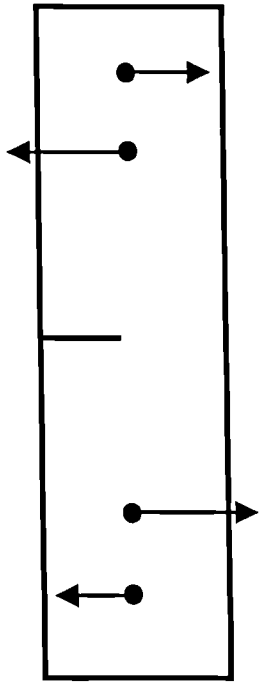

Figure 4-17. A sample of loading condition to produce ideal mode II.

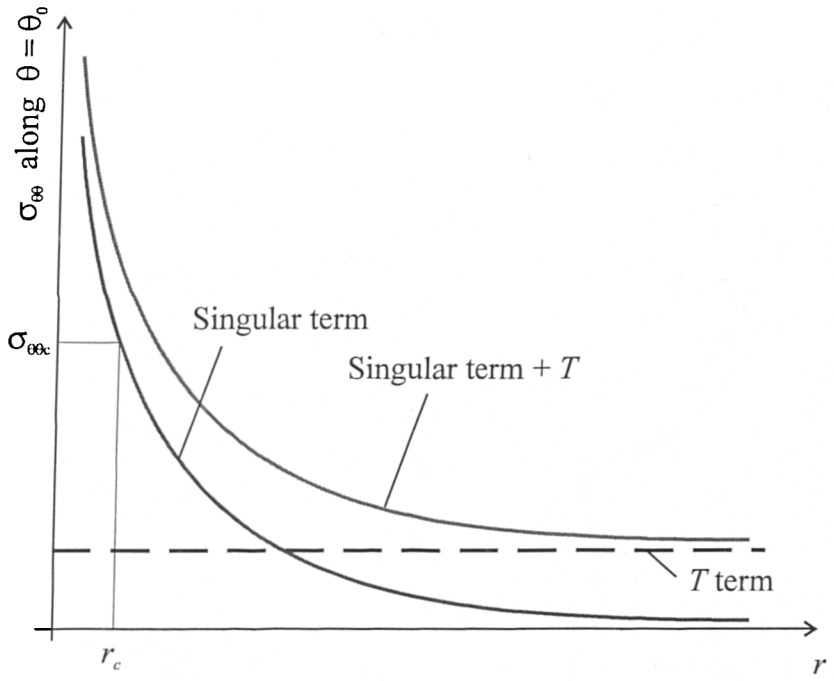

Figure 5-1. Elastic tangential stress along the direction of fracture initiation θ_0.

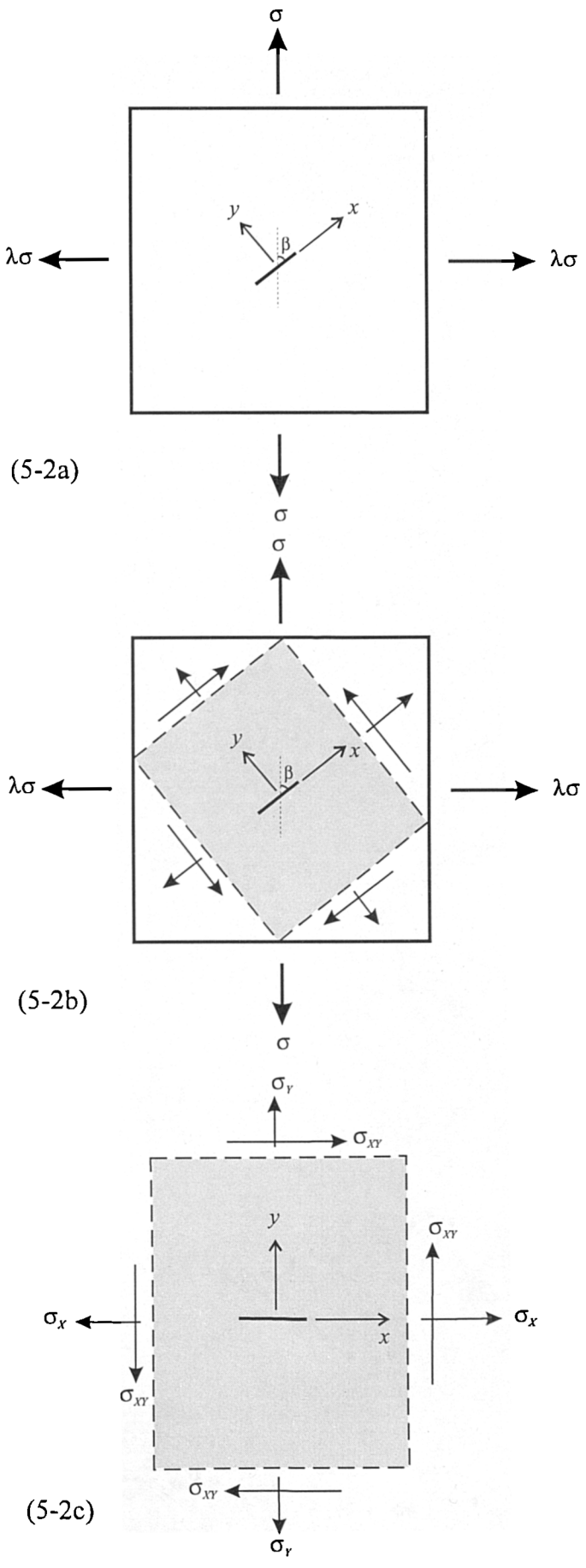

Figure 5-2. An angled internal crack in a biaxially loaded panel.

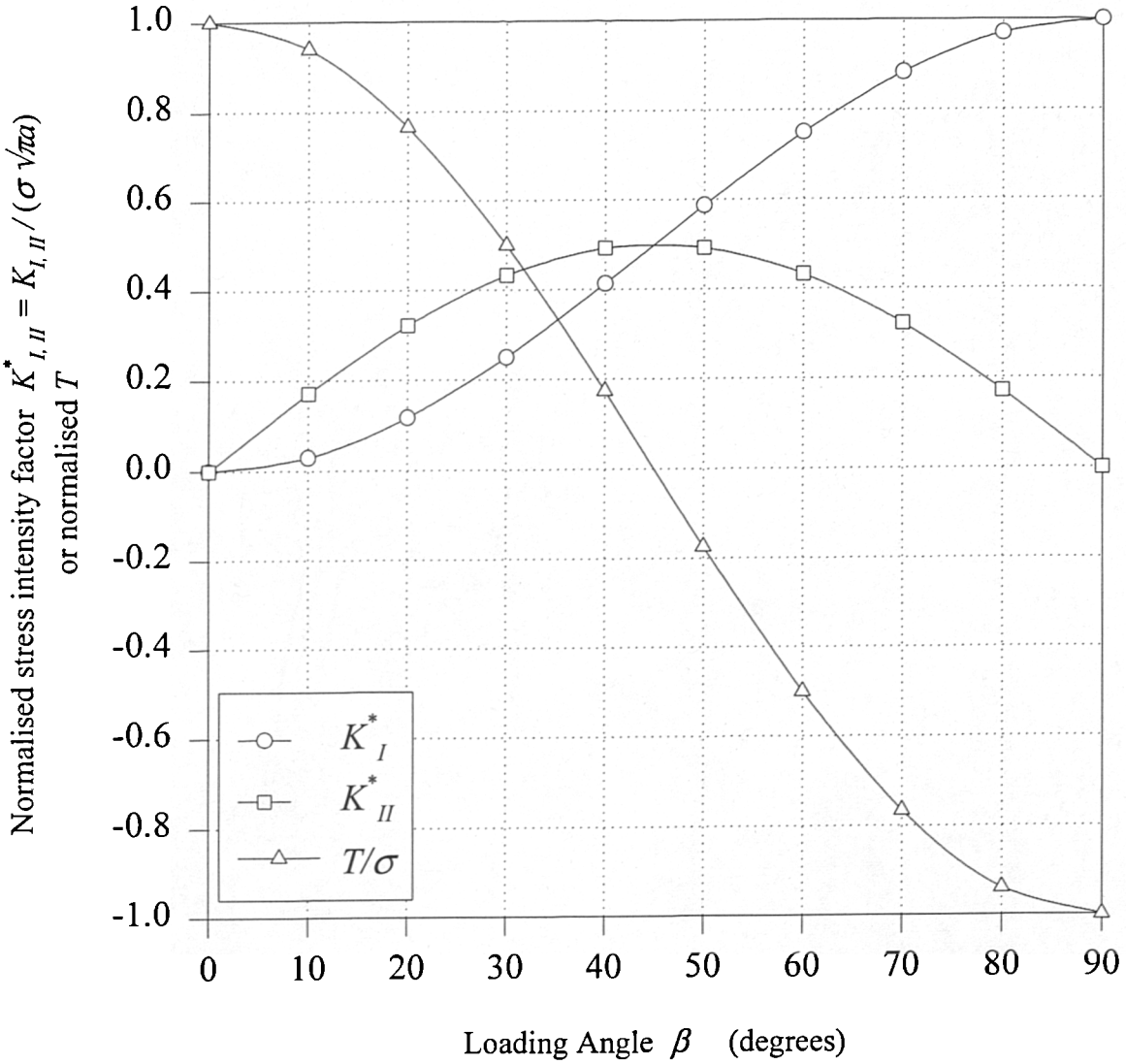

Figure 5-3. Variation of normalised K_I , K_{II} and T with loading angle β in a centrally cracked plate under uniaxial load.

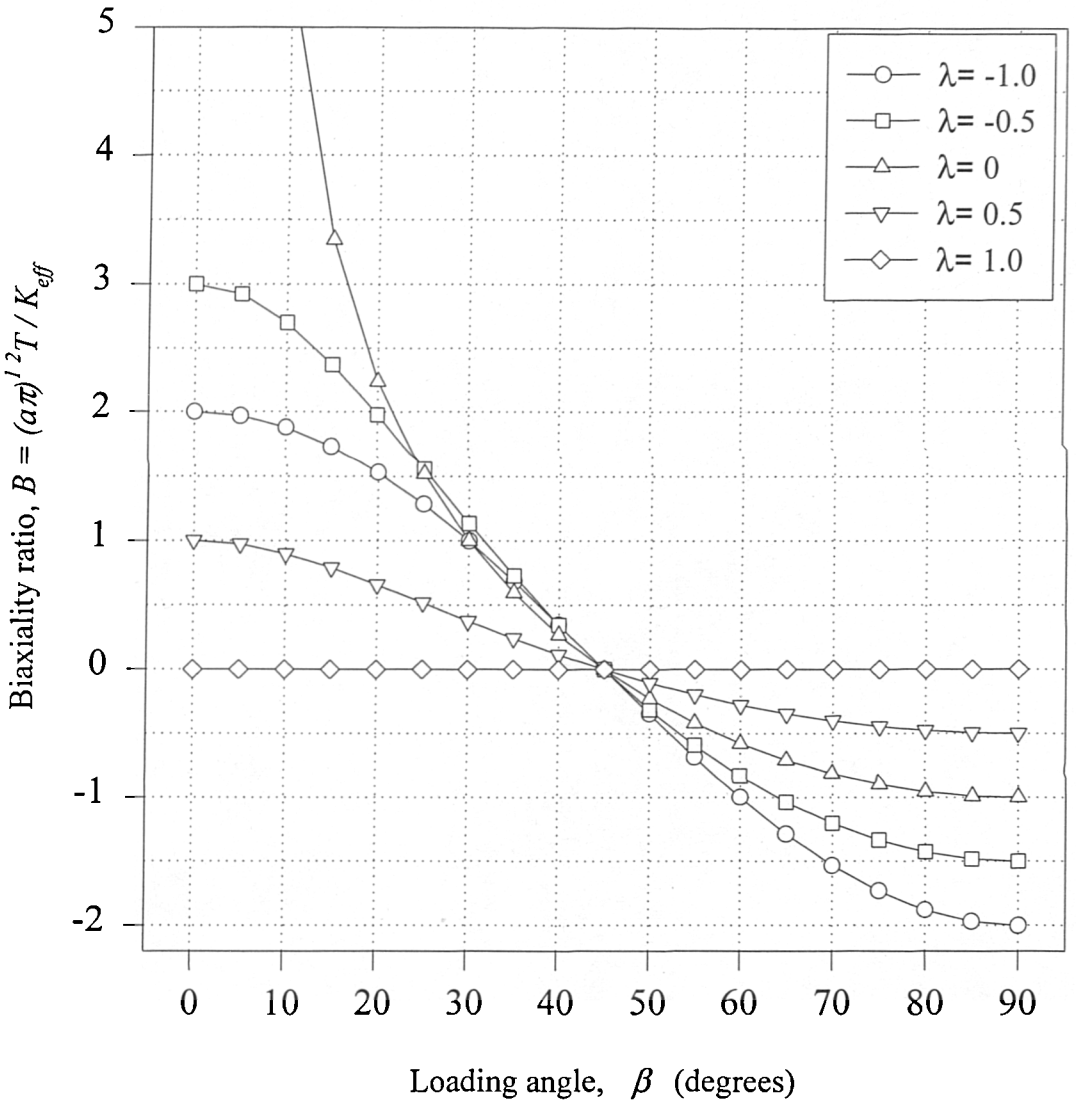

Figure 5-4. Variation of the biaxiality ratio with loading angle in a centrally cracked plate under biaxial uniform load for different values of the lateral load parameter λ.

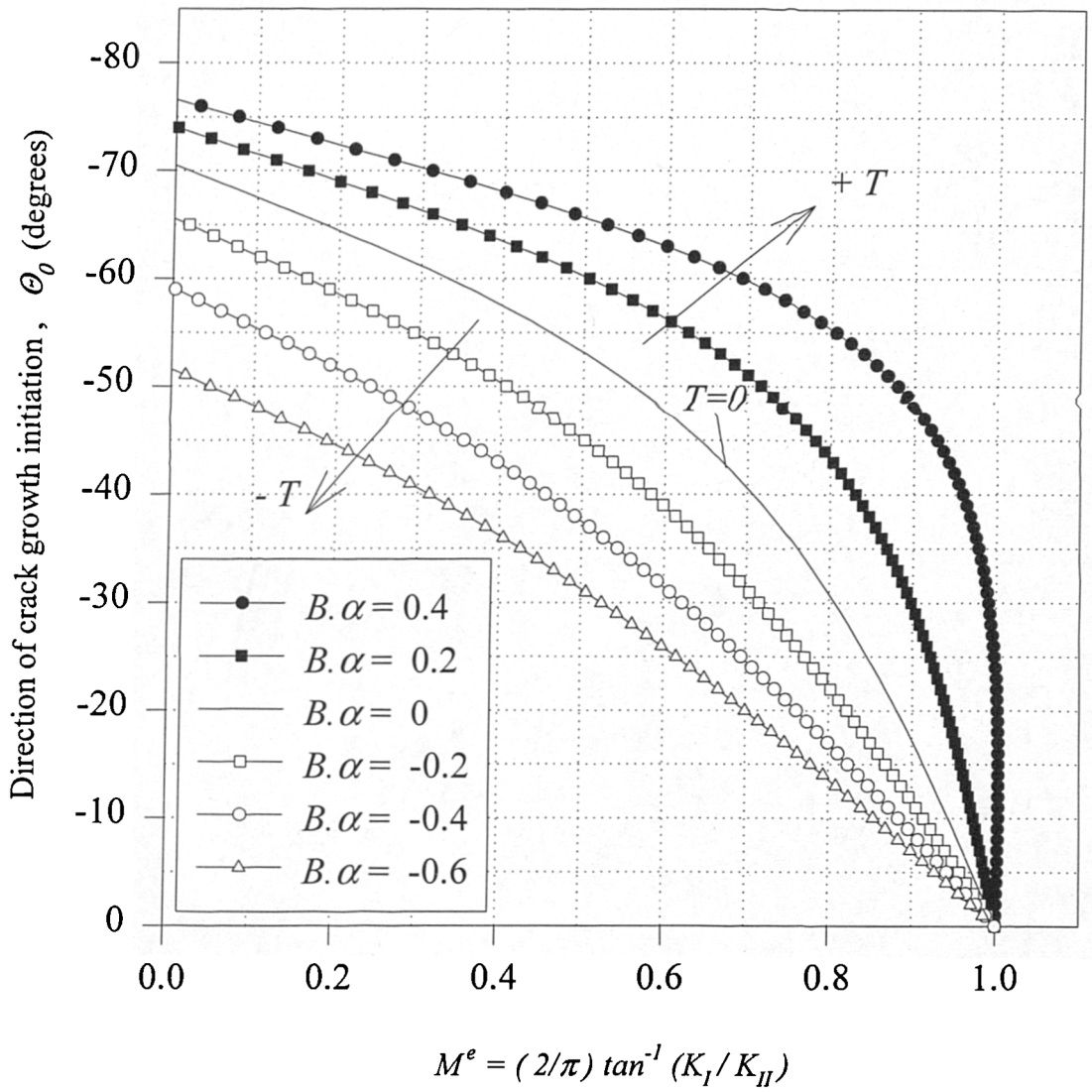

Figure 5-5. Effect of T on the direction of crack growth initiation in mixed mode fracture based on the generalised maximum tangential stress criterion.

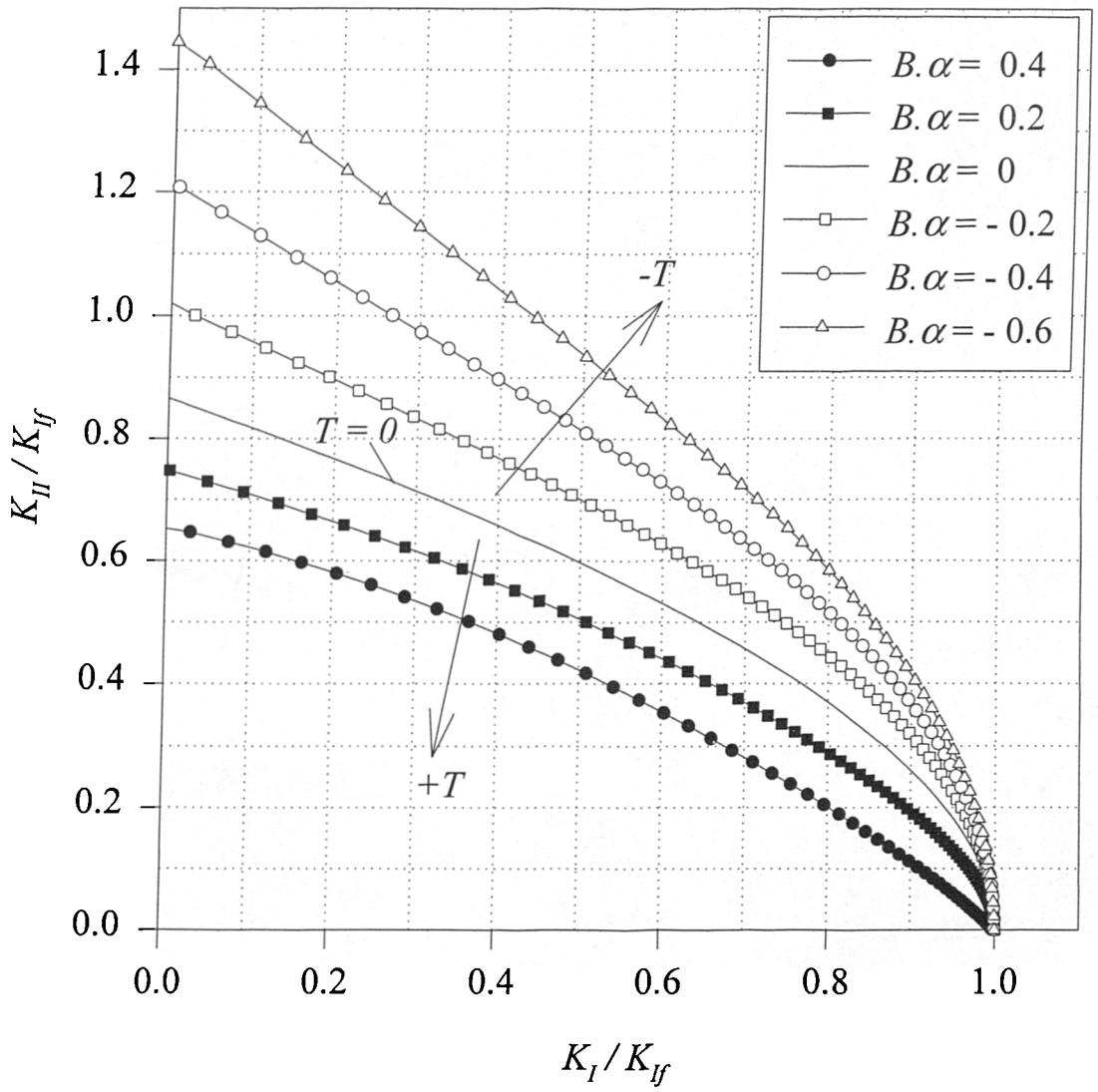

Figure 5-6. Mixed mode fracture loci based on the generalised maximum tangential stress criterion. $B=T.(\pi a)^{1/2}/K_{eff}$ and $\alpha=(2r_c/a)^{1/2}$.

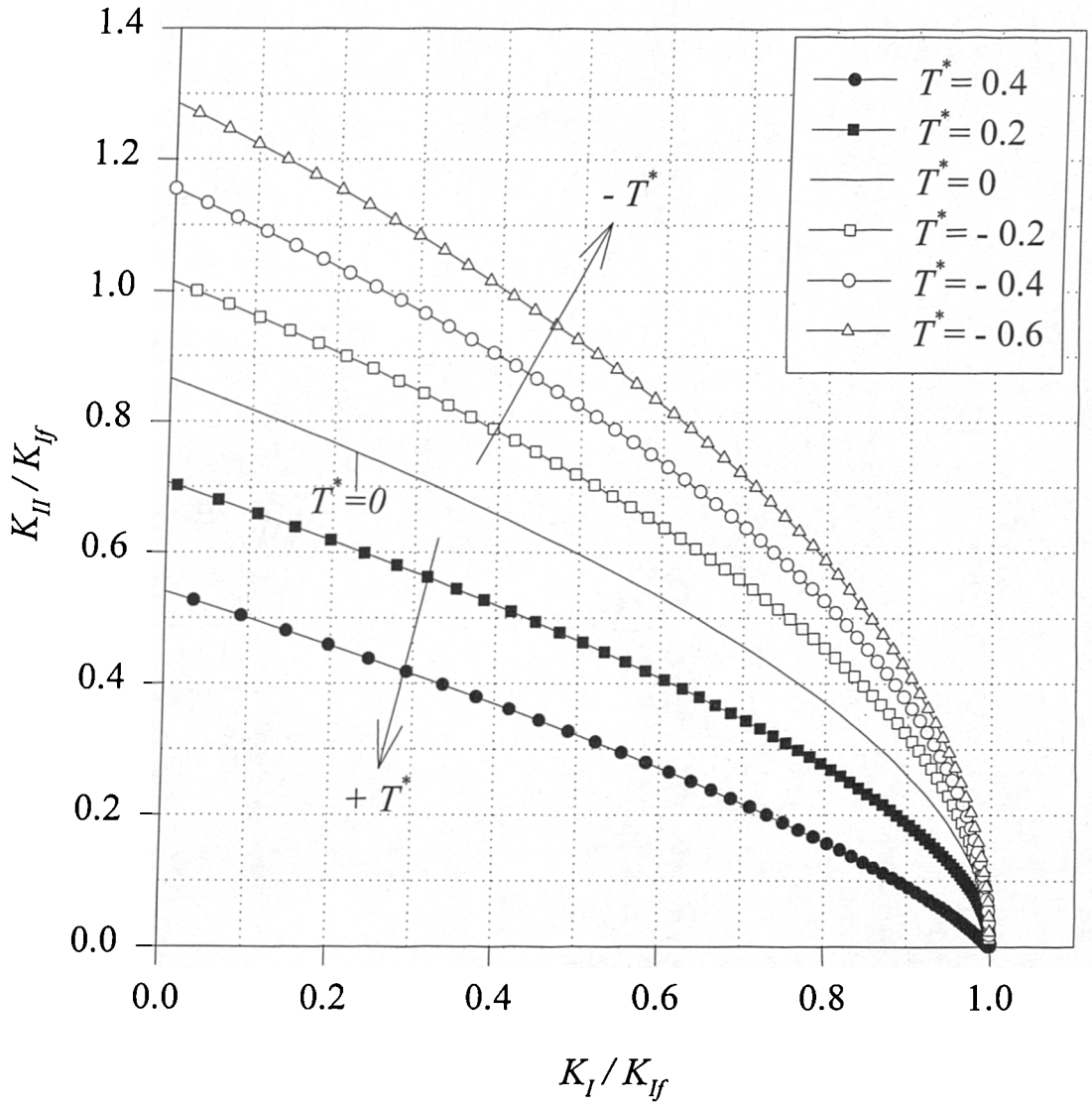

Figure 5-7. Mixed mode fracture loci based on the generalised maximum tangential stress criterion. $T^*=(2\pi r_c)^{1/2}T/K_{If}$.

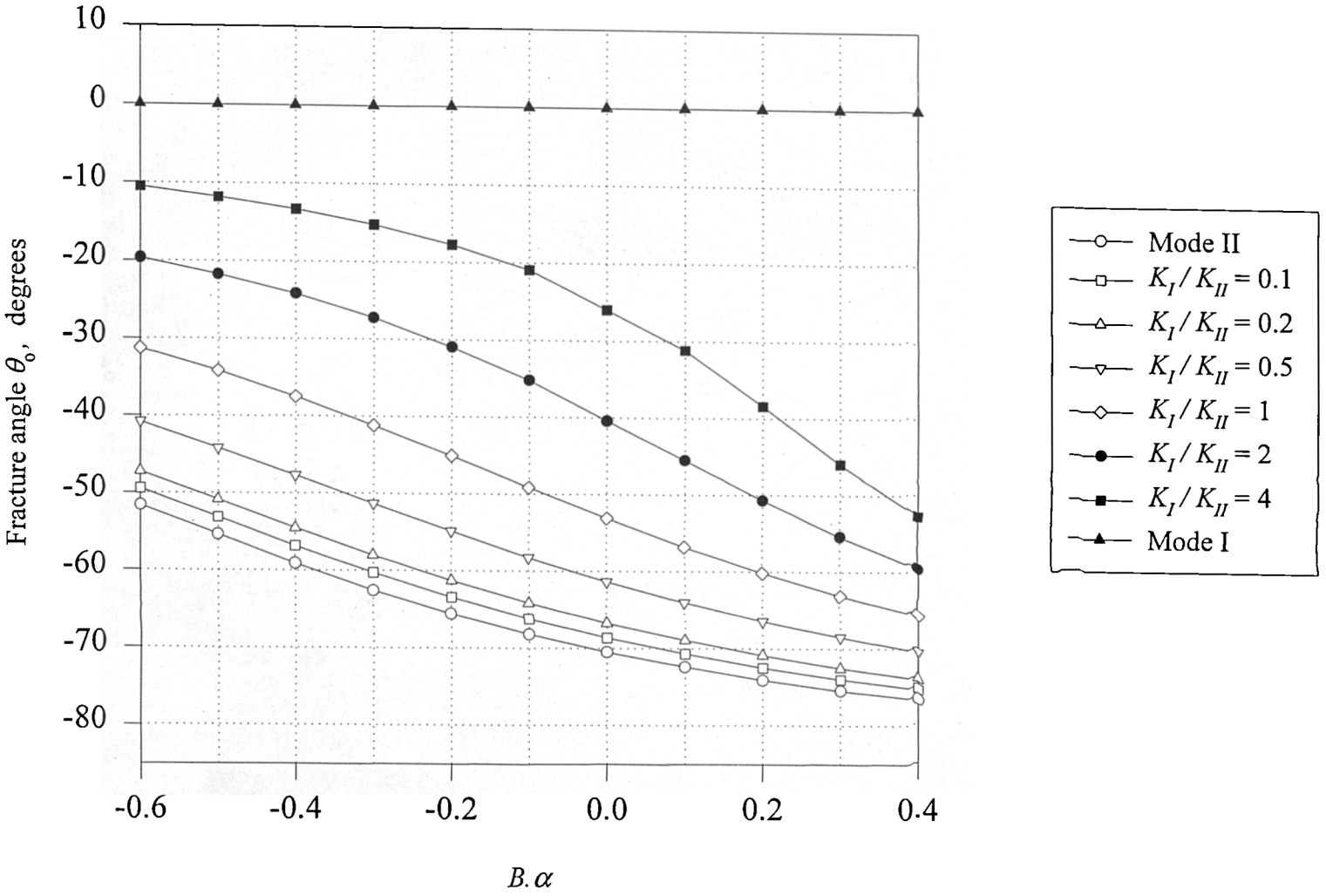

Figure 5-8. Effect of T on fracture initiation angle for different combinations of mode I and II, B is the biaxiality ratio, $\alpha = (2r_c/a)^{1/2}$.

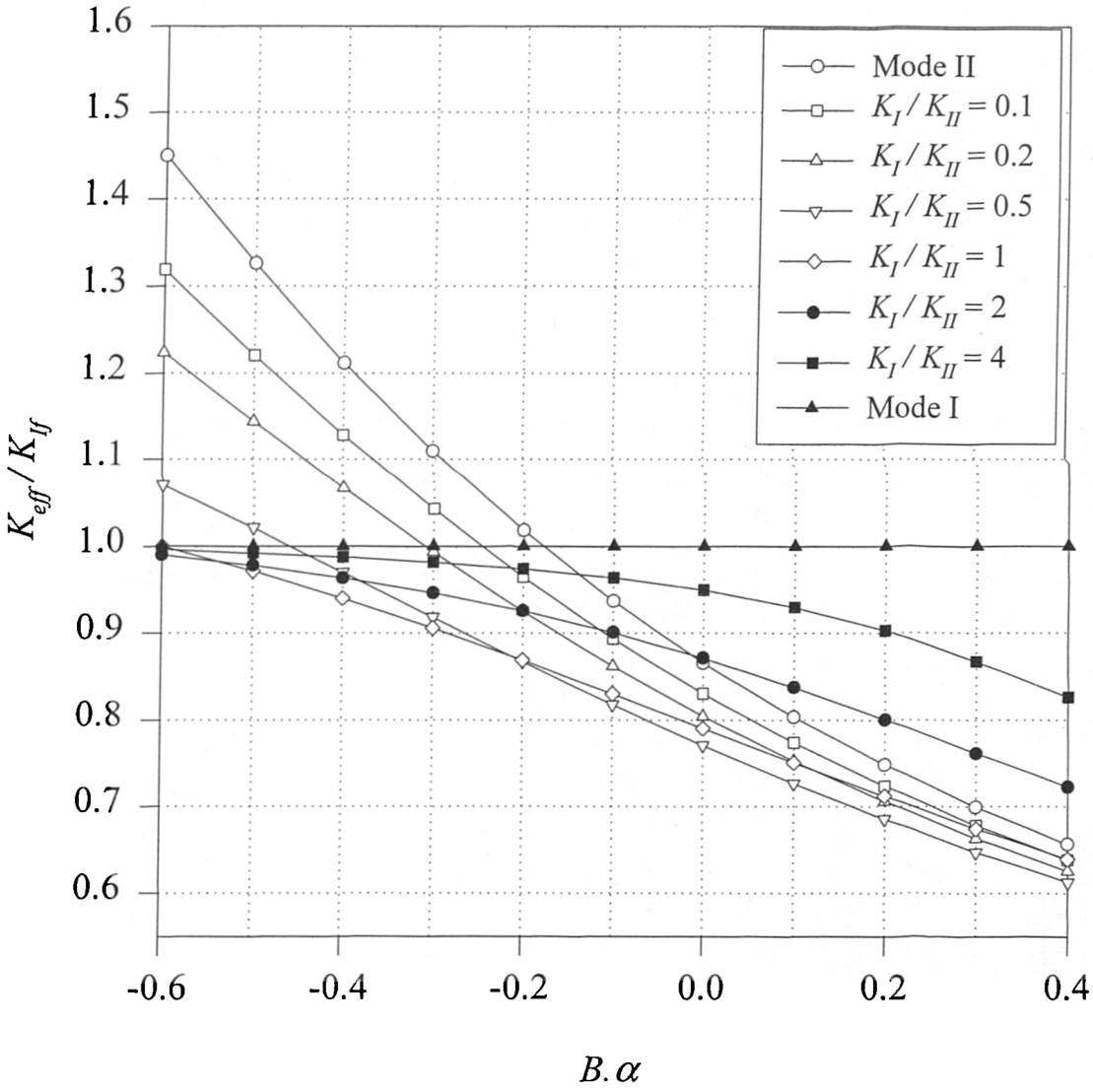

Figure 5-9. Effect of T on fracture toughness for different combinations of modes I and II, B is the biaxiality ratio, $\alpha = (2r_c/a)^{1/2}$

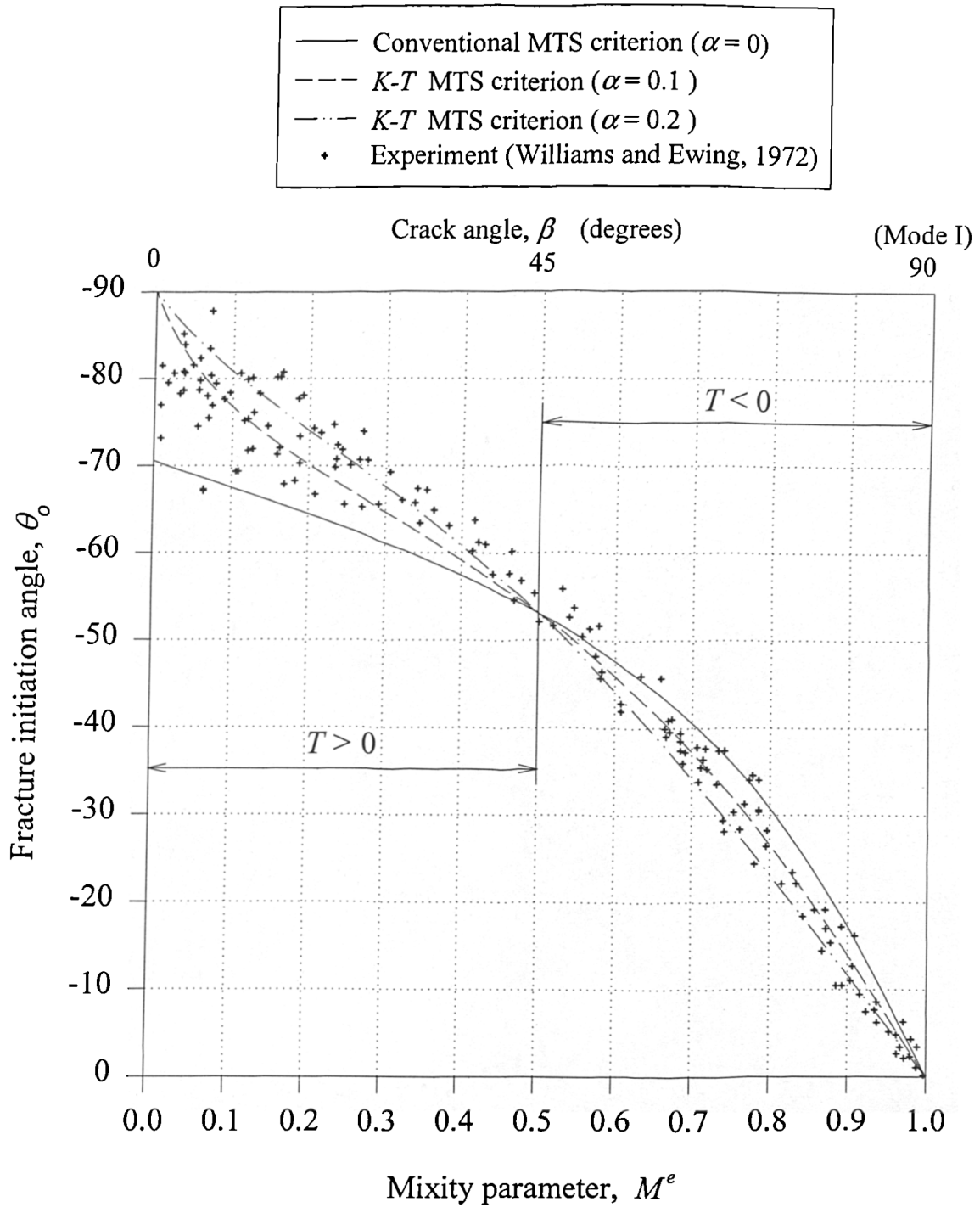

Fig 5-10. Direction of fracture initiation for the angled internal crack specimen, results obtained through experiment versus those predicted from the generalised MTS criterion.

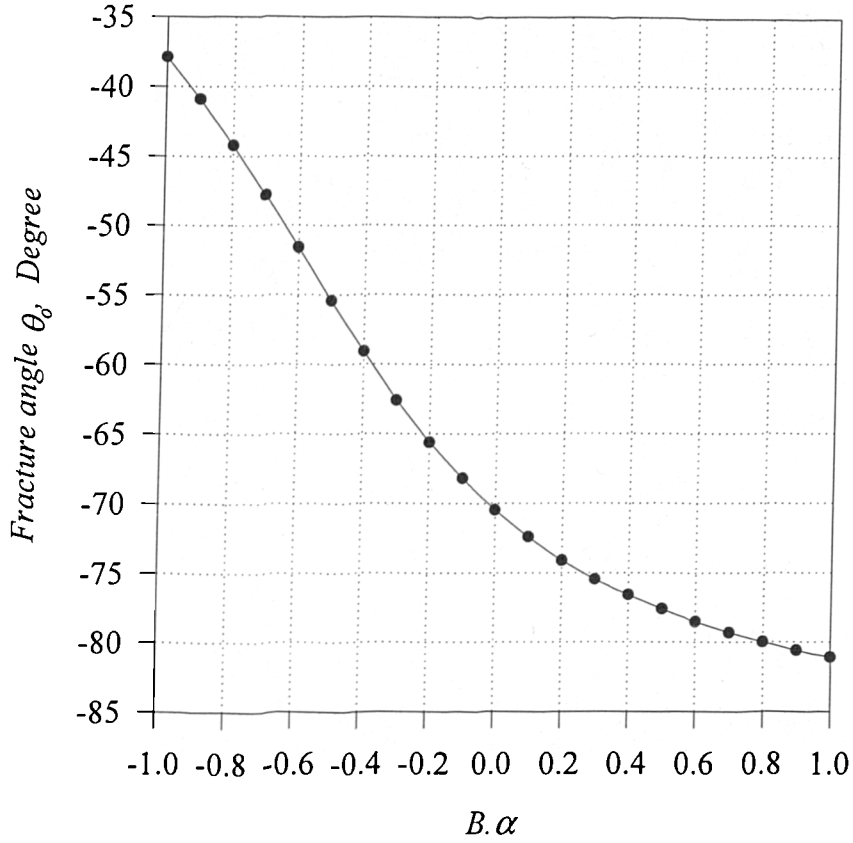

Figure 6-1. Effect of *T*-stress on fracture angle in mode II loading.
B= Biaxiality ratio, $\alpha = (2r_c/a)^{1/2}$

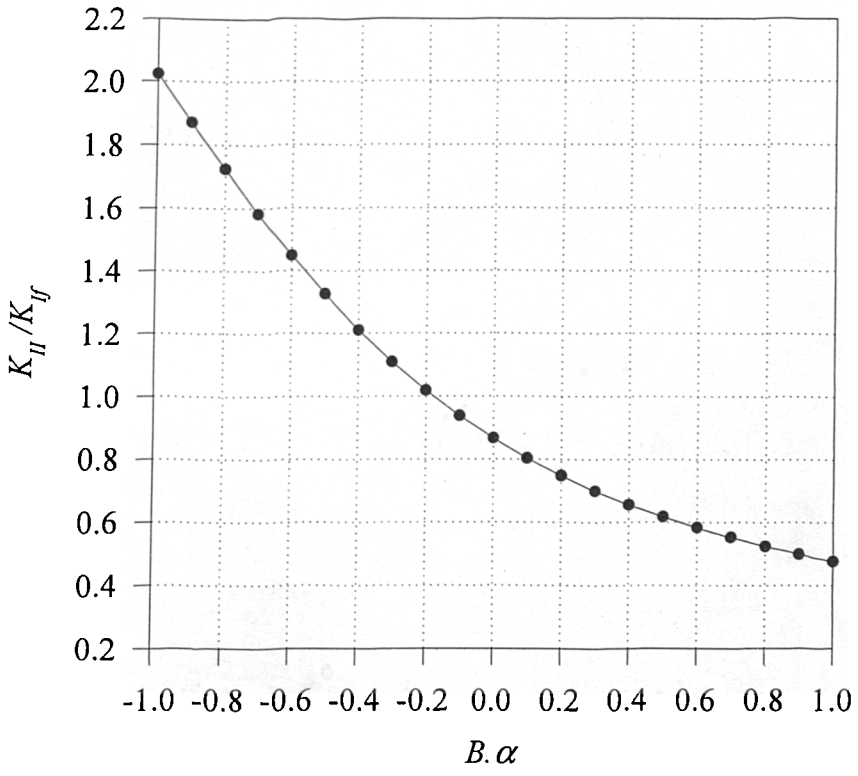

Figure 6-2. Effect of *T*-stress on mode II fracture toughness.
B= Biaxiality ratio, $\alpha = (2r_c/a)^{1/2}$

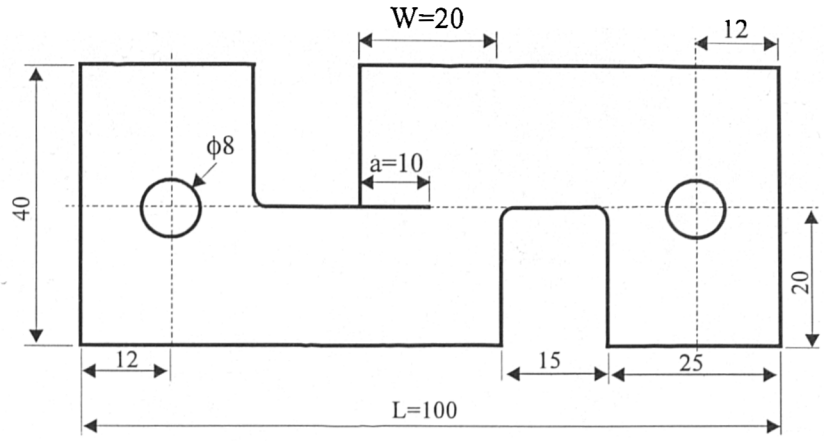

a. Mode II shear specimen, thickness = 20 mm.

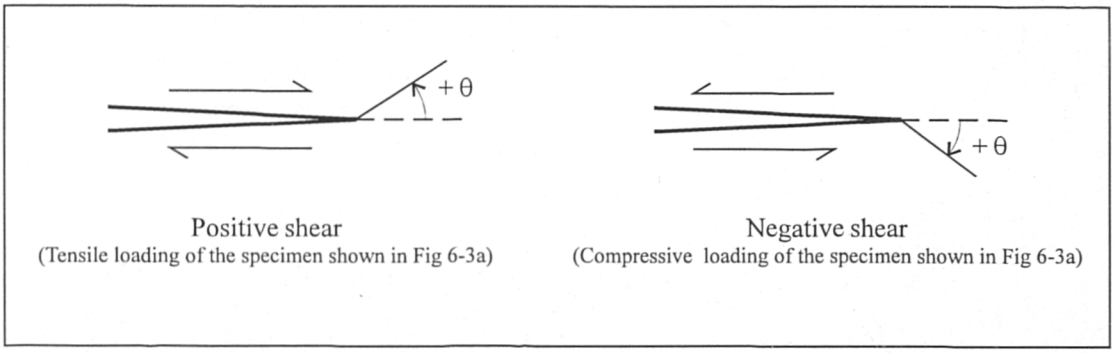

b. Definition for positive and negative shear in mode II loading.

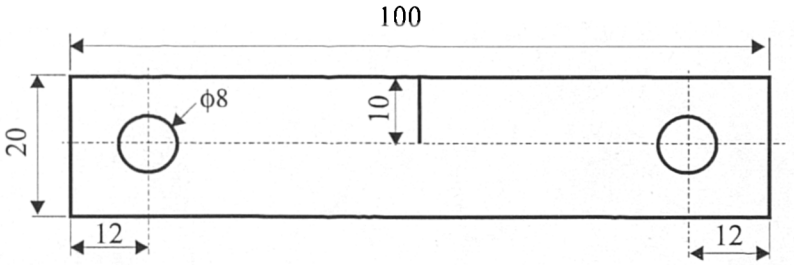

c. Mode I tension specimen, thickness = 20 mm

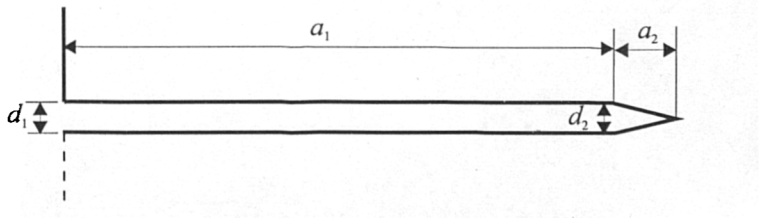

d. Parameters used to describe the length and width of cracks.

Figure 6-3. Mode II and mode I test specimens.
(all dimensions in mm)

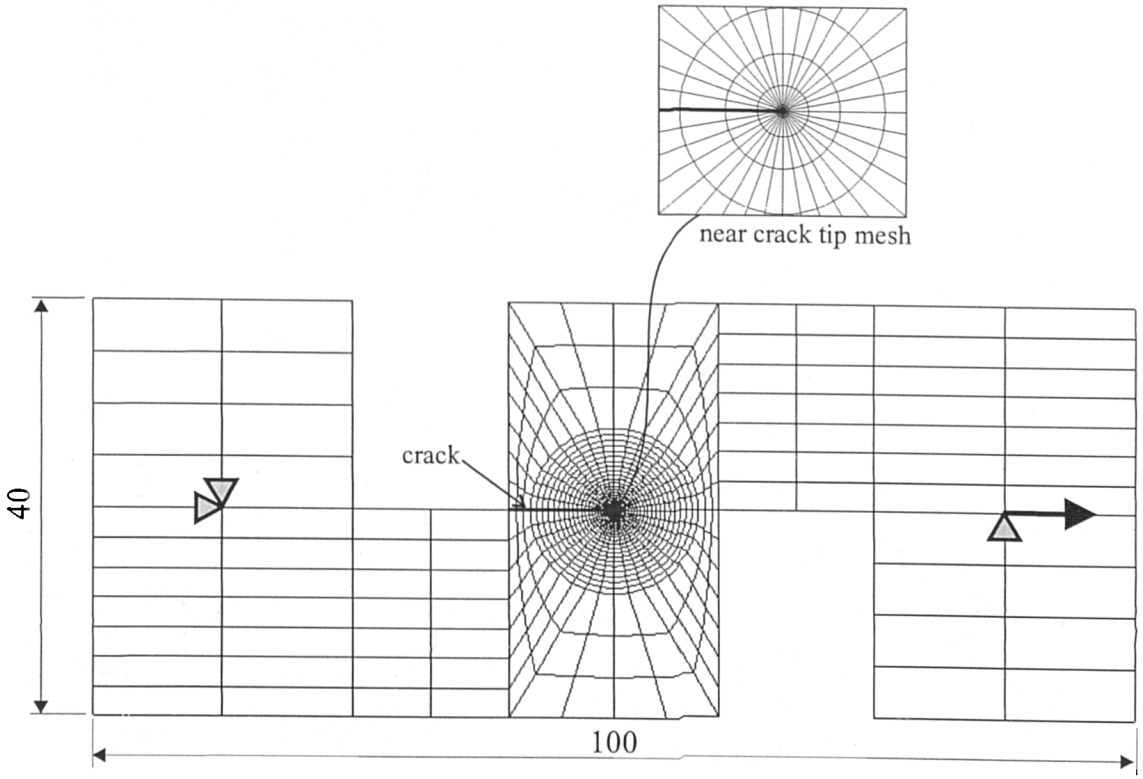

Figure 6-4. The mode II specimen mesh.

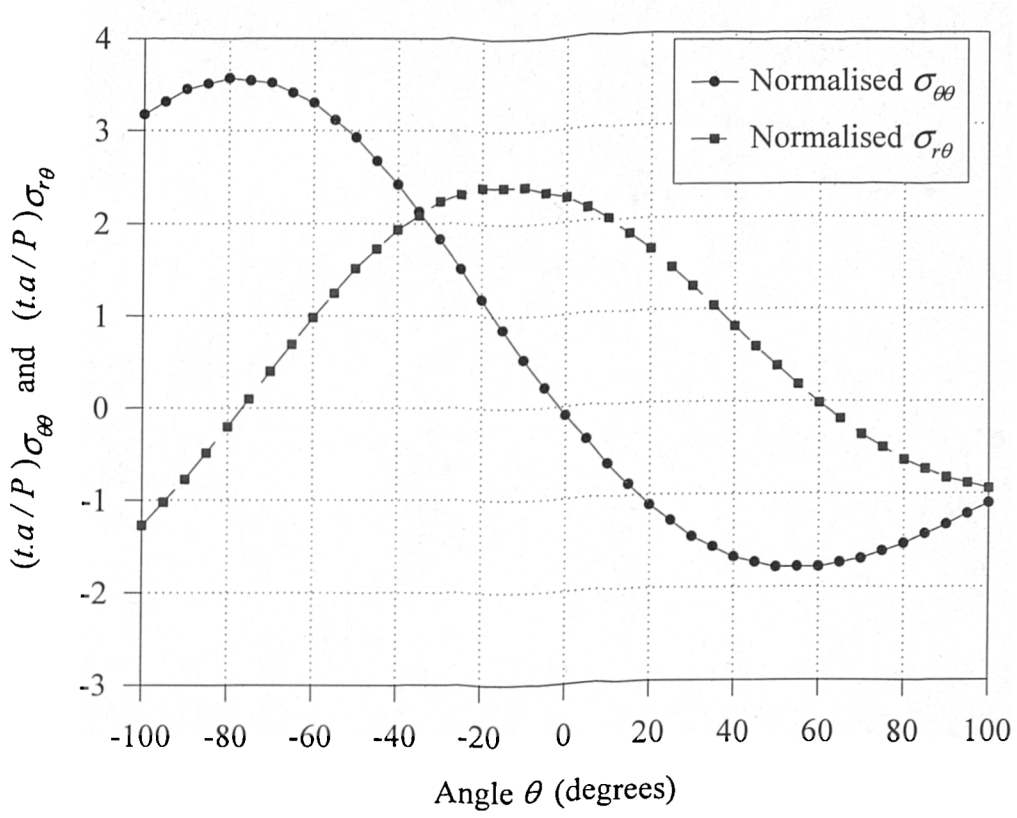

a) $+T$ shear specimen (Tensile loading).

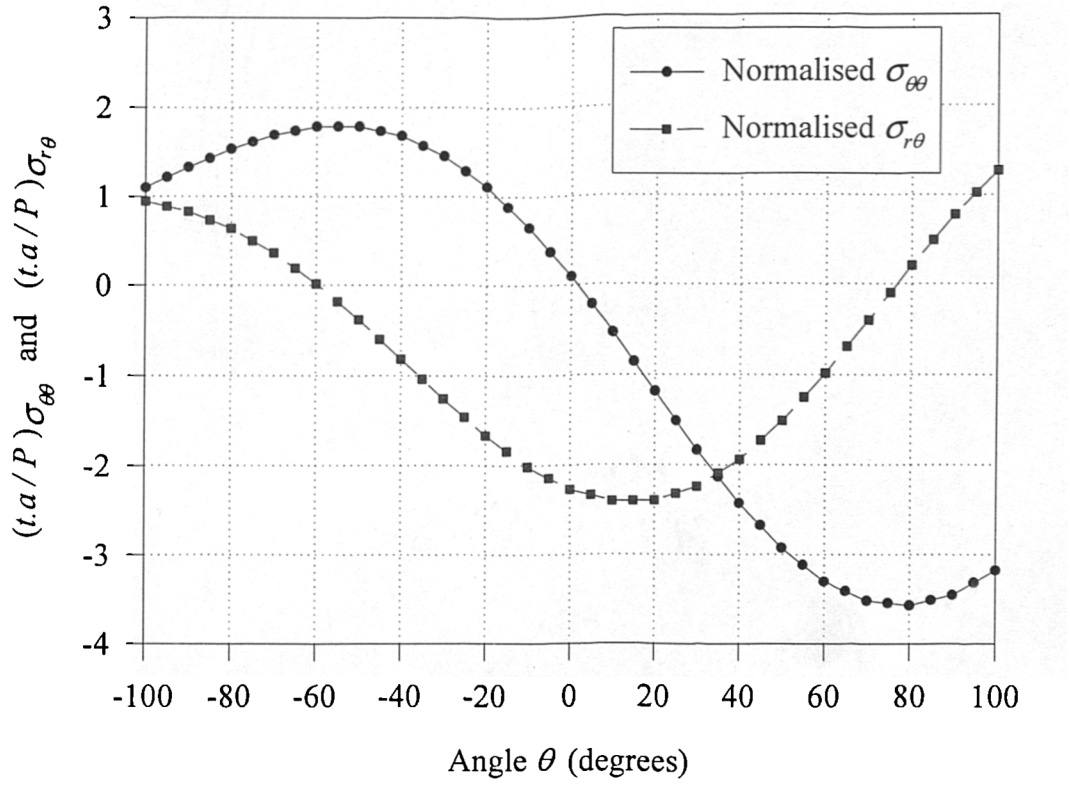

b) $-T$ shear specimen (Compressive loading)

Fig 6-5. Normalised tangential and shear stresses around the crack tip at a distance of r =0.27 mm, t =thickness, a =crack length, P =applied load.

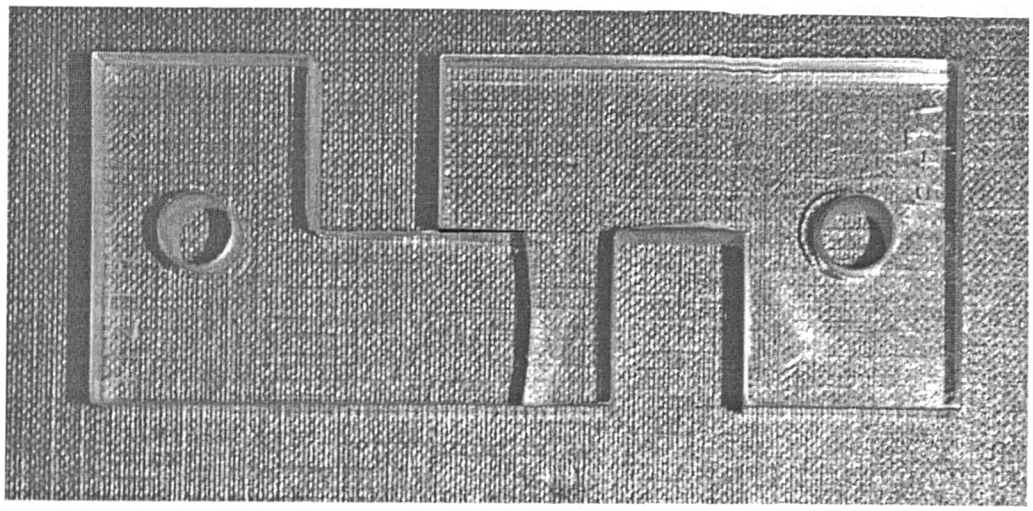

a. Positive *T* shear specimen (tensile loading).

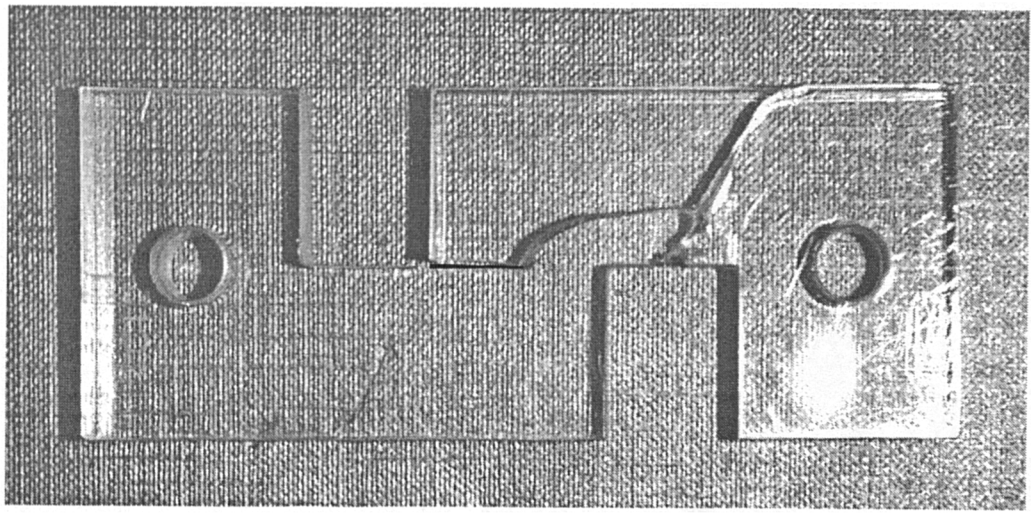

b. Negative *T* shear specimen (Compressive loading).

Figure 6-6. +*T* and -*T* shear specimens after testing.

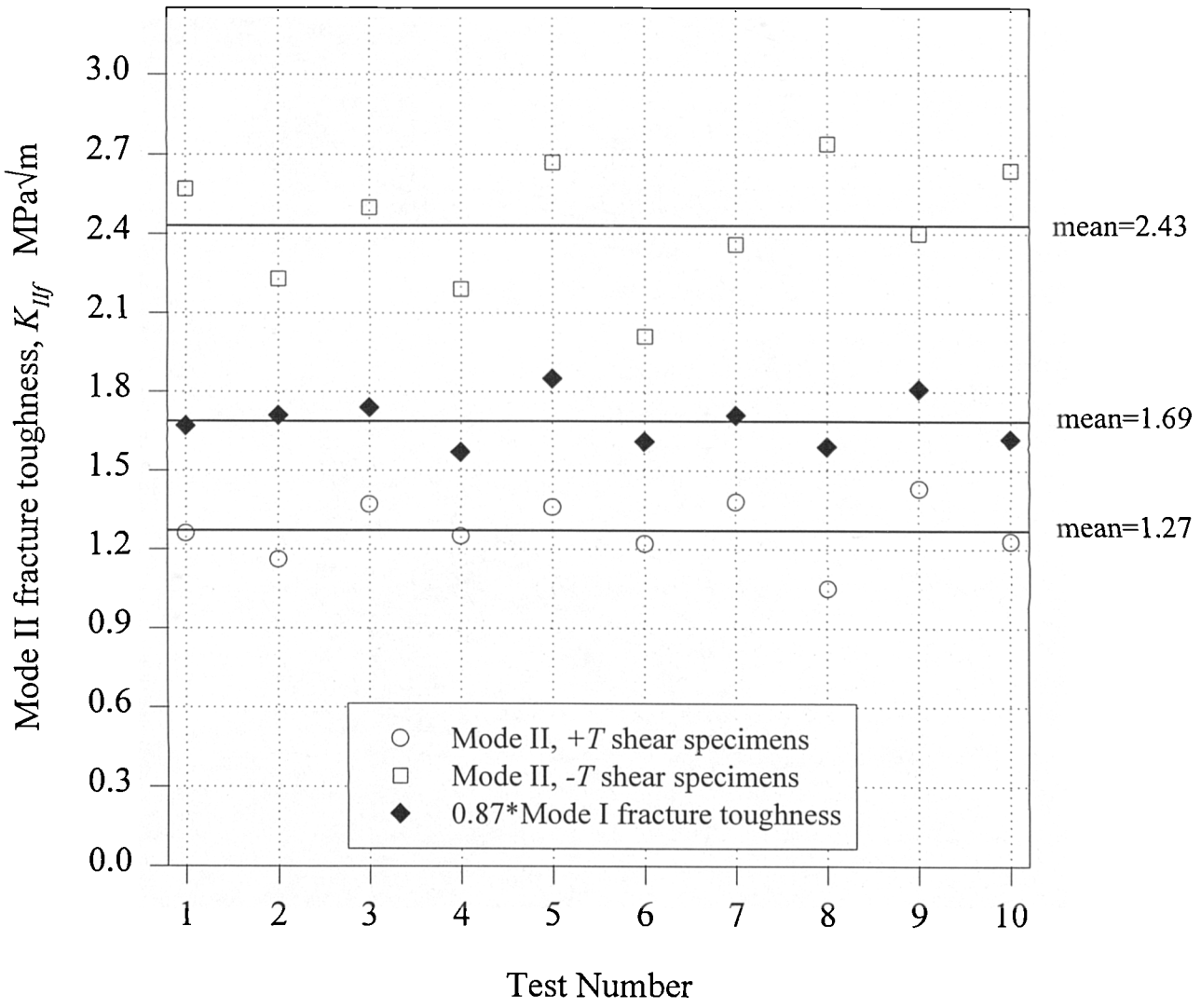

Figure 6-7. Experimental results for mode II fracture toughness.

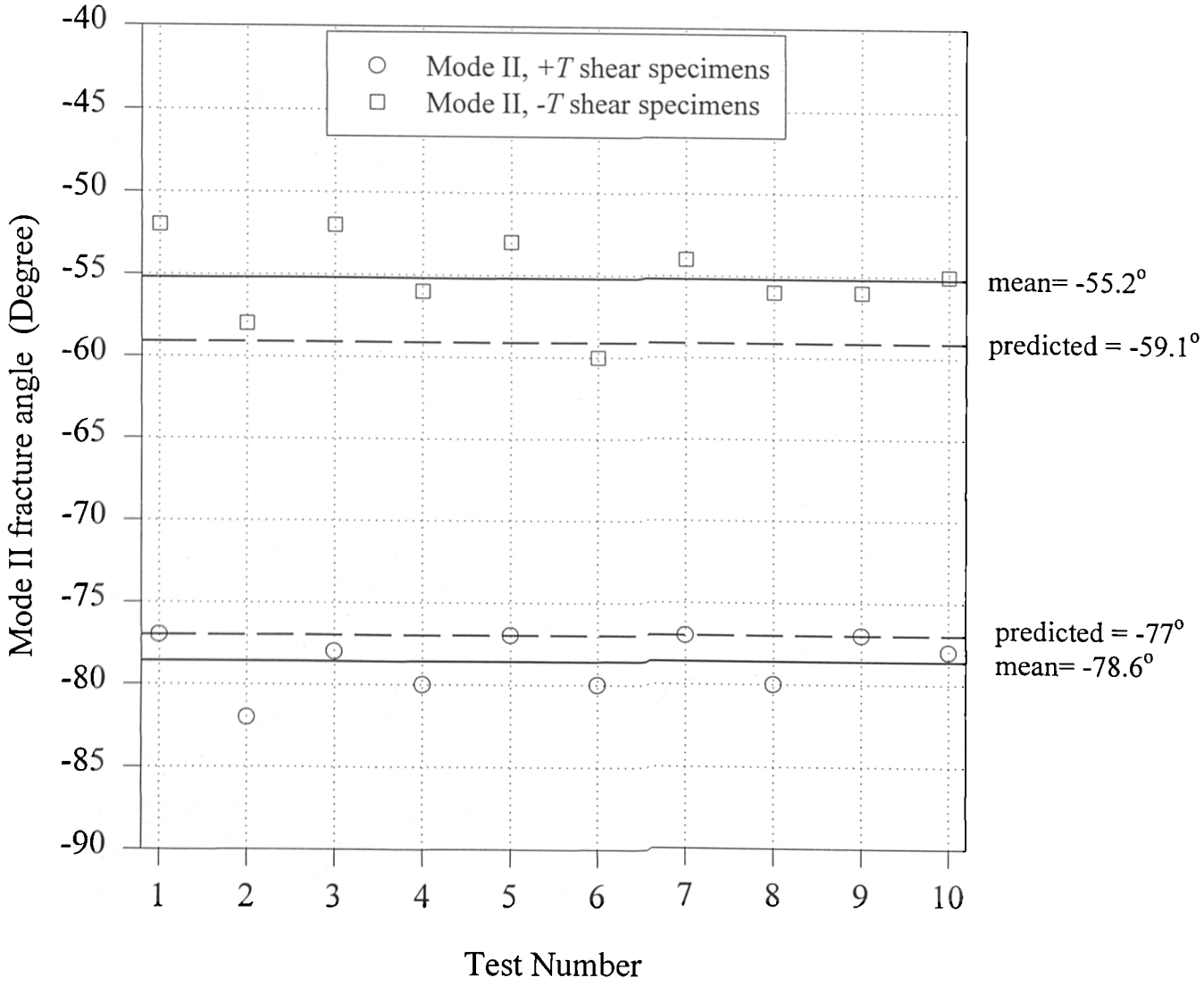

Figure 6-8. Fracture angles for mode II test specimens.

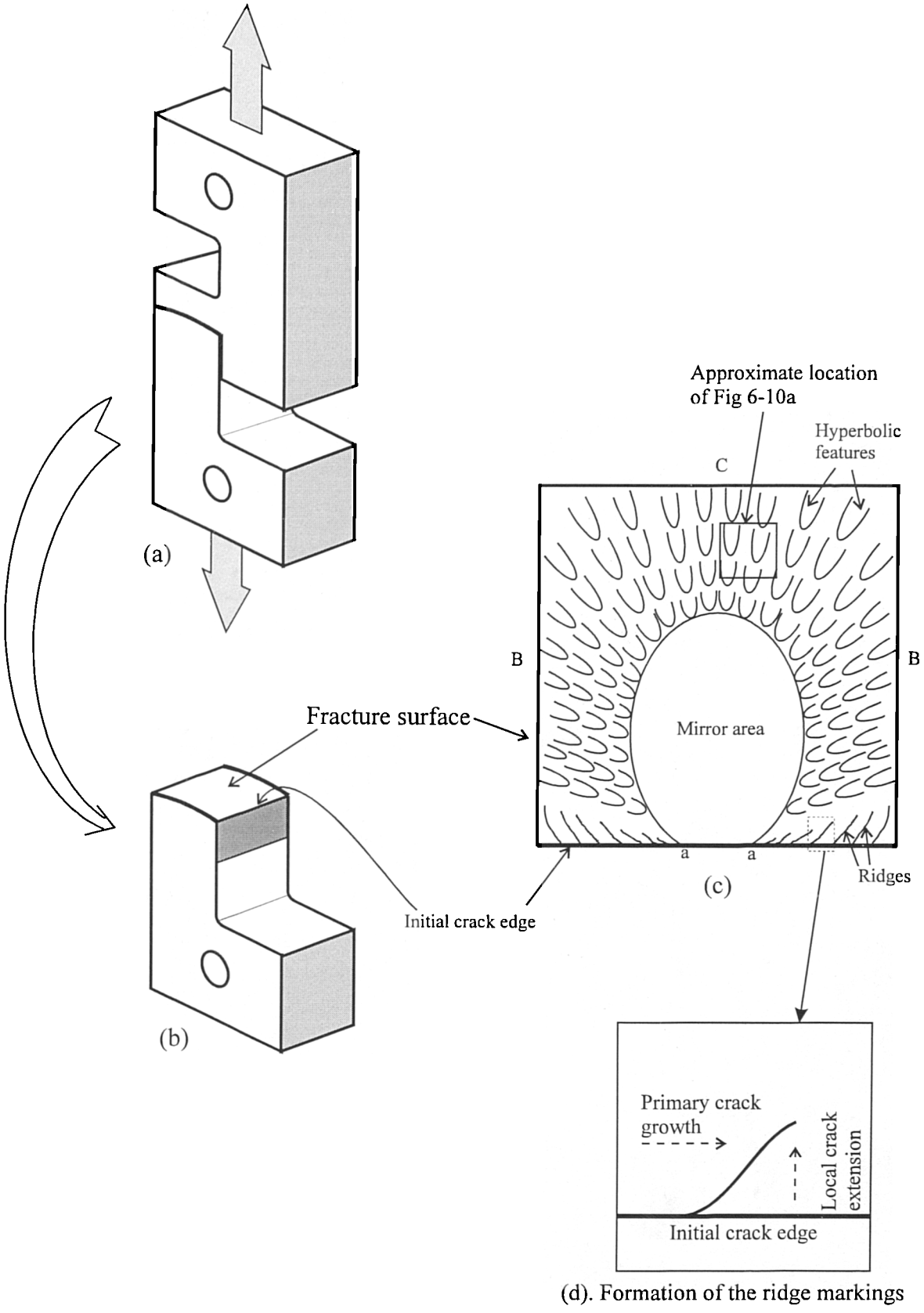

Figure 6-9. Fracture surface for the positive T shear specimen.

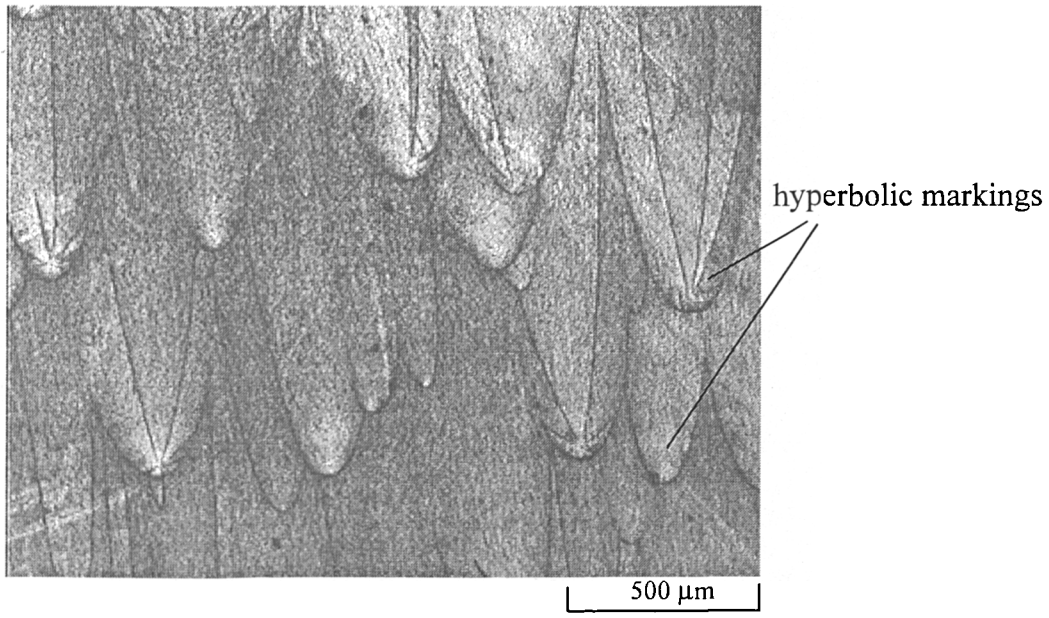

(a)

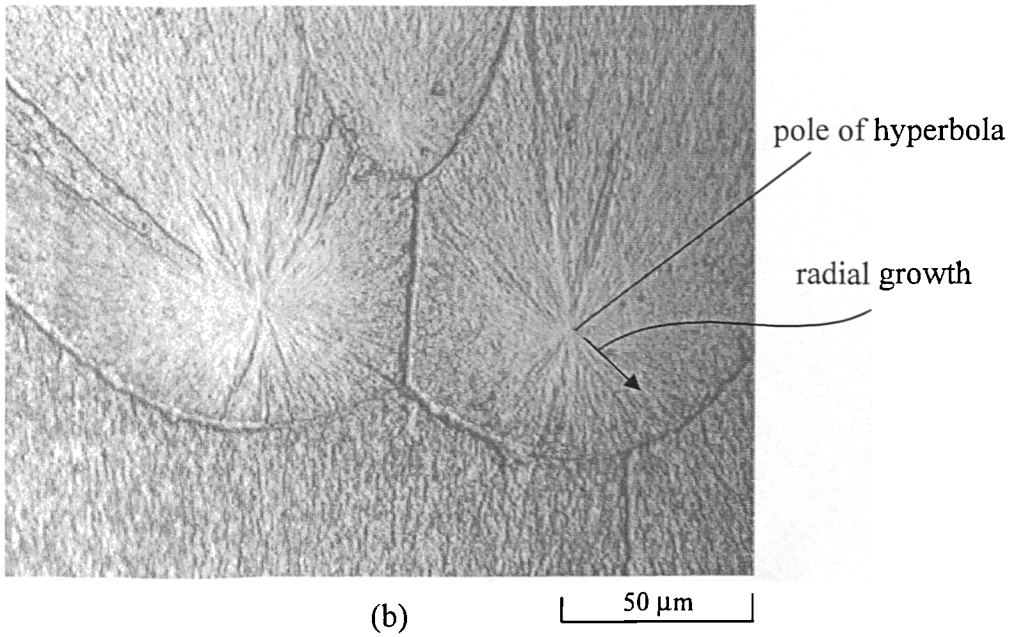

(b)

Figure 6-10. Microscopic picture of the hyperbolic markings.

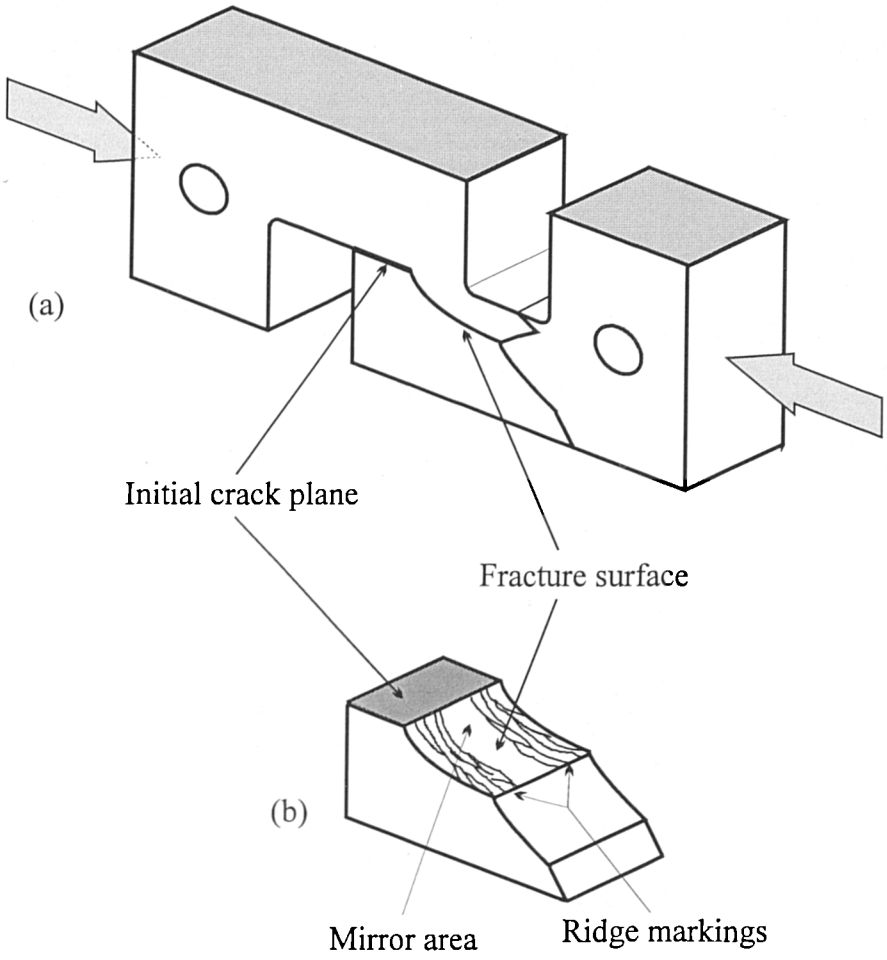

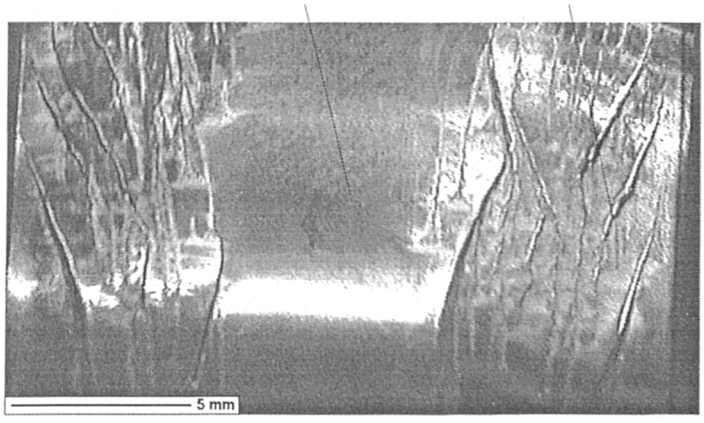

(c)

Figure 6-11 . Fracture surface for the negative *T* shear specimen.

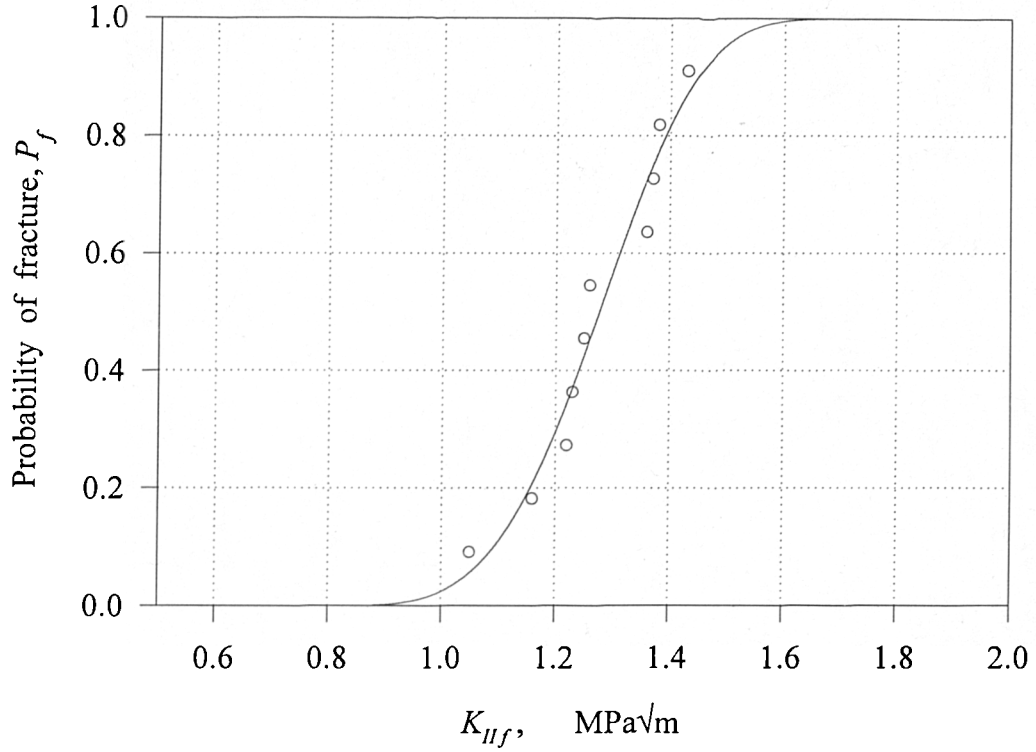

(a)

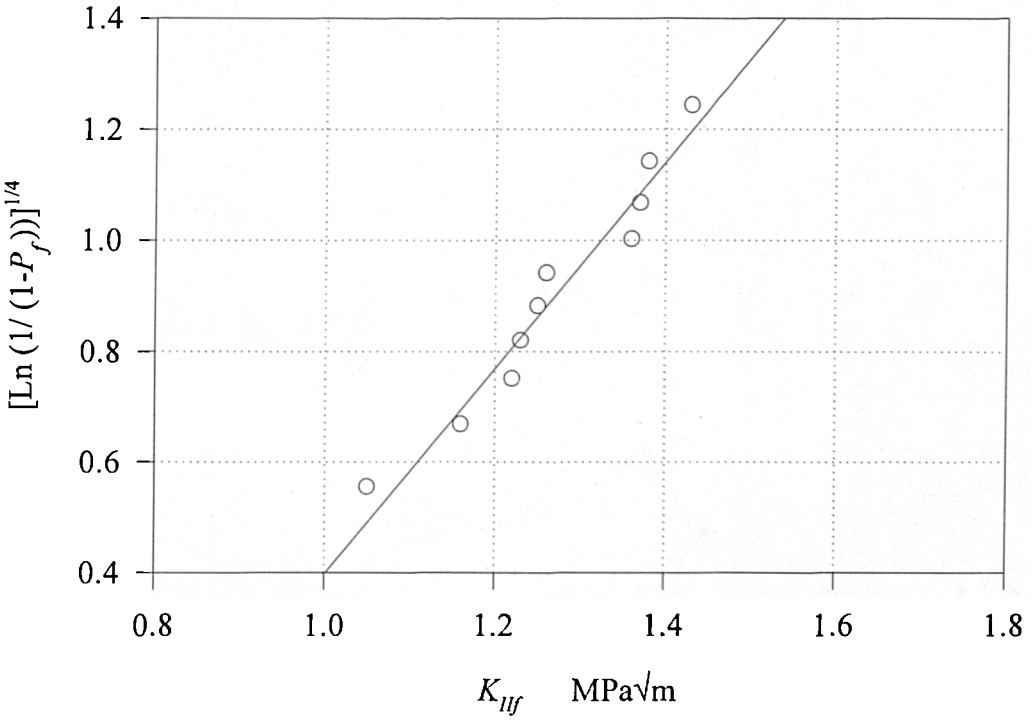

(b)

Figure 6-12. Statistical model for mode II fracture toughness in PMMA for the $+T$ shear tests. Fitting parameters, K_o=1.32, K_{min}=0.787

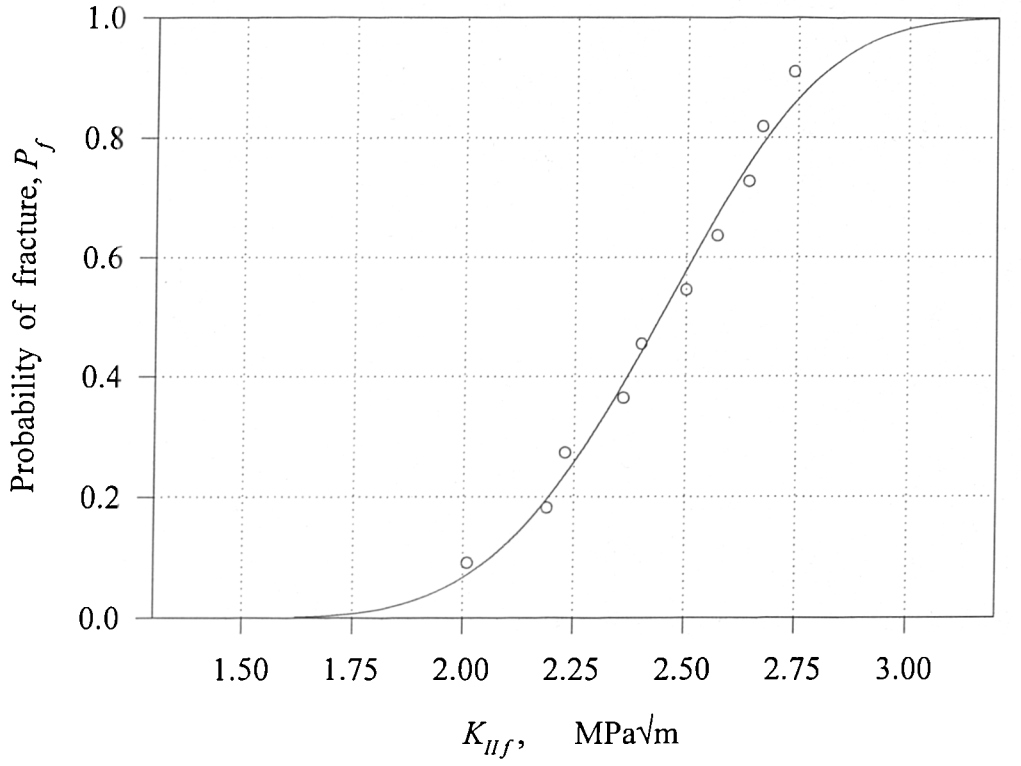

(a)

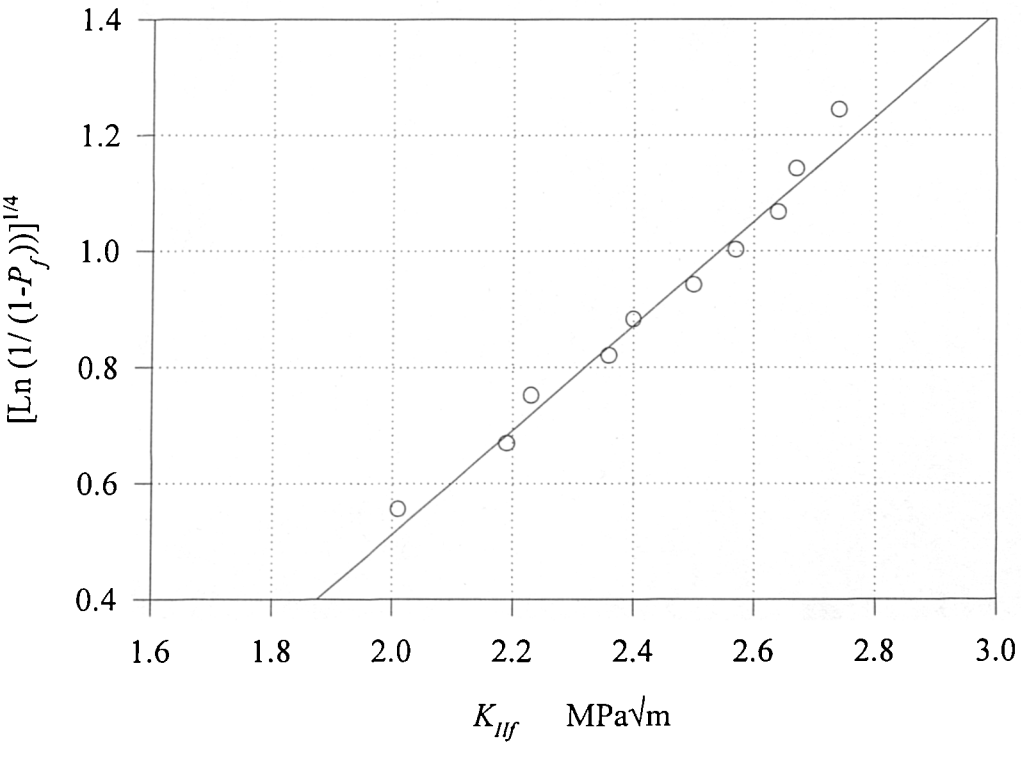

(b)

Figure 6-13. Statistical model for mode II fracture toughness in PMMA for the -T shear tests. Fitting parameters, K_o=2.54, K_{min}= 1.43

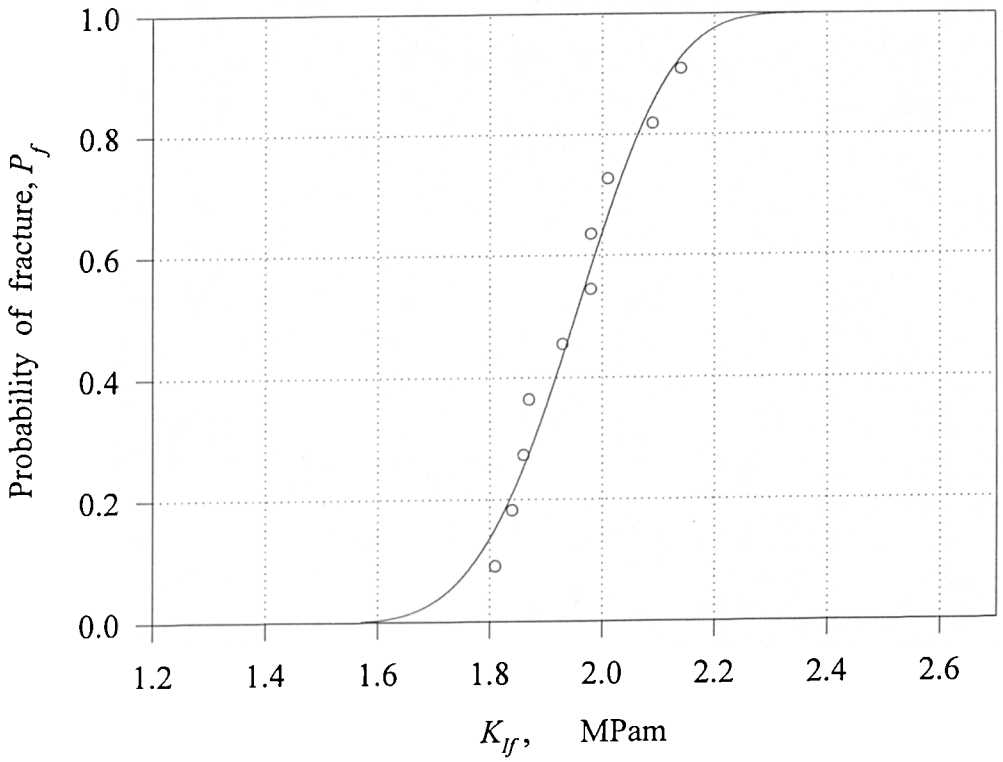

(a)

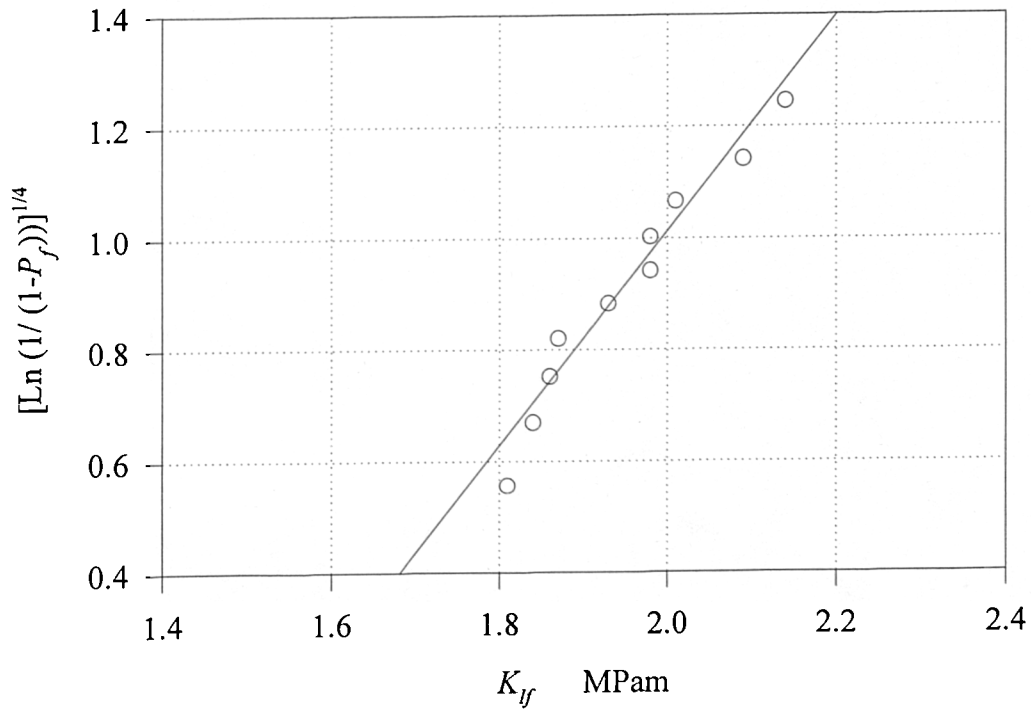

(b)

Fig 6-14. Probability of mode I fracture toughness in PMMA.
Fitting parameters, K_o=1.99, K_{min}=1.47

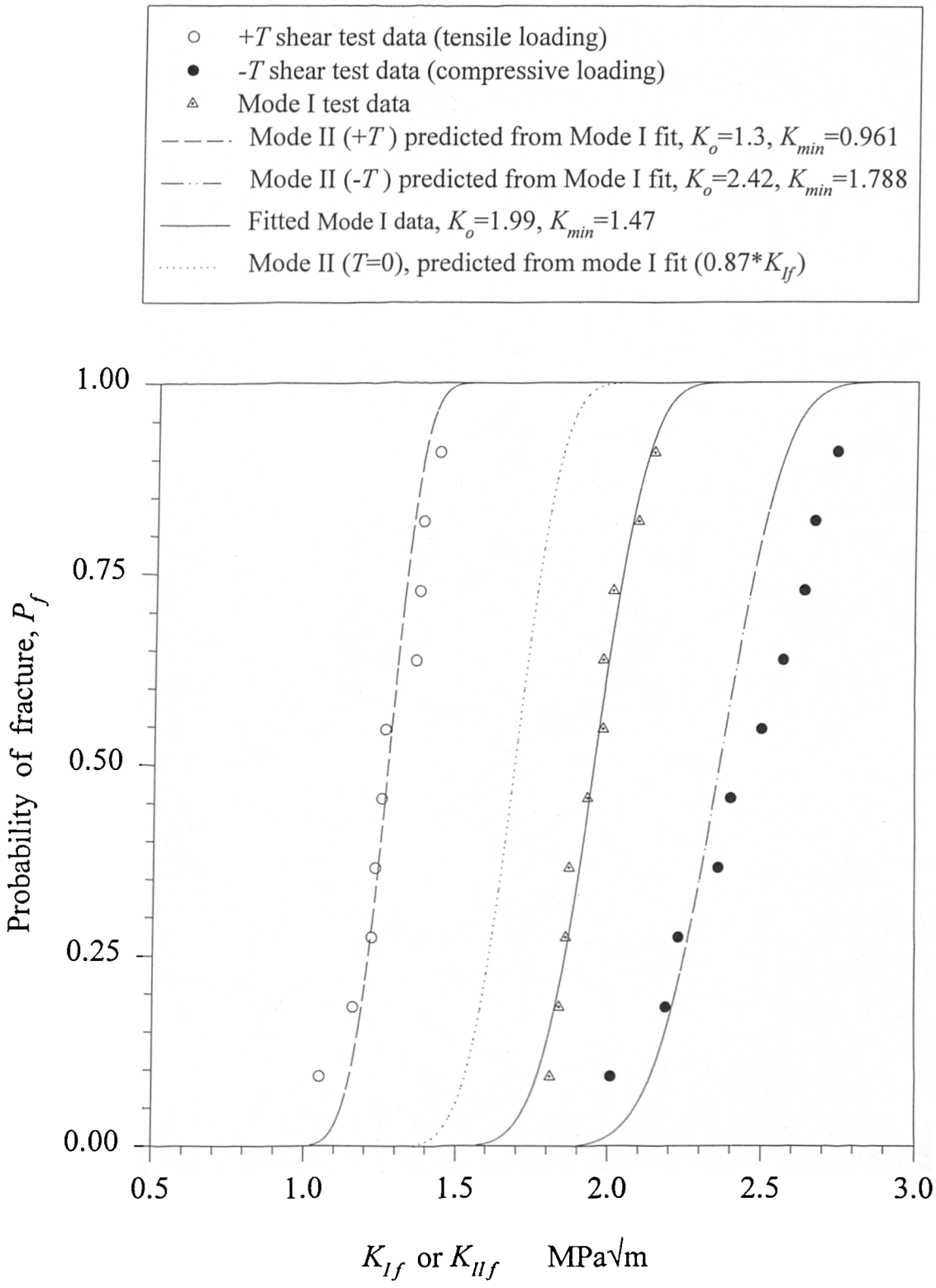

Fig 6-15. Probability of mode II fracture in PMMA for the $+T$ and $-T$ shear tests predicted from probability of mode I fracture toughness results.

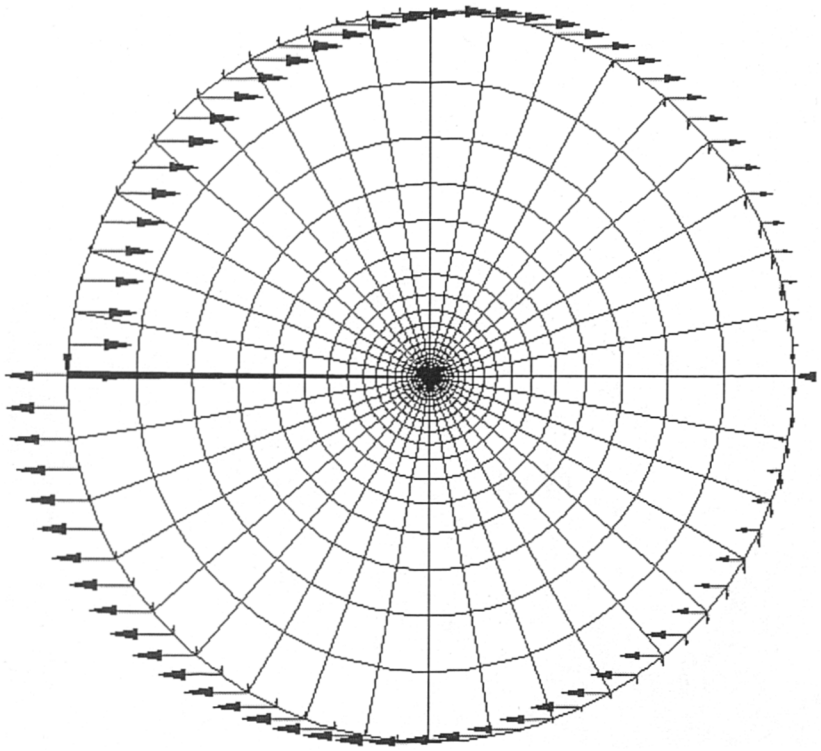

Figure 7-1. Finite element simulation of the mode II boundary layer model showing the displacement boundary conditions along the circular boundary (T=0).

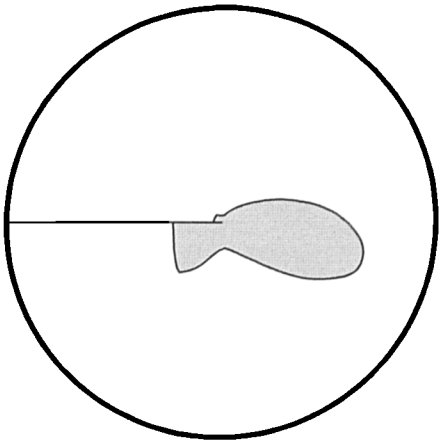

a. $T/\sigma_o = +0.4$

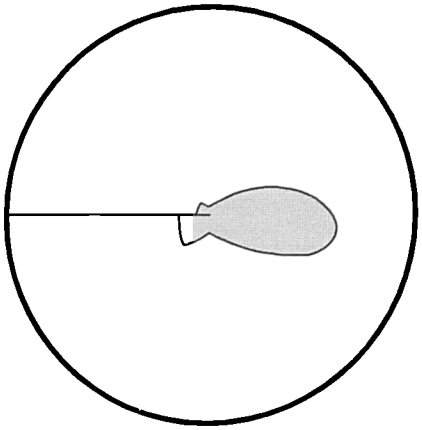

b. $T/\sigma_o = +0.2$

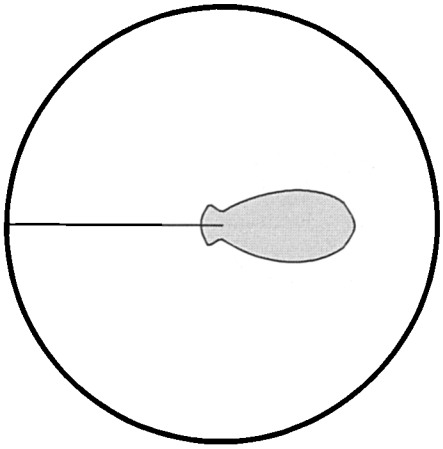

c. $T/\sigma_o = 0$

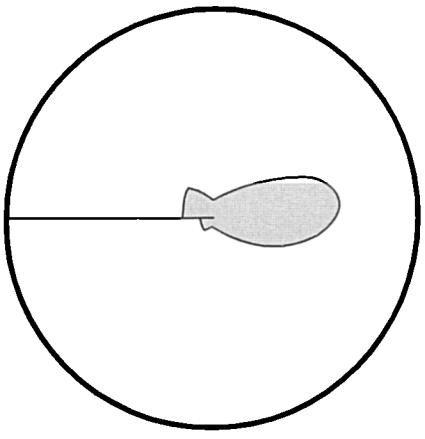

d. $T/\sigma_o = -0.2$

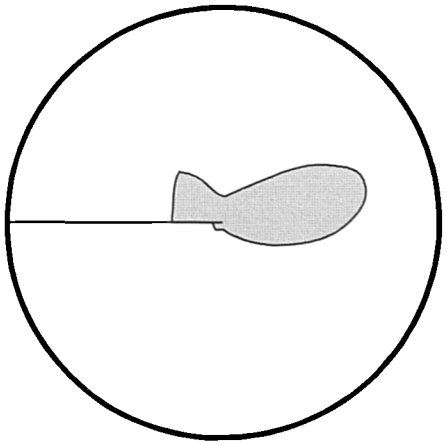

e. $T/\sigma_o = -0.4$

Figure 7-2. Effect of T-stress on the shape of plastic zone near the tip of a mode II crack in small scale yielding. (For all of the circles the dimensionless radius $r(\sigma_o / K_{II})^2$ is equal to 0.68)

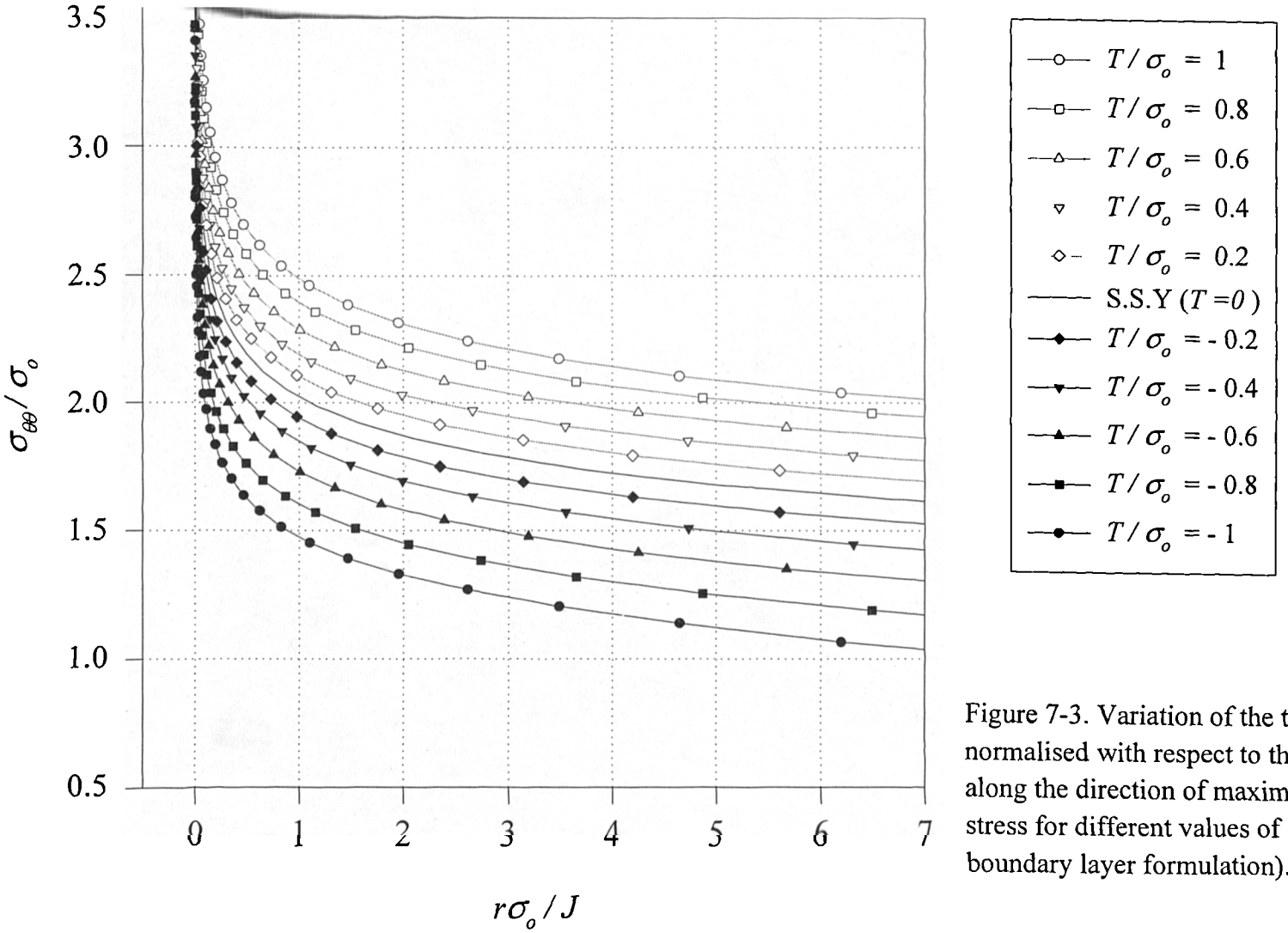

Figure 7-3. Variation of the tangential stress normalised with respect to the yield stress along the direction of maximum tangential stress for different values of T/σ_o (mode II boundary layer formulation).

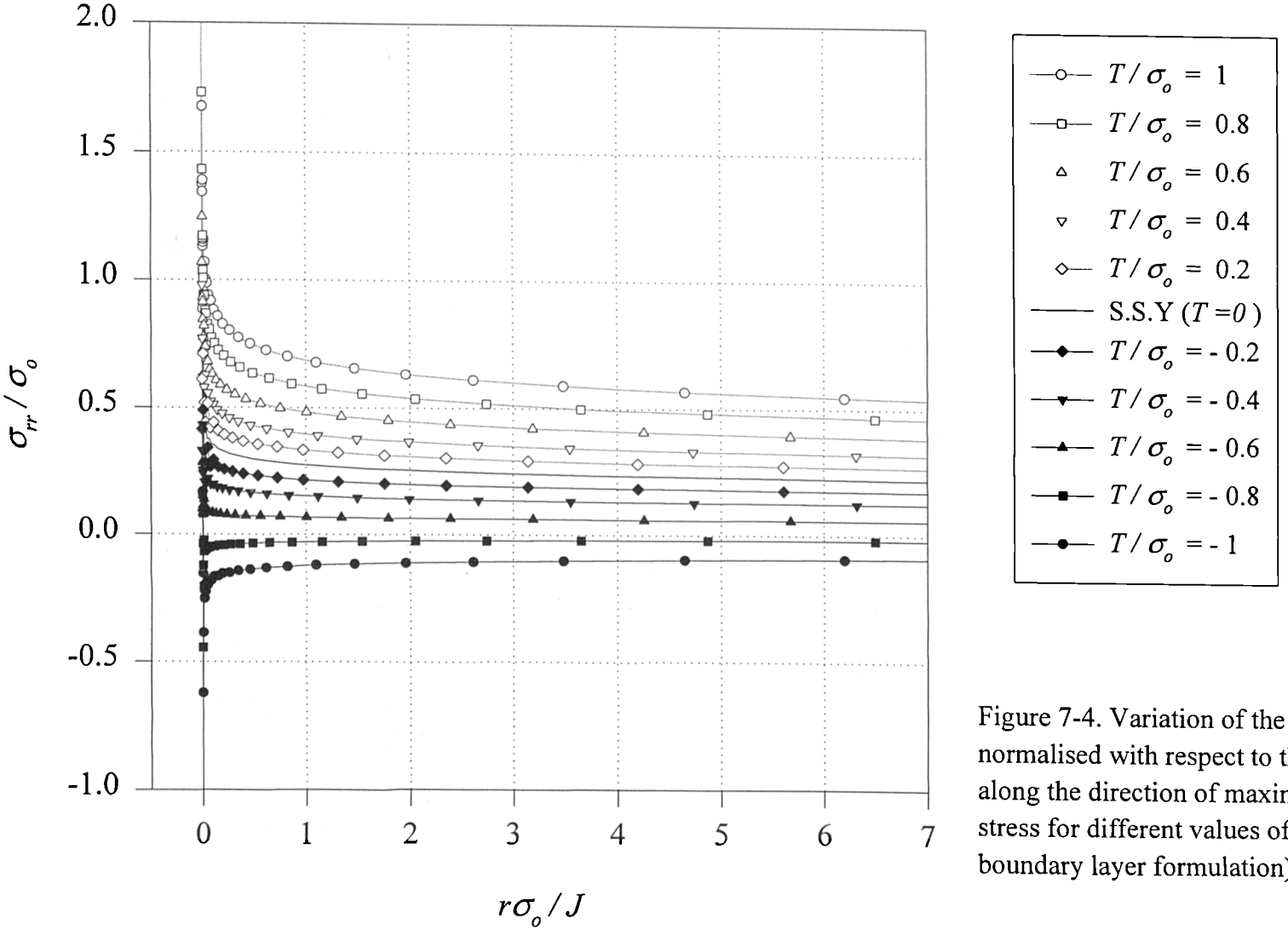

Figure 7-4. Variation of the radial stress normalised with respect to the yield stress along the direction of maximum tangential stress for different values of T/σ_o (mode II boundary layer formulation).

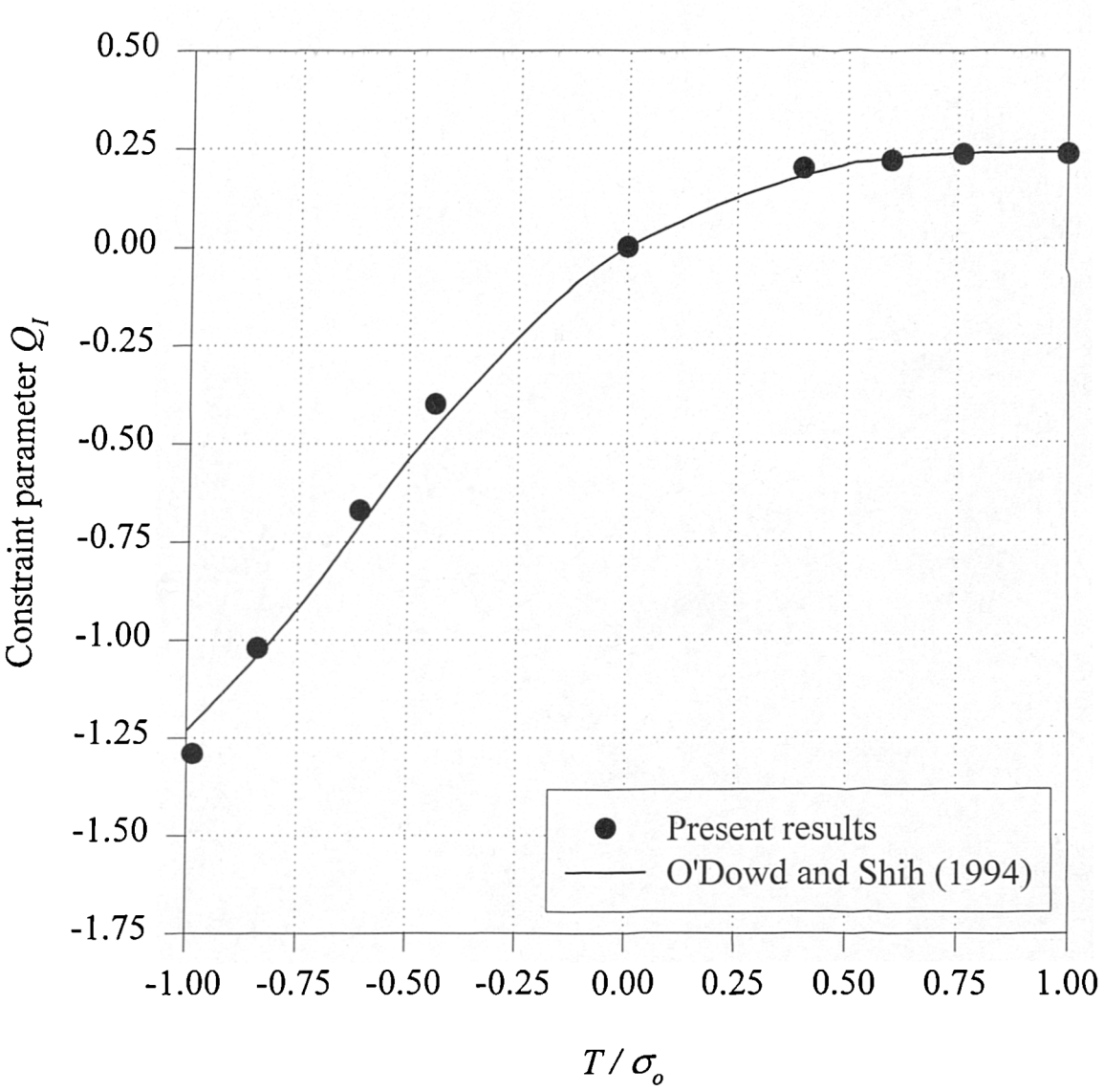

Figure 7-5. Relation between Q and T / σ_o in mode I for n=10.
(Present results compared with those of O'Dowd and Shih, 1994)

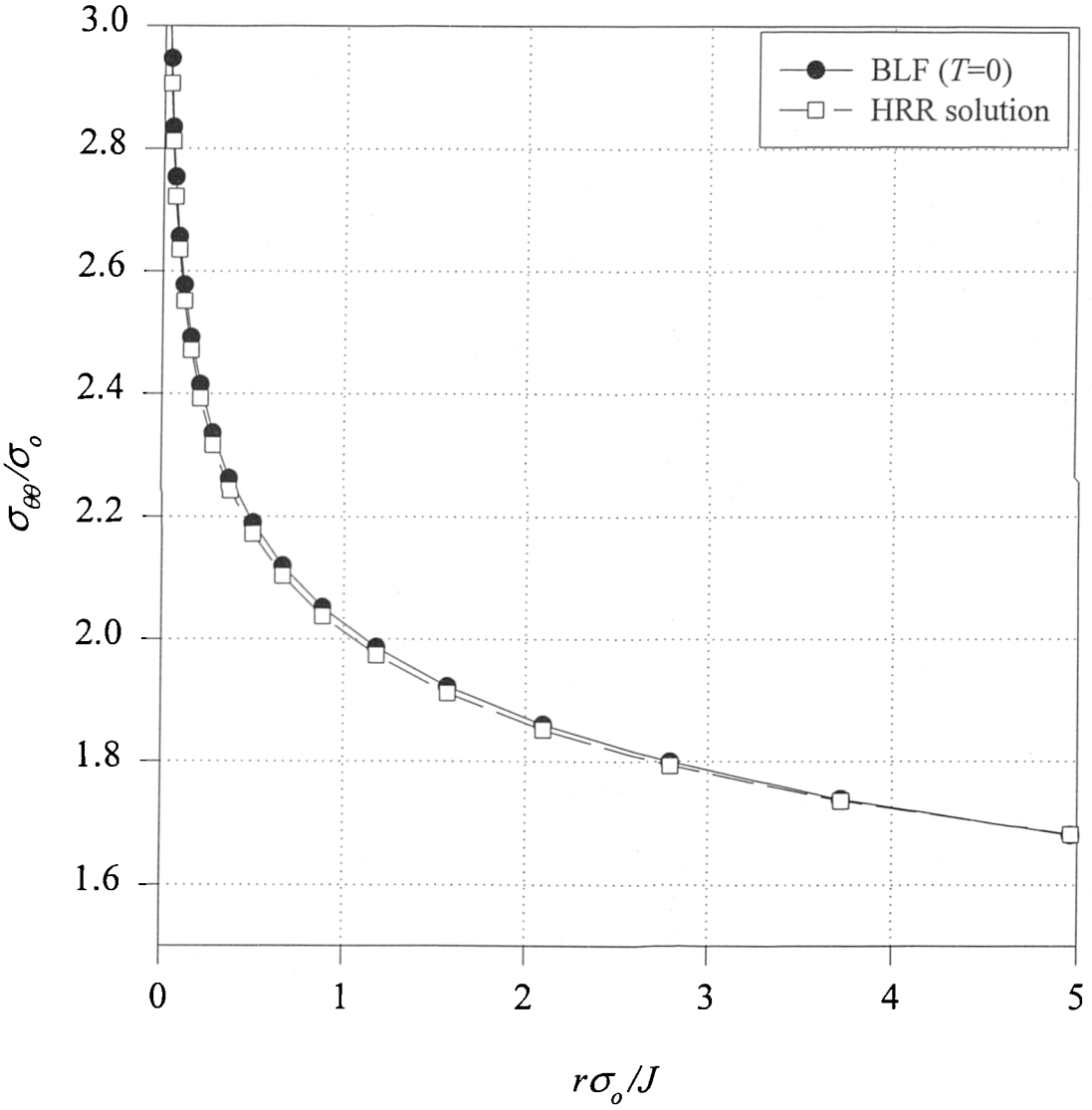

Figure 7-6. Singular term for the normalised tangential stress along the direction θ= -77 ° in mode II.
HRR solution compared with boundary layer formulation with T=0.

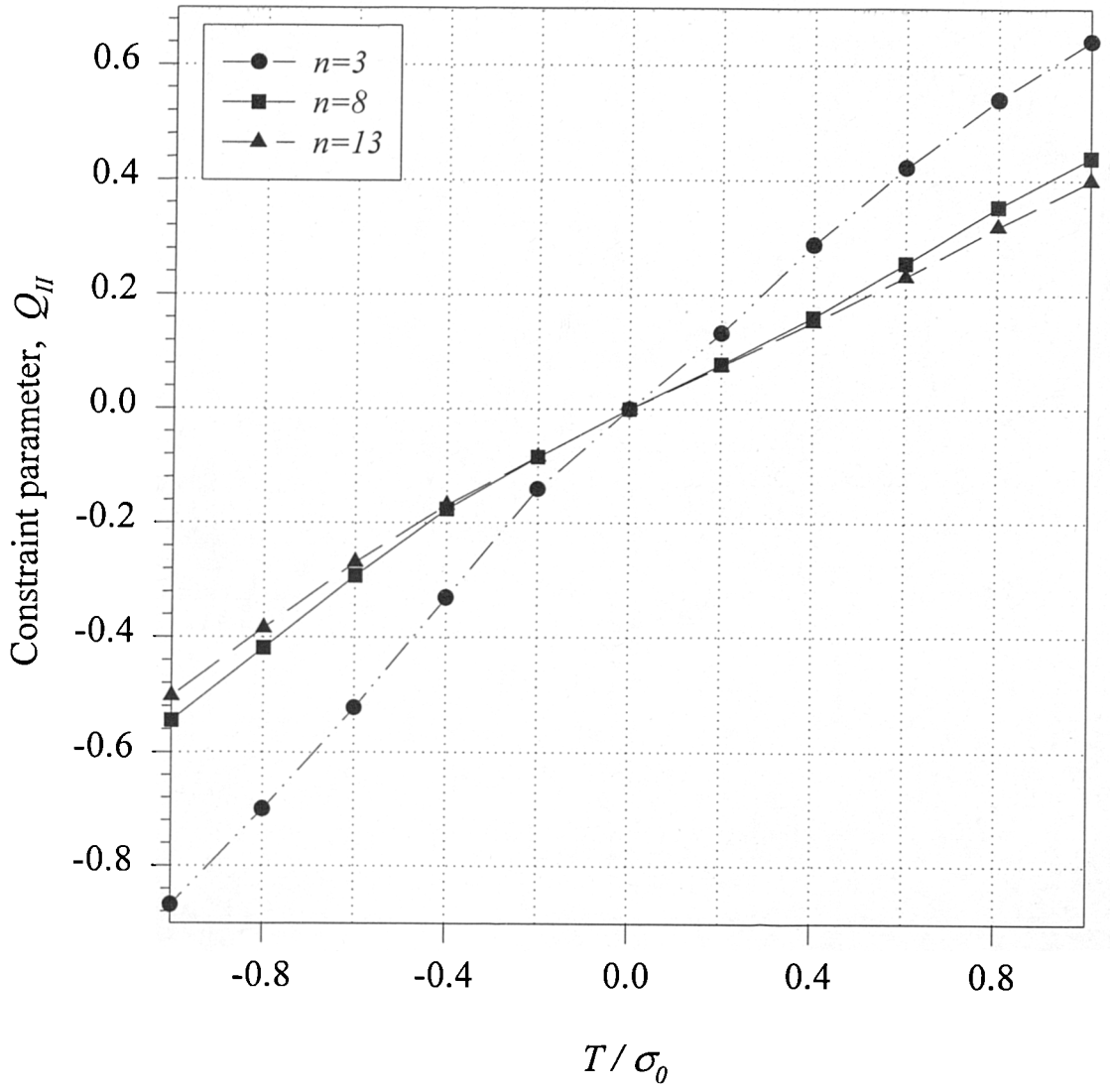

Figure 7-7. Relation between Q and T/σ_o in mode II for n=3, 8 and 13.

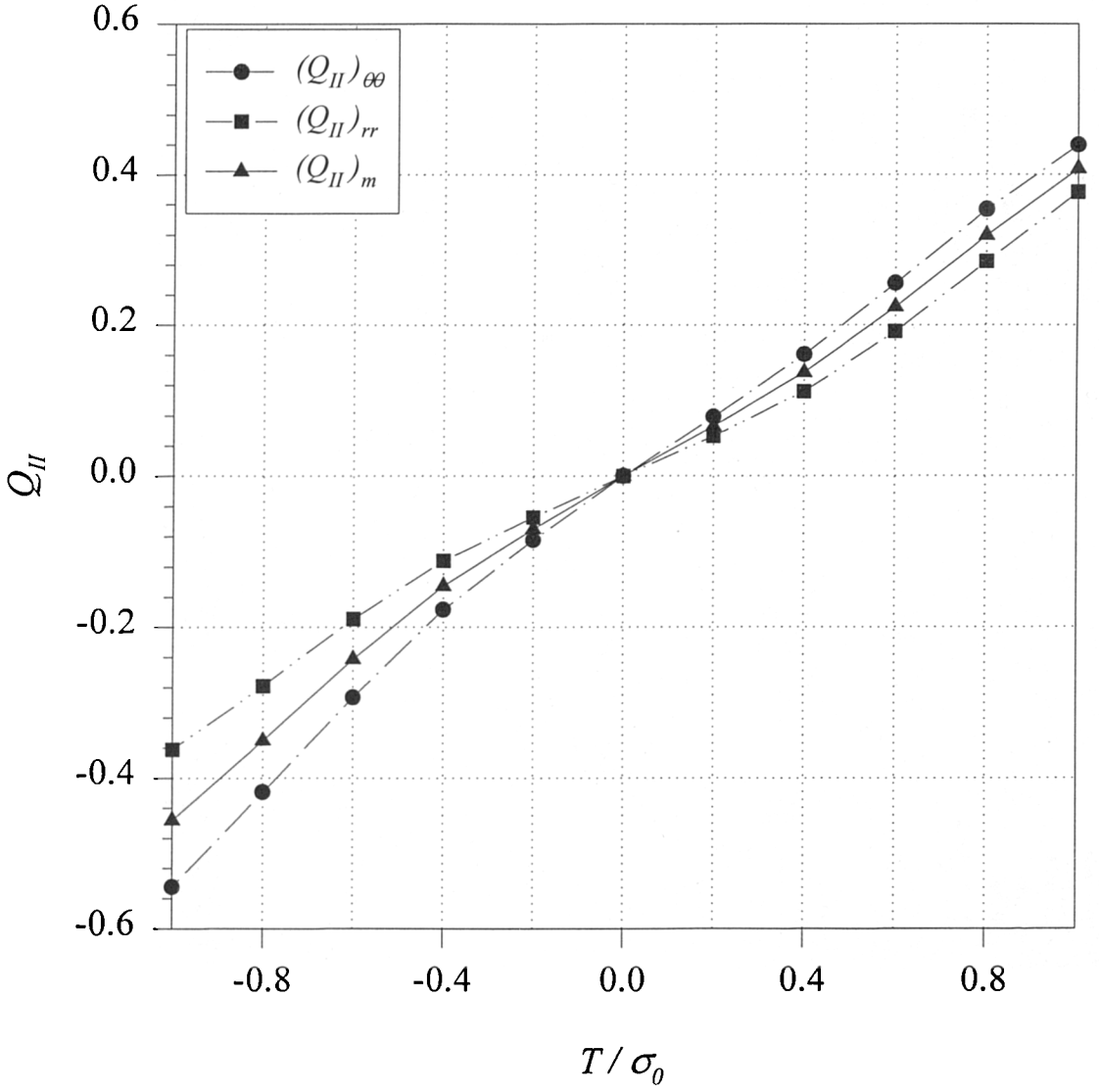

Figure 7-8. Q calculated in mode II along the direction of maximum tangential stress for $\sigma_{\theta\theta}$, σ_{rr} and σ_m for n=8.

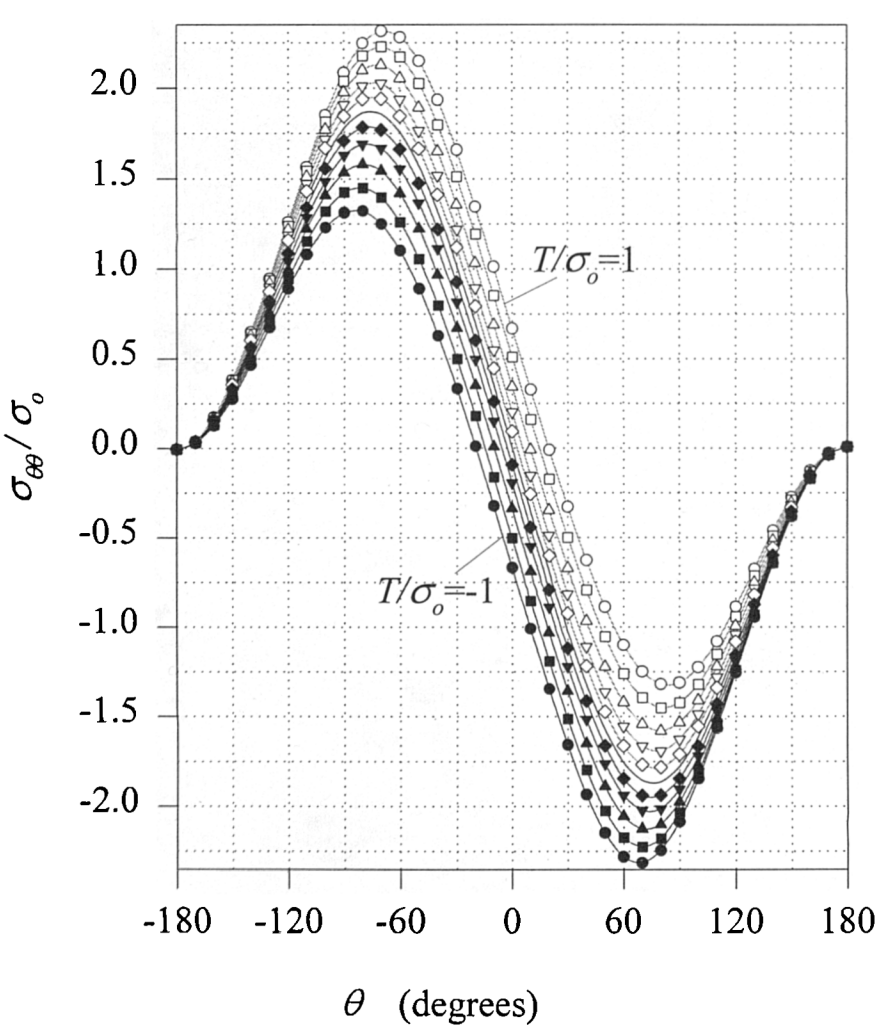

a. Stress field

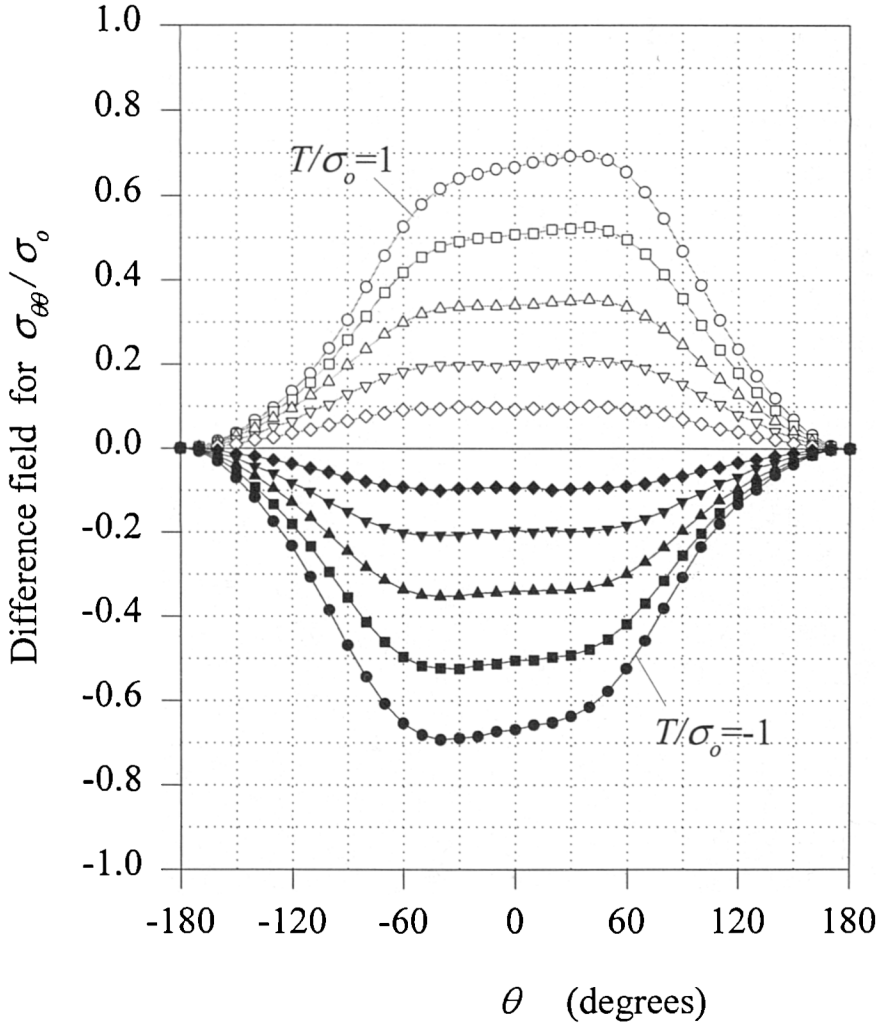

b. Difference field

Figure 7-9. Effect of T/σ_o on the angular distribution of $\sigma_{\theta\theta}/\sigma_o$.
(Symbols are defined in Figure 7-3)

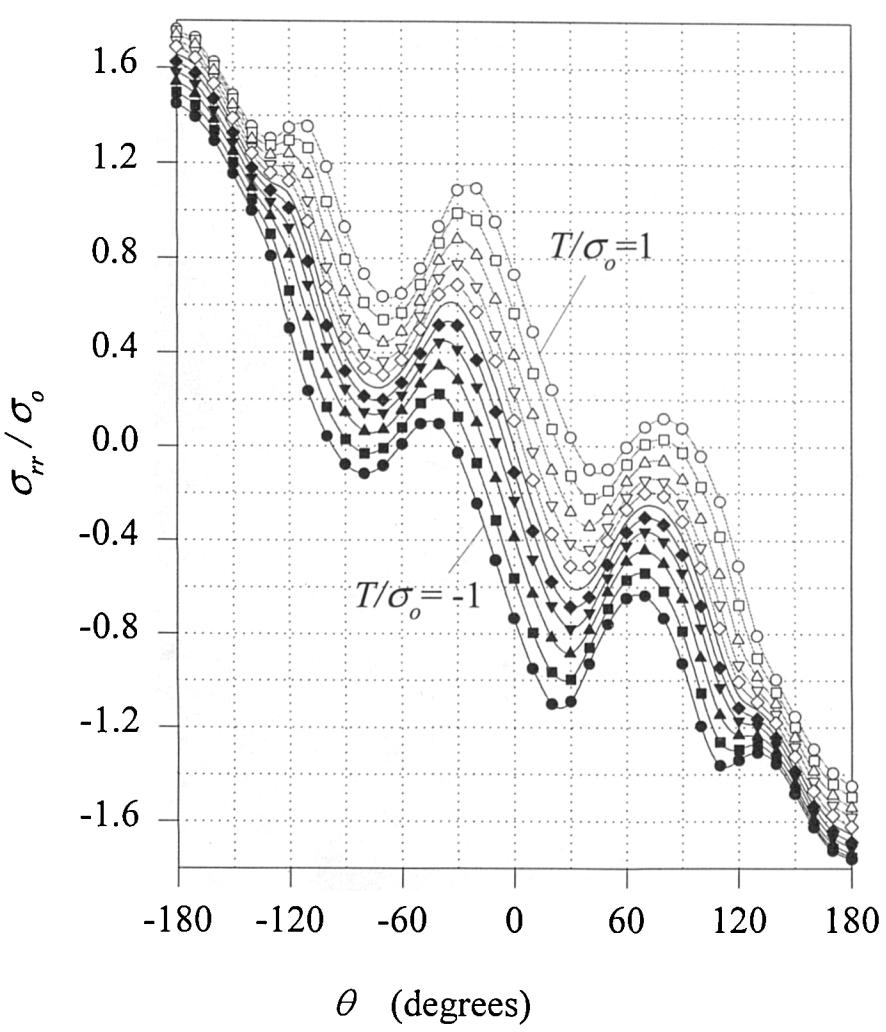

a. Stress field

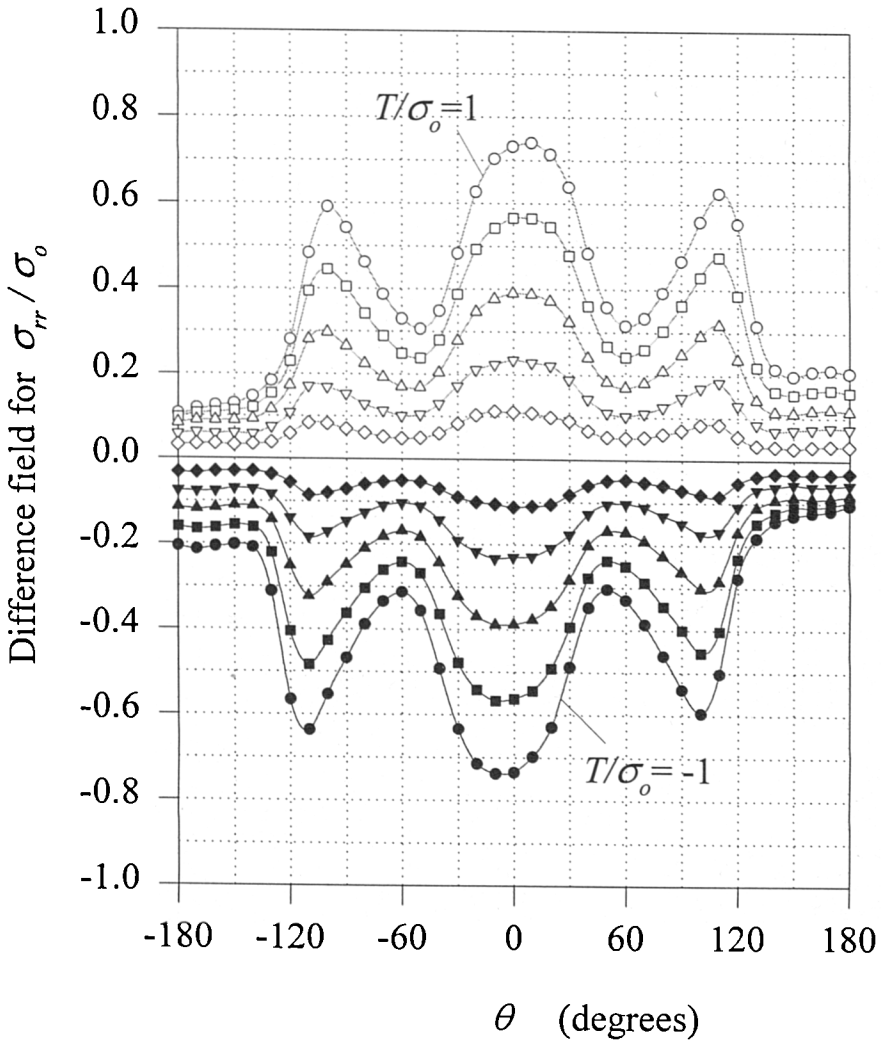

b. Difference field

Figure 7-10. Effect of T/σ_o on the angular distribution of σ_{rr}/σ_o.
(Symbols are defined in Figure 7-3)

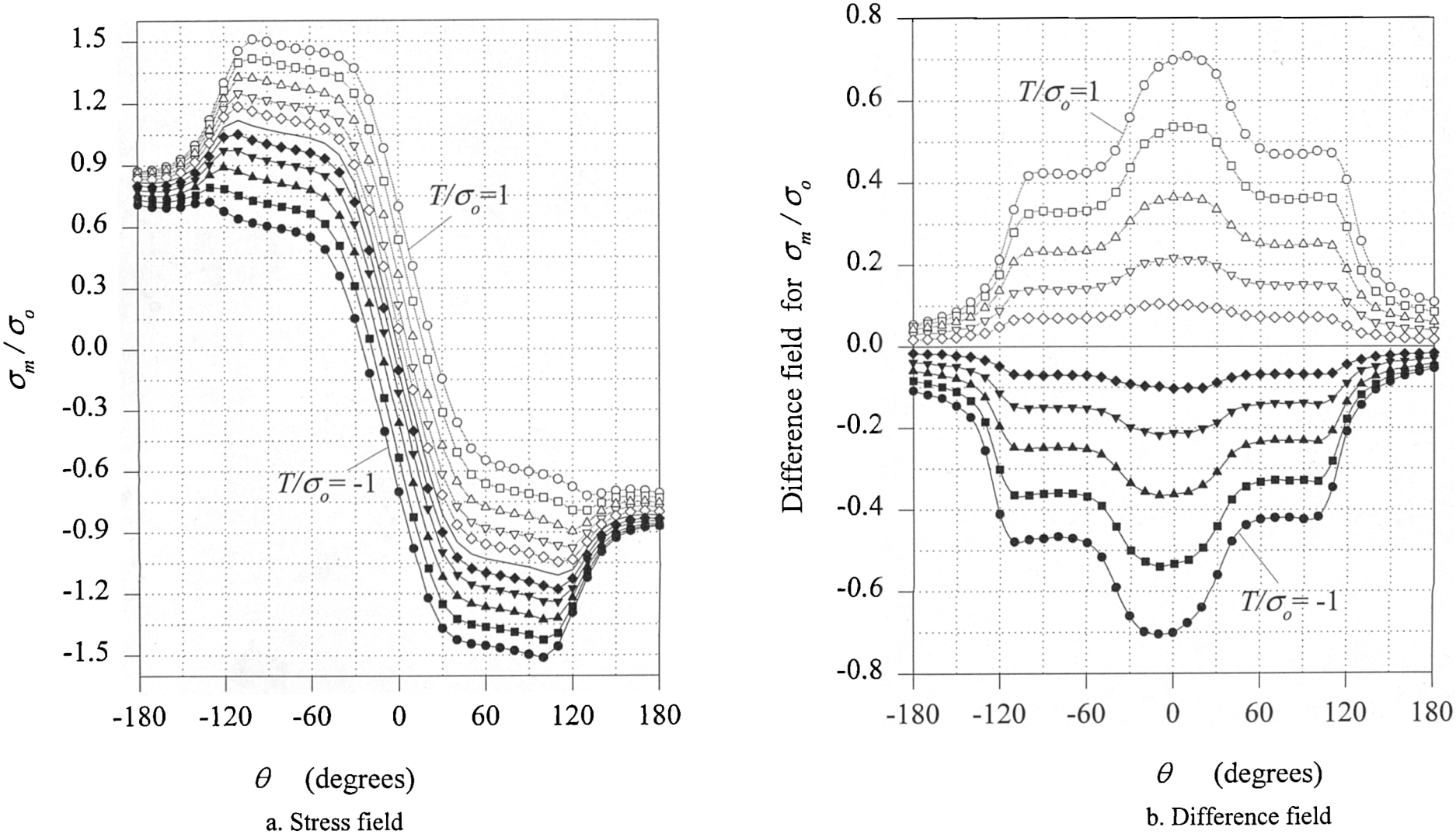

a. Stress field

b. Difference field

Figure 7-11. Effect of T/σ_o on the angular distribution of σ_m/σ_o.
(Symbols are defined in Figure 7-3)

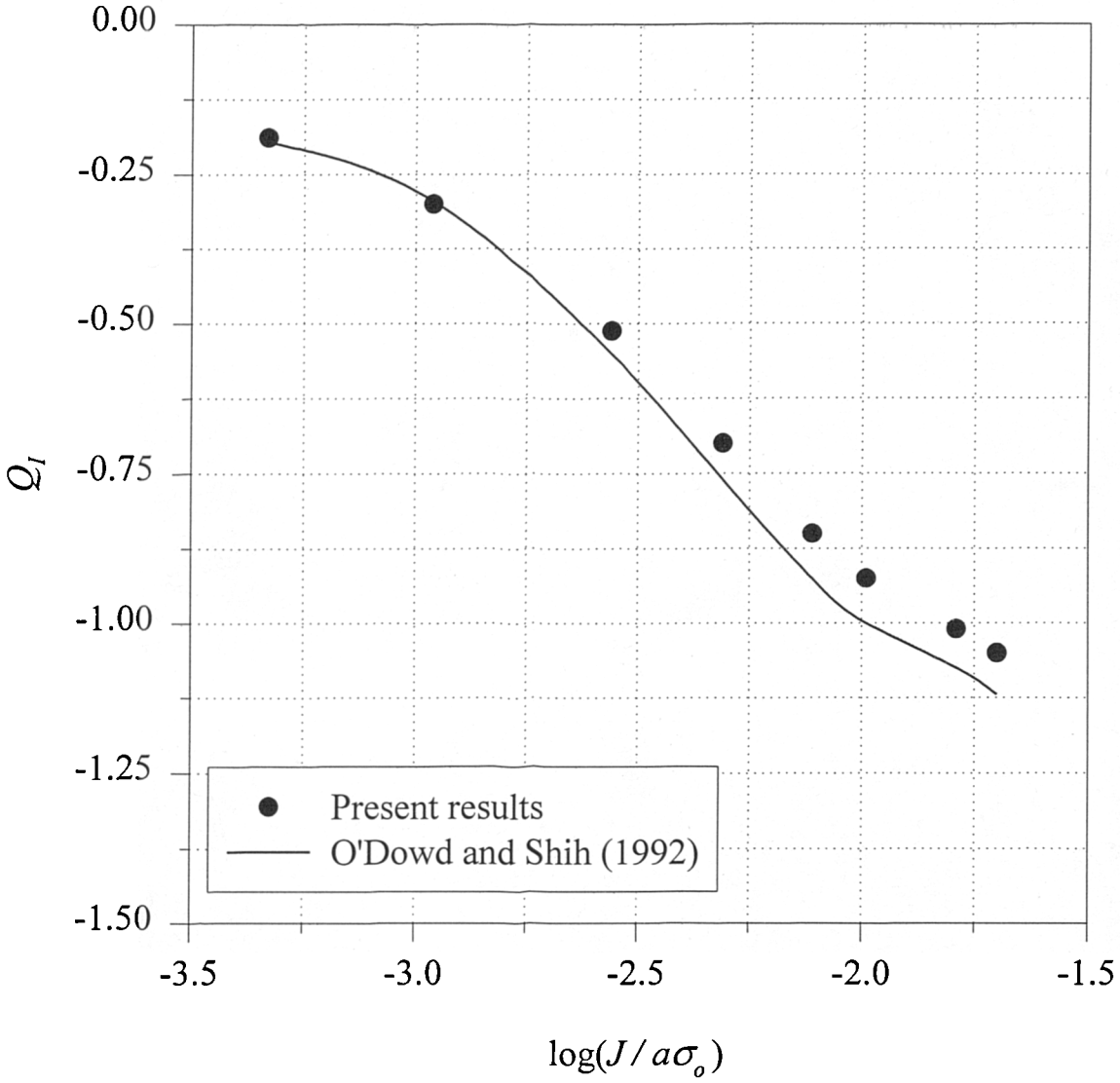

Figure 7-12. Variations of the mode I constraint parameter Q_I for a centrally cracked plate at different levels of load.
(Present results compared with those of O'Dowd and Shih, 1992)

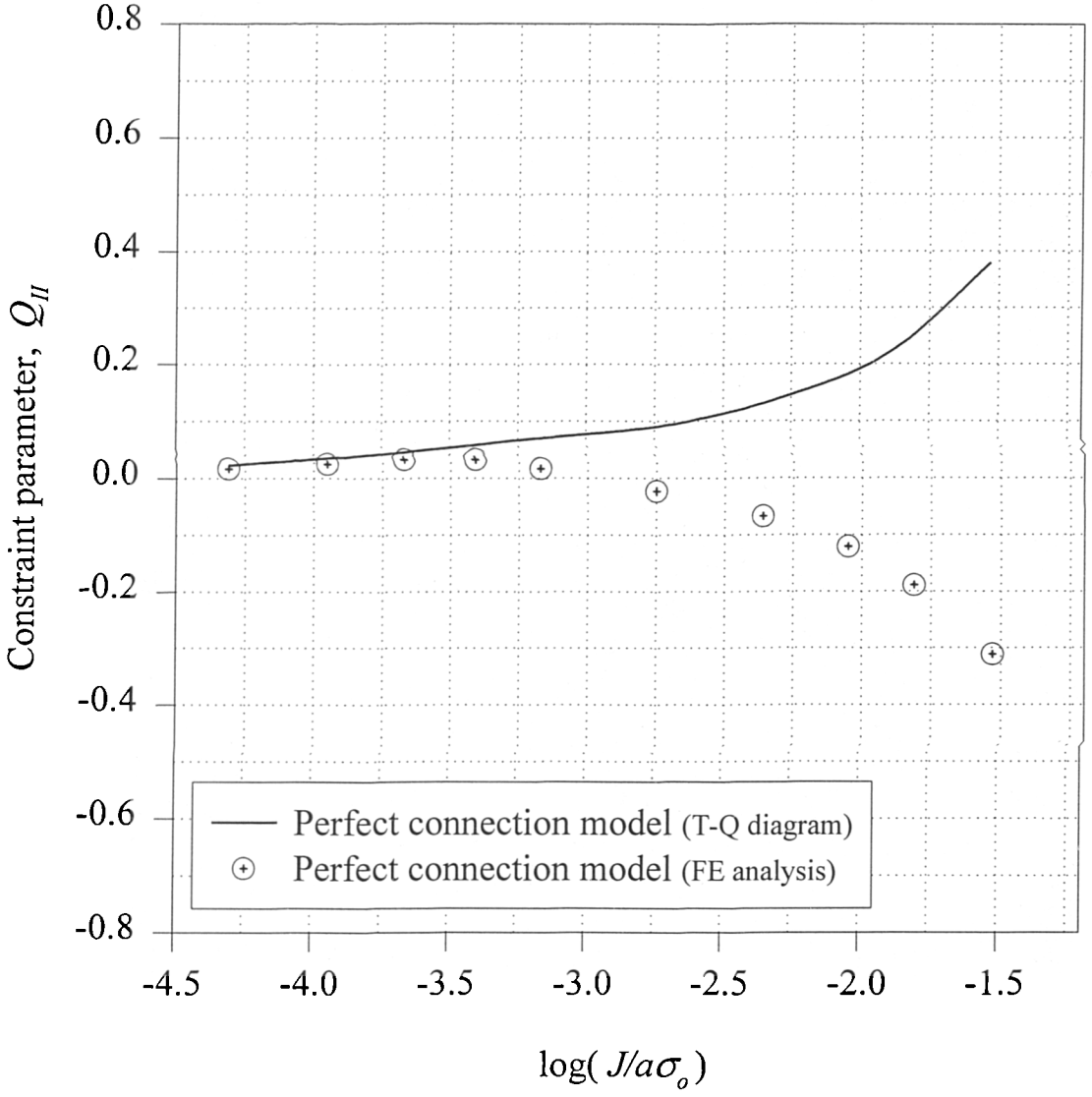

Figure 7-13. Variations of the mode II constraint parameter Q_{II} for the mixed mode specimen at different levels of shear load. (Perfect connection model).

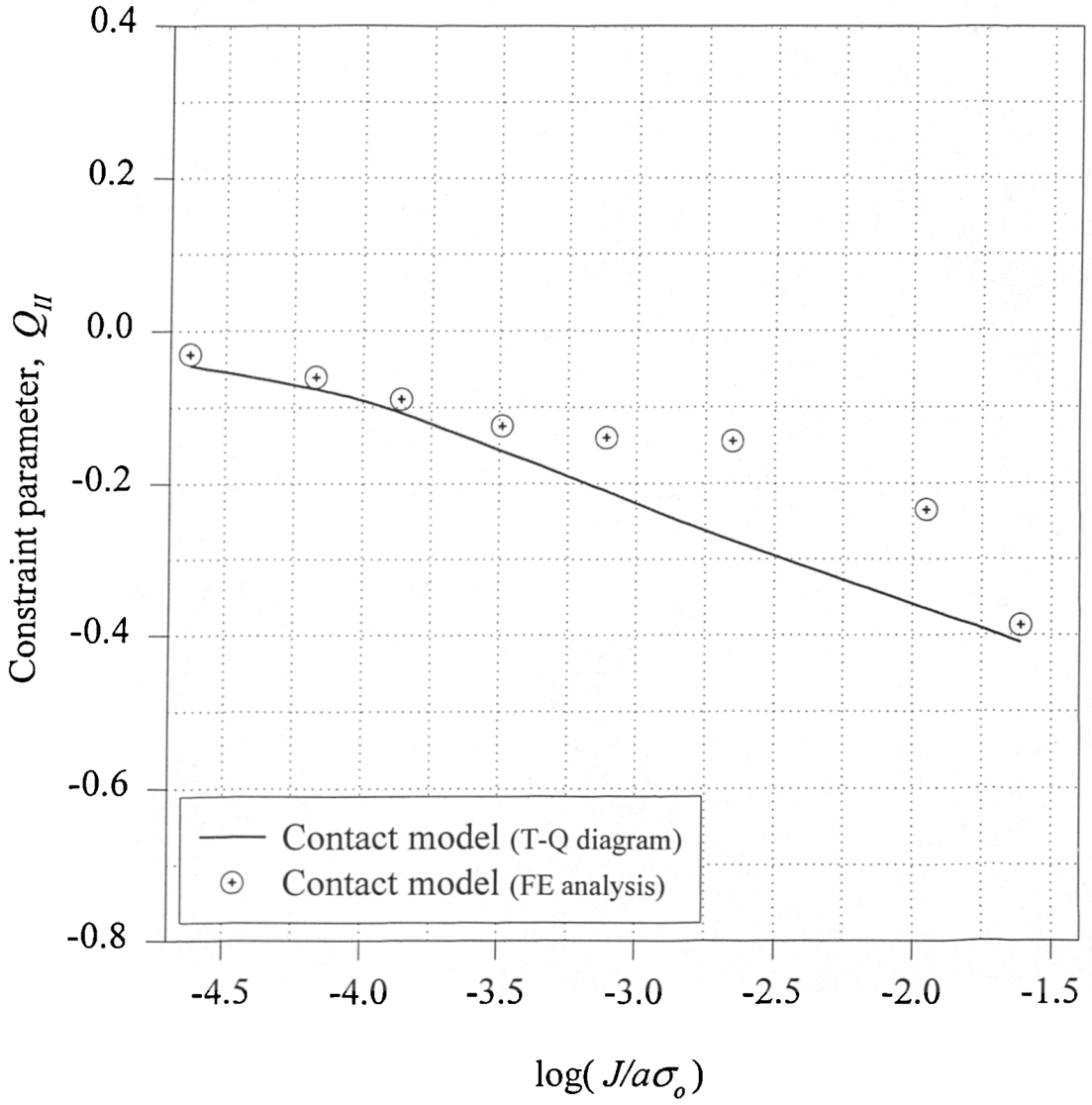

Figure 7-14. Variations of the mode II constraint parameter Q_{II} for the mixed mode specimen at different levels of shear load. (contact model).

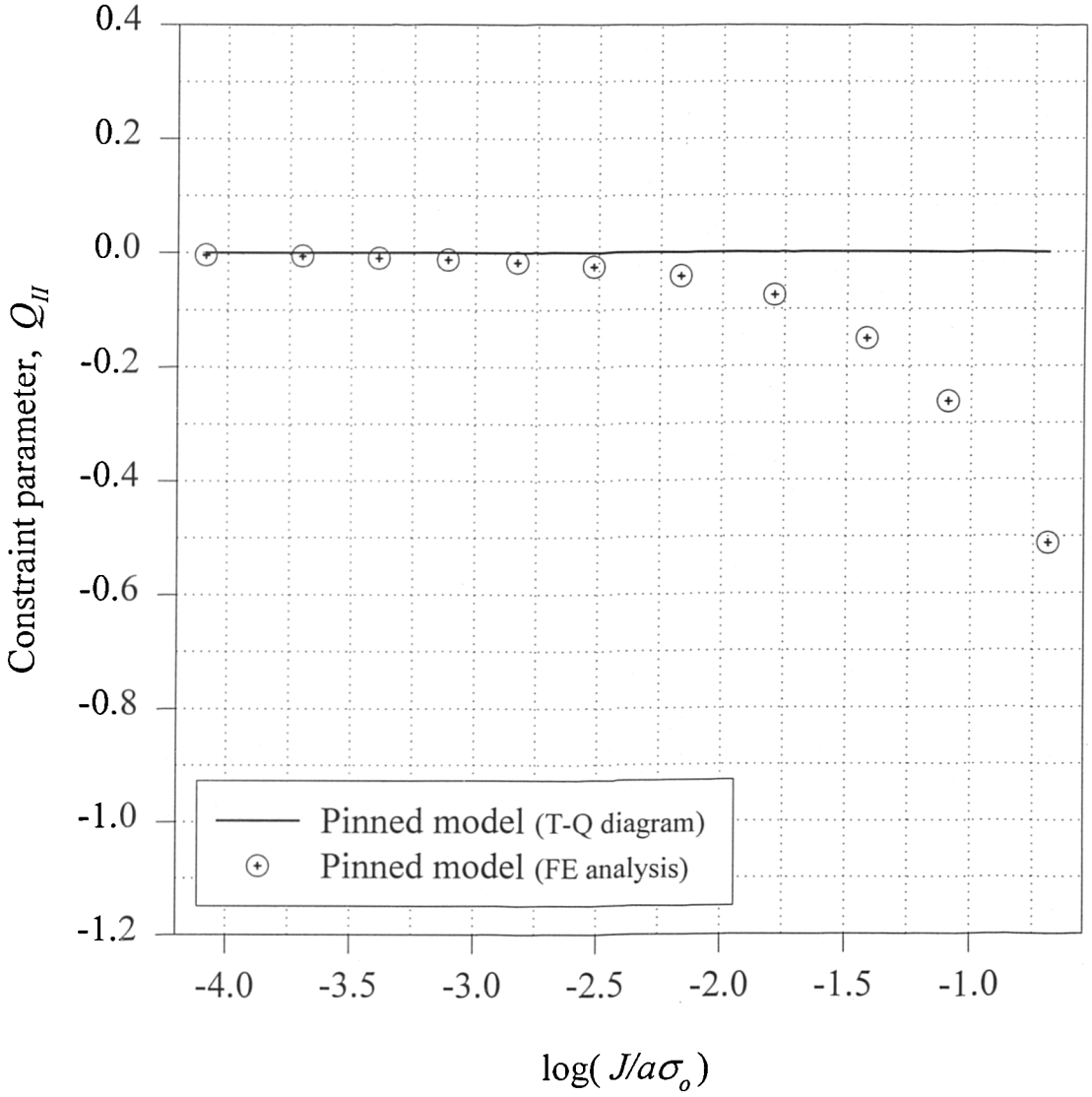

Figure 7-15. Variations of the mode II constraint parameter Q_{II} for the mixed mode specimen at different levels of shear load. (Pinned model).

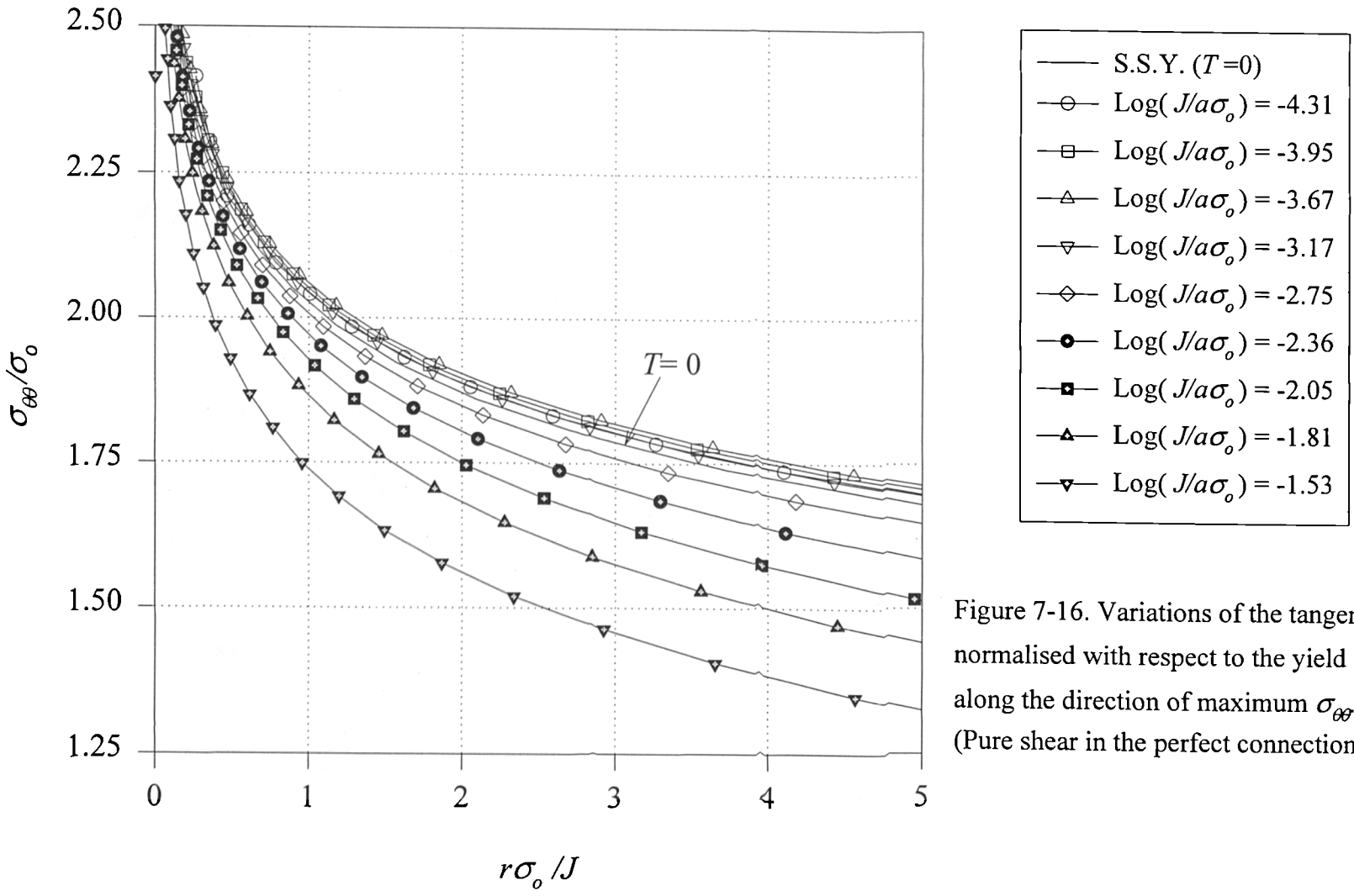

Figure 7-16. Variations of the tangential stress $\sigma_{\theta\theta}$ normalised with respect to the yield stress σ_o along the direction of maximum $\sigma_{\theta\theta}$ (Pure shear in the perfect connection model)

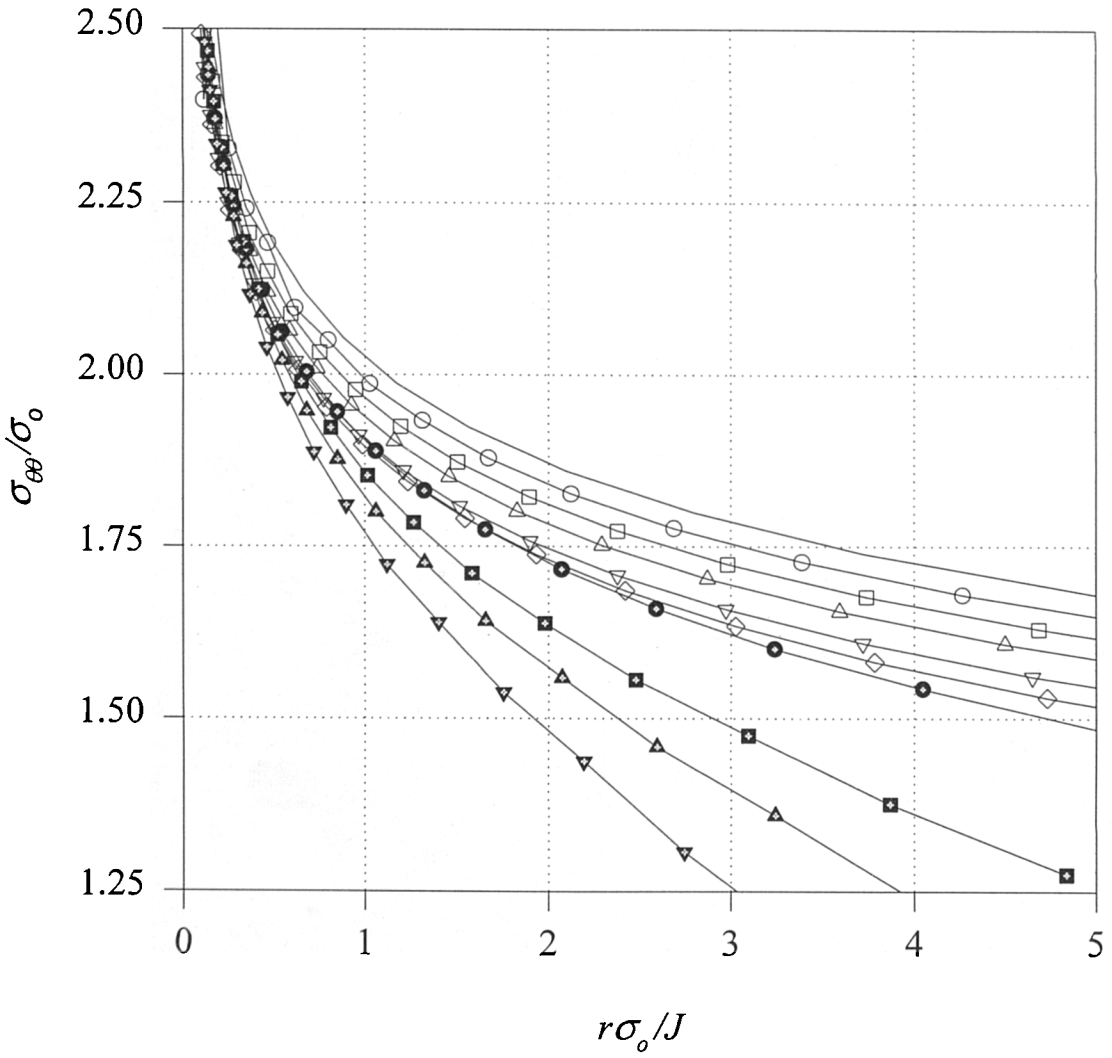

Figure 7-17. Variations of the tangential stress $\sigma_{\theta\theta}$ normalised with respect to the yield stress σ_o along the direction of maximum $\sigma_{\theta\theta}$ (Pure shear in the contact model)

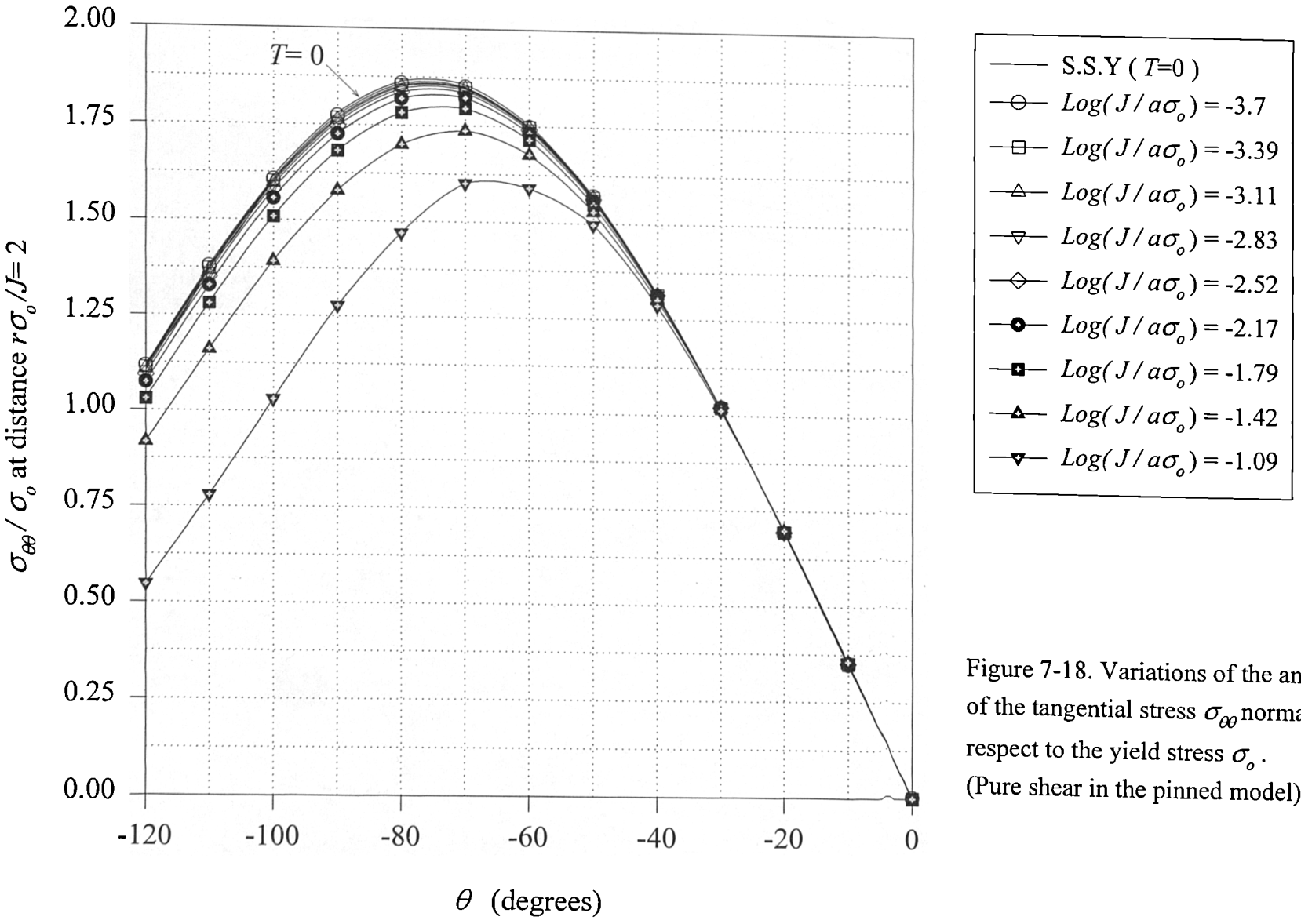

Figure 7-18. Variations of the angular distribution of the tangential stress $\sigma_{\theta\theta}$ normalised with respect to the yield stress σ_o.
(Pure shear in the pinned model)

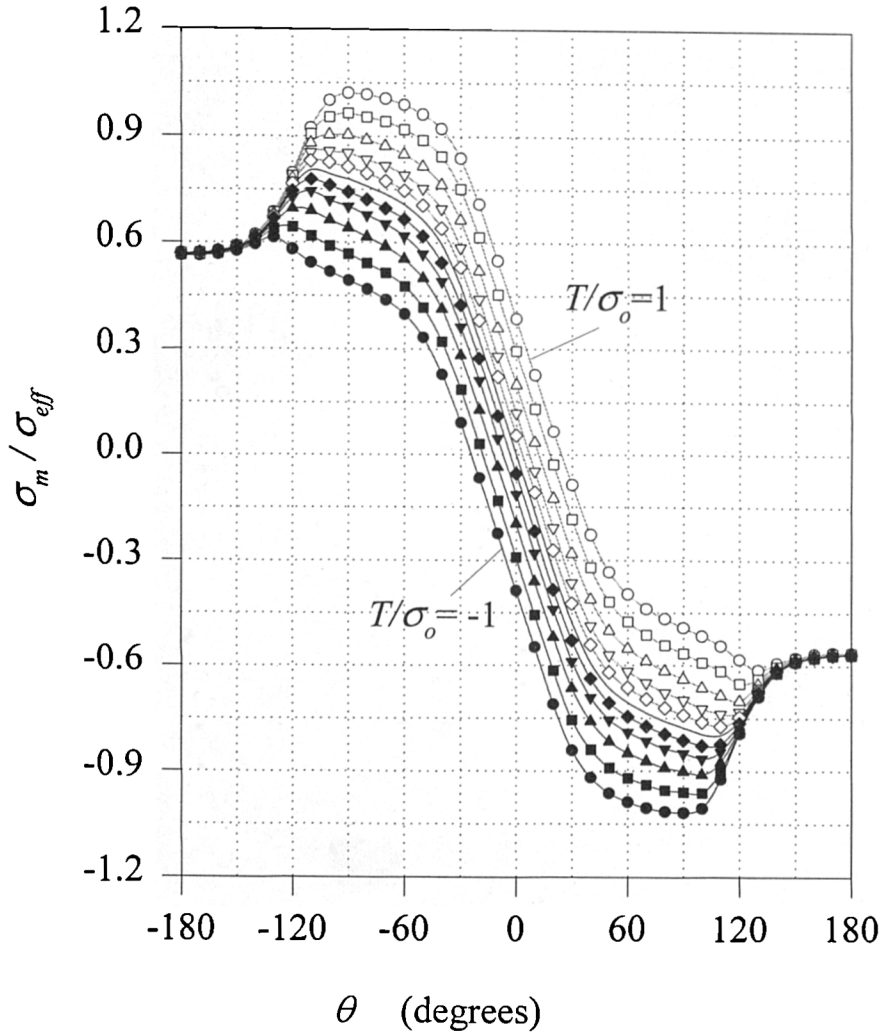

a. Stress field

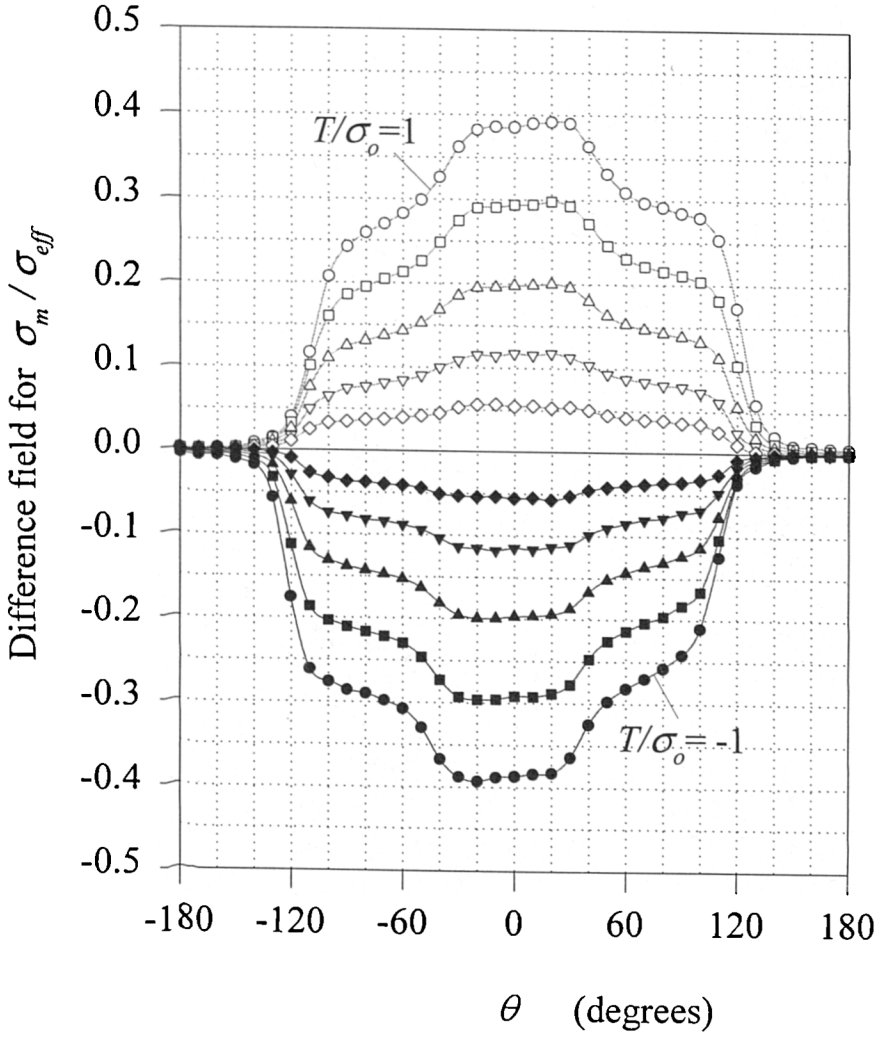

b. Difference field

Figure 7-19. Effect of T/σ_o on the angular distribution of σ_m/σ_{eff}
(Symbols are defined in Figure 7-3)

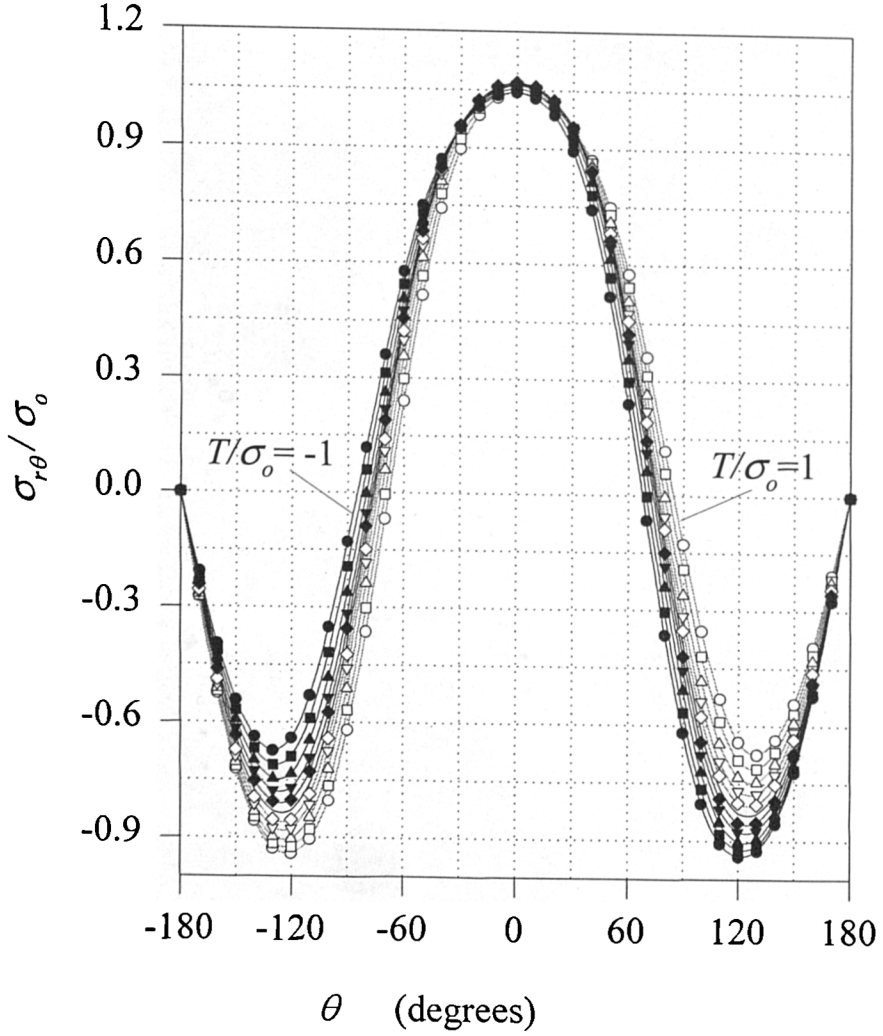

a. Stress field

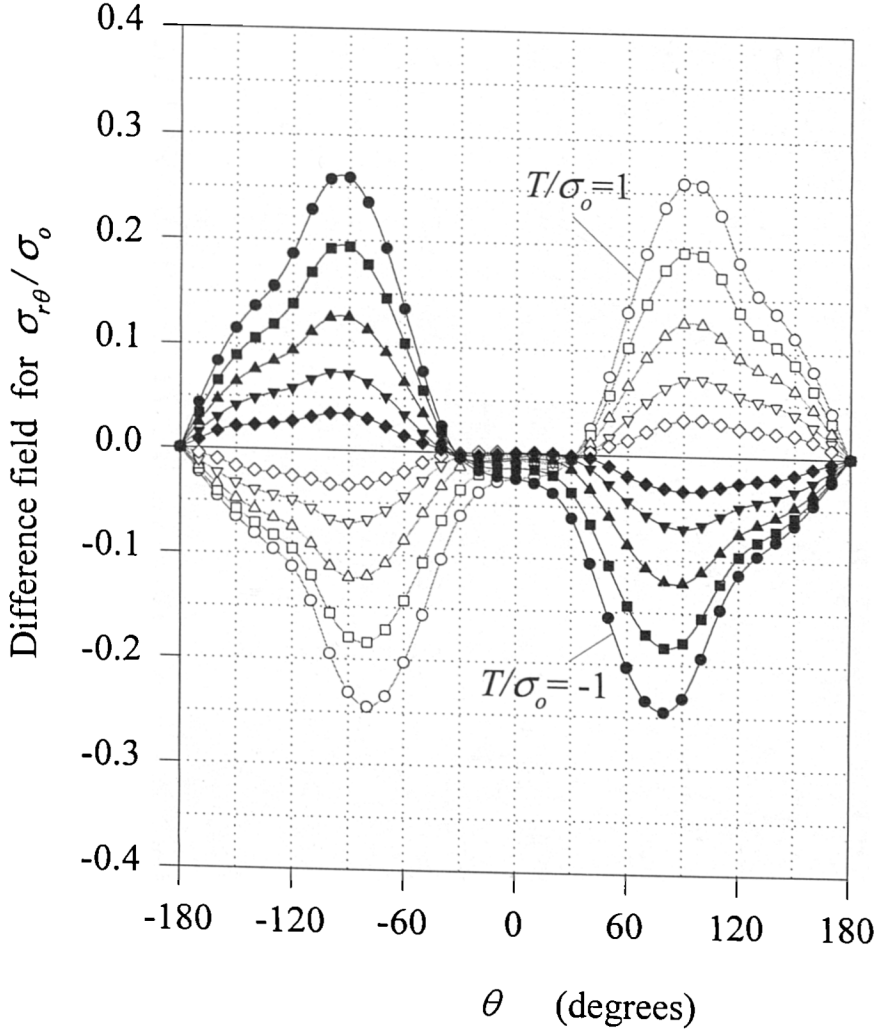

b. Difference field

Figure 7-20. Effect of T/σ_o on the angular distribution of $\sigma_{r\theta}/\sigma_o$.
(Symbols are defined in Figure 7-3)

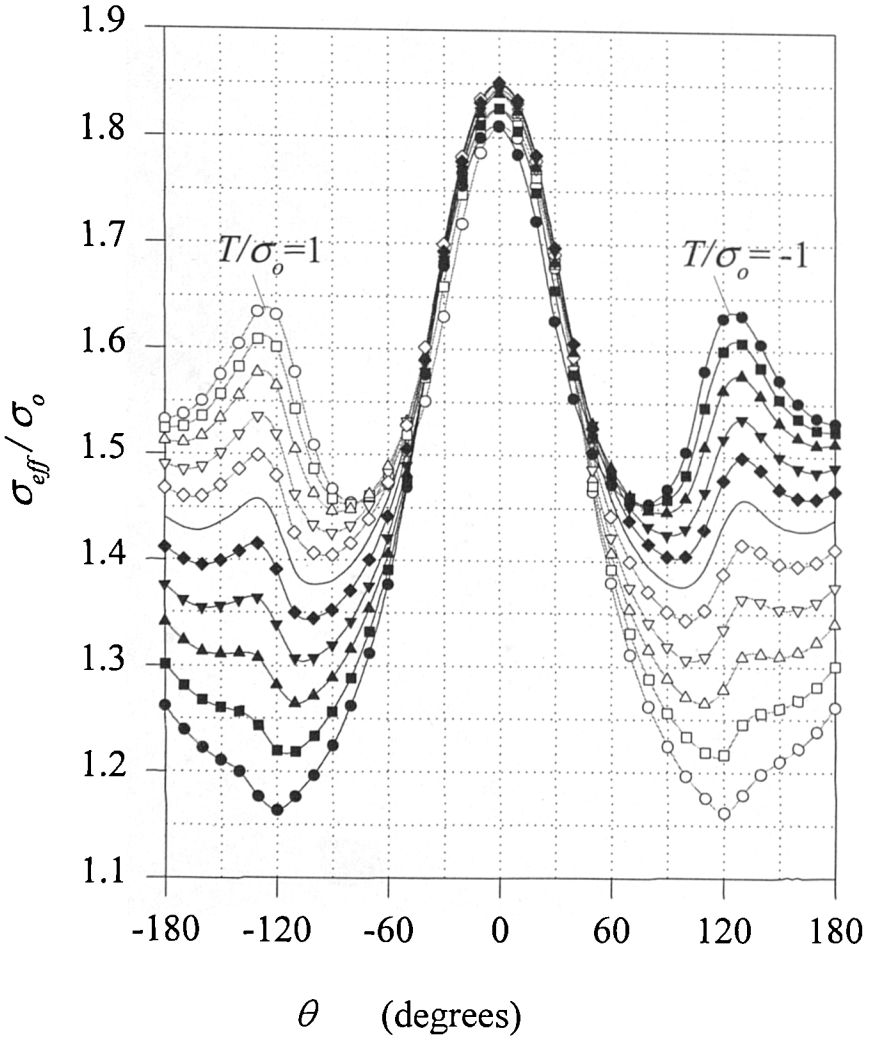

a. Stress field

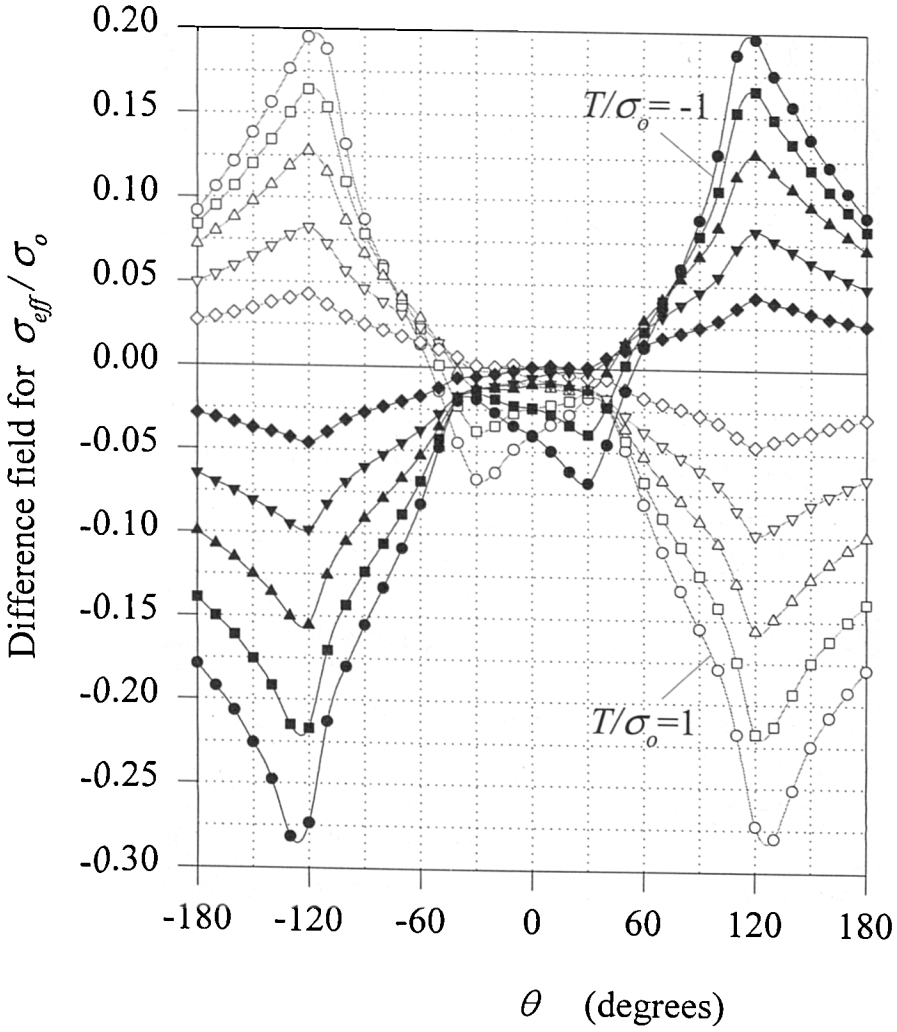

b. Difference field

Figure 7-21. Effect of T/σ_o on the angular distribution of σ_{eff}/σ_o.
(Symbols are defined in Figure 7-3)

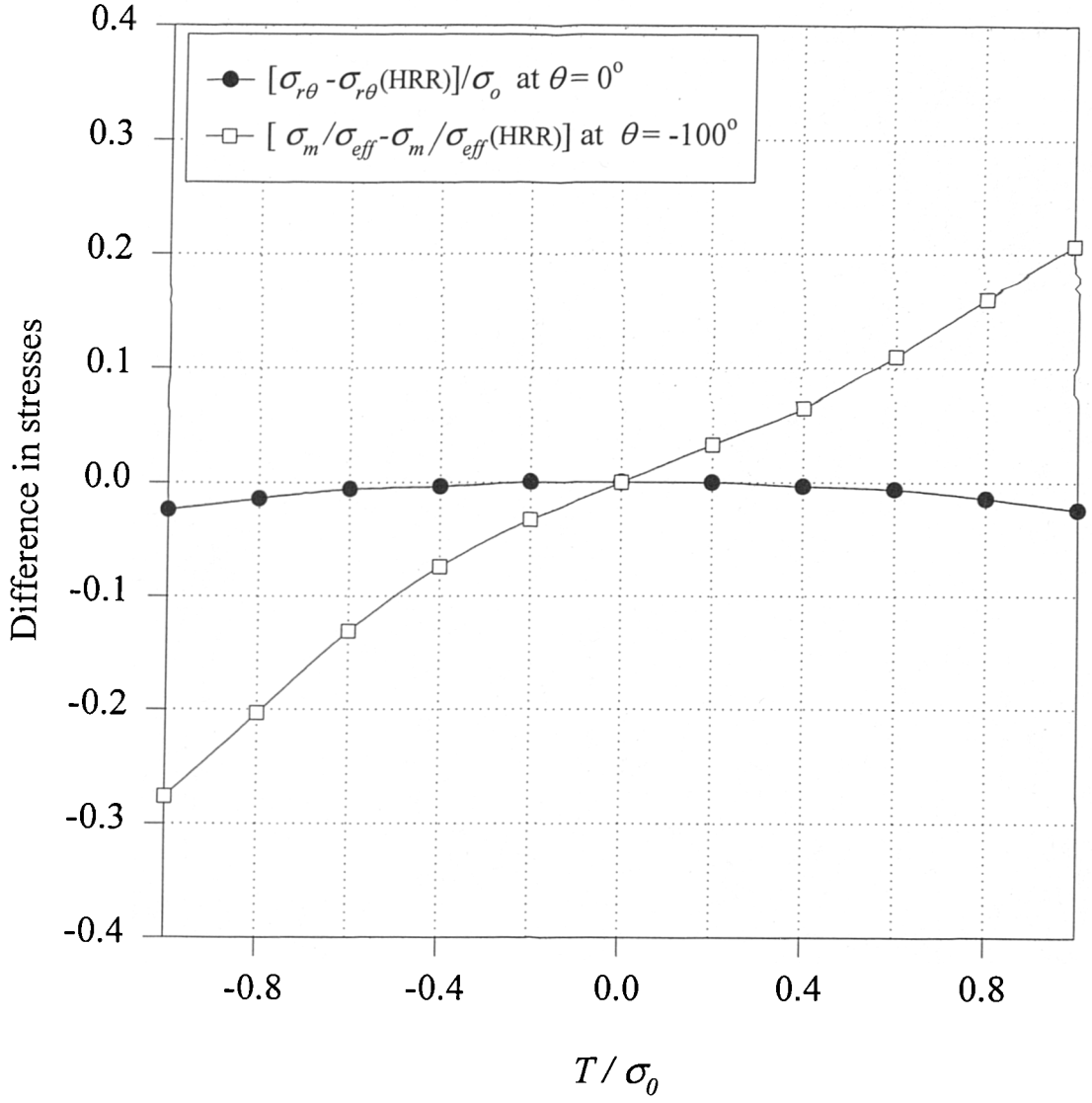

Figure 7-22. Influence of remote boundary T on near crack tip stresses for small scale yielding.

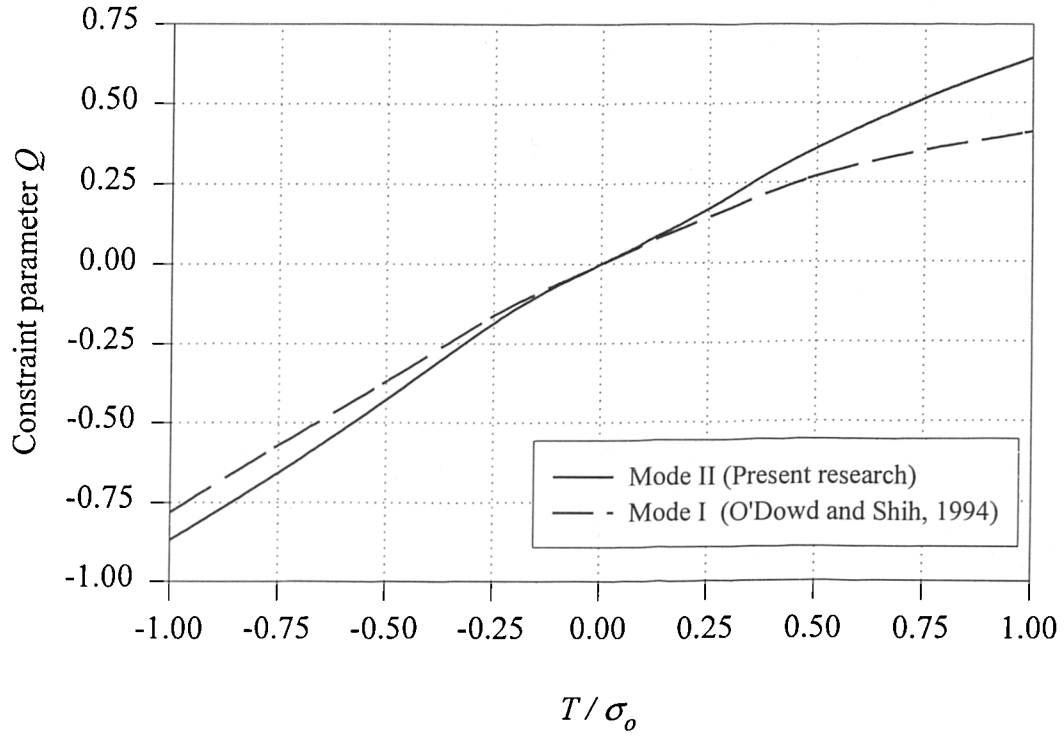

Figure 8-1. The Q-T diagram for n=3: Mode I compared with mode II.

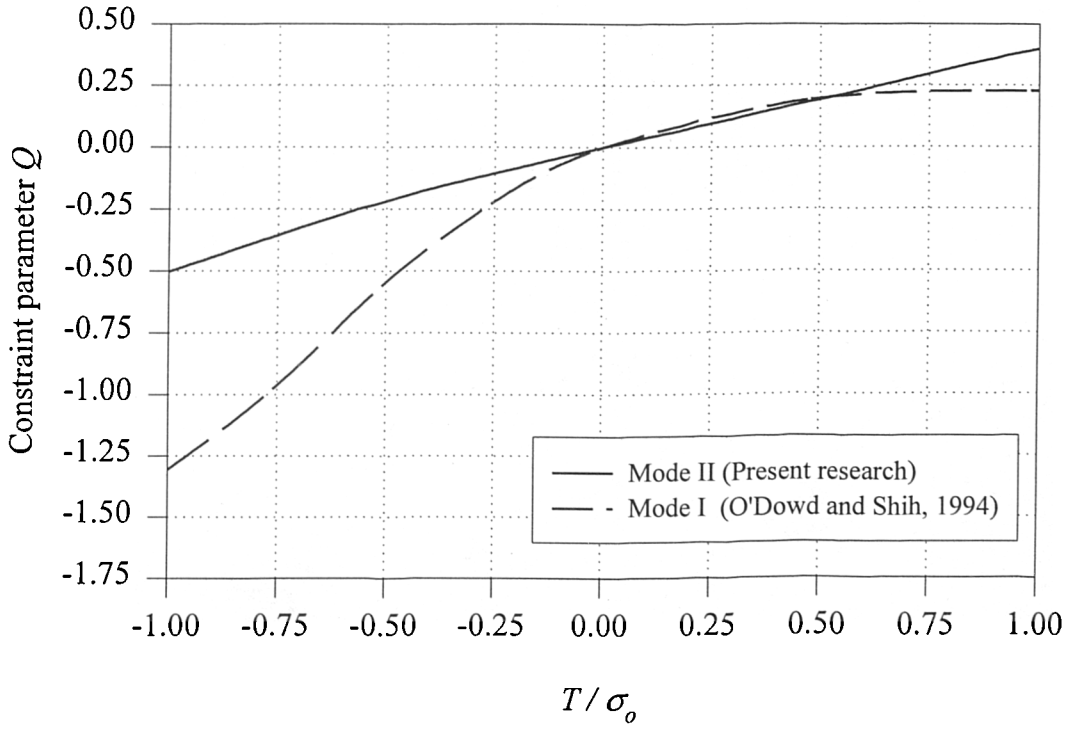

Figure 8-2. The Q-T diagram for n=13: Mode I compared with mode II.